FORSCHUNGSZENTRUM ROSSENDORF

WISSENSCHAFTLICH-TECHNISCHE BERICHTE
FZR-312
Januar 2001
ISSN 1437-322X

Institute of Bioinorganic and Radiopharmaceutical Chemistry

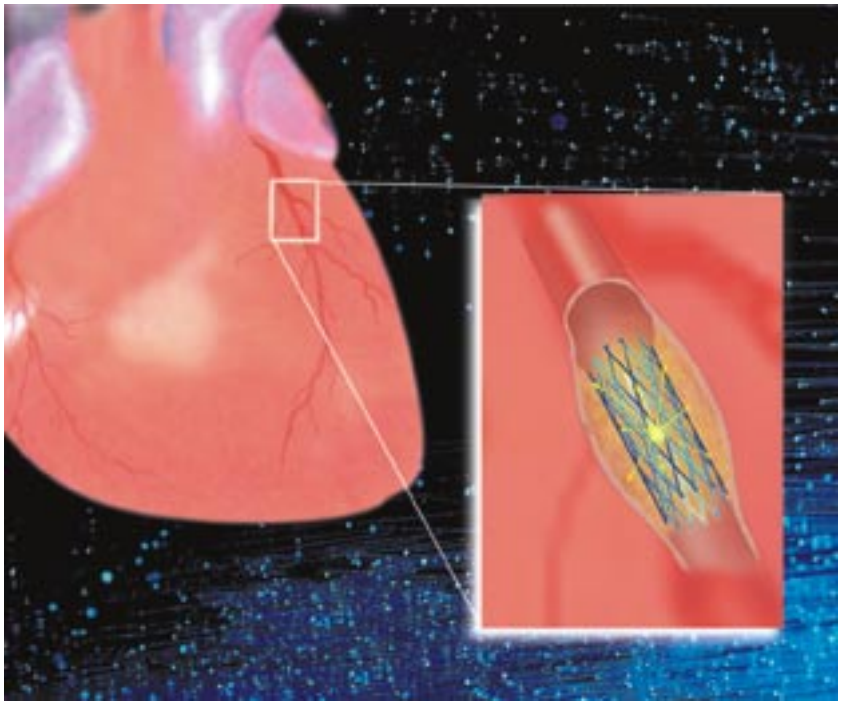

Annual Report 2000

Cover Picture:

Illustration of stent implantation in coronary artery after balloon angioplasty. Radioactively labelled stents prevent restenosis.

Forschungszentrum Rossendorf e.V.

Postfach 51 01 19 ; D-01314 Dresden
Bundesrepublik Deutschland
Telefon (0351) 260 3170
Telefax (0351) 260 3232
E-Mail johannsen@fz-rossendorf.de

FORSCHUNGSZENTRUM ROSSENDORF
WISSENSCHAFTLICH-TECHNISCHE BERICHTE
FZR-312
Januar 2001

Institute of Bioinorganic and Radiopharmaceutical Chemistry

Annual Report 2000

Editor:
Prof. Dr. B. Johannsen
Editorial staff: Dr. S. Seifert

FOREWORD

In 2000 the Rossendorf research centre (Forschungszentrum Rossendorf, FZR; homepage http://www.fz-rossendorf.de) continued and further developed its basic and application-oriented research. Research at the Institute of Bioinorganic and Radiopharmaceutical Chemistry, one of five institutes in the Research Centre, was focused on radiotracers as molecular probes to make the human body biochemically transparent with regard to individual molecular reactions. In this respect the potential for diagnostic application depends on the quality and versatility of radiopharmaceutical chemistry, which is the main discipline in our Institute. Areas in which the Institute was particularly active were the design of new radiotracers, both radiometal-based and natural organic molecules, the elaboration of radiolabelling concepts and procedures and the chemical and pharmacological evaluation of new tracers.

This was complemented by more clinically oriented activities in the Positron Emission Tomography Centre Rossendorf, which closely links the Institute with the Medical Faculty of the Dresden University of Technology. The PET Centre is manned by a joint team of staff members from both the Institute and the University Department of Nuclear Medicine.

During the period under review the Scientific Council as the advisory body to the German Federal Government and the state governments assessed the work of the Institute and commended the established areas of research.

With numerous contributions in the fields of radiopharmaceutical chemistry, tumour agents, tumour diagnosis and brain biochemistry this Annual Report will document the scientific progress made in 2000.

The achievements attained so far were only possible thanks to the dedication and commitment of the permanent and temporary staff, the Ph.D. students and collaborators inside and outside the Rossendorf Research Centre. I would like to extend my thanks to all of them. The Institute wishes to acknowledge in particular the support and assistance received from the Executive Board of the Rossendorf Research Centre, from the competent authorities and funding agencies.

Rossendorf, January 2001

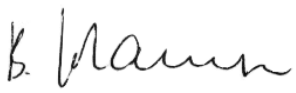

Prof. Dr. Bernd Johannsen

Contents

FOREWORD

I. RESEARCH REPORTS 1

RADIOPHARMACEUTICAL CHEMISTRY 3

1. $^{186/188}$Re Labelled Stents for Prophylaxis of Restenosis: First Animal Results 5
   B. Noll, L. Dinkelborg, P. Muschik, G. Tepe
2. Preparation of ^{188}Re Gluconate by Reduction of [^{188}Re]Perrhenate by Stannous Chloride 7
   B. Noll, H. Spies
3. Labelling of the Neurotensin(8-13) Derivative RP498s with ^{188}Re: Ligand Exchange versus Direct Labelling Approach 9
   K. Chavatte, B. Noll, H. Spies
4. Technetium and Rhenium Complexes with Modified Fatty Acid Ligands 12
   2. Synthesis of Novel Rhenium Complexes as Model Compounds of Technetium Tracers for Myocardial Metabolism Imaging
   C. M. Jung, H.-J. Pietzsch, J. Kropp, H. Spies
5. Technetium and Rhenium Complexes with Modified Fatty Acid Ligands 15
   3. Synthesis and Crystal Structure of an "SSS" Oxorhenium(V) Complex Bearing a ω-Mercapto Fatty Acid Ligand
   C. M. Jung, P. Leibnitz, H.-J. Pietzsch, H. Spies
6. Potentially Redox-Active Rhenium and Technetium Complexes Based on the Pyridinium/Dihydropyridine System 16
   3. Synthesis of Pyridinium/Dihydropyridine Bearing Rhenium(V) '3+1' Mixed-Ligand Complexes with Variable Spacer Lengths and N-Substituents
   A. Rother, T. Kniess, H. Spies, H. Jungclas
7. Potentially Redox-Active Rhenium and Technetium Complexes Based on the Pyridinium/Dihydropyridine-System 18
   4. Dependence of the Stability of Pyridinium/Dihydropyridine Bearing Rhenium(V) Mixed-Ligand Complexes on Variable Spacer Lengths and N-Substituents
   A. Rother, T. Kniess, H. Spies, H. Jungclas
8. Synthesis of a ^{99}Tc Complex with a Cationic Lipid as Initial Stage for Preparation of Tc-Labelled Cationic Lipid/DNA Complexes 21
   T. Kniess, G. Byk
9. Labelling Dithiol Ligands with the Tc-99m Synthon [^{99m}Tc(N)(PNP4)Cl_2] 23
   C. Bolzati, A. Duatti, A. Boschi, L. Uccelli, H.-J. Pietzsch, S. Seifert, H. Spies
10. Synthesis and Characterization of Trigonal-bipyramidal Technetium(III) Complexes with Tridendate/Bidendate NS_2/PS Coordination: A Novel Approach to Robust Tc Mixed-Ligand Chelates as Tools for Conjugating Biologically Active Molecules 25
    H.-J. Pietzsch, P. Leibnitz, F. Tisato, F. Refosco, S. Seifert, H.Spies
11. Preparation and Characterization of ^{99m}Technetium(III) Complexes with Tridentate and Bidentate Ligands ('3+2' Complexes) 27
    S. Seifert, H.-J. Pietzsch, R. Syhre, F. Tisato, H. Spies
12. Preparation and Characterization of New '3+1' Tc(V) Oxocomplexes Containing a Tridentate PNS or PNO Ligand and a Monothiol Ligand 32
    S. Seifert, C. M. Fernandes, R. Syhre, I. Santos, H. Spies
13. The Coordination of 4-Mercapto-5-methylthio-1.2-dithiol-3-thione with Technetium and Rhenium: First Results 35
    H.-J. Pietzsch, H. Stephan, H. Spies, W. Banße, H.J. Holdt
14. Bromoalkylated Tetradentate N_2S_2 Chelates and their Technetium Complexes 36
    I.Heimbold, A.Drews

15. EXAFS Analyses of Technetium and Rhenium Complexes 39
1. Stability Studies of Technetium(I) Tricarbonyl Dithioether Complexes in Solutions
S. Seifert, J.-U. Künstler, A. Gupta, H. Funke, T. Reich, C. Hennig, A. Roßberg, H.-J. Pietzsch, R. Alberto, B. Johannsen

16. EXAFS Analyses of Technetium and Rhenium Complexes 42
2. Reactivity of Technetium(I) Thioether Carbonyl Complexes against Histidine
S. Seifert, J.-U. Künstler, A. Gupta, H. Funke, T. Reich, H.-J. Pietzsch, R. Alberto, B. Johannsen

17. EXAFS Analyses of Technetium and Rhenium Complexes 45
3. Reaction of His, Gly and Small Model Peptides with the Precursor Complex $(NEt_4)_2[Tc(CO)_3Cl_3]$ in Solution
J.-U. Künstler, S. Seifert, T. Reich, B. Johannsen

18. EXAFS Analyses of Technetium and Rhenium Complexes 49
4. EXAFS Analyses of the Complexes $[Re(CO)_3(Phe)(PPh_3)]$ and $[Re(CO)_3(Phe)(H_2O)]$ – Comparison with the EXAFS Spectra of a Binuclear Oxorhenium(V) Complex Measured at Room Temperature and 15 K
J.-U. Künstler, S. Seifert, H.-J. Pietzsch, T. Reich, H. Funke, R. Alberto, B. Johannsen

19. ITC Analysis of Binding Perrhenate Using Monopyridinium-α-Cyclodextrin 54
H. Stephan, H. Spies, B. Johannsen, E. Nicoletti, F. P. Schmidtchen

20. Benzodiazepine Technetium Complexes 57
A. Drews, R. Syhre, P. Brust, A. Nudelman, H.- J. Pietzsch, B. Johannsen

21. Phenothiazine Technetium Complexes 60
A. Drews, R. Syhre, A. Nudelman, H.- J. Pietzsch, B. Johannsen

22. '3+1' Mixed-Ligand Oxorhenium (V) Complexes Bearing 1,2,3,4-Tetrahydro-quinoline and Quinoline 62
A. Zablotskaya, I. Segal, E. Lukevics, A. Drews, T. Kniess, H. Spies

23. Biological Study of '3+1' Mixed-Ligand Oxorhenium(V) Complex Bearing 1,2,3,4-Tetrahydroisoquinoline in the Monodentate Ligand 64
A. Zablotskaya, I. Segal, S. Germane, I. Shestakova, E. Lukevics, A. Drews, H. Spies

24. Psychotropic Activity of O-Organosilicon Containing 3-Thia, 3-Oxa and 3-Methyl-azapentane-1,5-Dithiolato-Oxorhenium(V) 66
A. Zablotskaya, I. Segal, S. Germane, E. Lukevics, H. Spies

25. Substrates of the Herpes-Simplex-Virus 1 Thymidine Kinase and Escherichia Coli Cytosine Deaminase for Monitoring Gene Expression 68
Part 1: Syntheses of New Modified Acyclic Purine and Pyrimidine Nucleosides
St. Noll, M. Grote, B. Große, B. Noll

26. Substrates of the Herpes-Simplex-Virus 1 Thymidine Kinase and Escherichia Coli Cytosine Deaminase for Monitoring Gene Expression 74
Part 2: Synthesis of New IVFRU Derived Nucleosides
T. Kniess, B. Noll

27. Substrates of the Herpes-Simplex-Virus 1 Thymidine Kinase and Escherichia Coli Cytosine Deaminase for Monitoring Gene Expression 77
Part 3: Synthesis of a Precursor for Labeling of 5-Iodo-2'-fluoro-2'-deoxy-uridine (FIRU) with [^{18}F]Fluorine
T. Kniess, St. Noll, B. Noll

28. Substrates of the Herpes-Simplex-Virus 1 Thymidine Kinase and Escherichia Coli Cytosine Deaminase for Monitoring Gene Expression 79
Part 4: Synthesis and Tosylation of 5-Hydroxymethyl-Cytosine
T. Kniess, St. Noll, B. Noll

29. Substrates of the Herpes-Simplex-Virus 1 Thymidine Kinase and Escherichia Coli Cytosine Deaminase for Monitoring Gene Expression 81
Part 5: Efficiency Study to Improve the ^{18}F-labelling of N^1-Methyl-9-[(1-hydroxy-3-[^{18}F]fluoro-2-propoxy)methyl]guanine by HPLC Detailed Control
B. Noll, M. Scheunemann, M. Grote, St. Noll

30. Substrates of the Herpes-Simplex-Virus 1 Thymidine Kinase and Escherichia Coli Cytosine Deaminase for Monitoring Gene Expression 84
Part 6: Results of a Fast and Simple Screening Method to Determine Possible Substrates for the Herpes-Simplex-Virus 1 Thymidine Kinase
M. Grote, B. Noll, St. Noll, T. Kniess, L. Scapozza

31. Substrates of the Herpes-Simplex-Virus 1 Thymidine Kinase and Escherichia Coli Cytosine Deaminase for Monitoring Gene Expression 88
Part 7: Preparation of Cytosine Deaminase from Escherichia Coli
M. Grote, A. Gupta, St. Noll, T. Kniess, B. Noll, H. K. Schackert, M.Hauses

32. Synthesis of S-([^{18}F]Fluoromethyl)-(+)-McN5652 - A Potential Radiotracer for Imaging the Serotonin Transporter 90
J. Zessin, O. Eskola, P. Brust, J. Bergman, J. Steinbach, P. Lehikoinen, O. Solin, B. Johannsen

33. Chemical Stability of S-([^{18}F]Fluoromethyl)-(+)-McN5652 94
J. Zessin, O. Eskola, J. Bergman, J. Steinbach, P. Lehikoinen, P. Brust, O. Solin

34. Self-Condensation Reaction of Pentamethinium Salts under Basic Conditions 96
B. Pawelke, P. Mäding, J. Steinbach, R. Schlecker

35. Simultaneous Preparation of 16α-[^{18}F]Fluoroestradiol-Sulphamates in an Automated Module. A High-Yield Procedure for 16α-[^{18}F]Fluoro-Estradiol-17β-Sulphamate 98
J. Römer, F. Füchtner, J. Steinbach, R. Lücke, C. Smuda, H. Kasch

36. Mass Spectroscopic Investigations of By-Products in the Synthesis of 16α-[^{18}F]Fluorestradiol-3,17β-Disulphamate 103
K. Fischer, J. Römer

37. Steroidal 16,17-O-Sulphuryl Derivatives as Suitable Precursors for ^{18}F-Labelled *trans* 16,17-Fluoro Hydrines 107
J. Römer, F. Füchtner, J. Steinbach, H. Kasch

38. 16α-Fluoro-Estradiol-3-Monosulphamate (FESMS) and 16α-Fluoro-Estradiol-3,17ß-Disulphamate (FESDS)– New Carbonic Anhydrase Inhibitors of High Potency 109
H. Rodig, J. Gross, A. Müller, H. Kasch, P. Brust

39. Synthesis of Labelled Advanced Glycation End Products Using N-Succinimidyl 4-[^{18}F]Fluorobenzoate 113
P. Mäding, Ch. Heichert, M. Scheunemann, R. Helling, T. Henle, J. Steinbach, B. Johannsen

40. Aspects of the 6-[^{18}F]Fluoro-L-DOPA Preparation: Effective Chromatographic Purification of the Reaction Mixture and Determination of Radiochemical Purity 116
F. Füchtner, J. Steinbach, R. Lücke, E. Kraus

41. Separation of Radioactively Labelled Compounds by on-line Combination of SEC and HPLC 120
H. Wittrisch, R. Bergmann, C. Heichert

42. Optimization of the Synthesis of [^{18}F]$FClO_3$ 124
A. Jordanova, J. Steinbach

43. Quality Assurance in Manufacturing Radiopharmaceuticals for Positron Emission Tomography (PET) 126
K. Smolinka, R. Syhre, F. Füchtner, J. Steinbach

44. Operation of the Rossendorf PET Cyclotron "CYCLONE 18/9" in 2000 128
St. Preusche, J. Steinbach

45. Modification of the ^{18}F Water Target Loading Procedure 131
St. Preusche, H. Ross

46. Measurement of Recovery Coefficients for HR+ and their Application in a Correction Method 133
H. Linemann, E. Will, B. Beuthien-Baumann, H. Kutzner

TUMOUR AGENTS AND TUMOUR DIAGNOSIS 136

47. 3-*O*-Methyl-6-[^{18}F]Fluoro-L-DOPA – a Promising PET Tracer for Tumour Imaging. Autoradiographic Description of the Biodistribution in a Tumour-Bearing Nude Mouse and in the Rat Brain 139
M. Kretzschmar, P. Brust , F. Füchtner, J. Steinbach, B. Johannsen

48. In Vitro Evaluation of [^{18}F]FHPG and [$^{124/125}$I]FIAU for their Potential of Monitoring Gene Therapy 142
A. Friedrich, M. Scheunemann, R. Haubner[1], O.N. Koufaki[2], S. Noll, R. Bergmann, H. Stephan, B. Noll, N. Avril, P. Brust, B. Johannsen

49. Separation of ^{18}F-Labelled Neurotensin Derivatives and its Metabolites 148
H. Wittrisch, R. Bergmann, K. Fischer, C. Heichert, P. Mäding, M. Scheunemann, P. Brust

50. Distribution of 16α-[^{18}F]Fluoro-Estradiol-3,17-β-Disulphamate (FESDS) in Rats and Tumour-Bearing Nude Mice 152
P. Brust, H. Rodig, R. Bergmann, J. Römer, M. Baumann, H. Kasch, F. Füchtner, J. Steinbach

51. Identification of Cancer Tissue by a Combination of FTIR Spectroscopy and PET 157
T. Richter, G. Steiner, R. Bergmann, H. Rodig, B. Johannsen, R. Salzer

52. Evaluation of FDG-PET in the Diagnostic Work-up of Patients with Squamous Cell Carcinomas of the Oral Cavitiy 162
M. Hlawitschka, J. Bredow, B. Beuthien-Baumann, E. Neise, U. Eckelt, W.-G. Franke

53. Assessment of 16α-[^{18}F]Fluoro-17β-Estradiol (FES) and 2-[^{18}F]Fluoro-2-Deoxy-D-Glucose (FDG) PET in the Pre-Operative Diagnosis of Breast Cancer 165
J. Bredow, B. Richter, B. Beuthien-Baumann, J. Römer, F. Füchtner, W. Distler, W.-G. Franke, B. Johannsen

54. Parametric Imaging of Oncological Brain PET Studies Using [^{18}F]OMFD 167
R. Hinz, J. Bredow

BRAIN BIOCHEMISTRY 171

55. Characterization of [^{11}C]McN5652 in Various Animal Species: Implications for Tracer Development 173
P. Brust, M. Kretzschmar, J. Zessin, R. Bergmann, A. Friedrich, F. Füchtner, R. Hinz, J. Steinbach

56. Ex-Vivo Autoradiographic Studies to Investigate the Pharmacological Specificity and Selectivity of [^{99m}Tc]TRODAT Binding in the Rat Brain 178
M. Kretzschmar, I. Heimbold, S. Seifert, P. Brust

57. Intrauterine Growth Restriction Induces Upregulation of Cerebral Aromatic Amino Acid Decarboxylase Activity in Newborn Piglets 181
P. Brust, R. Bauer, B. Walter, R. Bergmann, G. Vorwieger, E. El-Hallag, A. Fritz, R. Hinz, F. Füchtner, J. Steinbach, U. Zwiener

58. Transport of Carnitine at the Brain Endothelium *in vitro* 186
A. Friedrich, V. Ganapathy, P. Brust

59. Transport of L-Tryptophan at the Brain Endothelium *in vitro* 189
A. Friedrich, V. Ganapathy, P. Brust

60. Changes in the Cerebral Glucose Metabolism of Patients with Wilson's Disease 193
W. Burchert, B. Kunath, B. Beuthien-Baumann, U. Reuner, W.-G. Franke

61. Integration of Functional Brain PET Images and Intraoperative Brain Mapping Data into the BrainLab VectorVision Neuronavigation System 197
R. Steinmeier, S. B. Sobottka, B. Beuthien-Baumann, J. Bredow, G. Reiss, R. von Kummer, W.-G. Franke, G. Schackert

62. Longitudinal PET Study of the Cerebral Glucose Metabolism in Major Depression: Acute State and Clinical Remission 199
V. A. Holthoff, B. Beuthien-Baumann, W. Burchert, A. Triemer, P. Winiecki, W.-G. Franke, O. Bach

II. PUBLICATIONS, LECTURES, PATENTS AND AWARDS 201

III. SCIENTIFIC COOPERATION 211

IV. SEMINARS 217

V. ACKNOWLEDGEMENTS 223

VI. PERSONNEL 227

I. RESEARCH REPORTS

RADIOPHARMACEUTICAL CHEMISTRY

1. $^{186/188}$Re Labelled Stents for Prophylaxis of Restenosis: First Animal Results

B. Noll, L. Dinkelborg[1], P. Muschik[1], G. Tepe[2]
[1]Schering AG, Berlin, [2]Universität Tübingen

Introduction

Restenosis is a major problem occurring after angioplasty, atherectomy and implantation of stents. It was shown that external beam teletherapy (X-rays) and intravascular brachytherapy (e. g. Iridium-192 ribbon seeds, Re-188 filled catheters, P-32-coated stents) may prevent restenosis by inhibiting the proliferation of medial smooth muscle cells [1, 2]. But these methods require a high radiation dose during the short-time radiation and involve an additional risk for the patient. The hitherto studied approach to implanting ^{32}P into the stent surface requires the availability of a cyclotron. It was the aim of this study to label stents by an uncomplicated method with ^{186}Re and ^{188}Re and to investigate the potential of $^{186/188}$Rhenium labelled stents to prevent restenosis in an animal model.

Experimental

Stainless steel stents (2 cm long, Palmaz P204, Cordis, Warren, NJ) were labelled with ^{186}Re and ^{188}Re by a modified process ("kitlike") as described in the US patent application US006103295. The activity of each stent was determined by its γ-component in a scintillation chamber, the axial distribution of the activity in the stent was determined by gradually passing the labelled stent through a cylindrical collimator (slit width 2.0 mm).
The ^{186}Re stents were implanted with activities in several groups ranging from 3 MBq to 25 MBq. The delivered radiation dose (0.5 mm from a stent wire of a 4 mm stent) ranged from 38 Gy to 377 Gy. New Zealand White rabbits were fed a 0.5% cholesterol diet four weeks prior to the intervention. ^{186}Re ($T_{1/2}$=3.8 d) labelled Palmaz stents were placed in the infrarenal aorta of the rabbits after balloon denudation. Animals with implanted unlabelled stents served as controls. Whole-body scintigrams were obtained after 1, 4, 24 hours and after 7 and 14 days to determine the bleaching of Re-186 from the stents *in vivo*. Seven weeks later the animals were sacrificed and morphometry and immunohistology were performed.

Results

Depending on the labelling time and the amount of $^{186/188}$Re activity in the labelling solution, the stent can be labelled with a defined amount of activity. The labelling process is reproducible and the activity bound at the stent surface stable, the axial distribution of the $^{186/188}$Re activitivity is nearly constant (Fig.1). Challenge investigations in physiological saline solution and in human blood at 37°C showed that after 72 h not more than 5 % of the activity is lost. Thrombogenicity studies showed no differences between the labelled and the reference stents. The surface of the labelled stent was not negatively affected. (Fig.2)

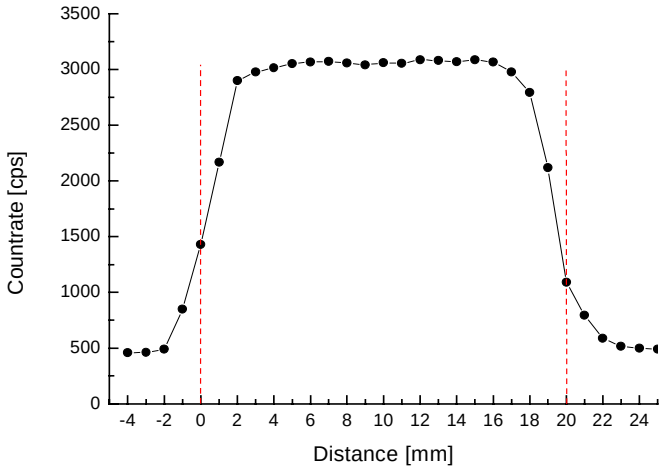

Fig 1. Determination of the axial distribution of ^{188}Re activity on a labelled Palmaz stent

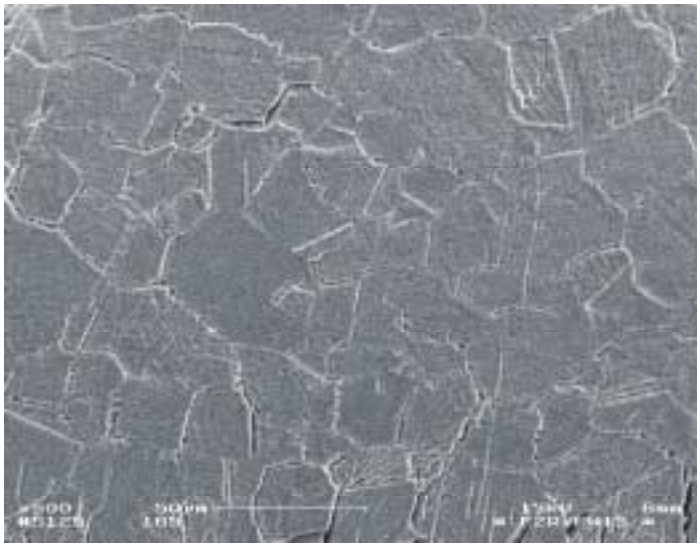

Fig. 2. Metallic grain observed by electron microscopy (500fold scale-up)

More than 90 % of the ^{186}Re remained on the stents two weeks after their implantation in the rabbits as was found by ROI analysis of the scintigrams. Seven weeks after stent implantation a neointima was found in the control group, which significantly differed from the treatment groups. A dose-dependent reduction of neointimal formation was observed. In the highest activity groups (16.0 and 25.3 MBq) neointimal growth was completely suppressed. With increasing radioactivity the media increasingly atrophied (Fig. 3).
No intraluminal thrombus formation was observed. The minor luminal accumulation of fibrin and fibroblasts directly at the stent struts implies that the delivered dose can even be reduced.

a b

Fig. 3. Cross-sections of rabbit aorta with stent grid seven weeks after implantation.
a- control, b-^{186}Re labelled stent

Further animal studies with ^{188}Re labelled stents as an alternative are in preparation.

Conclusions

Stents labelled with ^{186}Re and ^{188}Re are reproducible used over a large radioactivity range. The arterial implantation of ^{186}Re labelled stents was feasible and stable *in vivo*. The activity of 25 MBq totally inhibited neointimal formation. In further studies we will reduce the stent activity in order to determine the therapeutic window of ^{186}Re and ^{188}Re labelled stents.

References

[1] Fischell, T.A.; Kharma, B.K,; Fischell, D.R.; Loges, P.G.; Coffey, C.W. 2nd; Duggan, D.M.; Naftilan, A.J. Low-dose, beta-particle emission from 'stent' wire results in complete, localized inhibition of smooth muscle cell proliferation. Circulation. 90 (1994) 2956-63.
[2] Crocker, I.; McGinley, P.; Waksman, R.; Robinson, K.; King, S.B. 3rd; Beta-particle emission from stent wire. Circulation. 92 (1995) 1353-4.

2. Preparation of ^{188}Re Gluconate by Reduction of [^{188}Re]Perrhenate by Stannous Chloride

B. Noll, H. Spies

Re gluconate is a useful precursor for the preparation of numerous rhenium complexes in aqueous solution at the oxidation state +5 [1]. The preparation of ^{186}Re gluconate at 10^{-7} M level has been described previously [2]. These are experiments for the carrier free preparation of ^{188}Re gluconate from eluate of the ^{188}W/^{188}Re generator, since that is of special interest for radiotherapeutical preparations [3, 4]. Labelling experiments were carried out by variation of the stannous chloride concentration and the reaction time. To prevent possible radiolysis ascorbic acid as scavenger of radicals was added in some preparations.

Preparation

To a 0.5 M sodium gluconate solution the ^{188}Re eluate was added and argon was bubbled through the solution. The reduction was carried out by stepwise addition of the stannous chloride solution in a range from 0,5 mg/ml to 2 mg/ml at room temperature. The remaining content of perrhenate was determined by TLC on silica gel plastic sheets (Merck) and acetone as eluent. Analyses were done up to 120 min after adding the last amount of stannous chloride.

Results

The time dependence of the ^{188}Re gluconate formation at different amounts of stannous chloride is described in Fig. 1.

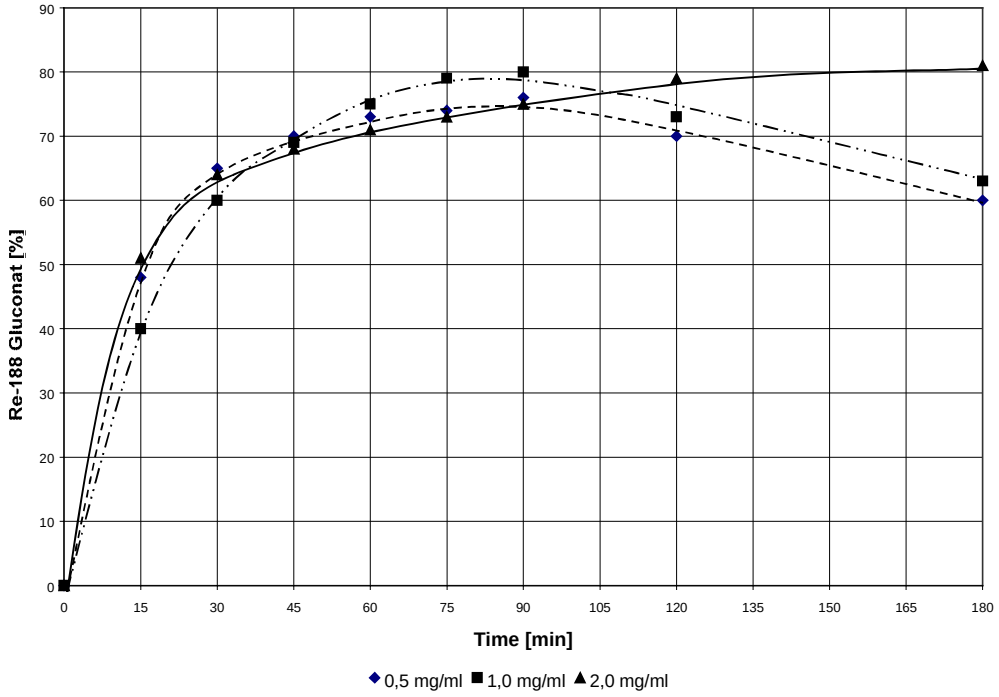

Fig. 1. Formation of ^{188}Re gluconate as a function of time and concentration of stannous chloride

The yield of ^{188}Re gluconate increases at stannous chloride concentrations lower than 1.0 mg/ml after about 90 min. At a stannous chloride concentration of 2.0 mg/ml the ^{188}Re gluconate is stable over a longer period.

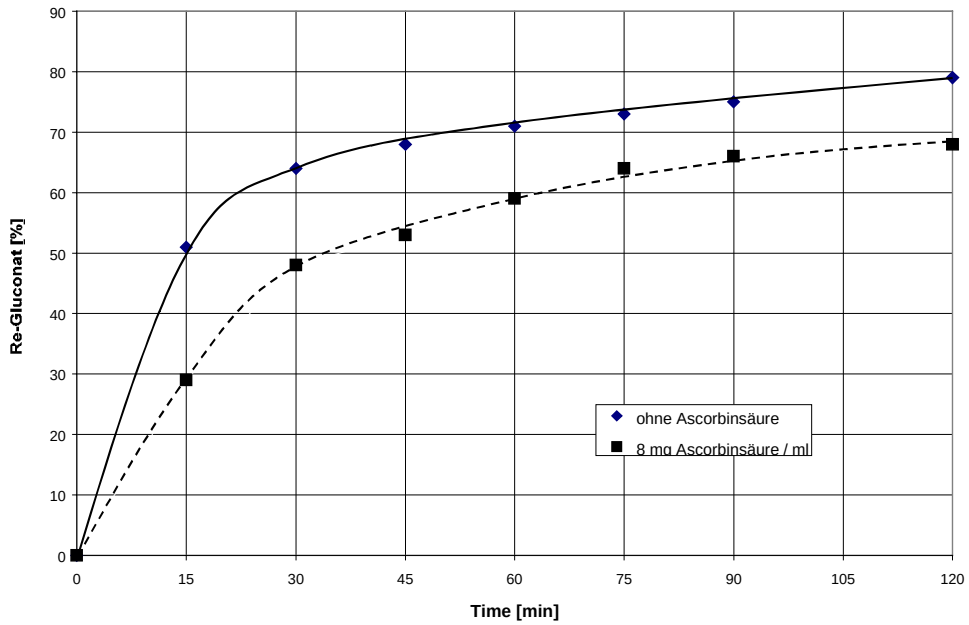

Fig. 2. Time dependence of an optimized preparation (2.0 mg $SnCl_2$/ml) without (----) and after adding of ascorbic acid (- - -)

Furthermore, the effect of ascorbic acid on yield and stability of ^{188}Re gluconate was studied. The yield of ^{188}Re gluconate is decreased about 10 % in the presence of ascorbic acid. The initially aimed effect-inhibition of radiolysis was not observed. After 20 h no increase of the perrhenate amount was observed, both preparations are stable over several hours.

Good analytical results are obtained on silicagel coated plastic sheets (Merck, without fluorescence indicator) and acetone as eluent, $[^{188}ReO_4]^-$ migrates with R_f = 0.9 and ^{188}Re gluconate with R_f = 0 - 0.1. On TLC plates containing a fluorescence indicator in the silicagel layer a lower amount of ^{188}Re gluconate and, respectively, an increase of the perrhenate content by about 20 % is observed. It is likely, that the indicator favours reoxidation of Re(V) species to perrhenate.

References

[1] Noll, B.; Kniess, T.; Friebe, M.; Spies, H.; Johannsen, B. Rhenium(V) gluconate, a suitable precursor for the preparation of rhenium(V) complexes. Isot. Environ. Health Stud. 32 (1996) 21-29.

[2] Noll, B.; Kniess, T; Spies, H. Synthesis of ^{186}Re gluconate by stannous chloride reduction of $^{186}ReO_4^-$, *Annual Report 1996*, Institute of Bioinorganic and Radiopharmaceutical Chemistry, FZR-165, pp. 106-107

[3] Zhu, Z.H.; Wu, Y.H.; Zhang, Z.Y.; Liu, Y.F. Direct labeling of antibodies IgG with rhenium-186 using sodium glucoheptonate., Radiochim. Acta 79 (1997) 105-108.

[4] Noll, B., Dinkelborg, L.; Hilger, H. ^{186}Re-Labelling of an endotheline derivative, *Report January 1998 – June 1999*, Institute of Bioinorganic and Radiopharmaceutical Chemistry, FZR-270, pp. 188-189.

3. Labelling of the Neurotensin(8-13) Derivative RP498s with ^{188}Re: Ligand Exchange versus Direct Labelling Approach

K. Chavatte[1], B. Noll, H. Spies.
[1]Vrije Universiteit Brussel

Introduction

Radiolabelled neurotensin (NT) analogues are of interest for diagnosis and internal radio therapeutic treatment of a broad spectrum of neuro-endocrine tumours. DiMet-Gly-Ser-Cys-Gly-[Arg-ψ(CH_2-NH)-Arg]-Pro-Tyr-Ile-Leu-OH (RP498s) is a derivative of the biologically active C-terminal part of neurotensin with an $N_2N'S$ type bifunctional chelator linked at its N-terminus. A reduced amide bond of the ψ(CH_2-NH) type was introduced between the amino acids Arg^8 and Arg^9 for biological (enzymatic) stability reasons. RP414 (Fig. 1) was shown to be successful in the formation of ^{99m}Tc(V) or Re(V) oxo complexes based on the reduction of pertechnetate or perrhenate to ^{99m}Tc(V) or Re(V) respectively using stannous gluconate at a pH of 5.5 - 6 [1].

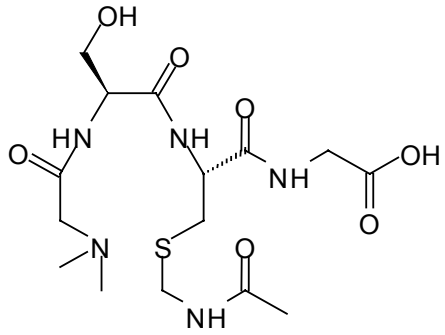

Fig. 1. RP414 a MAG_3-like bifunctional metal chelator

The labelling of RP498s with ^{188}Re was investigated in analogy with the labelling with ^{99m}Tc as earlier described [2]. ^{188}Re labelling follows two different approaches, i.e. ligand exchange reaction by means of ^{188}Re(V) gluconate as described by B. Noll *et al.* [3] and direct labelling using $SnCl_2$, beta-cyclodextrin and sodium tartrate as described by Bolzati *et al.* [4]. Quality control was performed by TLC.

Results

^{188}Re gluconate

^{188}Re gluconate was obtained in about 95 % radiochemical purity by reduction of 30 MBq of ^{188}Re eluate (^{188}W/^{188}Re generator, Oak Ridge National Laboratory) with stannous chloride in 0.5 M sodium gluconate at room temperature.

SP-TLC: Observed R_f values and yields (silica gel on plastic, acetone):

Re-gluconate:	0.1	(95 % for 1h*)
		(60 – 65 % at 4h)
Perrhenate:	0.7	(5 %)

^{188}Re RP498s by ligand exchange reaction

After addition of RP498s to the ^{188}Re gluconate solution and standing at room temperature, the radiolabelled peptide was observed as a double peak with an Rf of 0,1-0,2 (TLC: RP-18 F TLC plates, 5 x 10cm, Merck, Germany; eluent H_2O/MeCN//TFA 70/30//0). ^{188}Re gluconate and perrhenate both have R_f 0.9.

Fig. 1 shows the RP-TLC chromatogram as observed in the labelling of 1.41 mg of RP498s after 15 min reaction time. The position of the cold peptide on the RP-TLC plate was checked at 254 nm confirming an R_f of 0.1 - 0.2. The Re-labelled peptide clearly shows a front-shoulder / double peak that can be assigned to the syn and anti arrangement of the Re-O group in the chelator.

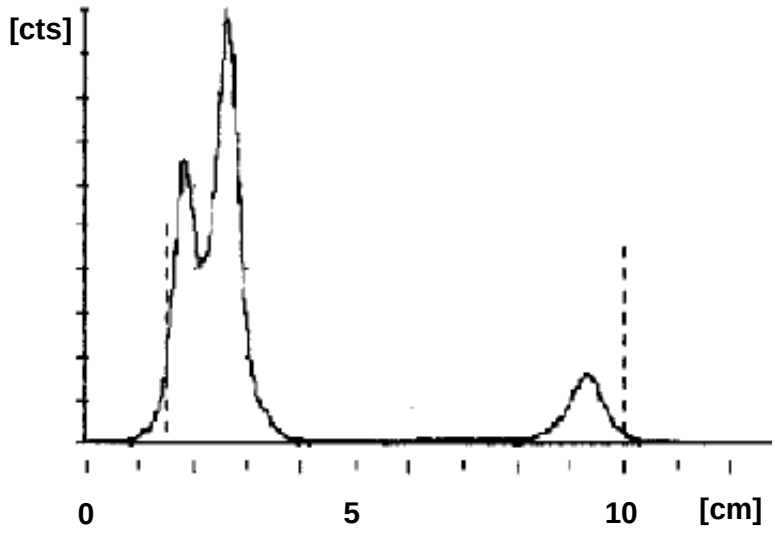

Fig. 2. RP-TLC-chromatogram of the reaction mixture using 1410 µg RP498s for labelling after 15min

The influence of the amount of peptide on the labeling yield is shown in Table 1. For relatively small amounts of peptide (250 µg), labelling yields of up to 85 % within 60 min can be obtained. Longer reaction times or larger amounts of peptide do not significantly increase the radiolabelling yields, ranging between 87 % and 91 %.

Table 1. Labelling of RP498s with ^{188}Re by ligand exchange method: Effect of the substrate amount and reaction time on radiochemical yied (RP-TLC analysis).

RP498s [µg]	^{188}Re- RP498s [%] after 15 min	60 min	150 min
250	77	85	87
810	85	87	90
1410	85	87	91

^{188}Re RP498s by direct labelling

This route follows the procedure put forward by Bolzati *et al.* [4], where the use of γ-cyclodextrin and oxalate makes it possible to label dithiolate ligands at room temperature.

In typical experiments 1.5 mg of RP498s together with 10mg of (2-hydroxypropyl)-β-cyclodextrin (Fluka Chemica, Switzerland) and 20mg / 40 mg of di-natriumtartrate-dihydrate were used for labeling. The pH value of the reaction mixture was 5.5. The reaction was left at room temperature. Samples were taken for RP-TLC after 15 min and 30 min.

Table 2 shows the labelling yields of ^{188}Re-RP498s. A clear effect is seen as regards both the reaction time and the amount of sodium tartrate used. Here, labelling yields of up to 81 % within 15 min were observed.

Table 2. Labelling of RP498s with ^{188}Re by direct labelling: Effect of sodium tartrate amount and reaction time on radiochemical yied (RP-TLC analysis).

Sodium tartrate [mg]	^{188}Re-RP498s [%] after 15 min	30 min
20	64	81
40	81	80

Conclusion

RP498s can be labelled with ^{188}Re by either ligand exchange or direct labelling methods. Both methods seem to be equal in efficiency. Within 15 min at room temperature, yields of up to 80 % and 85 % were observed for the proposed direct labelling method and the ligand exchange method.
The Re-labelled peptide clearly shows a front-shoulder / double peak that can be assigned to syn and anti isomers in the light of our previous experience with Re(V) tetradentate chelator chemistry [5].
Further investigations regarding the stability of the Re(V)-RP498s are in progress .

References

[1] Wong, E.; Fauconnier, T.; Bennett, S. Rhenium(V) and technetium(V) oxo bomplexes of an $N_2N'S$ peptidic chelator: Evidence of interconversion between the syn and anti conformations. Inorg. Chem. 36 (1997) 5799-5608.

[2] Chavatte, K.; Wong, E.; Fauconnier, T. *et al.* Rhenium(Re) and technetium (Tc-99m) oxocomplexes of neurotensin. J. Labelled Compd. Radiopharm. 42 (1999) 415-421.

[3] Noll, B.; Kniess, T.; Spies, H. Synthesis of ^{186}Re gluconate by stannous chloride reduction of $^{186}ReO_4^-$. *Annual Report 1996*, Institute of Bioinorganic and Radiopharmaceutical Chemistry, FZR-165 pp. 106-107.

[4] Bolzati, C.; Boschi, A.; Uccelli, L.; Duatti, A.; Franceschini, R.; Piffanelli, A. An alternative approach to the preparation of Re-188 radiopharmaceuticals from generator produced $^{188}ReO_4^-$: Efficient synthesis of Re-188(V)-meso-2,3-dimercaptosuccinic acid. Nucl. Med. Biol. 273 (2000) 309-314.

[5] Luyt, L.G.; Jenkins, H.A.; Hunter, D.H. An N_2S_2 bifunctional chelator for technetium-99m and rhenium: complexation, conjugation, and epimerization to a single isomer. Bioconjugate Chem. 103 (1999) 470-479.

4. Technetium and Rhenium Complexes with Modified Fatty Acid Ligands

2. Synthesis and Crystal Structure of an "SSS" Oxorhenium(V) Complex Bearing a ω-Mercapto Fatty Acid Ligand

C. M. Jung, P. Leibnitz[1], H.-J. Pietzsch, H. Spies
[1]Bundesanstalt für Materialforschung und -prüfung, Berlin

Introduction

In our attempt to develop fatty acid bearing technetium complexes for myocardial metabolism imaging, we reported the synthesis of a rhenium(V) model compound according to the '3+1' mixed-ligand concept [1]. In the present note we want to describe the preparation and X-ray analysis of an analogous oxorhenium complex chelated by an "SSS" tridentate and a modified ω-mercapto fatty acid. To the best of our knowledge, it is the first example of a crystal structure of a group 7 metal fatty acid complex.

Experimental

The utilized thia-inserted ω-mercapto fatty acid ligand was prepared in four steps by organic standard procedures, starting from commercially available 5-bromo valeric acid. The formation of the corresponding "SSS" complex **1** was achieved by ligand exchange on an appropriate oxorhenium(V) precursor [2].

Results and Discussion

Suitable crystals for X-ray single crystal analysis were obtained by slow evaporation of a saturated chloroform/acetonitrile solution of complex **1** at room temperature. The accompanying X-ray structure of **1** is shown in Fig. 1.

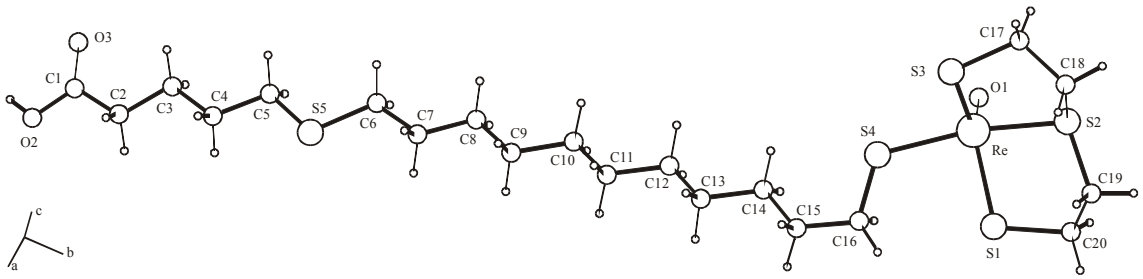

Fig. 1. X-ray structure of the fatty acid "SSS" oxorhenium(V) complex **1**.

As characteristic of "SSS"-coordinated '3+1' mixed-ligand complexes the four sulphur donor atoms are arranged in a square pyramidal geometry around the oxorhenium(V) core. The distorted basal surface of the pyramid exhibits a twisted orientation with respect to the planar arrangement of the fatty acid chain. The bond lengths and angles within the chelate moiety were found to be in the order of magnitude expected for this type of rhenium complexes.

References

[1] Spies, H.; Pietzsch, H.-J.; Kropp, J.; Fietz, T.; Jung, C. Tc-99m labelled fatty acids on the basis of 'n+1' mixed-ligand complexes? *Report January 1998 - June 1999*, Institute of Bioinorganic and Radiopharmaceutical Chemistry, FZR-270, pp. 145 - 147.

[2] Jung, C.M. Diplomarbeit 1999, Philipps-Universität Marburg, Fachbereich Chemie.

5. Technetium and Rhenium Complexes with Modified Fatty Acid Ligands

3. Synthesis of Novel Rhenium Complexes as Model Compounds of Technetium Tracers for Myocardial Metabolism Imaging

C. M. Jung, H.-J. Pietzsch, J. Kropp[1], H. Spies
[1]TU Dresden, Universitätsklinikum Carl Gustav Carus, Klinik und Polyklinik für Nuklearmedizin

Introduction

Naturally occurring long-chain fatty acids serve as the principal energy source of the normoxic myocardium. Radiolabelled fatty acids displaying efficient myocardial uptake and adequate retention are therefore attractive candidates for the clinical evaluation of regional discrepancies in the cardiac metabolism and energy turnover. In our efforts to find technetium-coordinated fatty acids with *in vivo* properties comparable to those of the currently favoured iodine-123-labelled derivatives, we concentrated on small-sized neutral chelating systems according to the 'n+1' design and on metal carbonyl moieties [1]. We prepared various nonradioactive rhenium complexes containing the metal core at the oxidation states +5, +3 or +1 as reference compounds for potential technetium tracers.

Experimental

Suitable ω-functionalized fatty acid ligands required for the 'n+1' mixed-ligand concept were synthesized, starting from the commercially available ω-bromo pentadecanoic acid [2]. Thiol groups were introduced by nucleophilic attack of sodium thiophosphate and subsequent acidic hydrolysis; the ω-isocyano unit was built up in four steps via the ω-azido and the ω-amino derivative by dehydration of the analogous ω-formanido acid.
In order to obtain ligands for the dithioether-carbonyl design, the bromo acid was coupled with 3-thia-1-butanethiol and 5-mercapto-3-thiapentanoic acid under basic conditions. Schiff base ligands attaching to the bromotricarbonylrhenium(I) moiety were obtained by reaction of ω-amino lauric acid salt with picolinaldehyde.

Results and Discussion

15-Mercapto pentadecanoic acid **1** was reacted with the two oxorhenium(V) precursors **2** and **3** to form the "SSS"- and "SNMeS"-coordinated '3+1' mixed ligand complexes **5** and **6** (Fig. 1). Replacement of the halide in precursor **2** by the thiol **1** in refluxing acetonitrile produced the reddish brown "SSS" complex **5** in excellent yields. The alternative '3+1' complex with "SNMeS" chelate was conveniently prepared in a one step synthesis of the protected tridentate **4**, the mercapto fatty acid **1** and the oxorhenium(V) precursor **3** under basic conditions. Subsequent chromatographic purification and crystallization from methanol yielded 64 % of **6** as a green powder.

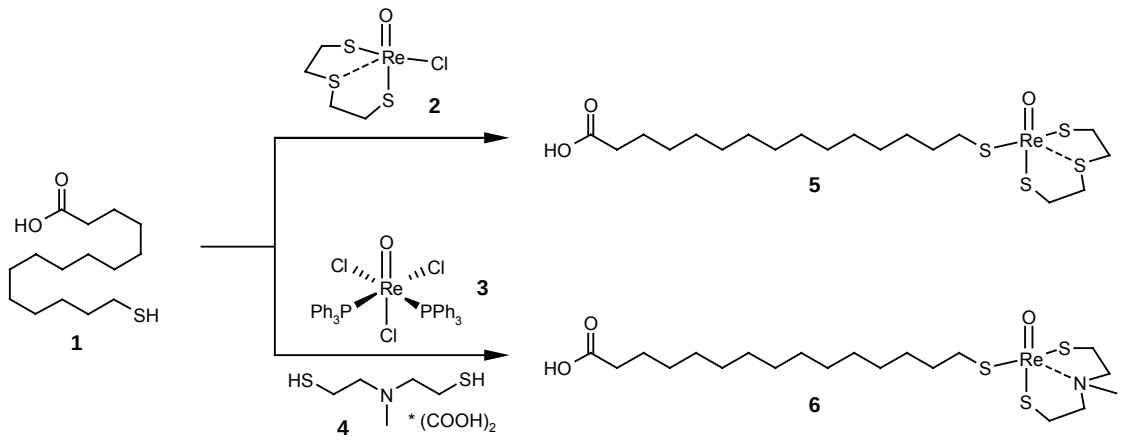

Fig. 1. Syntheses of fatty acid oxorhenium(V) complexes according to the '3+1' concept.

Considering the poor imitation of the lipophilic fatty acid chain by a polar oxometal chelate, the '4+1' version of the 'n+1' concept is expected to be superior to those using technetium and rhenium in the oxidation state +5. The trigonal-bipyramidal complex geometry allows extensive shielding of the metal(III) core. The five coordination sites are occupied by a tetradentate "NS_3" ligand and a monodentate isocyanide. The synthesis of such a '4+1' complex **9** was accomplished in moderate yields by exchange of the phosphane ligand in precursor **8** for the ω-isocyano fatty acid **7** at room temperature (Fig. 2).

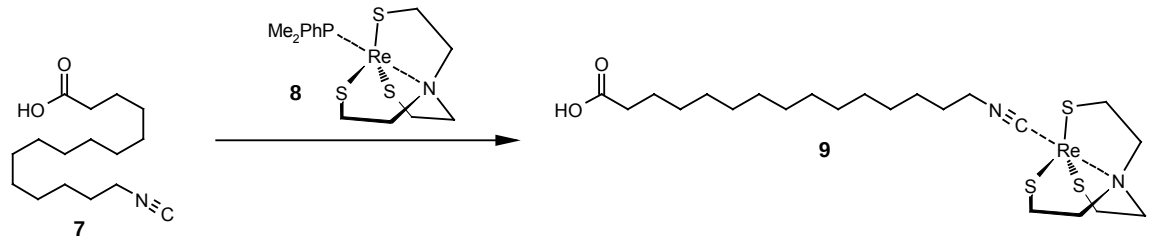

Fig. 2. Synthesis of a rhenium(III) fatty acid complex according to the '4+1' concept.

ALBERTO *et al.* recently introduced the "*fac*-$[M(CO)_3]^+$" fragment as a promising synthon for the labelling of biomolecules [3]. Due to the known tendency of the metal(I) core to interact strongly with soft donor ligands, dithioether units were used to attach fatty acids to the tricarbonylrhenium moiety. The sulphur atoms of the dithialigands **10** and **11** replace two bromine atoms of the precursor **12**. In complex **13** the third bromide substituent remains in the octahedral coordination sphere; in complex **14** however compensation of the electric charge is achieved by coordination of the adjacent carboxylate group (Fig. 3). Compounds **13** and **14** were received as colourless solids in moderate yields.

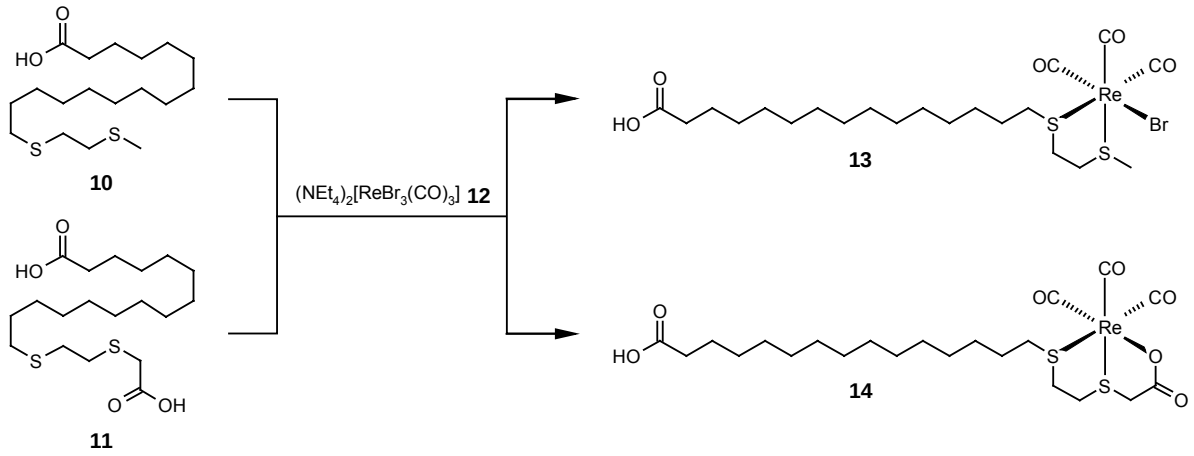

Fig. 3. Syntheses of fatty acid tricarbonylrhenium(I) complexes according to the dithioether design.

Apart from the thioether compounds, bidentate aromatic Schiff base ligands are exceedingly suitable for coordinating tricarbonylmetal(I) moieties [4]. The reaction between the organometallic precursor **12** and the soft nitrogen donor atoms of the fatty acid ligand **15** proceeds in the same way as mentioned above for dithioether units. Complex **16** was obtained in a satisfactory yield as a rich orange solid (Fig. 4).

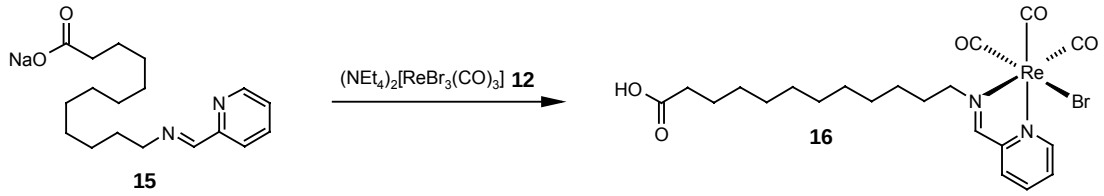

Fig. 4. Synthesis of a fatty acid tricarbonylrhenium(I) complex according to the Schiff base design.

References

[1] Spies, H.; Pietzsch, H.-J.; Kropp, J.; Fietz, T.; Jung, C. Tc-99m Labelled Fatty Acids on the Basis of 'n+1' Mixed-Ligand Complexes? *Report January 1998 - June 1999*, Institute of Bioinorganic and Radiopharmaceutical Chemistry, FZR-270, pp. 145-147.

[2] Jung, C.M. Diplomarbeit 1999, Philipps-Universität Marburg, Fachbereich Chemie.

[3] Alberto, R.; Schibli, R.; Abram, U.; Egli, A.; Knapp, F.F.; Schubiger, P.A. Potential of the "$[M(CO)_3]^+$" (M = Re, Tc) moiety for the labeling of biomolecules. Radiochim. Acta 79 (1997) 99-103.

[4] Alberto, R.; Schibli, R.; Schubiger, P. A.; Abram, U.; Pietzsch, H.-J.; Johnnsen, B. First application of *fac*-$[^{99m}Tc(OH_2)_3(CO)_3]^+$ in bioorganometallic chemistry: Design, structure, and in vitro affinity of a 5-HT_{1A} receptor ligand labeled with ^{99m}Tc. J. Am. Chem. Soc. 121 (1999) 6076-6077.

6. Potentially Redox-Active Rhenium and Technetium Complexes Based on the Pyridinium/Dihydropyridine System

3. Synthesis of Pyridinium/Dihydropyridine Bearing Rhenium(V) '3+1' Mixed-Ligand Complexes with Variable Spacer Lengths and N-Substituents

A. Rother, T. Kniess, H. Spies, H. Jungclas[1]
[1]Universität Marburg, Fachbereich Kernchemie

Introduction

Radiopharmaceutical chemistry is increasingly focused on tracers displaying an accumulation or transport that reflect relevant biochemical processes. One aim in this context is the visualization of the various redox processes occurring in the organism. Bodor *et al.* [1] used the NAD^+/NADH-analogous pyridinium/dihydropyridine system for drug transport across the blood-brain barrier. We wondered whether this principle could be exploited to develop redox-active ^{99m}Tc complexes. For this reason we initially investigated pyridinium/dihydropyridine-bearing rhenium(V) '3+1' mixed-ligand complexes, using rhenium as a surrogate for ^{99m}Tc. A main requirement for the suitability of these complexes is an appropriate lifetime of their dihydropyridine form. Since investigations showed that the dihydropyridine form of complex 1a undergoes rapid reoxidation in buffered aqueous solutions with half-lives between 1 and 5 min [2], dihydropyridine complexes of increased stability had to be synthesized.

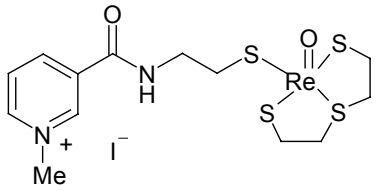

1a

Experimental

According to the literature dihydropyridines may be stabilized by substitution of the methyl group for isopropyl [3] or benzyl [4]. Series of pyridinium bearing rhenium(V) '3+1' mixed-ligand complexes were therefore synthesized. In addition to the alteration of the alkyl group at the pyridine nitrogen atom, the length of the spacer between the pyridinium group and the metal chelate was varied. The syntheses were performed according to the general reaction pathway in scheme 1.
Methyl-nicotinate and an aminoalcohol (chain-lengths of 2, 3 and 5 carbon atoms) were heated at 150 °C to relieve the methanol and to form 3(ω-hydroxyalkyl-carbamoyl)pyridine. Treatment of the hydroxyl group with thionyl chloride led to 3(ω-chloro-alkyl-carbamoyl)pyridine. The introduction of the thiol group was achieved by reacting the chloro group with sodium thiophosphate in a mixture of water and acetone according to a modified literature procedure [5]. Acid hydrolysis of the phosphoric acid thio-ester supplied the free thiol. The pyridine nitrogen atom was alkylated by an excess of either methyl iodide, isopropyl iodide or benzyl bromide. Alkylation of the sulphur was prevented by use of acetone as an aprotic solvent. The thiols produced in this way were reacted with the precursor chloro(3-thiapentane-1,5.dithiolato)oxorhenium(V) according to the '3+1' principle.
The resulting complexes were characterized by ^{1}H NMR, ^{13}C NMR and elemental analysis. Table 1 shows the list of synthesized complexes.

Table 1. List of synthesized pyridinium substituted '3+1' rhenium mixed-ligand complexes

Complex	R	X^-	N
1a	methyl-	I^-	2
1b	methyl-	I^-	3
1c	methyl-	I^-	5
2a	isopropyl-	I^-	2
2b	isopropyl-	I^-	3
2c	isopropyl-	I^-	5
3a	benzyl-	Br^-	2
3b	benzyl-	Br^-	5

Scheme 1. Reaction pathway for the preparation of pyridinium substituted '3+1' rhenium mixed-ligand complexes

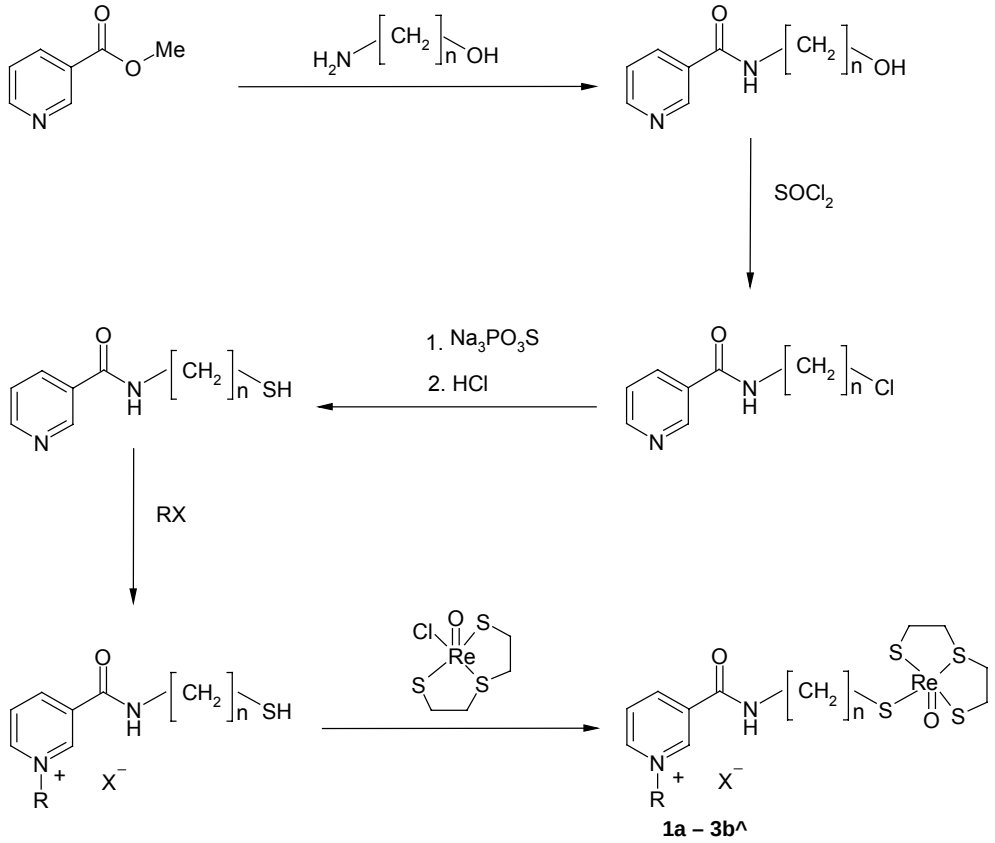

References

[1] Bodor, N.; Farag, H. H. Brain specific, sustained delivery of testosterone, using a redox chemical delivery system. J. Pharm. Sci. 73 (1984) 385-389.

[2] Rother, A.; Kniess, T.; Pütz, M.; Jungclas, H.; Spies, H.; Johannsen B. Nicotinamide-substituted complexes as redox markers – 2. Synthesis of a ^{99}Tc-dihydropyridine mixed-ligand complex and investigation of the stability in tissue homogenates. J. Labelled Compd. Radiopharm. 42 (1999) 673-681.

[3] Brewster, M. E.; Pop, E.; Braunstein, A. J.; Pop, A. C.; Druzgala, P J..; Dinculescu, A.; Anderson, W. R.; Elkoussi, A.; Bodor, N. The effect of dihydronicotinate N-substitution on the brain-targeting efficacy of a zidovudine chemical delivery system. Pharm. Res. 10 (1993) 1356-1361.

[4] Brewster, M. E.; Bartruff, M. S.; Anderson, W. R.; Druzgala, P. J.; Bodor, N.; Pop, E. Effect of molecular manipulation on the estrogenic activity of a brain-targeting estradiol chemical delivery system. J. Med. Chem. 37 (1994) 4237-4244.

[5] Bieniarz, C.; Cornwell, M. J. A facile high yielding method for the conversion of halides to mercaptans. Tetrahedron Lett. 34 (1993) 939-942.

7. Potentially Redox-Active Rhenium and Technetium Complexes Based on the Pyridinium/Dihydropyridine-System

4. Dependence of the Stability of Pyridinium/Dihydropyridine Bearing Rhenium(V) Mixed-Ligand Complexes on Variable Spacer Lengths and N-Substituents

A. Rother, T. Kniess, H. Spies, H. Jungclas[1]
[1]Universität Marburg, Fachbereich Kernchemie

Introduction

With respect to redox-active ^{99m}Tc-labelled radiotracers based on the pyridinium/dihydropyridine system we described the synthesis of series of rhenium(V) complexes of the following type [1, 2].

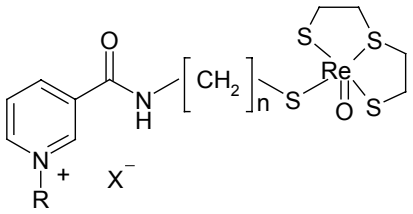

1a - 3b

In this paper the reduction of the pyridinium complexes into their dihydropyridine-form by sodium dithionite and investigations of the stability of these dihydropyridines against reoxidation are Kinetic measurements were performed by UV-vis spectrometry. The following complexes were analysed (Table 1).

Table 1. List of analysed pyridinium substituted '3+1' rhenium mixed-ligand complexes

Complex	R	N
1a	Methyl	2
1c	Methyl	5
2b	Isopropyl	3
3a	Benzyl	2
3b	Benzyl	5

Experimental

The complexes **1a – 3b** were reduced to their dihydropyridine form by an excess of sodium dithionite in alkaline solution. The reaction took place in the biphasic system of diethyl ether/water under reflux while vigorously stirring according to a literature procedure [3] (Fig. 1). In this way the lipophilic dihydropyridine complexes accumulate in the organic phase and can be separated, especially from the dithionite, which would falsify the results of the kinetic measurements. In the ethereal solution the dihydropyridine complexes show a much higher stability than in the aqueous phase and can be used for the further investigations.

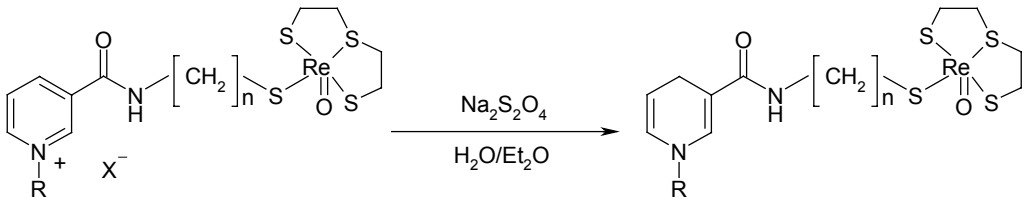

Fig. 1. Reduction of pyridinium substituted '3+1' rhenium mixed-ligand complexes

For kinetic measurements of the reoxidation of the dihydropyridine complexes 100 µL of the ethereal solution were injected into 2.0 mL of phosphate buffer (c = 0.1 mol*L^{-1}) with pH values between 6.7 and 7.6 in a quartz-glass cuvette and the ether was removed from the solution by a stream of argon. Then the reoxidation was followed by UV-vis spectrometry, using a diode array spectrometer with 1,024 diodes at appropriate intervals. The measurements were performed at 20 and 37 °C. The increasing intensity of the bond at 260 nm reflects the re-formation of the pyridinium complex,while the decrease in the bond at 360 nm is characteristic of the decay of the dihydropyridine complex. The appearance of isosbestic points at 245 and 315 nm may serve as proof of a pure two-compound system (Fig. 2a).
By fitting an exponential function to the decrease in intensity at 360 nm the half-lives of the reoxidation of the dihydropyridine complexes were determined (Fig. 2b).

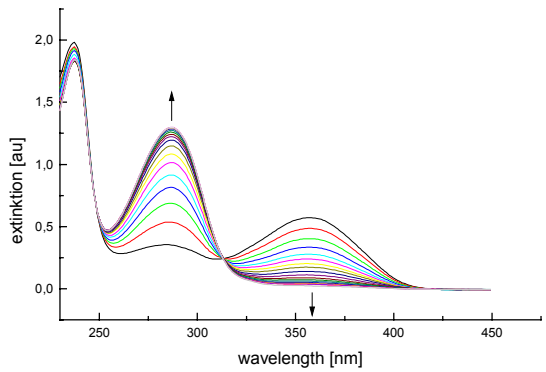

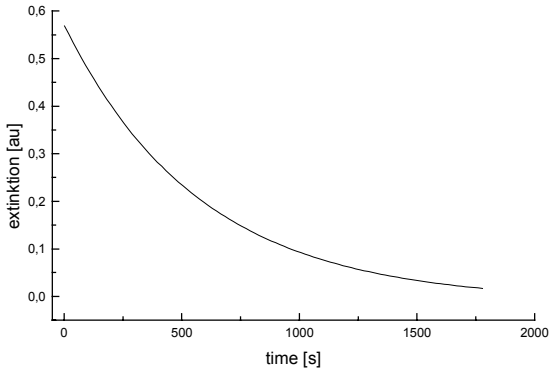

Fig. 2a (left). UV-vis-spectra of complex **1c** at pH = 7.6 and 20 °C about 25 min, the arrows show the course of measurement

Fig. 2b (right). Exponential decrease of the absorption of complex **1c** at 360 nm at pH = 7.6 and 20 °C over time

Results and Discussion

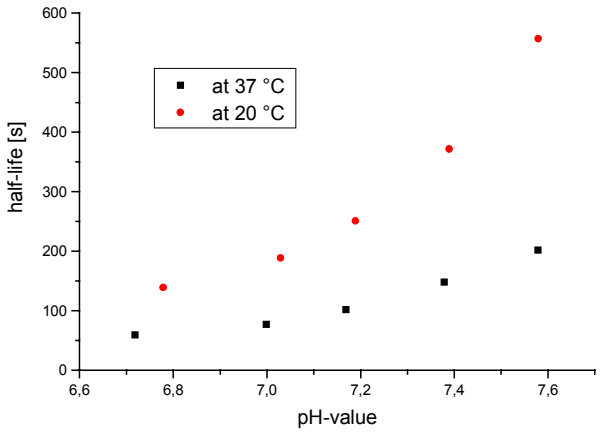

Fig. 3. Half-life of the reoxidation of complex **1c** as a function of the pH-value

Fig. 3 shows the half-lives of the reoxidation of complex **1c** as a function of the pH-value of the buffer. As a result two effects can be observed: the half-life decreases with increasing temperature and higher pH values result in a higher stability of the dihydropyridine complex.

Table 1 shows the highest and lowest half-lives of the analysed complexes.

Table 1. Highest and lowest half-lives of the analysed complexes

Reoxidation to complex	R	N	$t_{1/2(min)}$ / s	$t_{1/2(max)}$ / s
1a	methyl	2	53	394
1c	methyl	5	49	556
2b	isopropyl	3	58	586
5a	benzyl	2	335	1892
5b	benzyl	5	385	2266

It was thus shown that lengthening the spacer between the pyridinium group and the metal chelate does not significantly stabilize the dihydropyridine against reoxidation. Nor does the exchange of the methyl group for isopropyl result in enhanced stability. The replacement of methyl by benzyl however causes an increase in stability by a factor of 4 – 8. Nevertheless, the reoxidation of even the benzyl-substituted complexes still proceeds much too fast for application of the analogous ^{99m}Tc complex as a redox tracer. Complexes bearing a quinolinium/dihydroquinoline functionality are therefore synthesized at present. In addition, we are trying to proceed from the investigated '3+1' complexes to pyridinium complexes according to the '4+1' principle (Fig. 4).

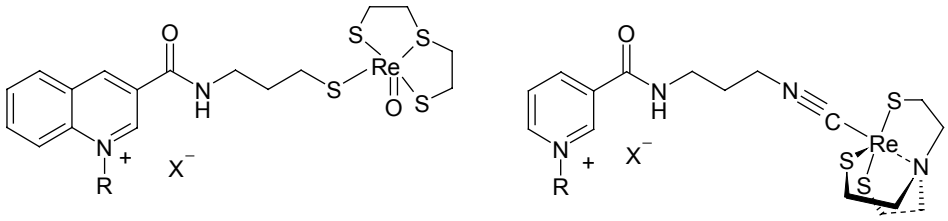

Fig. 4. Quinolinium subs**t**ituted '3+1' rhenium mixed-ligand complexes (**a**), pyridinium substituted '4+1' rhenium mixed-ligand complexes (**b**)

References

[1] Rother, A.; Kniess, T.; Pütz, M.; Jungclas, H.; Spies, H.; Johannsen B. Nicotinamide-substituted complexes as redox markers – 2. Synthesis of a ^{99}Tc-dihydropyridine mixed-ligand complex and investigation of the stability in tissue homogenates.
J. Labelled Compd. Radiopharm. 42 (1999) 673-681.

[2] Rother, A.; Kniess, T.; Spies, H.; Jungclas, H. Potentially redox-active rhenium and technetium complexes based on the pyridinium/dihydropyridine-system - 3. Synthesis of pyridiium/dihydropyridine bearing rhenium(V) '3+1'-mixed-ligand complexes with variable spacer lengths and N-substituents. *This report,* pp.

[3] Wong, Y. S.; Marazano, C.; Gnecco, D.; Das, B. C. 1,4-Dihydropyridines from dithionite reduction of pyridinium salts without electron-withdrawing groups as substituents.
Tetrahedron Lett. 35 (1994) 707-710.

8. Synthesis of a ^{99}Tc Complex with a Cationic Lipid as Initial Stage for Preparation of Tc-Labelled Cationic Lipid/DNA Complexes

T. Kniess, G. Byk[1]
[1]Laboratory of Peptidomimetics and Genetic Chemistry, Bar-Ilan University, Israel

Introduction

The approach of gene therapy in medicine which considers DNA as a therapeutic drug is currently undergoing first clinical trials. New perspectives are being opened up for gene transfer by viral vectors because of their high transfection efficiency. However, the use of viruses as DNA carriers for gene delivery presents major disadvantages: (1) the limited length of the DNA that can be introduced into a single viral particle, (2) the difficulties and cost of production and purification of the particles and (3) the immunological and pathological risks.
Synthetic vectors of the DNA represent a novel alternative to viruses since they display potentially less risks in terms of immunogenicity and propagation and are easier to produce under GMP conditions. In the last decade significant efforts have been invested in developing such non-viral methods for DNA delivery [1]. Some of these lipid/DNA complexes were launched into clinical trials at very early stages of development and produced varying results [2, 3]. The lack of physicochemical characterization of the self-assemblies prevented the interpretation, correlation and comparison of transgene expression with the biodistribution of the DNA complexes.
For a better understanding of biodistribution and final localization of the complexes formed with DNA, we propose to design novel cationic lipids bearing a chelating side chain able to complex with ^{99m}technetium, a probe for scintigraphic investigation. Here we describe the synthesis of a ^{99}Tc complex with a cationic lipid as the first stage of preparation of ^{99m}Tc-labelled cationic lipid/DNA complexes suitable for biodistribution studies on animals.

Experimental

General
The cationic lipid with the side chain able to complex was synthesized at Bar-Ilan University. Its structure was confirmed by mass spectroscopy. The labelling was carried out with $^{99/99m}$Tc gluconate. The reaction was observed by HPLC on an RP-2 column with a gradient of water (0.01 TFA) A and acetonitrile (0,01 TFA) B and a flow rate of 2ml/min. The gradient was as follows: 3 min 80 % A ,20 % B isocratic; 22 min 0 % A, 100 % B; 10 min 0% A, 100 % B isocratic; 5 min 80 % A, 20 % B. The inactive cationic lipid was detected by UV adsorbance at 220 nm, the Tc compounds were detected by γ detection and UV adsorbance.

Labelling procedure
18 mg of sodium gluconate was dissolved in 250 µl 0.01M $K^{99}TcO_4$ solution (2.5 µmol) to which 100 MBq $^{99m}TcO_4^-$ was added. The synthesis of $^{99/99m}$Tc gluconate was carried out by addition of 50 µl 0.01M $SnCl_2$ solution in 0.1M HCl (5µmol). The complete reduction of the pertechnetate was controlled by TLC.
A solution of 9.54 mg (10 µmol) of the cationic lipid in 100 µl sodium methanolate solution was added to this $^{99/99m}$Tc gluconate and the mixture was heated at 80 °C for 20 minutes. After cooling the reaction mixture was investigated by HPLC.

Results and Discussion

The structure of the cationic lipid is visible in Fig. 1. Its Tc chelating moiety was designed after the structure of mercaptoacetyltriglycine (MAG_3), the mercapto functionality is protected by an acetyl group to prevent oxidation during storage. Deprotection occurred by treatment with sodium methanolate before complexation.
Fig. 2a shows the HPLC chromatogram of the cationic lipid after deprotection with sodium methanolate with a retention time of 12.31 min. After reaction with $^{99/99m}$Tc gluconate a new peak at 14.44 min was observed by UV detection (Fig. 2b). Its counterpart was found by γ detection at 14.77 min (Fig. 2c). Unreacted starting material both of free ligand and of Tc gluconate (1.21 min) was detectable despite the molar excess of the former over the latter. The yield of the new Tc complex was found by radiochromatography to be 45 %. By carrying out the reaction without heating a very poor yield of complexation products was obtained.

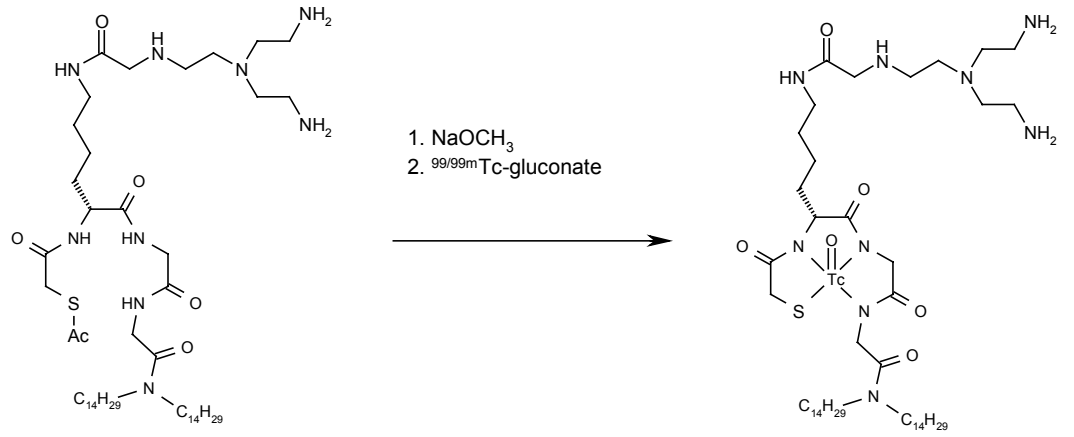

Fig. 1. Labelling of the cationic lipid with $^{99/99m}$Tc gluconate.

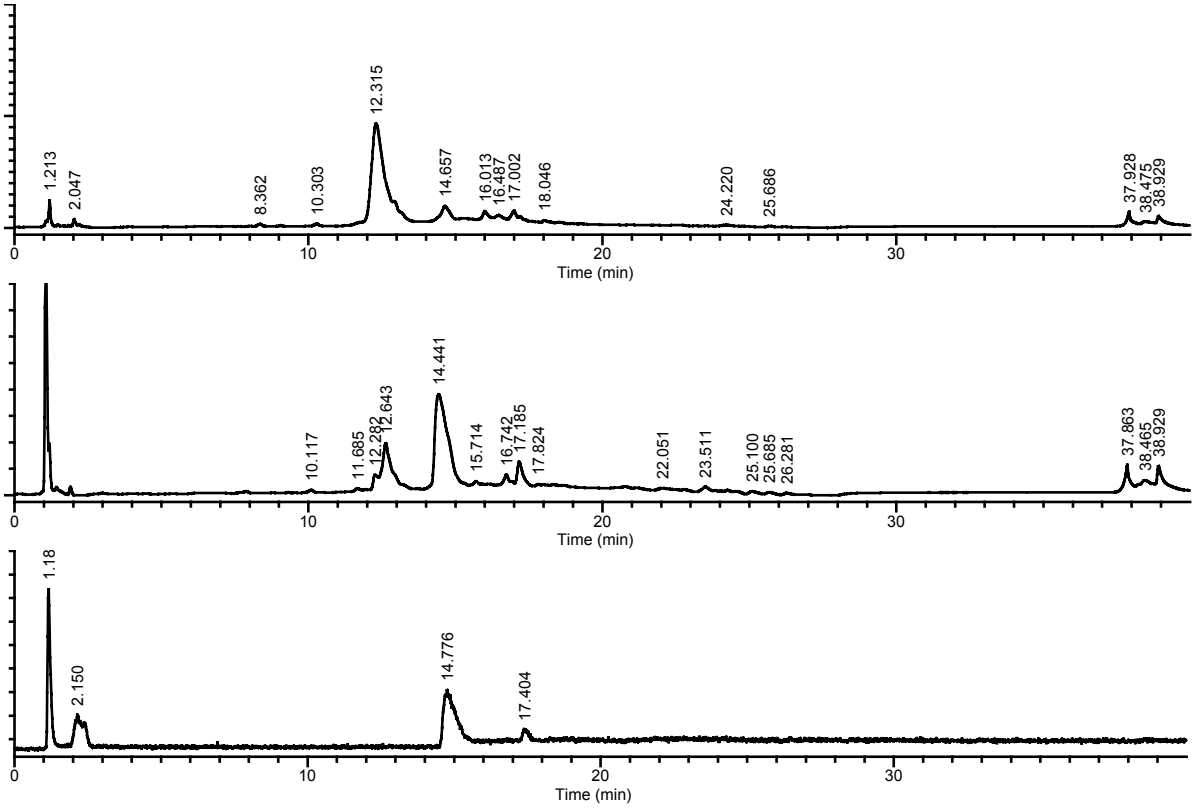

Fig. 2a,b,c. HPLC analyses of the reaction of the cationic lipid with $^{99/99m}$Tc gluconate

To sum up, we can report that we are able to prepare a complex of a cationic lipid with $^{99/99m}$Technetium. This encourages us to take the next steps, which include increasing the yield, isolation of the Tc complex and further complexation with DNA to obtain Tc-labelled cationic lipid/DNA complexes suitable for biodistribution studies.

References

[1] Byk, G.; Scherman, D. Novel cationic lipids for gene delivery and gene therapy. Exp. Opin. Ther. Patents 8 (1998) 1125-1141.

[2] Felgner, J.H.; Kumar, R.; Sridhar, C.N. Enhanced gene delivery and mechanism studies with a novel series of cationic lipid formulations. J. Biol. Chem., 269 (1994), 2550-2561.

[3] Lee, E.R.; Marshall, J.; Siegel, C.S. Detailed analysis of structures and formulations of cationic lipids for efficient gene transfer to lung. Hum. Gene Ther. 7 (1996) 1701-1717.

9. Labelling Dithiol Ligands with the Tc-99m Synthon [^{99m}Tc(N)(PNP4)Cl$_2$]

C. Bolzati[1], A. Duatti[1], A. Boschi[1], L. Uccelli[1], H.-J. Pietzsch, S. Seifert, H. Spies
[1]Laboratory of Nuclear Medicine, Department of Clinical & Experimental Medicine, University Ferrara, Italy.

Bis(phosphinoethyl)amine (PNP) ligands react with labile nitridotechnetium and nitridorhenium precursors to yield the novel complexes [MNCl$_2$(PNP)] (M = Tc, Re) [1]. The halide groups in these complexes can easily be exchanged by various bidentate ligands, such as mercaptoacetic acid, N-acetyl-L-cysteine or S-methyl-2-methyldithiocarbazate [2]. These are the results of the reaction of Tc-99m synthon [^{99m}Tc(N)(PNP4)Cl$_2$] with esters of dimercaptosuccinic acid, which are considered prototypes of dithiolate ligands.

Alternative procedures were employed for preparing neutral Tc-99m unsymmetrical nitrido complexes of the type [^{99m}Tc(N)(PNP4)(DT)], where DT represents a dithiol ligand. These are schematized in Chart 1.

Chart 1. Reaction routes to [^{99m}Tc(N)(PNP4)(DT)]

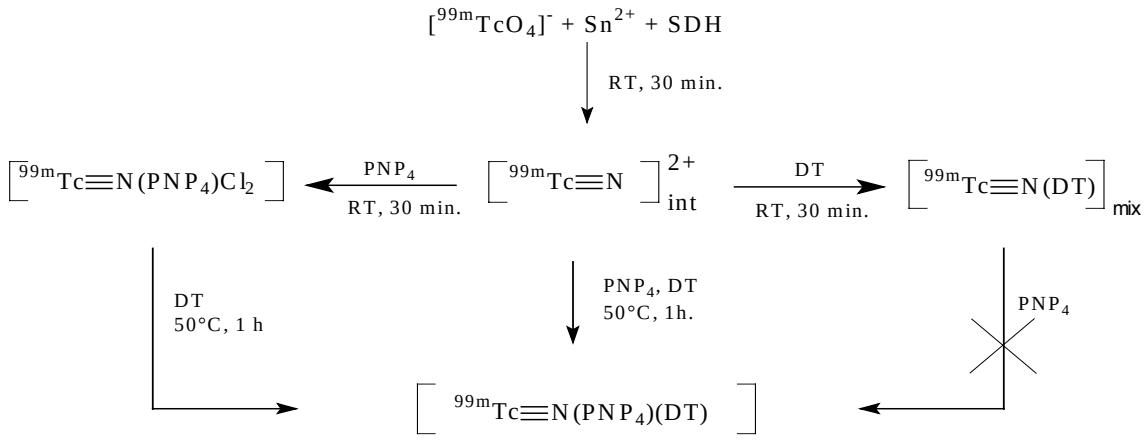

PNP_4= $[(CH_3)_2PC_2H_4]_2NCH_3$

DT= 

	R	R'	
DT1	-H	-COOH	*-meso*
DT2	$-COOC_2H_5$	$-COOC_2H_5$	*-meso*
DT3	$-COOCH_3$	$-COOCH_3$	*-meso*
DT4	$-COOCH_2CH(CH_3)_2$	$-COOCH_2CH(CH_3)_2$	*-meso*

Chromatographic characterization revealed that the chemical nature of the resulting complexes was independent of the method of preparation, i.e. that identical compounds obtained by different chemical procedures exhibited the same chromatographic properties.

The optimal labelling procedure involved two separate steps. The first step was required to generate a mixture of intermediate nitrido Tc-99m complexes, all containing the $[Tc{\equiv}N]^{2+}$ core as a result of the reduction of Tc-99m pertechnetate by tin(II) chloride in the presence of SDH as the donor of nitrido nitrogen atoms. As the second step the diphosphine ligand (PNP4) and the dithiol ligand were added to the reaction vial containing the mixture of Tc-99m nitrido precursors to afford the final products after 1 hour of heating at 50 °C. The complexes were purified by a PR-C18 cartridge, from which the Tc-99m species was eluted by 30% ethanol. The total radiochemical purity (by TLC) was 95 %. Fig. 1 shows a schematic drawing of the structure of the resulting complexes.

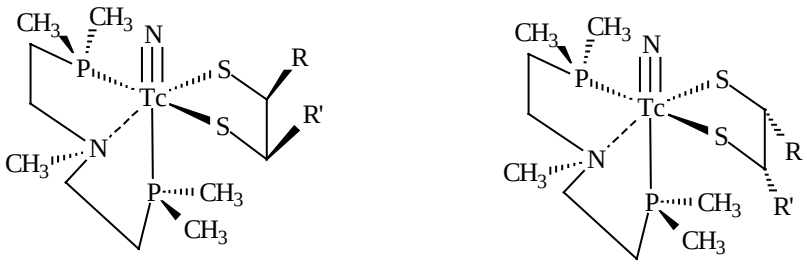

Fig.1. Proposed structure of syn- and anti- [^{99m}Tc(N)(PNP4)(DT)]

The PNP4 ligand is bound to the Tc≡N group by the two phosphorous atoms, while the dithiol ligand is coordinated by the two deprotonated sulfur atoms, thus yielding a final neutral compound.
All complexes were found to exist in two distinct isomeric forms, presumably differing in the relative *syn* or *anti* positions of the functional groups attached to the carbon backbone of the dithiol ligand relative to the Tc≡N multiple bond. The final isomeric ratio was approximately 50:50 in all cases and the two isomers were easily separated by TLC chromatography.

Table 1. R_f values and relative radiochemical yields for all isomeric complexes.

Complex	R_f	Yield [%]
[^{99m}TcN(PNP$_4$)(DT2)] a	0.4	42.3
[^{99m}TcN(PNP$_4$)(DT2)] b	0.3	40.8
[^{99m}TcN(PNP$_4$)(DT3)] a	0.36	45.8
[^{99m}TcN(PNP$_4$)(DT3)] b	0.28	42.3
[^{99m}TcN(PNP$_4$)(DT4)] a	0.3	46.2
[^{99m}TcN(PNP$_4$)(DT4)] b	0.25	42.6

The stability of all asymmetrical Tc-99m complexes towards transchelation by GSH and cysteine was investigated. No significant changes of RCPs were observed after 2 h of incubation, indicating that these compounds were almost inert towards substitution with cysteine and glutathione. On the contrary, the stability in the serum was found to be weak and all complexes were rapidly transformed into more hydrophilic species, which could presumably be identified as the same complexes having lost their lateral ester groups after hydrolysis by serum enzymes, a well-recognized phenomenon occurring *in-vivo* with ester substituents [3].

References

[1] (a) Duatti, A. Advances in the chemistry of technetium and rhenium from ligands and cores to biocomplexes. (a) in: *Technetium and Rhenium in Chemistry and Nuclear Medicine* 5 (M. Nicolini, U. Mazzi Eds.) SGEditoriali, Padova, (1999) pp. 3-17. (b) Bolzati, C.; Boschi, A.; Duatti, A.; Prakash, S.; Refosco, F.; Tisato, F.; Bandoli, G. Geometrically controlled selective formation of nitrido technetium(V) asymmetrical heterocomplexes with bidentate ligands.
J. Am. Chem. Soc. 122 (2000) 4510-4511.

[2] Tisato, F.; Refosco, F.; Cagnolini, A.; Bandoli, G.; Bolzati, C.; Ucceli, L.; Boschi, A., Prakash, S.; Duatti, A. Reliable syntheses os asymmetrical nitrido Tc(V) and Re(V) heterocomplexes. In: *Technetium and Rhenium in Chemistry and Nuclear Medicine* 5 (M. Nicolini, U. Mazzi Eds.) SGEditoriali, Padova, (1999) pp. 133-137.

[3] Seifert, S.; Syhre, R.; Spies, H.; Johannsen, B. Enzymatic hydrolysis of ester groups of mixed-ligand oxorhenium(V) and oxotechnetium(V) complexes. Appl. Radiat. Isot. 48 (1997) 1051- 1057.

10. Synthesis and Characterization of Trigonal-bipyramidal Technetium(III) Complexes with Tridendate/Bidendate NS_2/PS Coordination: A Novel Approach to Robust Tc Mixed-Ligand Chelates as Tools for Conjugating Biologically Active Molecules

H.-J. Pietzsch, P. Leibnitz[1], F. Tisato[2], F. Refosco[2], S. Seifert, H.Spies
[1]Bundesanstalt für Materialforschung- und testung, Berlin
[2]Istituto di Chimica e Tecnologie Inorganiche e dei Materiali Avanzati, Consiglio Nazionale delle Ricerche, Padova, Italy

Introduction

Oxo-free technetium in lower oxidation states, such as +3 and +1, is of increasing interest for coupling lipophilic Tc chelates to biologically active molecules, e.g. CNS receptor targeted agents [1]. After we reported on trigonal-bipyramidal mixed ligand technetium(III) complexes with 2,2',2"-nitrilotris-(ethanethiol) und isocyanides as co-ligands [2], which are neutral and non-polar since they contain sterically well shielded oxo-free Tc(III) ions, in the present paper we describe the basic chemistry of Tc complexes with analogous coordination geometry formed by the combination of a tridendate HS-E-SH ligand (E = $N(CH_3)$, S) with a bidendate PR_2-SH chelator. Syntheses procedures at the no-carrier-added level including challenge experiments with glutathione and biodistribution studies in rats will be described in [3].

Results and Discussion

As shown in Scheme 1 the complexes can be prepared in a two-step substitution/reduction procedure via a chlorine-containing oxotechnetium(V) complex (A). The alternative methode (B) is a one-step ligand exchange reaction of the labile tetrachloro oxotechnetate(V) with mixtures of the ligands and simultaneous reduction of the metal centre. Both reactions are characterized by a typical change in colour from orange to deep-violet indicating the transfer from Tc(V) to Tc(III).

Scheme 1. Reaction routes to Tc(III) complexes with "3+2" coordination (E = $N(CH_3)$, S)

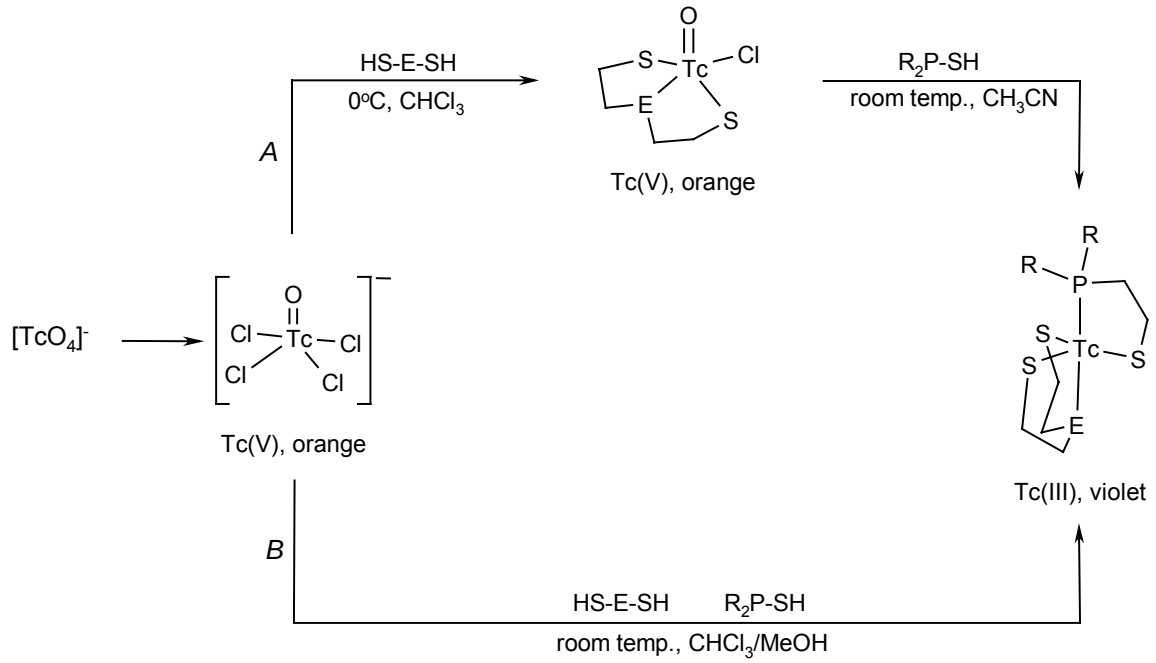

The complexes are characterized by elemental analyses as well as by NMR-, IR- and UV/Vis spectroscopy. X-ray structure analyses of two representatives confirm the expected trigonal-bipyramidal coordination geometry of this type of complexes (Figs. 1 and 2).

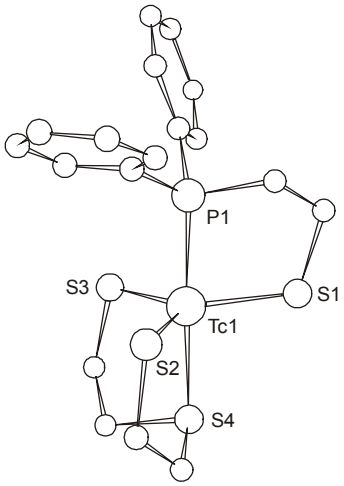

Fig. 1. Molecular structure of [Tc(SSS)(PS)]

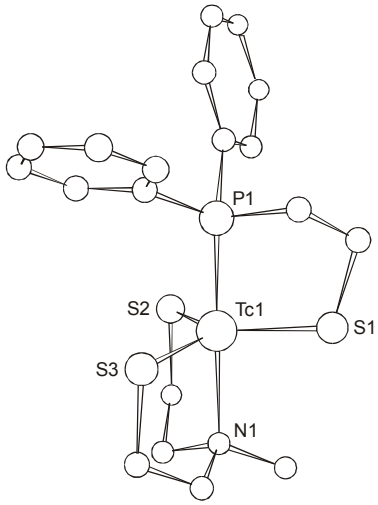

Fig. 2. Molecular structure of [Tc($SNCH_3S$)(PS)]

Conclusion

The common reaction of a tridendate HS-E-SH ligand (E = $N(CH_3)$, S) with a bidendate PR_2-SH chelator leads to the formation of non-polar, lipophilic technetium complexes which contain sterically shielded oxo-free Tc(III) ions. This combination enables easy functionalization in order to fine-tune physico-chemical properties of the complexes and to link the chelate unit to biomolecules. ^{99m}Tc complexes can easily be prepared at no-carrier-added level in high radiochemical yields. The complexes are stable towards re-oxidation and ligand exchange in challenge experiments with glutathione. This will be discussed in detail in [3].

References

[1] Pietzsch, H.-J.; Scheunemann, M.; Kretzschmar, M.; Elz, S.; Pertz, H. H.; Seifert, S.; Brust, P.; Spies, H.; Syhre, R.; Johannsen, B. Synthesis and autoradiographical evaluation of a novel high-affinity Tc-99m ligand for the 5-HT_{2A} receptor. Nucl. Med. Biol. 26 (1999) 865-875.

[2] Pietzsch, H.J., Gupta, A., Syhre, R., Spies, H. Synthesis and characterization of trigonal-bipyramidal technetium(III) complexes with tetradendate/monodendate NS_3/isocyanide coordination: Potencies of the “4+1“ Tc chelate system for the design of neutral, non-polar and lipophilic complexes stable *in vivo. Report July - December 1999,* Institute of Bioinorganic and Radiopharmaceutical Chemistry, FZR-283, pp. 84-88.

[3] Seifert, S.; Pietzsch, H.-J.; Syhre, R.; Tisato, F.; Spies, H. . Preparation and characterization of ^{99m}Technetium(III) complexes with tridentate and bidentate ligands (‘3+2‘ complexes). *This Report*, pp. 27-31.

11. Preparation and Characterization of ^{99m}Technetium(III) Complexes with Tridentate and Bidentate Ligands ('3+2' Complexes)

S. Seifert, H.-J. Pietzsch, R. Syhre, F. Tisato[1], H. Spies
[1]Istituto di Chimica e Tecnologie Inorganiche e dei Materiali Avanzati, Consiglio Nazionale delle Ricerche, Padova, Italy

Introduction

The search for neutral and stable mixed-ligand complexes of technetium at other oxidation states than +V led to the development of Tc complexes with '4+1' and '3+1+1' coordination. The trigonal-bipyramidal '4+1' Re and Tc complexes containing 2,2',2"-nitrilotris(ethanethiol) and isocyanides as co-ligands [1, 2, 3] are stable *in vitro* and *in vivo* while '3+1+1' complexes which contain a monothiol and a phosphine molecule besides the tridentate dithiol ligand, however, are unstable to oxidation as well as to ligand exchange [4, 5]. One approach to overcoming the stability problem of this type of complexes might be complexation of a bidentate ligand which contains the donor atoms P and S besides the tridentate ligand. In fact, the preparation of such '3+2' mixed-ligand Tc(III) complexes was successfully performed, while it was not possible to form the corresponding rhenium complexes [6].
The aim of this work was to prepare the technetium complexes at the n.c.a. level, to study their reactivities in various media and to check the biodistribution of a number of model complexes.

Experimental

No carrier added preparations of 3+2 technetium(III) complexes were studied with the tridentate ligands 3-thiapentane-1,5-dithiol (HS-$(CH_2)_2$-S-$(CH_2)_2$-SH), 3-methylazapentane-1,5-dithiol (HS-$(CH_2)_2$-N(CH_3)-$(CH_2)_2$-SH) and 3-oxapentane-1,5-dithiol (HS-$(CH_2)_2$-O-$(CH_2)_2$-SH) and the following bidentate ligands P-S1 – P-S5 shown in Table 1.

Table 1. Ligands used for preparation of 3+2 ^{99m}Tc complexes.

3+2 Complex	Bidentate ligand	
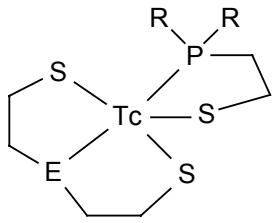 E = S, NMe, O R = alkyl, aryl	P-S1	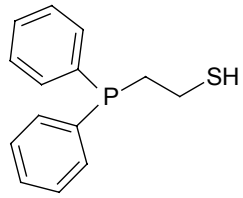
	P-S2	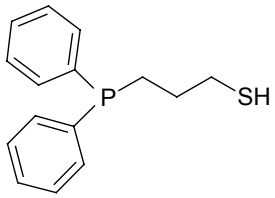
	P-S3	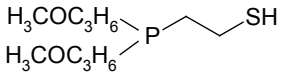
	P-S4	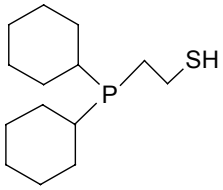
	P-S5	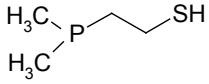

The preparation of the ^{99m}Tc complexes was achieved by reducing the pertechnetate by stannous chloride in the presence of both ligands. A mixture of ethanol, propylene glycol and acetonitrile was used. Short warming to 50 °C produces 60 – 90 % of the required labelled product. The preparations were purified by HPLC for stability and biodistribution studies using a semi-preparative Hypersil column (250 x 8 mm, 10 µm). The radiochemical purity and the stability of the preparations were determined by TLC and HPLC.
For stability studies the complex solution was diluted with 0.1 M phosphate buffer solution of pH 7.4 (Sörensen) to adjust the desired radioactive concentration to 20 – 30 MBq/ml. The equivalent volume of buffer, buffer with 2.0 mM GSH for challenge experiments, and plasma of rats was added to 0.5 ml of that solution and incubated at 37 °C.
Plasma analyses were performed with a Supelguard column (20 x 4.6 mm, 10 µm, flow rate 1.0 ml/min) using a linear gradient 95 % A to 40 % A in 15 min [A: isopropanol/0.1 % trifluoroacetic acid (TFA) (10/90), B: isopropanol/0.1 % TFA (90/10)].
Octanol/buffer partition coefficients of the ^{99m}Tc complexes were determined by the shake flask method.
Biodistribution studies in male Wistar rats (5 - 6 weeks old) were carried out in accordance with the relevant national regulations. 500 µl of ^{99m}Tc complex solution (500 kBq; saline, 15 % propylene glycol) were injected into the tail vein. 5 to 120 min p.i. the rats were sacrificed by heart puncture under ether anaesthesia. The selected organs were isolated for weighing and counting.

Results and Discussion

'3+2' mixed-ligand ^{99m}Tc(III) complexes of the general formula [Tc(SES/P-S)] (E = O, S, NMe) were prepared in a one-step procedure in neutral solutions, using optimized quantities of the bidentate as well as the tridentate ligands. While 0.05 mg of the P-S ligands is enough for preparation of the SNMeS and SOS complexes, the formation of SSS complexes requires 1.0 mg of P-S ligand. The optimum amount of tridentate ligands used for preparations was determined to be 0.05 mg as it was for preparations of the '3+1' Tc complexes [7].
A comparison of the chromatographic data of fully characterized ^{99}Tc reference complexes described in the article above confirms the identity with the ^{99m}Tc preparations.
Stability studies
'3+2' ^{99m}Tc complex solutions purified by HPLC are stable for hours. After dilution with saline or phosphate buffer solution they decompose slightly. Especially the SOS complexes are slowly transformed into more hydrophilic compounds. The reason for that slight instability is still unknown. Oxidation processes in these solutions cannot be excluded with certainty.
A very important result from the point of view of radiotracer design is the fact that no ligand-exchange reaction occurs when the complexes have been incubated with glutathione (GSH) solution. This is demonstrated in Fig. 1.

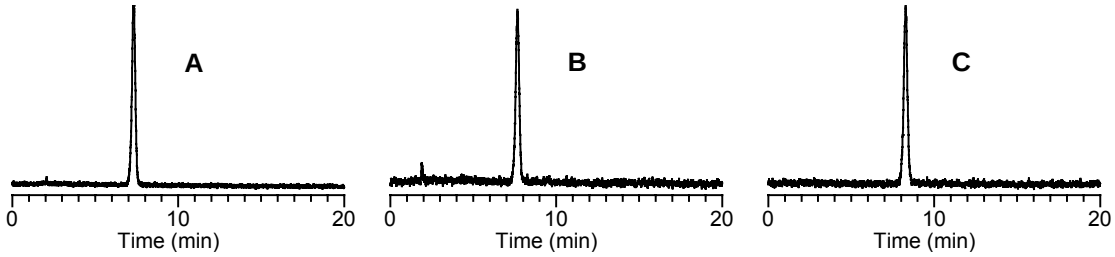

Fig. 1. ^{99m}Tc(SSS/P-S4) after 60 min incubation at 37 °C. A: complex solution after HPLC purification, B: in phosphate buffer pH 7.4, C: in 1 mM GSH solution.

When the complex solution is diluted with saline or phosphate buffer about 1:200, as is normally done for determination of the partition coefficient octanol/water, the radiochemical purity of the diluted sample decreases. After one hour this decrease is about 80 % for the complex [Tc(SNMeS/P-S5)]. Due to the formation of hydrophilic impurities the calculated partition coefficients are too low. For that reason we only diluted the original complex solution 1:1 with phosphate buffer solution of pH 7.4, immediately added octanol, shaked the solution for 5 minutes, separated the phases and measured the partition the following day in a Bohrloch scintillation counter (Table 2). In some cases the real log P values are perhaps slightly higher than the calculated ones, despite of beginning of decomposition.

These slight stability differences of the complexes are reflected by their incubation behaviour in rat plasma. While there is no indication of the SSS and SNMeS complexes binding to rat plasma, the SOS complexes are bound more or less to plasma proteins, especially to albumin (Fig. 2). It is not clear whether the complex themselves or their decomposition products are bound to albumin. It is likely but remains to be proved that the '3+2' Tc(III) complex with E = O is oxidized to Tc(V) oxo species which reacts with plasma proteins in the known way [8].

Table 2. Log $P_{o/w}$ values and reaction against rat plasma of various 3+2 ^{99m}Tc complexes.

Complex	Log $P_{o/w}$	Plasma binding
[Tc(SSS/P-S1)]	3.1	-
[Tc(SSS/P-S2)]	2.2	-
[Tc(SSS/P-S3)]	1.6	-
[Tc(SSS/P-S4)]	1.5	-
[Tc(SSS/P-S5)]	1.3	-
[Tc(SNMeS/P-S1)]	1.5	-
[Tc(SNMeS/P-S2)]	1.8	-
[Tc(SNMeS/P-S3)]	1.6	-
[Tc(SNMeS/P-S4)]	1.2	-
[Tc(SNMeS/P-S5)]	1.0	n. d.
[Tc(SOS/P-S1)]	1.5	+
[Tc(SOS/P-S2)]	1.2	+
[Tc(SOS/P-S4)]	1.6	+

n.d. = not determined because of decomposition of P-S5 ligand

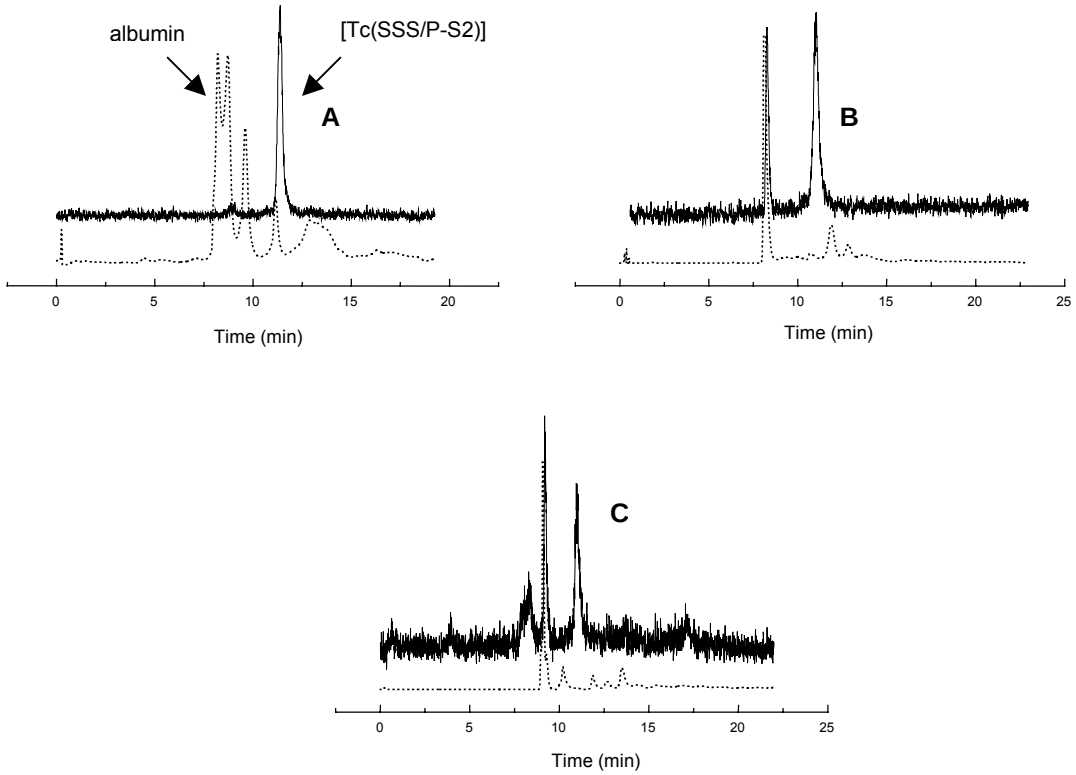

Fig. 2. Plasma binding of [Tc(SSS/P-S2)] and [Tc(SOS/P-S1)]. A: [Tc(SSS/P-S2)] after 5 min incubation at 37 °C; B: after 150 min; C: [Tc(SOS/P-S1)] after 5 min; dotted line: UV detection (220 nm), solid line: γ detection.

Most of the complexes are stable enough for their biological behaviour to be studied in animals.

Biodistribution studies

Biodistribution studies indicate that the ligand significantly influences the distribution pattern. Appreciable differences were observed, in particular in the brain, blood, lungs and liver of rats. All complexes listed in Table 2 are able to penetrate the blood-brain barrier of rats and show a relatively fast washout from the brain. The brain uptake is moderate for complexes with alkyl sustituents (P-S3 – P-S5) compared with complexes containing the phenyl substituted bidentate ligands P-S1 and P-S2. Differences in lipophilicity are assumed to govern the biodistribution patterns. However, no correlation was found between the brain uptake and the lipophilicity of complexes and, in general, no significant influence of tridentate ligands on the brain uptake was observed.

Table 3. Biodistribution of "3+2" ^{99m}Tc complexes in the blood pool (% injected dose /gram) and in selected organs (% injected dose) of Wistar rats (mean ± SD; n=5)

.	min p.i	Blood	Brain	Heart	Lungs	Kidneys	Liver
				P-S1			
SSS	5	0.3 ± 0.1	0.6 ± 0.04	0.5 ± 0.1	1.3 ± 0.5	1.8 ± 0.2	43.0 ± 1.2
	120	0.1 ± 0.01	<0.05	0.1 ± 0.01	0.4 ± 0.1	0.9 ± 0.2	21.2 ± 0.8
SNMeS	5	0.6 ± 0.1	1.0 ± 0.1	0.9 ± 0.2	2.7 ± 0.2	3.5 ± 0.3	37.2 ± 2.3
	120	0.1 ± 0.01	<0.05	0.1 ± 0.02	0.8 ± 0.1	0.7 ± 0.3	30.8 ± 1.7
SOS	5	1.5 ± 0.1	0.6 ± 0.1	0.6 ± 0.1	3.1 ± 0.1	2.1 ± 0.5	53.5 ± 0.7
	120	0.8 ± 0.2	<0.1	0.2 ± 0.1	3.4 ± 0.7	2.5 ± 0.2	47.8 ± 3.7
				P-S2			
SSS	5	0.4 ± 0.1	0.9 ± 0.2	0.7 ± 0.1	2.2 ± 0.5	3.1 ± 0.4	79.8 ± 6.4
	120	0.1 ± 0.01	<0.05	0.1 ± 0.01	1.1 ± 0.2	1.4 ± 0.3	56.7 ± 4.7
SNMeS	5	0.4 ± 0.04	0.5 ± 0.1	0.8 ± 0.1	1.5 ± 0.2	2.4 ± 0.2	41.3 ± 3.0
	120	0.2 ± 0.03	<0.1	0.1 ± 0.02	1.1 ± 0.2	2.2 ± 0.2	47.5 ± 0.9
SOS	5	0.9 ± 0.1	0.6 ± 0.01	0.6 ± 0.1	4.5 ± 0.4	2.0 ± 0.2	85.4 ± 3.4
	120	0.5 ± 0.1	<0.1	0.2 ± 0.03	5.7 ± 0.7	2.0 ± 0.2	79.3 ± 4.3
				P-S4			
SSS	5	0.6 ± 0.1	0.1 ± 0.01	0.9 ± 0.1	2.4 ± 0.4	2.1 ± 0.2	78.5 ± 5.1
	120	0.2 ± 0.01	<0.1	0.1 ± 0.01	0.7 ± 0.1	1.4 ± 0.2	33.3 ±1.2
SNMeS	5	1.8 ± 0.2	0.1 ± 0.02	0.6 ± 0.1	2.4 ± 0.4	2.2 ± 0.2	67.3 ± 2.1
	120	0.3 ± 0.02	<0.05	0.1 ± 0.02	0.6 ± 0.1	2.5 ± 0.1	35.6 ± 2.7
SOS	5	3.8 ± 0.6	0.3 ± 0.04	0.9 ± 0.1	3.8 ± 0.6	6.1 ± 0.3	44.7 ± 2.3
	120	2.3 ± 0.3	0.2 ± 0.1	0.4 ± 0.1	2.2 ± 0.4	9.9 ± 0.3	31.9 ± 1.1

Interestingly, complexes with the SOS chelate unit show a higher initial blood pool activity as well as a much slower blood clearance than the "SSS" or "SNMeS" complexes, an effect that is ascribed, in part, to the observed reactivity towards plasma proteins (Table 2). Furthermore, this chelate unit leads to a persistent high lung uptake. Similar distribution patterns were found for '3+1' complexes containing proteins as monodentate ligands [8].

The high liver uptake (40 - 85 % of the injected dose) does not directly correlate with the lipophilicity of these model complexes.

References

[1] Spies, H.; Glaser, M.; Pietzsch, H.-J.; Hahn, F. E., Kintzel, O.; Lügger, T. Trigonal-bipyramidale Technetium- und Rhenium-Komplexe mit vierzähnigen tripodalen NS_3 Liganden. Angew.Chem. 106 (1994) 1416-1419.

[2] Spies, H.; Glaser, M.; Pietzsch, H.-J.; Hahn, F. E., Kintzel, O.; Lügger, T. Synthesis and reactions of trigonal bipyramidal rhenium and technetium complexes with a tripodal NS_3 ligand. Inorg. Chim. Acta 240 (1995) 465-478.

[3] Pietzsch, H.-J.; Gupta, A.; Syhre, R.; Spies, H. Synthesis and characterization of trigonal-bipyramidal technetium(III) complexes with tetradendate/monodendate NS_3/isocyanide coordination: Potencies of the “4+1“ Tc chelate system for the design of neutral, non-polar and lipophilic complexes stable *in vivo. Report July – December 1999*, Institute of Bioinorganic and Radiopharmaceutical Chemistry, FZR-283, pp. 84-88.

[4] Pietzsch, H.-J.; Tisato, F.; Refosco, F.; Leibnitz, P.; Drews, A.; Seifert, S.; Spies, H. Synthesis and characterization of novel trigonal-bipyramidal technetium(III) mixed-ligand complexes with SES/S/P coordination (E = O, $N(CH_3)$, S). Inorg. Chem. 40 (2001) 59-64.

[5] Seifert, S.; Drews, A.; Gupta, A.; Pietzsch, H.-J.; Spies, H.; Johannsen, B. Stability Studies on ^{99m}Technetium(III) Complexes with Tridentate/Monodentate Thiol Ligands and Phosphine ("3+1+1" Complexes). Appl. Radiat. Isot. 53 (2000) 431-438.

[6] Nock, B.; Pietzsch, H.-J.; Tisato, F.; Maina, T.; Leibnitz, P.; Spies, H.; Chiotellis, E. Oxorhenium mixed-ligand complexes with the 2,6-dimercaptomethylpyridine ligand. Crystal structure of [2,6-dimercaptomethylpyridinato][p-methoxybenzenethiolato]oxorhenium(V). Inorg. Chim. Acta 304 (2000) 26-32.

[7] Seifert, S.; Pietzsch, H.-J.; Scheunemann, M.; Spies, H.; Syhre, R.; Johannsen, B. No carrier added preparations of '3+1' mixed-ligand ^{99m}Tc complexes. Appl. Radiat. Isot. 49 (1998) 5-11.

[8] Seifert, S.; Gupta, A.; Syhre, R.; Spies, H.; Johannsen, B. Ligand-exchange reaction of labile "3+1" ^{99m}Tc(V) complexes with SH group-containing proteins. Appl. Radiat. Isot. 54 (2001) 637-644.

12. Preparation and Characterization of New '3+1' Tc(V) Oxocomplexes Containing a Tridentate PNS or PNO Ligand and a Monothiol Ligand

S. Seifert, C. M. Fernandes[1], R. Syhre, I. Santos[1], H. Spies
[1]Inorganic and Radiopharmaceutical Chemistry Group, Chemistry Department, ITN, Sacavém, Portugal

Introduction

The stability of the so-called 3+1 approach for the synthesis of mixed-ligands Tc complexes, used in Tc tracer design, is strongly dependent on the nature of the tridentate as well as the monodentate ligand [1, 2].
The (tri)bidentate PNS(O) ligands (Scheme 1), developed and introduced by one of us, (I. Santos). present different coordination modes, depending on the reaction conditions [3].

Scheme 1

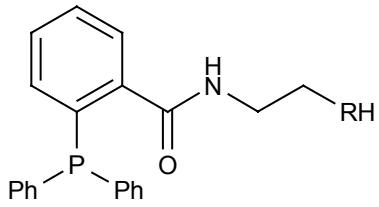

R = O (PNO), R = S (PNS)

With Re(V) different complexes have been synthesized and fully characterized [4]. Some of them are of the "3+1" mixed-ligand type [5]. Although the rhenium chemistry have investigated today, the Tc chemistry at the carrier added and non carrier added level is still lacking.
We report our studies to 3+1 oxotechnetium(V) complexes at the n.c.a. level, using the PNS and also the PNO tridentate ligands and different monodentate sulphur co-ligands, done within a short term scientific mission of C.M. Fernandes in Rossendorf.

Results and Discussion

3+1 ^{99m}TcO(PNS/RS) complexes
We studied complexation reactions at the n.c.a. level with the tridentate ligand PNS and with different monodentate sulphur donors (thiophenol, benzylmercaptan, cyclohexanthiol, mercaptopropionic acid, mercaptoacetyldiglycine and glutathione). The procedure is in accordance with the preparation of common 3+1 complexes described in [6].
The complex formation was optimized for the thiophenol ligand and yields of more than 90 % were reached using the following preparation conditions:

500 µl pertechnetate eluate, 50 µl propylene glycol, 1300 µl EtOH,
0.5 mg thiophenol and 0.05 mg PNS ligand.

Only 1 - 3 % of reduced hydrolyzed technetium were found by TLC. Similar results were obtained with lower quantities of ligands, when they were diminished in the same ratio. With only 0.01 mg thiophenol and 0.001 mg PNS ligand yields of > 90 % are possible.
The following stability and biodistribution studies were performed with this model complex only.
Stability studies
^{99m}TcO(PNS/PhS) was stable in saline and 0.01 M PBS pH 7.4 at 37 ºC during at least 2 hours (1:1 dilutions). It was not attacked by glutathione in 10 mM solutions at 37 ºC for 120 min.. The expected "3+1" mixed oxotechnetium(V) complex with glutathione and PNS (^{99m}TcO(PNS/GS) was prepared at a reference, but no impurity that would correspond to (^{99m}TcO(PNS/GS) was observed.
Biodistribution studies
The animal experiments were carried out according to the relevant national regulations. Organ distribution studies were performed on male Wistar rats (5 - 6 weeks old). 500 µl complex solution (500 KBq ^{99m}Tc) was injected into the tail vein. 5 min. and 120 min p.i. the rats were sacrificed by heart puncture under ether anaesthesia. The selected organs were isolated for weighing and counting. The results are presented in Table 1.

Table 1. Biodistribution of ^{99m}TcO(PNS/PhS) complex in rats (n = 5)

Organ	% injected dose ± s.d. 5 min. p.i.	120 min. p.i.
Brain	0.14 ± 0.03	0.11 ± 0.02
Spleen	0.95 ± 0.25	0.35 ± 0.11
Kidneys	4.16 ± 0.22	7.52 ± 0.41
Heart	0.93 ± 0.08	0.46 ± 0.03
Lungs	1.88 ± 0.16	0.80 ± 0.11
Liver	51.30 ± 1.40	26.60 ± 1.60

Preparation of $^{99/99m}$TcO(PNS/PhS)

The preparation of $^{99/99m}$TcO(PNS/PhS) was tried using $^{99/99m}$Tc(V) gluconate, $^{99/99m}TcO_4^-$ and $Bu_4N[^{99}TcOCl_4]$ as starting compounds. While aqueous solutions of Tc gluconate are not suitable for preparation of the desired complex because of insolubility of ligands in water, the complex could be prepared with $Bu_4N[^{99}TcOCl_4]$ but in a low yield (20 %).

We were able to prepare the complex $^{99/99m}$TcO(PNS/PhS) in good yields using nearly the same reaction conditions as for the n.c.a. preparation when 10^{-8} or 10^{-7} mole of ^{99}Tc are added in the form of sodium pertechnetate to the pertechnetate eluate.

After separation by HPLC the technetium complex was applied to mass spectrometric analyses (Fig. 2) The peak at m/z = 588 (M+1) corresponds to TcO(PNS/PhS).

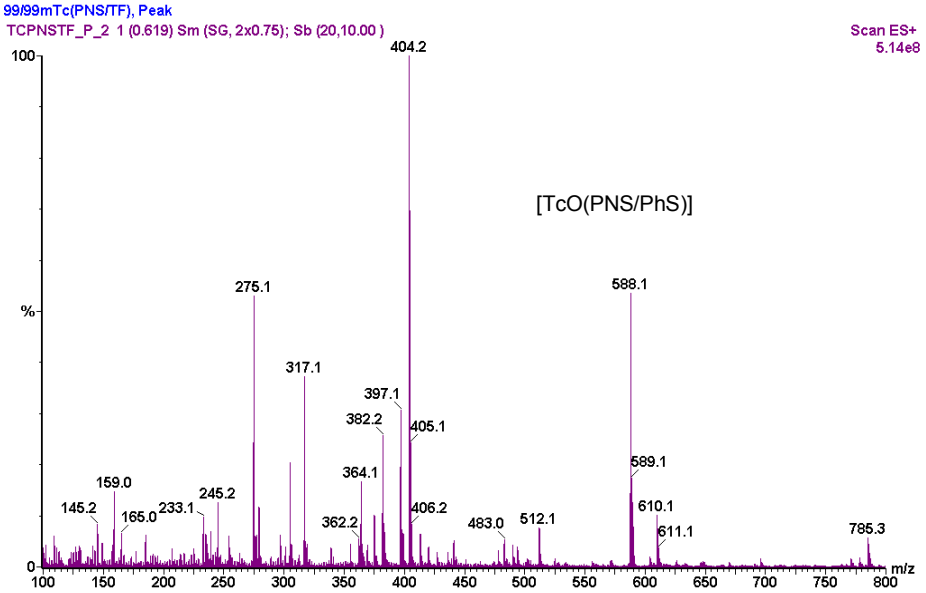

Fig. 2. ES$^+$ MS of [$^{99/99m}$TcO(PNS/PhS)]; m/z (found) 588 (M+1), m/z (calc.) 587 for [TcO(PNS/PhS)] ($C_{27}H_{23}NO_2PS_2Tc$)

3+1 ^{99m}TcO(PNO/RS) complexes

For the complexation reactions at the n.c.a. level with the tridentate ligand PNO and with thiophenol as monodentate ligand. the general labelling procedure as above is applicable, except the pH. With the PNO ligand alkaline conditions are required to form the 3+1 mixed-ligand complex (addition of 200 µl 0.1 N NaOH). With these labelling conditions ^{99m}TcO(PNO/PhS) was obtained in high yields (> 90 %). The complex was separated by HPLC and presents a good radiochemical purity after concentration. The complex stability is less than that for the ^{99m}TcO(PNS/PhS) complex when diluted with saline or GSH solution (Fig. 3). As it was observed for the ^{99m}TcO(PNS/PhS) complex, there is no exchange of the monodentate ligand by glutathione but the complex decomposes to more hydrophilic species.

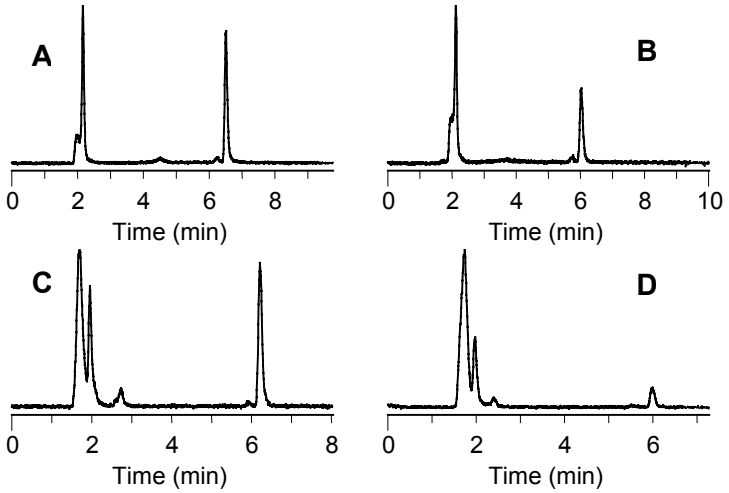

Fig. 3. Stability studies of ^{99m}TcO(PNO/PhS) complex by HPLC; stability in saline at 37 ºC, **A**: after 30 min; **B**: after 60 min incubation; stability in 1 mM GSH at 37 ºC, **C**: after 30 min; **D**: after 60 min incubation.

Summarizing we are able to prepare '3+1' oxotechnetium(V) complexes at the n.c.a. level, using the PNO and the PNS tridentate ligands and different monodentate sulphur co-ligands. The '3+1' complexes show different *in vitro* stability. While ^{99m}TcO(PNS/PhS) is a stable complex the corresponding PNO complex is unstable under the same conditions. So, the tridentate ligand used seems to play a very important role in the complex stabilization.
The complexes do not exchange the monodentate ligand against glutathione as observed for common 3+1 complexes, but they decompose after dilution in different rates and form more hydrophilic unknown radiochemical species. The results obtained with the ^{99m}TcO(PNS/PhS) complex are very promising. In further work the used high lipophilic PNS ligand should be replaced by more hydrophilic derivatives and biologically interesting monothiols should be used as co-ligands.

References

[1] Syhre, R.; Seifert, S.; Spies, H.; Gupta, A. and Johannsen, B. Stability versus reactivity of "3+1"mixed-ligand technetium-99m complexes *in vitro* and *in vivo*. Eur. J. Nucl. Med. 25 (1998) 793-796.
[2] Gupta, A.; Seifert, S.; Syhre, R.; Brust, P.; Johannsen, B. Reactivity of mixed ligand 3+1 ^{99m}Tc(V) complexes towards glutathione. Radiochim. Acta, in press.
[3] Correia, J. D. G.; Domingos, Â.; Santos, I. Neutral trichlorooxorhenium(V) complexes containing heterofuncionalized phosphine ligands of the type PN_2 and PNO. Eur. J. Inorg. Chem. (2000) 1523-1529.
[4] Correia, J. D. G.; Domingos, Â.; Paulo, A.; Santos, I. Novel six-coordinated oxorhenium complexes with ligands containing PN_2 and PNO donor atom sets: Synthesis and structural characterization. J. Chem. Soc., Dalton Trans. 14 (2000) 2477-2482.
[5] Correia, J. D. G.; Domingos, A.; Santos, I. unpublished results.
[6] Seifert, S.; Pietzsch, H.-J.; Scheunemann, M.; Spies, H.; Syhre, R.; Johannsen, B. No carrier added preparations of '3+1' mixed-ligand ^{99m}Tc complexes. Appl. Radiat. Isot. 49 (1998), 5-11.

13. The Coordination of 4-Mercapto-5-Methylthio-1.2-Dithiol-3-Thione with Technetium and Rhenium: First Results

H.-J. Pietzsch, H. Stephan, H. Spies, W. Banße[1], H.J. Holdt[1]
[1]Institut für Anorganische Chemie und Didaktik der Chemie, Universität Potsdam

4-Mercapto-5-methylthio-1,2-dithiol-3-thione **(1)** reacts with Zn^{2+}, Cd^{2+}, and Mn^{2+} to give neutral complexes [M (**1**)$_2$] [1]. We became interested in this sulfur-rich compound as a potential ligand for the radioactive nuclides of technetium and rhenium. Because of the well documented high thiophilicity of Tc and Re , stable complexes are expected to be formed. A Tc complex of 4,5-dimercapto-1,3-dithiol-2-thione (L) was earlier described [2]. Unlike this dithiolate ligand which forms an anionic complex $[TcO(L)_2]^-$, only one mercapto group in **(1)** is available for coordination. On the one hand this requires participation of the thione group in the coordination and favours the formation of neutral species. On the other, the 5-thiol position may be used to introduce biomolecules, thus enabling stable "Tc-labelling".
Experiments to bind technetium and rhenium at the oxidation states V, III, and I will be made. Here we report first experiments to coordinate 4,5-mercapto-1.2-dithiol-3-thione derived ligands with Re(V).

Results

4-Mercapto-5-methylthio-1,2-dithiol-3-thione **(1)** was allowed to react with tetrachloro-oxorhenate(V). Thus, 56 mg (0.094 mmol) of the Re(V) precursor $NBu_4[ReOCl_4]$ was dissolved in 2 ml methanol and a solution of 40 mg (0.19 mmol) of **(1)** in 3 ml chloroform was added at room temperature. An orange-coloured solid precipitated. After stirring for 30 min. the solid was separated and washed with chloroform and methanol. The solid was extracted by hot acetonitrile, from which a complex **(2)** resulted as an orange powder (m.p.: 215 – 216 °C). Yield: 48 mg (77 % rel. to $NBu_4[ReOCl_4]$). Based on the elemental analysis we assume the formula $C_8H_{10}OS_{10}ClRe$. The infrared spectrum shows an intensive band at 972 cm^{-1} assigned to Re=O.

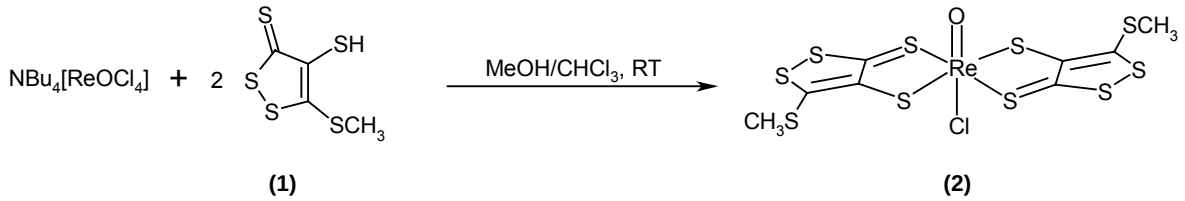

Fig. 1. Reaction scheme of the formation of the rhenium complex **(2)**

Relying on these experimental results a coordination pattern of **(2)** is derived, where two ligands are bound to the oxorhenium core. To become neutral, a chlorine also coordinates, most likely trans to the oxo group.
As the hitherto described complexes of **(1),** the rhenium complex **(2)** is slightly soluble in common solvents.

References

[1] Rudershausen, S. Synthese und Koordinationschemie mono- und dialkylierter Derivate des 1,2-Dithiol-3-thion-4,5-dithiolates und acyclisch-substituierter und verkronter Thiodesaurine sowie verkronter 1,3-Dithiafulvene. Thesis, Universität Rostock (1998).
[2] Spies, H.; Johannsen, B. Oxotechnetium(V)bis(dithiolato) complexes. Inorg. Chim. Acta 48 (1981) 255-258

14. Bromoalkylated Tetradentate N_2S_2 Chelates and their Technetium Complexes

I.Heimbold, A.Drews

Introduction

Tetradentate N_2S_2 ligands are known to form stable monooxo complexes with technetium(V) and rhenium(V). They therefore play an important role in the search for new Tc-radiopharmaceuticals [1 - 3]. To improve the utility of these ligands we synthesized bromopentyl- and bromohexyl- funtionalized derivatives of the amine-amide-dithiol (AADT) ligand and the diaminodithiol (DADT) ligand.

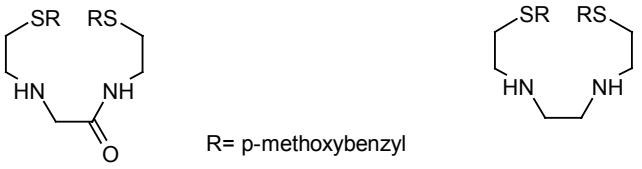

AADT **DADT**

Simple alkylation reactions make it possible to attach these chelates to receptor-specific molecules which are to be labelled with technetium or rhenium.
Here we report on the synthesis of bromoalkyl AADT and bromoalkyl DADT. For a better understanding of the labelling reaction with ^{99}Tc which involves simultaneously deprotection of the thiol groups we studied this reaction for bromohexyl AADT and bromohexyl DADT.

Results and Discussion

Alkylation of the tetradentate AADT ligand occurs with an excess of dibromohexane or dibromopentane in dioxane using K_2CO_3 as a base. Bromoalkyl AADTs were purified by flash chromatography on silica gel using first chloroform for separation of excessive dibromoalkyl and then chloroform / methanol (100:1) to yield the desired product (60 – 80 %).
The reduction of bromoalkyl AADTs was achieved with BH_3/THF by refluxing for several hours. Purification occurs by flash chromatography with chloroform /methanol (20:1) to yield the bromoalkyl DADTs in a 30 to 70 % yield.

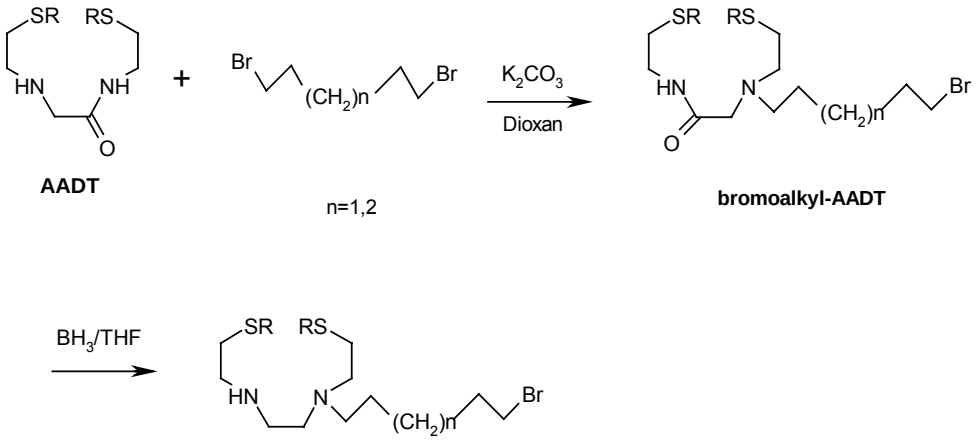

AADT

n=1,2

bromoalkyl-AADT

bromoalkyl-DADT

General procedure

Alkylation
0.43 g (1.0 mmol) of the AADT ligand was dissolved in dioxane. 10.0 mmol of dibromoalkyl and 0.28 g (2.0 mmol) K_2CO_3 were added and the mixture was refluxed for about 20 hours. Then the solution was filtered, evaporated and purified by liquid chromatography on silica gel with at first chloroform to yield the excessive dibromoalkyl and then chloroform / methanol (100:1) to yield the bromoalkyl AADT.

6-Bromohexyl AADT (yield: 0.48 g, 80 %)
^{1}H NMR (400 MHz, $CDCl_3$): δ = 1.22-1.29 (m, 2H, hexylchain), 1.30-1.38 (m, 4H, CH_2-AADT), 1.81 (quint, 2H, hexylchain), 2.35 (t, 2H), 2.42 (t, 2H), 2.48 (t, 2H), 2.56 (t, 2H), 2.96 (s, 2H, -CH_2-C=O), 3.29-3.37 (m, 4H, CH_2-AADT and –CH_2-Br), 3.57 (s, 2H, -S-CH_2-Ph), 3.60 (s, 2H, -S-CH_2-Ph), 3.75 (s, 3H, -O-CH_3), 3.76 (s, 3H, -O-CH_3), 6.80-6.83 (m, 4H, $H_{arom.}$), 7.17-7.21 (m, 4H, $H_{arom.}$), 7.73 (t, 1H, -NH).
^{13}C NMR (100 MHz, $CDCl_3$): δ = 26.61, 27.32, 28.17, 29.72, 31.24, 32.85, 34.11, 35.23, 36.02, 37.82, 54.54, 55.07, 55.45 (O-CH_3), 55.47 (O-CH_3), 58.68, 114.11 ($C_{arom.}$), 114.13 ($C_{arom.}$), 130.07 ($C_{arom.}$), 130.15 ($C_{arom.}$), 130.18 ($C_{arom.}$), 130.29 ($C_{arom.}$), 158.82 ($C_{arom.}$-p-methoxy), 158.87 (C_{arom}-p-methoxy), 171.78 (C=O).

5-Bromopentyl AADT (yield: 0.34 g, 60 %)
^{1}H NMR (400 MHz, $CDCl_3$): δ =1.39-1.71(m, 6H), 1.82 (quint, 2H, pentylchain), 2.48-2.55 (m, 6H), 3.02 (s, 2H, -CH_2-C=O), 3.37 (quart.,2H, CH_2-AADT), 3.46 (t, 2H, -CH_2-Br), 3.62 (s, 2H, -S-CH_2-Ph), 3.65 (s, 2H, -S-CH_2-Ph), 3.75 (s, 3H, -O-CH_3), 3.76 (s, 3H, -O-CH_3), 6.76-6.82(m, 4H, $H_{arom.}$), 7.17-7.22 (m, 4H, $H_{arom.}$) 7.79 (t, 1H, NH).
^{13}C NMR (100 MHz, $CDCl_3$): δ = 27.50, 29.52, 31.12, 32.71, 33.90, 34.95, 35.24, 35.86, 37.75, 53.82, 55.45(O-CH_3), 55.48(O-CH_3), 57.97, 58.61, 114.09($C_{arom.}$), 114.15($C_{arom.}$), 130.08 ($C_{arom.}$), 130.17 ($C_{arom.}$), 130.32 ($C_{arom.}$), 130.45 ($C_{arom.}$), 158.83 (C_{arom}-p-methoxy), 158.89 (C_{arom}-p-methoxy), 171.34 (C=O).

Reduction
0.5 mmol of bromoalkyl AADT was dissolved in dry THF under argon and 3.0 ml of BH_3/THF (1M) were added. The reaction mixture was allowed to reflux for about 10 hours. Then it was cooled down to 0 °C and water was dropwise added until the gas development was finished. The solution was evaporated to dryness, the residue dissolved in 30 ml ethanol and 5ml of concentrated HCl were added. This mixture was refluxed for one hour and then evaporated. The residue was dissolved in water and $KHCO_3$ (10 %) was added until pH 8 - 9. The bromoalkyl DADT was extracted with chloroform, dried over $MgSO_4$ and evaporated to dryness. The resulting oil was purified by liquid chromatography on silica gel with chloroform / methanol (20:1)

6-Bromohexyl DADT (yield: 0.2 g, 70 %)
^{1}H NMR (400 MHz, $CDCl_3$): δ = 1.20-1.25 (m, 2H), 1.32-1.39 (m, 4H), 1.72 (quint, 2H, hexylchain), 2.31 (t, 2H), 2.42-2.52 (m, 10H), 2.69 (t, 2H), 3.46 (t, 2H, -CH_2-Br), 3.59 (s, 2H, -S-CH_2-Ph), 3.60 (s, 2H, -S-CH_2-Ph), 3.71 (s, 3H, -O-CH_3), 3.72 (s, 3H, -O-CH_3), 6.76-6.78 (m,4H, $H_{arom.}$), 7.15-7.17 (m, 4H, $H_{arom.}$), 7.76 (t, 1H, NH).
^{13}C NMR (100 MHz, $CDCl_3$): δ = 26.82, 26.96, 27.32, 29.39, 31.59, 32.76, 35.72, 36.08, 45.29, 47.44, 48.77, 53.83, 53.84, 54.37, 55.44(O-CH_3), 55.45(O-CH_3), 114.08($C_{arom.}$), 114.10($C_{arom.}$), 130.08($C_{arom.}$), 130.11($C_{arom.}$), 130.16($C_{arom.}$), 130.50($C_{arom.}$), 158.78(C_{arom}-p-methoxy), 158.81(C_{arom}-p-methoxy).

5-Bromopentyl DADT (yield: 85 mg, 30 %)
^{1}H NMR (400 MHz, $CDCl_3$): δ = 1.36-1.68(m, 6H), 1.79 (quint, 2H, pentylchain), 2.38-2.58 (m, 12H), 3.28(t, 2H, -CH_2-Br), 3.60 (s, 2H, -S-CH_2-Ph), 3.65 (s, 2H, -S-CH_2-Ph), 3.76 (s, 3H, -O-CH_3), 3.77 (s, 3H, -O-CH_3), 6.74-6.80(m, 4H, $H_{arom.}$), 7.18-7.22 (m, 4H, $H_{arom.}$), 7.78 (t, 1H, NH).
^{13}C NMR (100 MHz, $CDCl_3$): δ = = 27.51, 29.52, 32.71, 33.90, 35.24, 35.86, 37.75, 45.27, 47.42, 48.75, 53.80, 53.83, 54.35, 55.44(O-CH_3), 55.46(O-CH_3), 114.09($C_{arom.}$), 114.10($C_{arom.}$), 130.09($C_{arom.}$), 130.10($C_{arom.}$), 130.15($C_{arom.}$), 130.49($C_{arom.}$), 158.77(C_{arom}-p-methoxy), 158.80(C_{arom}-p-methoxy).

Labelling reaction with ^{99}Tc
The preparation of the ^{99}Tc compounds **Tc1** and **Tc2** simultaneously with deprotection of the thiol groups of the ligands was performed by transchelation from [^{99}Tc]technetium gluconate under the following conditions: 9 mg of the tetradentate ligand (6-bromohexyl AADT and 6-bromohexyl DADT) was dissolved in 2.0 ml ethanol while adding 0.2 ml of 37 % HCl, 0.2 ml of ^{99}Tc pertechnetate solution (0.05 M, 0.6 MBq)), 0.2 ml (40 MBq) ^{99m}Tc pertechnetate and 0.5 ml stannous chloride solution, which contained 2 mg of stannous chloride and 25 mg sodium gluconate. The mixture was stirred at 80 – 100 °C for 6 h.

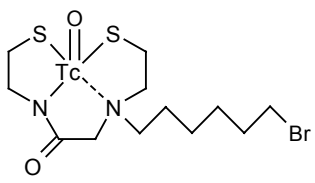

Tc 1

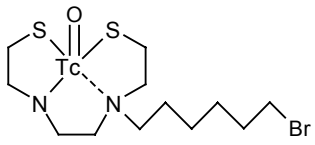

Tc 2

After neutralization with 1 N NaOH, the mixture was partitioned between $CHCl_3$ and bidistillated water. The layers were separated and the organic phase was concentrated.
The reaction was examined by an HPLC system (Hypersil ODS column, Knauer, 250 x 4mm, 10 µm, flow rate 1ml/min) using a linear gradient system [t(min)/%A] (0/50), (5/100) of methanol (A) and 0.01M phosphate buffer (Sörensen) of pH 7.4 (B).
The compounds were purified, using a semipreparative Hypersil ODS column (Knauer, 250 x 8 mm, 10 µm, flow rate 2 ml/min) under the same mobile phase conditions as described above.

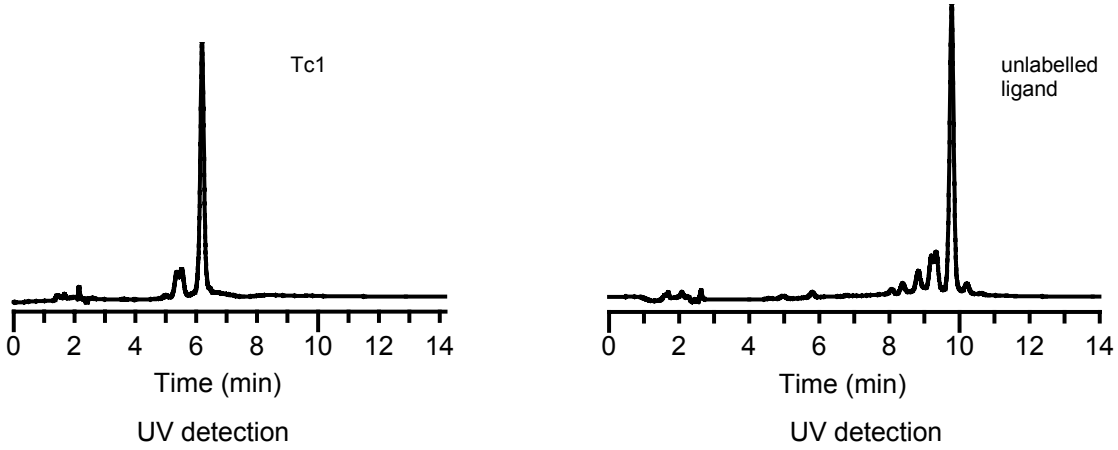

Fig. 1. HPLC pattern of purified **Tc1** and the protected, unlabelled ligand

The **Tc1** complex was obtained in a yield of 20 % after a first HPLC purification. The retention time of the **Tc2** complex was 6.8 min, obtained in the same way as the **Tc1** complex from the analytical HPLC system. Unfortunately, the **Tc2** complex was only observed in a yield of < 5 % after HPLC purification.

To sum up the bromoalkyl AADT and DADT ligands were prepared in good yields. The yields of 5-bromopentyl DADT should be further optimized. The results demonstrate that simultaneously labelling and deprotection of these tetradentate ligands is possible. The yields of the DADT ligand labelling were very low, but an optimization will probably lead to better results.
The bromoalkyl AADTs and DADTs are good tools for further investigations of radiopharmaceuticals with tetradentate chelate units. Some first encouraging results of coupling with receptor-specific molecules have been obtained.

References

[1] Kung, M.-P.; Stevenson, D.A.; Plössl, K.; Meegalla, S.K.; Beckwith, A.; Essman, W.D.; Mu, M.; Lucki, I.; Kung, H.F. [^{99m}Tc]TRODAT-1: a novel technetium-99m complex as a dopamine transporter imaging agent. Eur. J. Nucl. Med. 24 (1997) 372.

[2] Madras, B.K.; Jones, A.G.; Mahmood, A.; Zimmermann, R.E.; Garada, B.; Holman, B.L.; Davison, A.; Blundell, P.; Meltzer, P.C. Technepine: A high-affinity ^{99m}Technetium probe to label the dopamine transporter in brain by SPECT imaging. Synapse 22 (1996) 239.

[2] O'Neil, J.P.; Wilson, S.R.; Katzenellenbogen, J.A. Preparation and structural characterization of monoamine-monoamide bis(thiol) oxo complexes of technetium(V) and rhenium(V). Inorg. Chem. 33 (1994) 319.

15. EXAFS Analyses of Technetium and Rhenium Complexes

1. Stability Studies of Technetium(I) Tricarbonyl Dithioether Complexes in Solutions

S. Seifert, J.-U. Künstler, A. Gupta, H. Funke[1], T. Reich[1], C. Hennig[1], A. Roßberg[1], H.-J. Pietzsch, R. Alberto[2], B. Johannsen
[1]Institute of Radiochemistry, [2]Institute of Inorganic Chemistry, University of Zurich, Switzerland

Introduction

Among a broad variety of complex compounds differing in the oxidation state of the technetium atom and the denticity and composition of ligands used, the Tc(I) carbonyl complexes represent a new promising approach to low valent, non-polar and inert technetium compounds [1, 2, 3]. Intensive investigations in the Tc carbonyl chemistry showed the availability of an organometallic Tc(I) aqua ion, $[Tc(OH_2)_3(CO)_3]^+$, which acts under normal pressure [4, 5] as a precursor for the preparation of complexes containing the small $[Tc(CO)_3]^+$ moiety starting from TcO_4^-.
In the present paper we describe the preparation and characterization of some ^{99}Tc(I) and ^{99m}Tc(I) carbonyl thioether complexes and their reaction products in aqueous solution. Besides chromatographic methods for the characterisation of the no-carrier-added (n.c.a.) Tc complexes and their reaction products, we used Extended X-ray Absorption Fine Structure (EXAFS) spectroscopy and mass spectrometry for the identification of the ^{99}Tc congeners (K-edge at 21.044 keV).

Experimental

The ^{99}Tc precursor complex $(NEt_4)_2[TcCl_3(CO)_3]$ was prepared according to the standard procedure [6]. The thioether complex **Tc1** ($[TcCl(CO)_3L]$, L = 3,6-dithiaoctane) was prepared by addition of equimolar amounts of the thioether ligand to the methanolic precursor complex solution, separation of NEt_4Cl (filtration of the solution after addition of tetrahydrofurane), removing of the solvent by vacuum evaporation and washing of the white residue with water and diethyl ether. The complex **Tc1a** ($[Tc(H_2O)(CO)_3L]^+$) was obtained by dissolution of complex **Tc1** in water/methanol (1/1) and removing the chloride by addition of one equivalent of $AgNO_3$ to the solution.
The corresponding ^{99m}Tc complexes were prepared and analysed as described in [6].
The complexes were characterized by chromatographic methods, electrospray mass spectrometry and EXAFS analysis.
EXAFS measurements of the technetium compounds were performed, using the Rossendorf Beamline (ROBL) facility at the European Synchrotron Radiation Facility (ESRF) in Grenoble, France [7].
The sample preparation and experimental EXAFS data are described in [8].

Results and Discussion

As known from n.c.a. studies of technetium dithioether complexes of the general formula $[TcX(CO)_3L]$ (X = Cl, L = bidentate thioether ligand), the chloride ion is in all probability substituted in aqueous solution by water [6]. The resulting cationic complex $[Tc(OH_2)(CO)_3L^2]^+$ can reversibly be converted into the neutral species by adding an excess of sodium chloride.

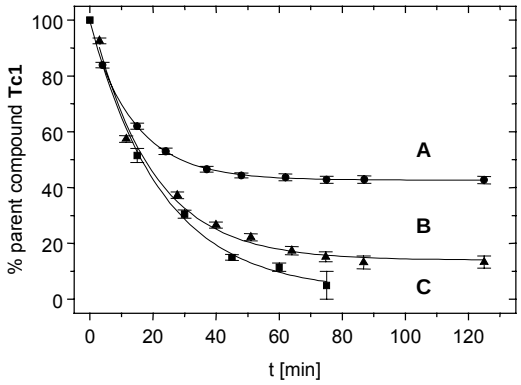

Fig. 1. Time course of conversion of the complex **Tc1** into the complex **Tc1a** in a solution of 45 % H_2O / 45 % MeOH / 10 % propylene glycol at various Tc concentrations determined by HPLC.
A: 10^{-2} M, **B**: 10^{-3} M, **C**: n.c.a. solution.

The fastest chloride exchange reaction was observed in the n.c.a. solution. At this low concentration level the transformation into the aqua complex **Tc1a** proceeds nearly completely and the rate of the reaction should be pseudo first order since the water concentration can be considered as constant. In

fact, the time course of the converting reaction fits the equation for a pseudo first order reaction. With increasing ^{99}Tc concentrations the conversion results in an establishment of the equilibrium (Fig. 1).
The cationic charge of the conversion product was confirmed by paper electrophoresis as well as by capillary electrophoresis.
Mass spectrometric analyses and EXAFS measurements of the ^{99}Tc complexes **Tc1** and **Tc1a** confirm the compositions $[TcCl(CO)_3L]$ and $[Tc(OH_2)(CO)_3L]^+$.
Besides the molecule mass for complex **Tc1a** (m/z = 351) the fragmentation product $[^{99}Tc(CO)_3L]$ (m/z = 333) was found. The same fragmentation product was also found in the sample **Tc1**. For obvious reasons, the chloride ion and water were easily split off during ionization. Instead of the molecule ion peak of **Tc1** the sodium adduct was detected (m/z = 391).
EXAFS spectroscopy was applied to investigate the coordination spheres of these complexes. The complex **Tc1** was analysed both as powder and liquid sample. The identity of the EXAFS data and their Fourier transforms of both the solid and the dissolved **Tc1** can be seen in Fig. 2.

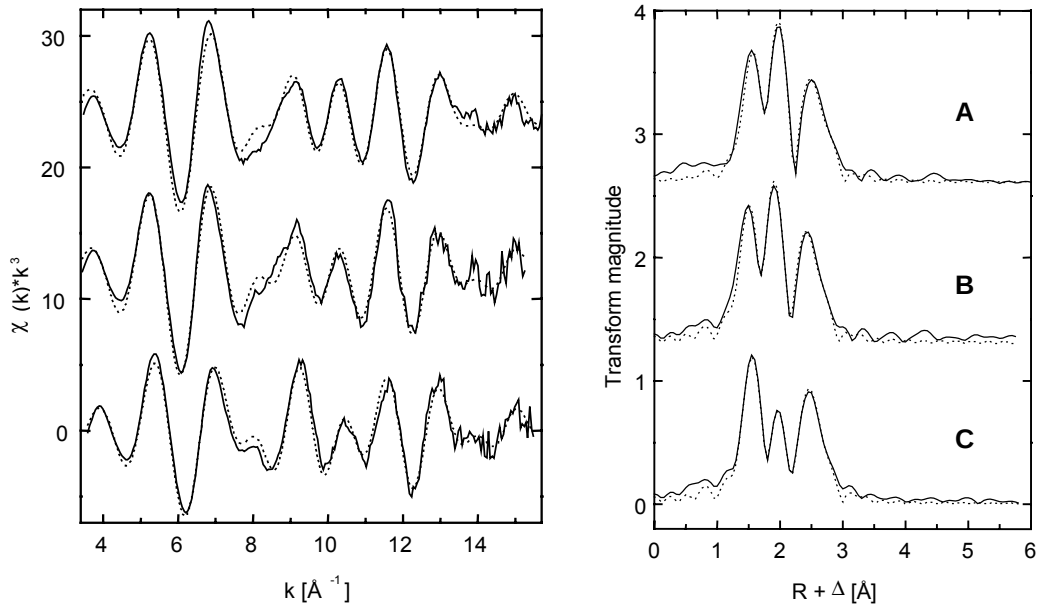

Fig. 2. Tc K-edge k^3-weighted EXAFS spectra and the corresponding Fourier transforms of samples **Tc1** and **Tc1a**. **A**: **Tc1** solid, **B**: **Tc1** dissolved in saline/methanol, **C**: **Tc1a** dissolved in water/methanol. (solid line: experimental data, dotted line: fit).

Table 1. Structural parameters obtained by the Tc K-edge k^3-weighted EXAFS spectrum of **Tc1** and **Tc1a** (R: bond distance, N: coordination number, σ^2: Debye-Waller factor, standard deviation in parentheses).

	Tc1 (powder)			**Tc1** (dissolved in methanol/saline)			**Tc1a** (dissolved in methanol/water)		
Path	R [Å]	N	σ^2 [10^{-3} Å^2]	R [Å]	N	σ^2 [10^{-3} Å^2]	R [Å]	N	σ^2 [10^{-3} Å^2]
Tc-C	1.92(1)	3.7(2)	2.3(2)	1.92(1)	4.0(3)	3.1(3)	1.92(1)	3.3(3)	2.2(5)
Tc-Cl	2.49(1)[1)]	1.3(1)[1)]	4.9(2)[1)]	2.49(1)[1)]	1.3(1)[1)]	5.1(3)[1)]			
Tc-O							2.19(1)	1.2(1)[1)]	2.2(8)
Tc-S	2.49(1)[1)]	2.7(2)[1)]	4.9(2)[1)]	2.49(1)[1)]	2.7(2)[1)]	5.1(3)[1)]	2.49(1)	2.5(2)[1)]	5.6(4)
Tc-C-O (3 legs)	3.07(1)[2)]	5.9(2)[2)]	3.4(2)[2)]	3.06(1)[2)]	5.7(3)[2)]	3.0(3)[2)]	3.06(1)[2)]	5.0(2)[2)]	3.1(3)[2)]
Tc-C-O (4 legs)	3.07(1)[2)]	2.9(1)[2)]	3.4(2)[2)]	3.06(1)[2)]	2.8(2)[2)]	3.0(3)[2)]	3.06(1)[2)]	2.5(1)[2)]	3.1(3)[2)]

[1) 2)] In each column, identically marked parameters were forced to have constant ratios during the fits.

From EXAFS fit results (Table 1), nearly the same coordination numbers and bond lengths of the different groups of backscatterers as for the rhenium reference complex can be concluded for the tech-

netium carbonyl complex **Tc1**. The Fourier transform of the experimental EXAFS data, corresponding to the distribution function of the neighbours in R-space, shows three clearly resolved peaks. The left peak represents the C coordination shell, the middle the S and Cl atoms (**Tc1**) or the O atom (**Tc1a**) and the right peak is the O coordination shell of the CO. When Cl is substituted by water (see **C** in Fig. 2) the magnitude of the second peak of the Fourier transform is smaller because oxygen is a weak back-scatterer compared to chlorine. The initial fit with freely floated parameters R, N, σ^2 for the Tc-S and Tc-Cl paths resulted in very high standard deviations of these parameters and a smaller difference in bond lengths than the expected resolutions of 0.13 Å. In addition, the scattering phases and amplitudes for the Tc-S and Tc-Cl paths are nearly identical since S and Cl are neighbouring elements in the periodic table. To model the Tc-S and Tc-Cl coordination shells with a higher degree of precision, their R and σ^2 values were fixed to be equal and the ratio of N(Tc-S) to N(Tc-Cl) was set to two during the fit.
The relative short distance of 2.19 Å demonstrates the strong coordination of water in complex **Tc1a**. The Tc-C and Tc-S distances are in agreement with those found by X-ray diffraction analyses of similar Re complexes [9] and are not changed by exchange of chlorine against water.

References

[1] Alberto, R., Schibli, R., Egli, A., Schubiger, P. A., Herrmann, W. A., Artus, G., Abram, U., Kaden, T. A. Metal carbonyl syntheses XXII. Low pressure carbonylation of $[MOCl_4]^-$ and $[MO_4]^-$: The Tc(I) and Re(I) complexes $[NEt_4]_2[MCl_3(CO)_3]$. J. Organomet. Chem. 493 (1995) 119.

[2] Alberto R. High- and low-valency organometallic compounds of technetium and rhenium. Topics in Current Chemistry 176 (1996) 149, Springer-Verlag, Berlin, Heidelberg.

[3] Schibli, R., Alberto, R., Abram, U., Abram, S., Egli, A., Schubiger, P.A., Kaden, T.A. Structural and Tc-99 NMR investigations of complexes with fac-$[Tc(CO)_3]^+$ moieties and macrocyclic thioethers of various ring sizes: Synthesis and X-ray structure of the complexes fac-[Tc(9-ane-S-3)$(CO)_3$]Br, fac-$[Tc_2(tosylate)_2$(18-ane-S-6)$(CO)_6]$, and fac-$[Tc_2$(20-ane-S-6-OH)$(CO)_6]$[tosylate]$_2$. Inorg. Chem. 37 (1998) 3509.

[4] Alberto, R., Schibli, R., Egli, A., Schubiger, A.P., Abram, U., Kaden, T.A. A novel organometallic aqua complex of technetium for the labeling of biomolecules: Synthesis of $[^{99m}Tc(OH_2)_3(CO)_3]^+$ from $[^{99m}TcO_4]^-$ in aqueous solution and its reaction with a bifunctional ligand. J. Am. Chem. Soc. 120 (1998) 7987.

[5] Alberto, R., Schibli, R., Schubiger, A.P., Abram, U., Pietzsch, H.-J., Johannsen, B. First application of fac-[Tc-99m$(OH_2)_3(CO)_3]^+$ in bioorganometallic chemistry: Design, structure, and *in vitro* affinity of a 5-HT_{1A} receptor ligand labeled with Tc-99m. J. Am. Chem. Soc. 121 (1999) 6076.

[6] Pietzsch, H.-J., Gupta, A., Reisgys, M., Drews, A., Seifert, S., Syhre, R., Spies, H., Alberto, R., Abram, U., Schubiger, P. A., Johannsen, B. Chemical and biological characterization of technetium(I) and rhenium(i) tricarbonyl complexes with dithioether ligands serving as linkers for coupling the "$Tc(CO)_3$" and "$Re(CO)_3$" moieties to biologically active molecules. Bioconjugate Chem. 11 (2000) 414.

[7] Matz, W., Schell, N., Bernhard, G., Prokert, F., Reich, T., Claußner, J., Oehme, W., Schlenk, R., Dienel, S., Funke, H., Eichhorn, F., Betzl, M., Pröhl, D., Strauch, U., Hüttig, G., Krug, H., Neumann, W., Brendler, V., Reichel, P.,. Denecke, M.A., Nitsche, H. ROBL - a CRG beamline for radiochemistry and materials research at the ESRF. J. Synchrotron Rad. 6 (1999) 1076.

[8] Seifert, S.; Kuenstler, J.-U.; Gupta, A.; Funke, H.; Reich, T.; Hennig, C.; Rossberg, A.; Pietzsch, H.-J.; Alberto, R.; Johannsen, B. EXAFS analyses of technetium(I) carbonyl complexes - stability studies in solutions. Radiochim. Acta 88 (2000) 239-245.

[9] Alberto, R., Schibli, R., Angst, D., Schubiger, P. A., Abram, U., Abram, S., Kaden, Th. A. Application of technetium and rhenium carbonyl chemistry to nuclear medicine. Preparation of $[NEt_4]_2[TcCl_3(CO)_3]$ from $[NBu_4][TcO_4]$ and structure of $[NEt_4][Tc_2(\mu\text{-}Cl)_3(CO)_6]$; structures of the model complexes $[NEt_4][Re_2(\mu\text{-}OEt)_2(\mu\text{-}OAc)(CO)_6]$ and $[ReBr(\{\text{-}CH_2S(CH_2)_2Cl\}_2)(CO)_3]$. Transition Met. Chem. 22 (1997) 597.

16. EXAFS Analyses of Technetium and Rhenium Complexes

2. Reactivity of Technetium(I) Thioether Carbonyl Complexes against Histidine

S. Seifert, J.-U. Künstler, A. Gupta, H. Funke[1], T. Reich[1], H.-J. Pietzsch, R. Alberto[2], B. Johannsen
[1]Institute of Radiochemistry, [2]Institute of Inorganic Chemistry, University of Zurich, Switzerland

Introduction

The precursor complex ion $[^{99m}Tc(CO)_3(H_2O)_3]^+$ and also the Tc(I) thioether carbonyl complexes show a strong tendency to bind to plasma and other blood proteins [1, 2]. The highest plasma binding was found for the cationic complex $[Tc(CO)_3(H_2O)(S\text{-}S)]^+$ but also the neutral complexes $[Tc(CO)_3Cl(S\text{-}S)]$ and $[Tc(CO)_3(S\text{-}S\text{-}O)]$ (S-S-O = tridentate carboxylato dithioether ligand) exhibit a plasma binding of more than 50 %. On the other side we found that ^{99m}Tc(I) tricarbonyl complexes with N-donor ligands like histidine or Schiff bases are not bound to plasma proteins. It can be assumed that the strong binding of thioether carbonyl complexes to proteins of plasma is caused by a ligand exchange reaction. It is known from the biobehaviour as well as challenge experiments of so-called 3+1 complexes of Re(V) and Tc(V) with monothiols like glutathione that the original monothiol of the 3+1 complex is substituted by glutathione *in vitro* and *in vivo*. Likely, the Tc(I) thioether carbonyl complexes react with N-donor groups of proteins. For that reason we studied the behaviour of some Tc(I) thioether carbonyl complexes, **Tc1**: $[Tc(CO)_3ClL^1]$ (L^1 = 3,6-dithiaoctane), **Tc1a**: $[Tc(CO)_3(H_2O)L^1]^+$, **Tc2**: $[Tc(CO)_3L^2]$ (L^2 = 1-carboxylato-3,6-dithiaheptane) in aqueous solutions containing histidine as high potential ligand for complexing the $[Tc(CO)_3]^+$ moiety.
EXAFS measurements of the ^{99}Tc compounds were performed, using the Rossendorf beamline (ROBL) facility at the European Synchrotron Radiation Facility (ESRF) in Grenoble, France [3]. Experimental and results are described in detail in [4].

Results and Discussion

We found that the complexes **Tc1**, **Tc1a** and **Tc2** react with histidine to the products **Tc1b** and **Tc2b** in aqueous solution which are identically with the reference $[Tc(CO)_3His]$, **Tc3** (Fig. 1).

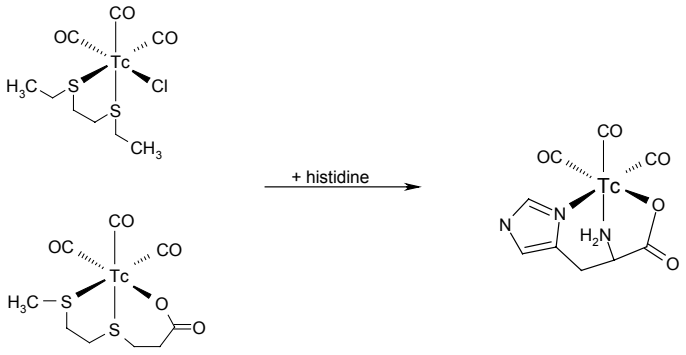

Fig. 1. Reaction of Tc thioether carbonyl complexes with histidine.

A comparison of HPLC analyses data of ^{99}Tc and ^{99m}Tc histidine carbonyl complexes prepared by reaction of the precursor complex with histidine and by ligand exchange reaction of the dithioether complexes with histidine confirm the structural identity of the ^{99}Tc and ^{99m}Tc complexes. The bidentate dithioether ligand L^1 is substituted by histidine in a higher exchange rate than the tridentate carboxylato dithioether ligand L^2, thereby the conversion of **Tc1** into **Tc1a** was prevented by addition of saline. The exchange results in a complete conversion of **Tc1**, **Tc1a** or **Tc2** into **Tc3**.
The lower stability of **Tc1** in comparison with **Tc2** is also reflected in the fact that **Tc1** shows a distinct higher protein binding in plasma and blood [1]. Capillary electrophoresis studies confirm the neutrality of complexes **Tc1**, **Tc2**, **Tc3**, which are detected together with the neutral marker acetone, and the positive charge of **Tc1a** at pH 7.0. Moreover, **Tc2** and **Tc3** shows neutrality at pH 2.5 and 9.3, which confirms the coordination of the carboxylic group. The results of ESI-MS analysis are in agreement with the expected molecular weights of all ^{99}Tc complexes.

EXAFS analyses

To obtain a satisfactory interpretation of the EXAFS spectra and the corresponding Fourier transforms the following single-scattering paths including the C, N/O and S/Cl coordination shells and multiple-scattering paths to model the oxygen atom of carbon monoxide were taken into account (Table 1). All other possible scattering paths did not lead to a significant improvement of the fit results.

The Fourier transforms of the experimental EXAFS data of **Tc1** and **Tc2** show three well resolved peaks and two clearly resolved peaks for **Tc1b**, **Tc2b** and **Tc3**. Peak A represents mainly the C coordination shell but also the coordination of the N and O atoms (**Tc1b**, **Tc2**, **Tc2b**, **Tc3**), peak B the S and Cl atoms (**Tc1**) or the S and partly the O atom (**Tc2**) and peak C the O coordination shell of CO. The coordination of an O atom from the carboxylic group (**Tc2**) in comparison with the coordination of a Cl atom (**Tc1**) causes a decrease in magnitude of peak B of the Fourier transform because oxygen is a weak back-scatterer compared to chlorine (Fig. 2).

The estimated atomic distances in **Tc1** and **Tc2** are almost the same as those found by single-crystal X-ray diffraction analyses of Re carbonyl complexes containing similar dithioether ligands, which we recently published [1]. The estimated coordination numbers agree with the expected values.

The EXAFS spectra, their Fourier transforms and the fit results of **Tc1b** and **Tc2b** are almost identical to the results of EXAFS analysis of reference **Tc3**. This fact proves the substitution of bidentate dithioether and tridentate carboxylato dithioether ligands by histidine, which coordinates in a tridentate manner. The obtained atomic distances are in agreement with those found for the Re congener by single-crystal X-ray diffraction analysis [5].

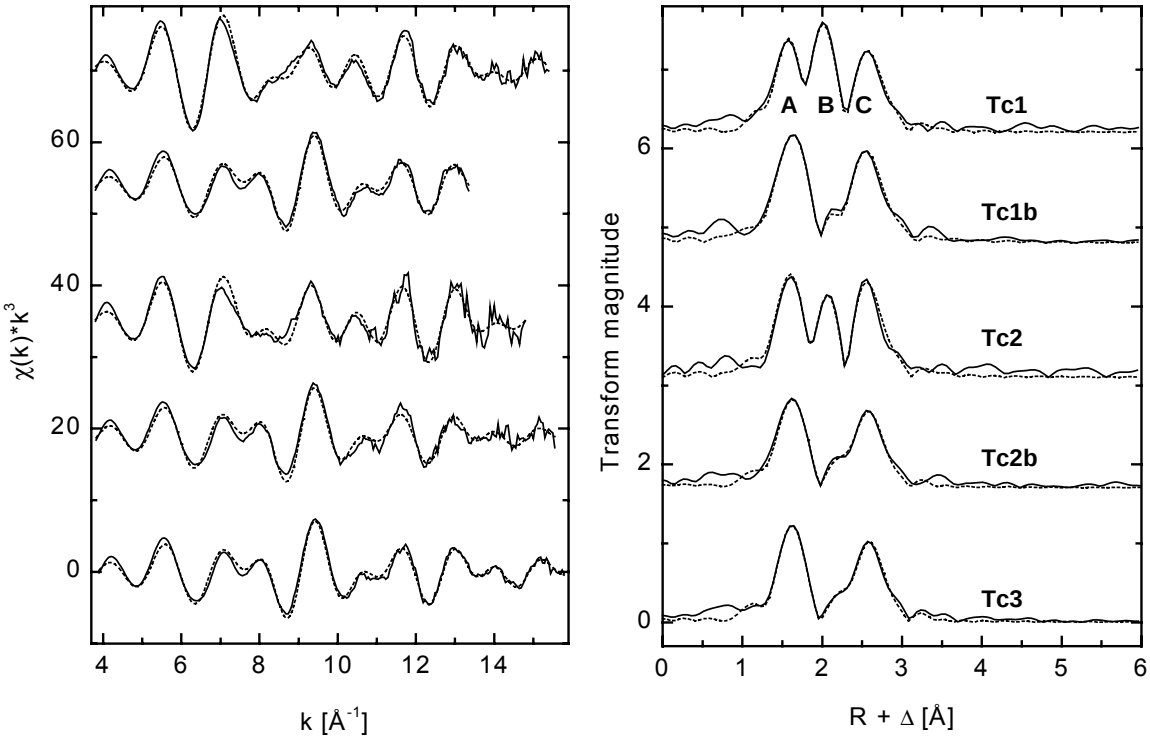

Fig. 2. Tc K-edge k^3-weighted EXAFS spectra and the corresponding Fourier transforms (solid line: experimental data, dotted line: fit). **Tc1**: $[Tc(CO)_3ClL^1]$, **Tc1b**: **Tc1** after the reaction with histidine; **Tc2**: $[Tc(CO)_3L^2]$, **Tc2b**: **Tc2** after the reaction with histidine; **Tc3**: $[Tc(CO)_3His]$.

Table 1. Structural parameters obtained by the Tc K-edge k^3-weighted EXAFS spectra of **Tc1**, **Tc1b**, **Tc2**, **Tc2b** and **Tc3** (R: atomic distance, N: coordination number, σ^2: Debye-Waller factor).

	Path	Tc-S or Tc-S/Cl	Tc-O or Tc-N/O	Tc-C	Tc-CO (2, 3 and 4 legs)
Tc1	R [Å]	2.49 ± 0.02		1.92 ± 0.02	3.07 ± 0.02 [1)]
	N	3.9 ± 0.9		3.4 ± 0.6 [1)]	6.8 ± 1.1 [1) a)]
					3.4 ± 0.6 [1) b)]
	σ^2 [10^{-3} Å^2]	5.0 ± 0.9		2.3 ± 0.8	3.7 ± 0.6 [1)]
Tc1b	R [Å]		2.21 ± 0.02	1.90 ± 0.02	3.07 ± 0.02 [1)]
	N		3.0 ± 1.2	3.0 ± 1.0 [1)]	6.1 ± 2.0 [1) a)]
					3.0 ± 1.0 [1) b)]
	σ^2 [10^{-3} Å^2]		2.6 ± 2.7	1.6 ± 1.7	2.9 ± 1.1 [1)]
Tc2	R [Å]	2.50 ± 0.02	2.21 ± 0.02	1.92 ± 0.02	3.07 ± 0.02 [1)]
	N	2.1 ± 0.6 [1)]	1.0 ± 0.3 [1)]	3.0 [2)]	6.0 [2) a)]
					3.0 [2) b)]
	σ^2 [10^{-3} Å^2]	3.3 ± 1.7	1.1 ± 3.1	1.0 ± 0.7	2.7 ± 0.7 [1)]
Tc2b	R [Å]		2.20 ± 0.02	1.91 ± 0.02	3.07 ± 0.02 [1)]
	N		3.0 ± 1.1	3.4 ± 0.9 [1)]	6.9 ± 1.8 [1) a)]
					3.4 ± 0.9 [1) b)]
	σ^2 [10^{-3} Å^2]		2.7 ± 2.1	2.6 ± 1.3	3.7 ± 0.9 [1)]
Tc3	R [Å]		2.20 ± 0.02	1.91 ± 0.02	3.06 ± 0.02 [1)]
	N		3.2 ± 0.8	3.1 ± 0.6 [1)]	6.3 ± 1.1 [1) a)]
					3.1 ± 0.6 [1) b)]
	σ^2 [10^{-3} Å^2]		3.0 ± 1.5	1.5 ± 0.8	3.0 ± 0.6 [1)]

[1)] In each line, identically marked parameters were forced to have constant ratios during the fits.
[2)] These parameters were hold constant.
[a)] Path Tc-CO (3 legs).
[b)] Path Tc-CO (2 legs) and path Tc-CO (4 legs).

Acknowledgements

We acknowledge the European Synchrotron Radiation Facility for provision of synchrotron radiation facilities and we would like to thank Christoph Hennig and Andre Roßberg for assistance during the EXAFS measurements.

References

[1] Pietzsch, H.-J.; Gupta, A.; Reisgys, M.; Drews, A.; Seifert, S.; Syhre, R.; Spies, H.; Alberto, R.; Abram, U.; Schubiger, P.A.; Johannsen, B. Chemical and biological characterization of technetium(I) and rhenium(I) tricarbonyl complexes with dithioether ligands serving as linkers for coupling the $Tc(CO)_3$ and $Re(CO)_3$ moieties to biologically active molecules. Bioconjugate Chem. 11 (2000) 414-424.

[2] Egli, A.; Alberto, R.; Tannahill, L.; Schibli, R.; Abram, U.; Schaffland, A.; Waibel, R.; Tourwe, D.; Jeannin, L.; Iterbeke, K.; Schubiger, P.A. Organometallic ^{99m}Tc-aquaion labels peptide to an unprecedented high specific activity. J. Nucl. Med. 40 (1999) 1913-1917.

[3] Matz, W.; Schell, N., Bernhard, G.; Prokert, F.; Reich, T.; Claußner, J.; Oehme, W.; Schlenk, R., Dienel, S.; Funke, H., Eichhorn, F., Betzl, M.; Pröhl, D., Strauch, U.; Hüttig, G.; Krug, H.; Neumann, W.; Brendler, V.; Reichel, P.;. Denecke, M. A.; Nitsche, H. ROBL - a CRG beamline for radiochemistry and materials research at the ESRF. J. Synchrotron Rad. 6 (1999) 1076.

[4] Künstler, J.-U.; Seifert, S.; Reich, T.; Funke, H.; Johannsen, B. EXAFS analyses of technetium(I) tricarbonyl complexes – ligand exchange studies. Speciation, Techniques and Facilities for Radioactive Materials at Synchrotron Light Sources, Workshop Proceedings Grenoble, France 10-12. 09. 2000 (accepted).

[5] Schibli, R.; La Bella, R.; Alberto, R.; Garcia-Garayoa, E.; Ortner, K.; Abram, U.; Schubiger, P. A. Influence of the denticity of ligand systems on the in vitro and in vivo behavior of ^{99m}Tc(I)-tricarbonyl complexes: A hint for the future functionalization of biomolecules. Bioconj. Chem. 11 (2000) 345-351.

17. EXAFS Analyses of Technetium and Rhenium Complexes

3. Reaction of His, Gly and Small Model Peptides with the Precursor Complex $(NEt_4)_2[Tc(CO)_3Cl_3]$ in Solution

J.-U. Künstler, S. Seifert, T. Reich[1], B. Johannsen
[1]Institute of Radiochemistry

Introduction

The recently introduced $[Tc(CO)_3]^+$ building block is of high interest for the design of ^{99m}Tc labelled peptides. Coordination of peptide sequences or amino acids – particularly histidine – with the $[Tc(CO)_3]^+$ moiety can be obtained by ligand exchange reactions, using the precursor $[Tc(CO)_3Cl_3]^{2-}$. On the other hand, peptide sequences were able to replace less stable ligands bound to the $[Tc(CO)_3]^+$ moiety, resulting in strong protein binding of some Tc(I) tricarbonyl complexes in vivo [1, 2].
The aim of this work was to study the exchange of the chloride ligands of $[Tc(CO)_3Cl_3]^{2-}$ by His, Gly and simple peptides at the ^{99}Tc level. Gly-Gly and Gly-Gly-Gly, which offer three or four ligating groups, served as models for a peptide backbone. His-Gly, Gly-His, His-Gly-Gly, Gly-His-Lys and Gly-Gly-His are prototypical peptide sequences containing pendant or integrated histidine and representing tri- or tetradentate ligands. The possibility of detecting any other than the ligating atoms of the amino acids and peptides was to be checked by Tc K-edge EXAFS analysis.

Experimental

The precursor complex $(NEt_4)_2[Tc(CO)_3Cl_3]$ was synthesized according to [3]. The precursor complex (2.5×10^{-5} mol) was dissolved in 2 ml water/methanol (1/1) and His, Gly-His, His-Gly, Gly-Gly-Gly, His-Gly-Gly, Gly-Gly-His, Gly-His-Lys (in an approximately 1.2-fold excess) and Gly, Gly-Gly (approximately 2-fold excess) were added. The samples were named **TcHis**, **TcGlyHis**, **TcHisGly**, **TcGlyGlyGly**, **TcHisGlyGly**, **TcGlyGlyHis**, **TcGlyHisLys**, **TcGly** and **TcGlyGly**. The final stage of the ligand exchange reaction was checked by HPLC and ESI mass spectrometry.
The Tc K-edge EXAFS spectra were recorded at the Rossendorf beamline [4]. All samples were measured in solution (Tc concentration ≈ 0.01 M, transmission mode, sample thickness ≈ 1 or 2 cm) at room temperature. The spectra were recorded in steps of 0.05 $Å^{-1}$ with gradually increasing counting time per data point from 2 to 20 s. The EXAFS spectra were obtained from two or three averaged scans. The EXAFS spectra were evaluated, using the program package EXAFSPAK; single and multiple effective scattering amplitude and wave phase-shift functions were generated with the theoretical EXAFS modeling code FEFF6 [5, 6]. Constraints between parameters of various scattering paths were set for the fits. For all paths the shift in threshold energy was forced to be the same. All other variables were freely floated, unless stated otherwise in the table of the results. The amplitude reduction factor was held constant at 0.9 for all fits.

Results and Discussion

In the studied systems amino, amido, carboxylato groups of the amino acids or peptides, chloride and the solvent molecules water and methanol represent possible ligands for the $[Tc(CO)_3]^+$ moiety, which requires three-fold coordination.
HPLC was performed to check whether a predominant single Tc species or several Tc species were formed in the solution, assuming that one peak in the $ß^-$ trace corresponds to one Tc species. In the reaction with Gly-Gly-Gly and the peptides with the C-terminal His, several Tc species were found simultaneously in each sample in contrast to the reaction products with the other amino acids or peptides. From a mixture of Tc species the main compound was isolated by semipreparative HPLC, but instability of the compounds was observed by rechromatography.
For all samples except for **TcGly**, we found m/z values of the ions $[Tc(CO)_3(L)]^-$ and $[Tc(CO)_3(L)]^+$ (L: amino acid or peptide charged minus one) using ESI-MS. For **TcGly** a m/z value of $[Tc(CO)_3GlyCl]^-$ was obtained, while the species with two Gly ligands or water and Gly bound to the $[Tc(CO)_3]^+$ moiety were not observed in the mass spectrum. Coordination of chloride with the $[Tc(CO)_3]^+$ moiety was not found for **TcGly** by EXAFS analysis (see below). A possible explanation for the contradiction could be seen in the ionization mechanism of the electrospray techniques. When charged sample droplets evaporate, their surface charge density increases until a “Coulomb explosion“ occurs which produces daughter droplets [7]. The chloride concentration increases in the droplet because of solvent evaporation and the equilibrium shifts to the species $[Tc(CO)_3GlyCl]^-$.

EXAFS measurements

We carried out EXAFS measurements only of samples showing one peak in the HPLC chromatogram (ß$^-$-ray detection).

To obtain a satisfactory interpretation of the EXAFS spectra and the Fourier transforms, single-scattering paths including the C, N/O coordination shells and multiple-scattering paths to model the oxygen atom of the carbonyl goups were taken into account. For evaluation of the EXAFS spectra effective scattering amplitude and wave phase-shift functions were generated, using simple atom clusters consisting of a Tc atom ideal-octahedrally surrounded by three facial CO groups and three N or O atoms or two N or O atoms and one Cl atom. In the Fourier transform peak A represents the C atom of the carbon monoxide and the mixed N/O coordination shell of the coordinated amino acids, peptides or solvent molecules, and peak B is the oxygen coordination shell of carbon monoxide (Figure 1). Fitting the experimental EXAFS data simultaneously with freely floated Debye-Waller factors, δ^2, and other parameters (see Table 1) resulted in high confidence limits for the coordination number, N, (about ± 1.0) and δ^2 of the N/O coordination shell. N and δ^2 are highly correlated variables in each EXAFS wave. As peak A in the Fourier transform is dominated by the backscattering off the C atoms, parameters describing the Tc-N/O scattering were obtained with a lower precision; δ^2 were therefore fixed at 0.003 Å^{-2} deduced from initial fit results.

Fitting the experimental EXAFS function with Tc-Cl single-scattering paths failed for all samples. Hence Cl coordination with the $[Tc(CO)_3]^+$ moiety can be excluded for all investigated samples, i. e. the chloride ligands of the precursor were substituted by amino acids, peptides or molecules of the solvent. The EXAFS measurements also confirm the mononuclear nature of the investigated complexes. The estimated atomic distances of the CO ligands square with those obtained for other Re(I) or Tc(I) tricarbonyl complexes. Single-crystal X-ray diffraction analyses of mononuclear Re(I) tricarbonyl complexes with imidazole, histamine, picolinic acid or picolinamine-N,N-diacetic acid show Re-N distances of 2.17, 2.08 Å (pyridine), 2.17 to 2.22 Å (imidazole), 2.18, 2.32 Å (amino group) and Re-O bond lengths of 2.14, 2.10 Å (carboxylic group) [3, 8]. The structure of $[Re(CO)_3His]$ with bond lengths of 2.19 Å (Re-N) and 2.15 Å (Re-O) was recently published [9]. The estimated bond lengths of the mixed Tc-N/O coordination shells are therefore in the expected range for similar Re complexes.

Several publications investigate peptide coordination, using XAFS analysis. The involvement of the peptide backbone chain in the metal chelate rings is proved in special cases by the multiple scattering approach, including carbonyl groups of the peptide backbone and backscattering from the peptide backbone carbon atoms. Detection of the oxygen of the peptide backbone carbonyl groups can be improved by the nearly colinear arrangement of the central atom and the carbonyl group resulting in a significant amplitude enhancement by foreward-scattering by the intervening C atom. This effect, however, drops off very rapidly for bond angles below 150° [10]. For instance, in the complex $[TcO(MAG_2)]^-$, six carbon atoms (Tc-C distance ≈ 2.95 Å) and three carbonyl groups (Tc-O distance ≈ 4.07 Å) of the peptide backbone are included in the chelate rings. These C or O atoms have only very small differences in their distance from the central atom, the angle Tc-C-O is about 160° [11]. The analogous coordination shells of a Re congener were detected by Re L_{III}-edge EXAFS analysis. In the Fourier transform, however, the height of the peak indicating the Re-O coordination shell of the peptide backbone carbonyl groups exceeds the background only three times [12]. In the investigated Tc complexes the coordination shells mentioned are also expected at roughly the same distance from the central atom. In the Fourier transform a peak expected at roughly 3.5 R + Δ [Å] on account of Tc-O backscattering of the peptide backbone carbonyl groups was not observed, perhaps due to the number of these ligands being too low, and/or the Tc-C-O arrangement deviates more from a linear one. The carbon atoms of the peptide backbone are expected at approximately the same distance as the oxygen atoms of carbon monoxide. They cannot be detected because of overlap with the very strong backscattering off the three oxygen atoms, which is enhanced by a strong multiple-scattering effect.

The evaluation of the EXAFS spectra for the investigated type of complexes shows that no detection of the imidazole ring is possible, which will be discussed in [13].

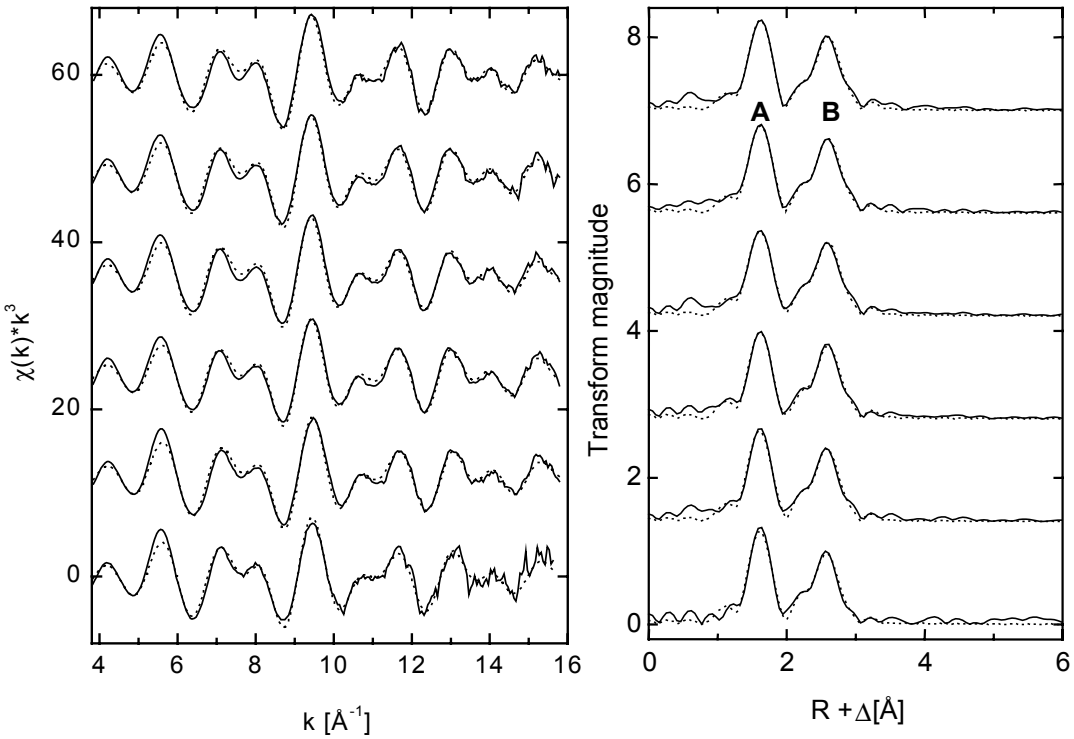

Fig. 1. Tc K-edge k^3-weighted EXAFS spectra and corresponding Fourier transforms of **TcHis** (above), **TcHisGly**, **TcHisGlyGly**, **TcGlyHisLys**, **TcGly**, **TcGlyGly** (below); solid line: experimental data, dotted line: fit.

Table 1. Structural parameters obtained by the Tc K-edge k^3-weighted EXAFS spectra of the samples **TcHis**, **TcHisGly**, **TcHisGlyGly**, **TcGlyHisLys**, **TcGly**, **TcGlyGly** (R: atomic distance, N: coordination number, σ^2: Debye-Waller factor).

Coordination shell	Sample	R [Å] [a)]	N	σ^2 [10^{-3} Å^2]
Tc-C	**TcHis**	1.91	3.2 ± 0.5	1.6 ± 0.7
	TcHisGly	1.91	3.2 ± 0.5	1.7 ± 0.6
	TcHisGlyGly	1.91	3.2 ± 0.5	1.8 ± 0.6
	TcGlyHisLys	1.91	2.7 ± 0.4	1.0 ± 0.6
	TcGly	1.90	3.1 ± 0.5	1.4 ± 0.6
	TcGlyGly	1.90	2.9 ± 0.6	1.0 ± 0.8
Tc-N/O	**TcHis**	2.20	3.2 ± 0.4	3.0 [1)]
	TcHisGly	2.20	3.1 ± 0.4	3.0 [1)]
	TcHisGlyGly	2.21	2.9 ± 0.4	3.0 [1)]
	TcGlyHisLys	2.20	2.8 ± 0.3	3.0 [1)]
	TcGly	2.20	3.2 ± 0.4	3.0 [1)]
	TcGlyGly	2.20	3.3 ± 0.5	3.0 [1)]
Tc-O_{CO} [2)]	**TcHis**	3.06	3.1 ± 0.4	2.9 ± 0.6
	TcHisGly	3.06	3.0 ± 0.4	2.8 ± 0.6
	TcHisGlyGly	3.06	3.2 ± 0.4	3.1 ± 0.6
	TcGlyHisLys	3.06	2.9 ± 0.3	2.9 ± 0.6
	TcGly	3.05	3.1 ± 0.4	3.2 ± 0.7
	TcGlyGly	3.05	3.3 ± 0.6	3.6 ± 0.9

[a)] The confidence limit is ± 0.02 Å.
[1)] The parameter were fixed.
[2)] The three scattering paths (2, 3 and 4 legs) were included. For the different paths, each of the parameters R, N and σ^2 were forced to have constant ratios during the fits.

To sum up, the reaction of the precursor $[Tc(CO)_3Cl_3]^{2-}$ with His, Gly and small peptides containing these amino acids was studied by HPLC, ESI-MS and EXAFS analysis in solution. EXAFS measurements confirmed the exchange of chloride, the mononuclear structure and typical structural parameters expected for such type of complexes. For all complexes, the same local structure was observed. Detection of any other than the ligating atoms of the amino acids or peptides was not possible. That could be realized in complexes in which the central atom is surrounded by a relatively large number of C atoms and carbonyl groups of the peptide backbone or imidazole rings and if the various coordination shells have a small distribution in distance; the angle between the central atom and the oxygen of the carbonyl groups is almost linear, and there is little overlapping with strong scattering paths (such as that from carbon monoxide). Furthermore, changing the experimental conditions to reduce the background (measurement at low temperature) and enlargement of the k-range of the EXAFS spectrum may improve the detectibility of those coordination shells.

Acknowledgments

We thank Harald Funke, Christoph Hennig and Andre Rossberg for their assistance during the EXAFS measurements at the ESRF at ROBL.

References

[1] Alberto, R.; Schibli, R.; Waibel, R.; Abram, U.; Schubiger, P. A. Basic aqueous chemistry of $[M(OH)_2(CO)_3]^+$ (M = Re; Tc) directed towards radiopharmaceutical application. Coordination Chem. Rev. 190-192 (1999), 901-919.

[2] Pietzsch, H.-J.; Gupta, A.; Reisgys, M.; Drews, A.; Seifert, S.; Syhre, R.; Spies, H.; Alberto, R.; Abram, U.; Schubiger, P. A.; Johannsen, B. Chemical and biological characterization of technetium(I) and rhenium(I) tricarbonyl complexes with dithioether ligands serving as linkers for coupling the $Tc(CO)_3$ and $Re(CO)_3$ moieties to biologically active molecules. Bioconj. Chem. 11 (2000) 414-424.

[3] Schibli R. Normaldrucksynthese von $[TcCl_3(CO)_3]^{2-}$ und $[ReCl_3(CO)_3]^{2-}$ und ihr Substitutionsverhalten im Hinblick auf Anwendungen in der Nuklearmedizin. Universität Basel, Thesis (1996).

[4] Matz, W.; Schell, N.; Bernhard, G.; Prokert, F.; Reich, T.; Claußner, J.; Oehme, W.; Schlenk, R.; Dienel, S.; Funke, H.; Eichhorn, F.; Betzl, M.; Pröhl, D.; Strauch, U.; Hüttig, G.; Krug, H.; Neumann, W.; Brendler, V.; Reichel, P.; Denecke, M. A.; Nitsche, H. ROBL - a CRG beamline for radiochemistry and materials research at the ESRF. J. Synchrotron Rad. 6 (1999) 1076-1085.

[5] George, G. N.; Pickering, I. J. EXAFSPAK: A Suite of Computer Programms for Analysis of X-ray Absorption Spectra. Stanford Synchrotron Radiation Laboratory, Stanford, CA, USA (1995).

[6] Zabinsky, S. I.; Rehr, J. J.; Ankudinov, A.; Albers, R. C.; Eller, M. J. Multiple-scattering calculations of X-ray-absorption spectra. Phys. Rev. B 52 (1995) 2995-3009.

[7] Fenn, J. B.; Mann, M.; Meng, C. K.; Wong, S. F. Electrospray ionization-principles and practice. Mass Spectrometry Rev. 9 (1990) 37-70.

[8] Alberto, R.; Schibli, R.; Egli, A.; Schubiger, A. P. A novel organometallic aqua complex of technetium for the labeling of biomolecules: synthesis of $[^{99m}Tc(OH_2)_3(CO)_3]^+$ from $[^{99m}TcO_4]^-$ in aqueous solution and its reaction with a bifunctional ligand. J. Am. Chem. Soc. 120 (1998), 7987-7988.

[9] Schibli, R.; La Bella, R.; Alberto, R.; Garcia-Garayoa, E.; Ortner, K.; Abram, U.; Schubiger, P.A. Influence of the denticity of ligand systems on the in vitro and in vivo behavior of $^{99m}Tc(I)$ tricarbonyl complexes: a hint for the future functionalization of biomolecules. Bioconjugate Chem. 11 (2000), 345-351.

[10] Teo, B. K. EXAFS: Basic Principles and Data Analysis. Berlin Springer-Verlag (1998).

[11] Johannsen, B.; Noll, B.; Leibnitz, P.; Reck, G.; Noll, S.; Spies, H. Occurrence and nature of different Tc(V) and Re(V) complexes with mercapto/amide ligands. Radiochim. Acta 63 (1993) 133-137.

[12] Jankowsky, R. Strukturuntersuchung an Peptidkomplexen von Technetium und Rhenium. TU Dresden, Thesis (1998).

[13] Künstler, J.-U.; Seifert, S.; Reich, T.; Funke, H.; Johannsen, B. EXAFS analyses of technetium(I) tricarbonyl complexes – ligand exchange studies. Speciation, Techniques and Facilities for Radioactive Materials at Synchrotron Light Sources, Workshop Proceedings Grenoble, France 10-12. 09. 2000 (accepted).

18. EXAFS Analyses of Technetium and Rhenium Complexes

4. EXAFS Analyses of the Complexes $[Re(CO)_3(Phe)(PPh_3)]$ and $[Re(CO)_3(Phe)(H_2O)]$ – Comparison with the EXAFS Spectra of a Binuclear Oxorhenium(V) Complex Measured at Room Temperature and 15 K

J.-U. Künstler, S. Seifert, H.-J. Pietzsch, T. Reich[1], H. Funke[1], R. Alberto[2], B. Johannsen
[1]Institute of Radiochemistry, [2]Institute of Inorganic Chemistry, University of Zurich, Switzerland

Introduction

One of us (R. Alberto) obtained two rhenium complexes in solid form with the assumed formula $[Re(CO)_3(Phe)(H_2O)]$, **Re1**, and as reference $[Re(CO)_3(Phe)(PPh_3)]$, **Re2.** For **Re1**, a binuclear structure can be discussed. We wanted to carry out EXAFS measurements to compare structural parameters of these complexes and to clarify whether **Re1** is a mononuclear or a binuclear complex. The well-characterized complex $[ReO(S\text{-}S)_2Cl_2]_2O$, **Re3**, (S-S = 5,8-dithiadodecane) served as a reference for an oxygen bridged binuclear complex [1].
Moreover, EXAFS spectra of the binuclear reference complex were recorded both at room temperature (RT) and 15 K in order to evaluate the new possibility for XAFS measurements at temperatures down to 15 K for Re or Tc EXAFS studies which is available at the Rossendorf beamline since the end of 1999.

Experimental

All EXAFS spectra were recorded in transmission mode at the Re L_{III}-edge (10535 eV) using a water-cooled Si(111) double-crystal monochromator of fixed-exit type. The complexes were measured as solids. 17 mg of **Re1**, 40 mg of **Re2** and 20 mg of **Re3** were mixed with 200 mg Teflon powder and pressed into pellets, respectively. The spectra were recorded in steps of 0.05 $Å^{-1}$ with gradually increasing counting time per data point from 2 to 30 s for **Re1, Re2** and to 20 s for **Re3**. The energy of the first inflection point of the Re L_{III}-edge spectrum was defined as 10535 eV, and the ionization energy for the Re L_{III} electron was arbitrarily set to 10555 eV. All samples were measured at room temperature. In addition, sample **Re3** was also measured at a temperature of 15 K using a closed-cycle He cryostat.
The EXAFS spectra for **Re1** and **Re2** were obtained from two averaged scans and the EXAFS spectra for **Re3** from single scans, respectively. The EXAFS spectra were evaluated using the program package EXAFSPAK; single and multiple effective scattering amplitude and wave phase-shift functions were generated with the theoretical EXAFS modeling code FEFF6 [2, 3]. For the fits, constrains between parameters of different scattering paths were set. For all paths the shift in threshold energy was forced to be the same. All other variables were freely floated if not stated otherwise in the table with the results. The amplitude reduction factor was held constant at 0.9 for all fits.

Results and Discussion

EXAFS analyses of the complexes $[Re(CO)_3(Phe)(PPh_3)]$ and $[Re(CO)_3(Phe)(H_2O)]$
To obtain a satisfactory interpretation of the EXAFS spectra and the Fourier transforms, single-scattering paths including the C, N/O or P coordination shells and multiple-scattering paths to model the oxygen atom of the carbonyl groups were taken into account. For evaluation of the EXAFS spectra, effective scattering amplitude and wave phase-shift functions were generated using simple atom clusters consisting of a Re atom which is ideal-octahedrally surrounded by three facial CO groups and three N or O atoms for **Re1** and two N or O atoms and one P atom for **Re2**.
In the Fourier transform, peak A represents mainly the C coordination shell, peak B the P atom (**Re2**) and peak C the O coordination shell of CO (Fig. 1). The coordination of the N and O atoms contributes mainly to peaks A and B. The coordination of an O atom from the assumed water coordination (**Re1**) in comparison with the coordination of a P atom (**Re2**) causes the loss of peak B in the Fourier transform because oxygen is a weaker back-scatterer compared to phosphorus. EXAFS analysis of **Re1** shows approximately the same structural parameters for the N/O, C and CO coordination shells like the reference **Re2** except the fact that the coordination number for the N/O coordination shell is increased by one and no P coordination shell is found (Table 1). This fact confirms the coordination of an additional O-ligand like water in **Re1**.
The estimated atomic distances are almost the same as found by single-crystal X-ray diffraction analyses and EXAFS measurements of similar ligands-bearing Re or Tc tricarbonyl complexes [4 - 6]. The obtained coordination numbers agree with the expected values.

EXAFS spectroscopy is extremely useful for detecting metal-metal interactions [7]. Backscattering from a heavy atom like Re in a binuclear Re complex has a strong effect on the EXAFS spectrum and causes a characteristic peak in the Fourier transform. For a μ–oxo Re complex, an intensive peak at roughly 4 R + Δ [Å] in the Fourier transform is expected (see Fig. 3 and Table 2). That is not observed for **Re1** - hence, it follows that **Re1** represents a mononuclear complex. The mononuclear structure of **Re2** is also confirmed.

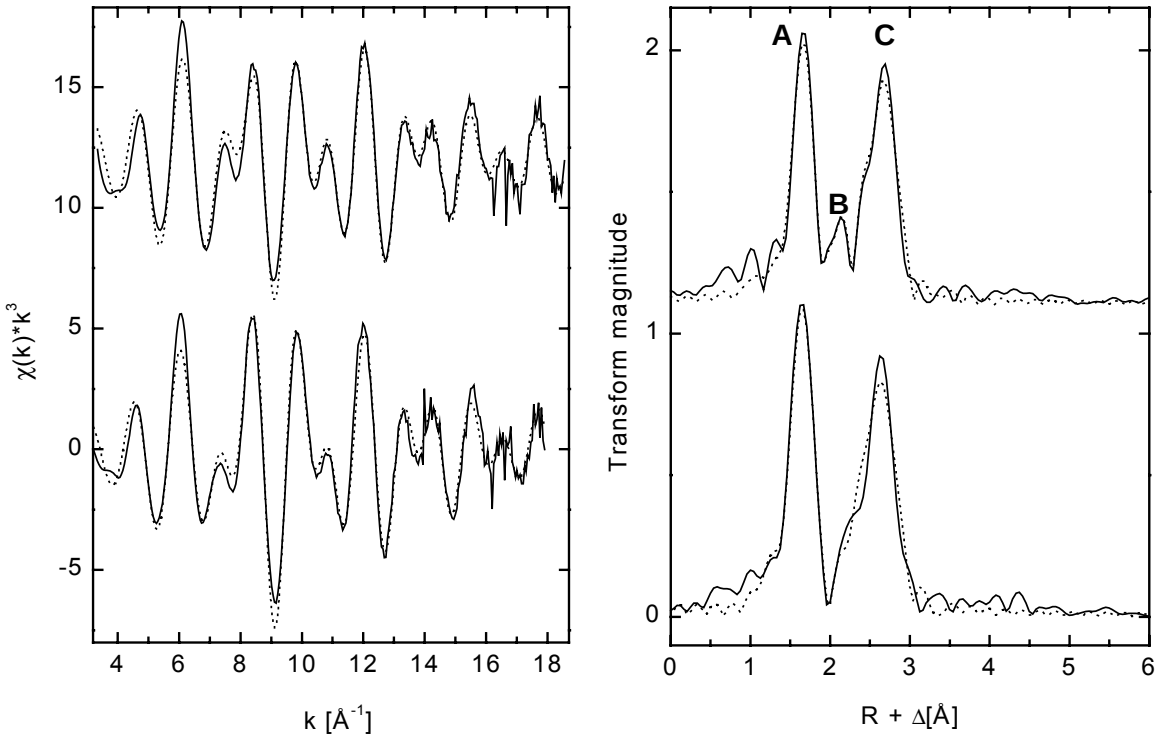

Fig. 1. Re L_{III}-edge k^3-weighted EXAFS spectra and corresponding Fourier transforms of **Re2** (above) and **Re1** (below); solid line: experimental data, dotted line: fit.

Table 1. Structural parameters obtained by the Re L_{III}-edge k^3-weighted EXAFS spectra of **Re1** and **Re2** (R: atomic distance, N: coordination number, σ^2: Debye-Waller factor).

	Re1			**Re2**		
Path	R [Å] [a)]	N	σ^2 [10^{-3} Å^2]	R [Å] [a)]	N	σ^2 [10^{-3} Å^2]
Re-C	1.91	2.9 ± 0.5 [1)]	1.8 ± 0.7	1.92	2.7 ± 0.4 [1)]	1.6 ± 0.6
Re-N/O	**2.16**	**3.5 ± 0.8**	4.1 ± 1.3	**2.19**	**2.4 ± 0.4** [2)]	3.6 ± 1.1
Re-P				**2.50**	**1.2 ± 0.2** [2)]	5.9 ± 2.1
Re-C-O (3 legs)	3.06 [1)]	5.9 ± 1.0 [1)]	2.3 ± 0.5 [1)]	3.07 [1)]	5.3 ± 0.8 [1)]	2.2 ± 0.4 [1)]
Re-C-O (2 and 4 legs)	3.06 [1)]	2.9 ± 0.5 [1)]	2.3 ± 0.5 [1)]	3.07 [1)]	2.7 ± 0.4 [1)]	2.2 ± 0.4 [1)]

[a)] The confidence limit is ± 0.02 Å.
[2)] In each column, identically marked parameters were forced to have constant ratios during the fits.

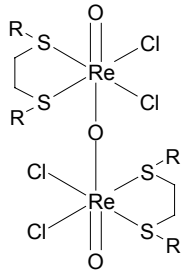

Fig. 2 Representation of $[ReO(S\text{-}S)_2Cl_2]_2O$, **Re3**, (S-S = 5,8-dithiadodecane) used as reference for an oxygen bridged binuclear complex.

EXAFS analyses of **Re3** show a shape of the Fourier transform and structural parameters which are evidently for a binuclear complex (Fig 3. and Table 2).
To obtain a satisfactory interpretation of the EXAFS spectra and the corresponding Fourier transforms, the following single-scattering paths had to be included in the fit to the experimental EXAFS data: Re-S/Cl (N = 4); Re-O (Re=O, N = 1) and Re-O (Re-O-Re, N = 1). Given in parentheses are the coordination numbers N derived from the single-crystal X-ray diffraction analysis [1]. To model the Re coordination shell, the equivalent multiple-scattering paths Re-O-Re-Re and Re-Re-O-Re (3-legs, degeneracy of 2), the non-degenerated path Re-O-Re-O-Re (4-legs) and the single-scattering path Re-Re were taken into account (Table 2). All other possible scattering paths did not lead to a significant improvement of the fit results. Effective scattering amplitude and wave phase-shift functions were generated using a simple atom cluster consisting of a Re atom which is ideal-octahedrally surrounded by four equatorial S or Cl atoms and one axial O atom and oppositely axial O and Re atoms linear arranged.
The peak system A in the Fourier transform represents the coordination of the O, S and Cl atoms and the peak B the coordination shell of the second Re atom (Fig. 3). The estimated atomic distances square with those obtained by single-crystal X-ray diffraction analysis (Table 2).

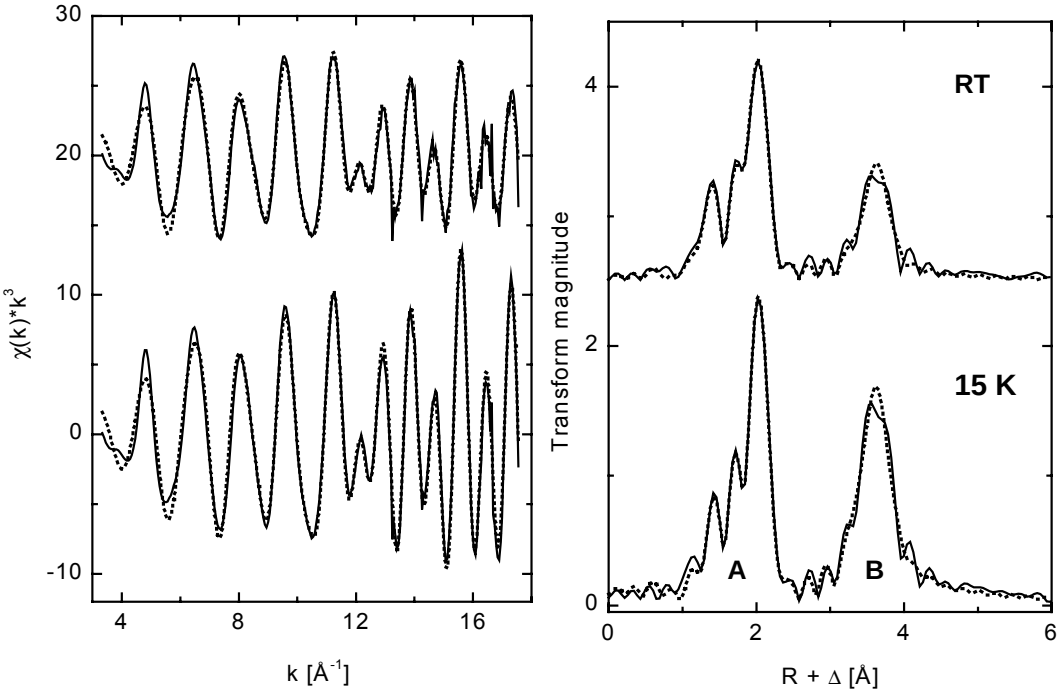

Fig. 3. Re L_{III}-edge k^3-weighted EXAFS spectra and corresponding Fourier transforms of **Re3** measured at RT and 15 K; solid line: experimental data, dotted line: fit.

Table 2. Structural parameters obtained by the Re L_{III}-edge k^3-weighted EXAFS spectra of **Re3** measured at RT and 15 K (R: atomic distance, N: coordination number, σ^2: Debye-Waller factor) - Comparison with atomic distances obtained by single-crystal X-ray diffraction analysis.

Path	T	R [Å]		N	σ^2 [10^{-3} Å]
		EXAFS [a]	XRD [3]		
Re-O (Re=O)	RT	1.70	1.72	1.0 ± 0.3 [1]	0.8 ± 1.1
	15 K	1.70		0.9 ± 0.3 [1]	0.4 ± 1.8
Re-O (Re-O-Re)	RT	1.93	1.93	1.0 ± 0.3 [1]	2.3 ± 1.4
	15 K	1.93		0.9 ± 0.3 [1]	1.0 ± 1.2
Re-S/Cl	RT	2.41	2.41	4.2 ± 0.4	3.6 ± 0.5
	15 K	2.41		4.2 ± 0.3	2.4 ± 0.3
Re-O-Re (3 legs)	RT	3.85 [1]	3.85	1.7 ± 0.6 [2]	2.0 ± 0.7 [1]
	15 K	3.85 [1]		1.7 ± 0.4 [2]	0.6 ± 0.4 [1]
Re-O-Re (4 legs) and Re-O-Re (2 legs)	RT	3.85 [1]	3.86 (4 legs) 3.83 (2 legs)	0.9 ± 0.3 [2]	2.0 ± 0.7 [1]
	15 K	3.85 [1]		0.9 ± 0.2 [2]	0.6 ± 0.4 [1]

[a] The confidence limit is ± 0.02 Å.
[1] [2] In each column, identically marked parameters were forced to have constant ratios during the fit.
[3] [1]

Measurement at 15 K results in a decrease of noise. The Debye-Waller factor, σ^2, is the mean-square relative displacement of absorber and backscatterer atoms caused by thermal vibrations and static disorder. The measurement at low temperature results in a decreasing of the thermal vibration and therefore of σ^2 (Table 2). That causes an increase of the EXAFS amplitude. This effect increases exponentially as k increases. In the Fourier transform the peaks are narrowed and enlarged in height (Fig. 2) [8]. In special cases, detection of backscatterer atoms which are not detectable at RT could be possible at low temperatures.
The expected resolution in distance, δR, is given by the ratio $\delta R = \pi / 2 \Delta k$ (Δk: k range of the EXAFS data). To improve the resolution in distance, it is necessary to enlarge Δk, i. e., the energy range of an EXAFS measurement. Usually, the evaluation of an EXAFS spectrum recorded at RT is limited by noise at higher k values. For Re compounds it is not possible to enlarge Δk because the Re L_{III}-edge spectrum at 10535 eV overlaps with the L_{II}-edge at 11959 eV. On the other hand EXAFS spectra of Tc compounds can be obtained with a larger Δk due to the possibility to measure at the Tc K-edge at 21044 eV. The Re K-edge (71676 eV) is outside of the energy range of the synchrotron beam (5 – 35 keV) which is provided by the Rossendorf beamline [9]. Hence, EXAFS analyses should be carried out on the Tc congeners to fully exploit the advantages of a measurement at low temperature. Generally, the measurement at low temperature connected with an enlargement of the available Δk of an EXAFS spectrum results in a better resolution of the coordination shells and a determination of the structural parameters with a higher degree of precision.

Acknowledgments

We would like to thank Christoph Hennig and Andre Roßberg for assistance during the EXAFS measurements.

References

[1] Pietzsch, H.-J.; Spies, H.; Leibnitz, P.; Reck, G. Technetium and rhenium complexes with thioether ligands – IV. synthesis and structural characterization of binuclear oxorhenium(V) complexes with bidentate thioether coordination. Polyhedron 14 (1995) 1849-1853.
[2] George, G.N.; Pickering, I.J. EXAFSPAK: A Suite of Computer Programms for Analysis of X-ray Absorption Spectra. Stanford Synchrotron Radiation Laboratory, Stanford, CA, USA (1995).
[3] Zabinsky, S.I.; Rehr, J.J.; Ankudinov, A.; Albers, R.C.; Eller, M.J. Multiple-scattering calculations of X-ray-absorption spectra. Phys. Rev. B 52 (1995) 2995-3009.
[4] Schibli, R.; La Bella, R.; Alberto, R.; Garcia-Garayoa, E.; Ortner, K.; Abram, U.; Schubiger, P.A. Influence of the denticity of ligand systems on the in vitro and in vivo behavior of ^{99m}Tc(I)- tricar-

bonyl complexes: A hint for the future functionalization of biomolecules. Bioconjugate Chem. 11 (2000) 345-351.
[5] Schibli, R. Normaldrucksynthese von $[TcCl_3(CO)_3]^{2-}$ und $[ReCl_3(CO)_3]^{2-}$ und ihr Substitutionsverhalten im Hinblick auf Anwendung in der Nuklearmedizin. University of Basel, Thesis (1996).
[6] Künstler, J.-U.; Seifert, S.; Reich, T.; Funke, H.; Johannsen, B. EXAFS analyses of technetium(I) tricarbonyl complexes – ligand exchange studies. Speciation, Techniques and Facilities for Radioactive Materials at Synchrotron Light Sources, Workshop Proceedings Grenoble, France 10-12. 09. 2000 (accepted).
[7] Penner-Hahn, J.E. X-ray absorption spectroscopy in coordination chemistry. Coord. Chem. Rev. 190-192 (1999) 1101-1123.
[8] Teo, B.K. EXAFS: Basic Principles and Data Analysis. Berlin Spriner-Verlag (1988).
[9] Matz, W.; Schell, N.; Bernhard, G.; Prokert, F.; Reich, T.; Claußner, J.; Oehme, W.; Schlenk, R.; Dienel, S.; Funke, H.; Eichhorn, F.; Betzl, M.; Pröhl, D.; Strauch, U.; Hüttig, G.; Krug, H.; Neumann, W.; Brendler, V.; Reichel, P.; Denecke, M. A.; Nitsche, H. ROBL - a CRG beamline for radiochemistry and materials research at the ESRF. J. Synchrotron Rad. 6 (1999) 1076-1085.

19. ITC Analysis of Binding Perrhenate Using Monopyridinium-α-Cyclodextrin

H. Stephan, H. Spies, B. Johannsen, E. Nicoletti[1], F. P. Schmidtchen[1]
[1]Institut für Organische Chemie und Biochemie, Technische Universität München

Introduction

Owing to their suitable nuclear properties the β-particle emitting radionuclides ^{186}Re and ^{188}Re are gaining in importance in the development of therapeutic agents in nuclear medicine [1 - 3]. ^{188}Re is conveniently available as "carrier free" perrhenate anion from a ^{188}W/^{188}Re generator system. Hence it appears highly desirable to directly complex this anion in the generator eluate. The binding of such a large, lowly charged anion requires hosts which are able to form inclusion compounds. In this nexus cyclodextrins may be very promising agents [4 - 6]. Especially the cage cavity of α-cyclodextrin [470...530 pm) should be ideally suited for inclusion of the perrhenate anion having a diameter of 520 pm [7]. In order to enhance the binding strength to the monovalent perrhenate anion a pyridinium moiety is introduced into the α-cyclodextrin scaffold (cf. Fig. 1).
In this paper we report the thermodynamic data of the complexation of the anions perrhenate and perchlorate [8] by α-cyclodextrin (α-CD) and monopyridinium-α-cyclodextrin (Pyr-α-CD) in aqueous solution. The complexation behaviour was studied by isothermal titration calorimetry (ITC).

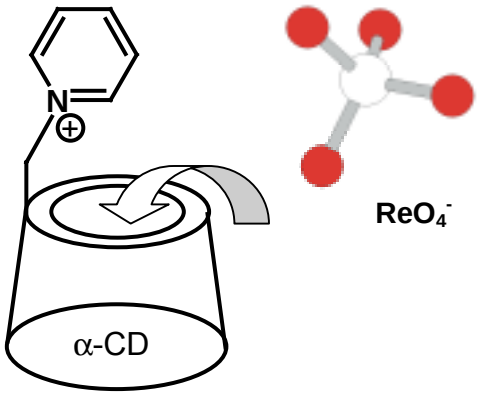

Fig. 1. Conceptual sketch of binding perrhenate by monopyridinium-α-cyclodextrin

Experimental

All chemicals were reagent grade and used as obtained. α-CD was received from Fluka. Pyr-α-CD was prepared according the route described by Matsui *et al.* [9, 10]. Thus, α-CD was sharply dried in vacuum (0.05 Torr) at 105 °C for 2 days. After reaction with 2-mesitylenesulphonyl chloride the monosubstituted C(6)-O-sulfonylated α-cyclodextrin was isolated, using column chromatography (RP-8). This product was converted into 6-deoxy-6-(1-pyridino)-α-cyclodextrin by refluxing in dry pyridine. Cation exchange (Sephadex C-25) was applied for purification. Elution with ammonium hydrogencarbonate solution followed by evaporation to dryness produced to the corresponding hydrogencarbonate salt. 0.04 M stock solutions of α-CD and Pyr-α-CD in aqueous NaCl (0.9%) were prepared. These solutions were diluted to the appropriate concentration for calorimetric titration, using aqueous NaCl. The experiments were performed in an isothermal titration calorimeter (MicroCal Inc., Northampton/USA) at 303 K. The degassed host solution (0.01...0.015 M CD in aqueous NaCl) was filled into the sample cell (1.3 ml) and 0.15 M $NaClO_4$ ($NaReO_4$) in aqueous NaCl was titrated, using a burette syringe (250 µl). 50 injections of 4.5 µl for α-CD and 60 injections of 2 µl for Pyr-α-CD were chosen at 300 second intervals. Blank titration was carried out under the same experimental conditions (metal salt solution into aqueous NaCl). Data collection and analysis were performed with MicroCal-Origin ITC software.

Results and Discussion

The thermodynamic parameters for the association of α-CD with sodium perchlorate were at first determined and compared with known data from the literature (cf. Table 1). There was a good agreement between our experimental results with the literature data [12, 14 - 17]. The thermodynamic parameters obtained by *Hansen* [11] and *Kaifer* [13] slightly differed from the other results, obviously due to the choice of an unsuitable concentration range for calorimetric titration.
Table 2 summarizes the thermodynamic parameters for the complexation of perchlorate and perrhenate with α-CD and Pyr-α-CD. In all cases a clean 1:1 host-guest association was pointed out by ITC analysis (cf. Fig. 2). The association constant of α-CD with perrhenate was 2.6 times higher than with perchlorate. This was mainly caused by a less negative entropic contribution for the perrhenate inclusion. As expected the K_{ass} value increased when the pyridinium unit is introduced into the cyclodextrin skeleton. In addition to stabilizing the anion in the cyclodextrin cage by *van-der-Waals* interactions and forming hydrogen bonds, electrostatic attraction amplified the host-guest binding.

Table 1. Thermodynamic parameters for the complexation of α-CD with perchlorate

K [M^{-1}]	ΔG^0 [kJ·mol^{-1}]	ΔH^0 [kJ·mol^{-1}]	$T\Delta S^0$ [kJ·mol^{-1}]	Method	Reference
24 ± 0.5*	-8.0	-25.4 ± 0.3	-17.4	Cal (ITC)	This work
19.9**	-7.5	-41 ± 5	-29	Cal (IPC)	[11]
42 ± 2**	-9.0	-25.9 ± 0.3	-16.9	Cal (IPC)	[12]
66 ± 5**	-10.4	-15.8 ± 1	- 5.4	Cal (FMC)	[13]
45.8**	-9.5	-26.4 ± 0.8	- 16.4	Pot	[14]
28.9**				Cond	[15, 16]
29.4**				Spec	[17]

*: 303 K, **: 298 K, IPC: Isoperibolic calorimeter, FMC: Flow microreaction calorimeter, Pot: pH potentiometry
Cond: Conductance measurements, Spec: Spectrophotometric measurements

Table 2. Thermodynamic parameters for the complexation of perchlorate and perrhenate with α-CD and Pyr-α-CD under ITC study in aqueous NaCl at 303 K

System	K [M^{-1}]	ΔG^0 [kJ·mol^{-1}]	ΔH^0 [kJ·mol^{-1}]	$T\Delta S^0$ [kJ·mol^{-1}]
$NaClO_4$/α-CD	24 ± 0.5	-8.0	-25.4 ± 0.3	-17.4
$NaReO_4$/α-CD	62.4 ± 2.2	-10.4	-23.9 ± 0.4	-13.5
$NaClO_4$/Pyr-α-CD	130 ± 2.5	-12.2	-31.9 ± 0.3	-19.7
$NaReO_4$/Pyr-α-CD	124 ± 1.7	-12.2	-32.1 ± 0.2	-19.9

The thermodynamic parameters for complexation of perchlorate and perrhenate with Pyr-α-CD are almost the same. In comparison with the unsubstituted CD, the monopyridinium host shows a more favourable enthalpic term. On the other hand, the more negative value of TΔS compensates part of free energy for host-guest complexation.

To sum up, derivatives of α-CD seem to be well suitable for binding perrhenate in aqueous solution. However, in view of the complexation of $^{188}ReO_4^-$ in the generator eluate, the stability of host-guest complexes has to improved. One way of doing this may be the progressive replacement of the 6-hydroxy group in α-CD by positively charged functional groups. In this relation it is known that the hexapyridino derivative of α-CD forms complexes with iodide, obtaining an association constant of almost 10^6 M^{-1} in water [10]. Furthermore the entropic term for the complexation reaction of perrhenate with α-CD derivatives has to be more favourable. The most promising way of achieving this seems to be the preorganization of host molecules.

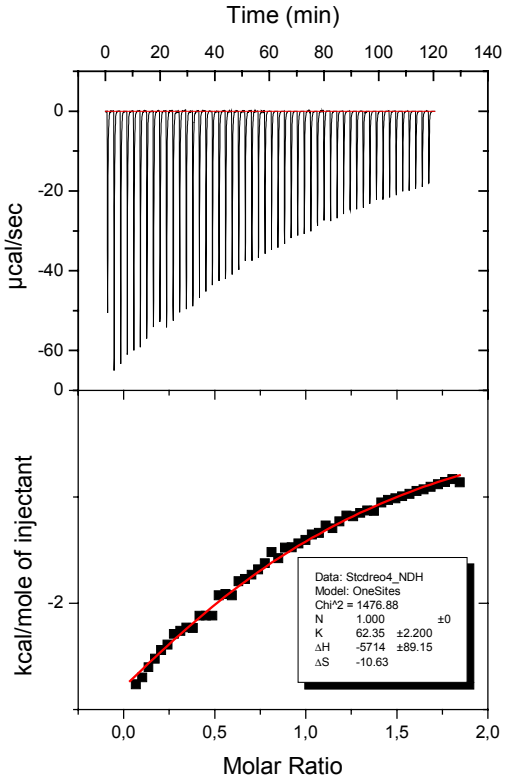

Fig. 2. ITC analysis of the α-CD-perrhenate host-guest binding

References

[1] Volkert, W.A.; Hoffman, T.J. Therapeutic radiopharmaceuticals. Chem. Rev. 99 (1999) 2269-92.

[2] Heeg, M.J.; Jurisson, S.S. The role of inorganic chemistry in the development of radiometal agents for cancer therapy. Acc. Chem. Res. 32 (1999) 1053-60.

[3] Blower, P.J.; Prakash, S. The chemistry of rhenium in nuclear medicine. Perspectives on Bioinorganic Chemistry, JAI Press 1999, 4 (1999) 91-143.

[4] Saenger, W.: Cyclodextrin-Einschlußverbindungen in Forschung und Industrie. Angew. Chem. 92 (1980) 343-61.

[5] Li, S.; Purdy, W.C. Cyclodextrins and their applications in analytical chemistry. Chem. Rev. 92 (1992) 1457-70.

[6] Rekharsky, M.V.; Inoue, Y. Complexation thermodynamics of cyclodextrins. Chem. Rev. 98 (1998) 1875-1917.

[7] Marcus, Y. Ion Properties, Marcel Dekker 1997, New York-Basel-Hong Kong.

[8] Perchlorate was chosen as reference anion, because there are many experimental data about the association with α-cyclodextrin.

[9] Matsui, Y.; Fujie, M.; Hanaoka, K. Host-guest complexation of mono[6-(1-pyridino)-6-deoxy]- α-cyclodextrin with several inorganic anions. Bull. Chem. Soc. Jpn. 62 (1989) 1451-57.

[10] Matsui, Y.; Fujie, M.; Sakate, H. Host-guest complexation of 6-deoxy-6-(1-pyridino) derivaties of α-cyclodextrin (cyclomaltohexaose) with inorganic anions in aqueous solution. Carbohydr. Res. 192 (1989) 91-95.

[11] Lewis, E.A.; Hansen, L.D. Thermodynamics of binding of guest molecules to α- and β-cyclodextrins. J. Chem. Soc., Perkin Trans. 2 (1973) 2081-85.

[12] Spencer, J.N.; He, Q.; Ke, X.; Wu, Z.; Fetter, E. Complexation of inorganic anions and small organic molecules with alpha-cyclodextrin in water. J. Sol. Chem. 27 (1998) 1009-19.

[13] Godínez, L.A.; Schulze-Fiehn, B.G.; Patel, S.; Criss, C.M.; Evanseck, J.D.; Kaifer, A.E. Observation and interpretation of anomalous inorganic anion binding with α- and β-cyclodextrins in aqueous media. Supramol. Chem. 8 (1996) 17-22.

[14] Gelb, R.I.; Schwartz, L.M.; Radeos, M.; Laufer, D.A. Cycloamylose complexation of inorganic anions. J. Phys. Chem. 87 (1983) 3349-54.

[15] Wojcik, J.F.; Rohrbach, R.P. Small anion binding to cycloamylose. Equilibrium constants. J. Phys. Chem. 79 (1975) 2251-53.

[16] Rohrbach, R.P.; Rodriguez, L.J.; Eyring, E.M.; Wojcik, J.F. An equilibrium and kinetic investigation of salt-cycloamylose complexes. J. Phys. Chem. 81 (1977) 944-48.

[17] Cramer, F.; Saenger, W.; Spatz, H.-Ch. Inclusion compounds. XIX. The formation of inclusion compounds of α-cyclodextrin in aqueous solutions. Thermodynamics and kinetics. J. Am. Chem. Soc. 89 (1967) 14-20.

20. Benzodiazepine Technetium Complexes

A. Drews, R. Syhre, P. Brust, A. Nudelman[1], H.- J. Pietzsch, B. Johannsen
[1]Bar Ilan Universität, Raman Gan, Israel

Introduction

Benzodiazepines are known to have clinically relevant anxiolytic, muscle relaxant and anticonvulsant effects and they are among the most widely prescribed psychotropic medications [1]. Some of these drugs have been used to develop ^{11}C and ^{123}I labelled radiopharmaceuticals for benzodiazepine receptor studies in neurologic disorders [2, 3].
We are interested in ^{99m}Tc- labelled benzodiazepines. Technetium carbonyl complexes with a benzodiazepine ligand were described by Marchi *et al.* [4].
In this study we synthesized "3+1" technetium complexes (**Tc1**, **Tc2**) bearing demoxepam [5] derivative moieties by reduction of pertechnetate with stannous chloride in a mixture of monothiol ligands (7-chloro-1,3-dihydro-5-phenyl-2H-1,4-benzodiazepin-1-(propylthiol)-2-oxo-4-oxide) (**L1**) and (7-chloro-1,3-dihydro-5-phenyl-2H-1,4-benzodiazepin-1-(butylthiol)-2-oxo-4-oxide) (**L2**) with a tridentate dithiol ligand (3-methylazapentane-1.5-dithiol) (**SNMeS**).
The new complex Tc1 was investigated for its *in-vitro* benzodiazepine receptor affinity [6, 7]. The biodistribution of both compounds (Tc1, Tc2) was studied in rats.

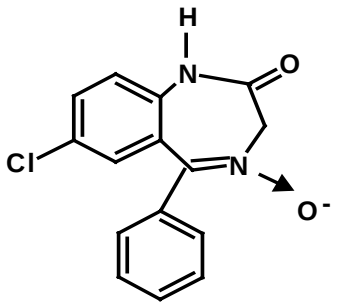

Fig.1. Demoxepam

Experimental

Preparation of the technetium complexes

C.a. preparation
The synthesis of the [^{99}Tc]Tc1 reference compound was performed by transchelation from ^{99}Tc gluconate. It was purified by semipreparative HPLC on a Hypersil ODS column and by passing it through a silica gel column with ethyl acetate / MeOH (1:1) as an eluent.
The synthesis of the [^{99}Tc]Tc2 reference compound was carried out as described in this report [8].
The ^{99}Tc compounds were characterized by mass spectrometry on a Micromass Tandem Quadrupole Mass Spectrometer (Quattro LC) operating in the MS mode. Mass spectral data were recorded in the positive ESI mode, using a cone voltage of 30 - 35 V. A solution of about 0.1 mg of the ^{99}Tc complex in 1 ml acetonitrile was injected at a flow rate of 5 µl/min.
The values confirmed the assumed composition:
MS-**Tc1** ES^+: m/z (found) 624 (M+), m/z (calc.) 623 for [^{99}TcO(SNMeS)/L1]
MS-**Tc2** ES^+: m/z (found) 638 (M^+), m/z (calc.) 637 for [^{99}TcO(SNMeS)/L2].
N.c.a. preparation
The oxotechnetium(V)complexes were synthesized in a reaction as described by Seifert et al [9, 10] and purified as desribed in this report [8].
The partition coefficient was measured by the shake-flask method.

Receptor binding assay
The preparation of rat occipital cortex was performed as previously described [11]. The [^{99}Tc]**Tc1** compound for the benzodiazepine receptor was used for the binding assay.
To determine the IC_{50} value for this compound, various concentrations of the [^{99}Tc]**Tc1** complex were incubated with cold Tris/HCl buffer (50 mM, pH 7.4) containing 0.12 nM [^{3}H]flunitrazepam and 0.16 mg/ml protein in a final volume of 5 ml. Non specific binding was determined by addition of 10 mM

GABA to the incubate. Incubation was at 7 °C for 90 min. The binding assay was terminated by rapid filtration through GF/B fibre filters (Whatman). The filters were rapidly washed three times with 5 ml of ice cold buffer, transferred into 4 ml of scintillation fluid (Ultima-Gold, Packard) and analysed for radio-activity (by liquid scintillation counting (Beckman-LS600-LL).
The protein content was estimated according to the method of Lowry *et al.* [12].

Biodistribution experiments
The biodistribution in rats was carried out as described in the previous report [8].

Results and Discussion

As shown in Table 1, ^{99}Tc complexes were obtained in 20 to 30 % yields after purification. The ^{99m}Tc complexes were obtained in 50 to 80 % yields in a radiochemical purity of over 95 % after purification. The [^{99}Tc]**Tc1** compound displayed a low *in-vitro* affinity of 467 ± 6 nM to the benzodiazepine receptor. The partition coefficients (log $P_{O/W}$) of both ^{99m}Tc complexes (**Tc1, Tc2**) are very similar, regardless of the small variation in the spacer length (C_3 versus C_4) of the benzodiazepine moiety.

Table 1. 3+1 mixed-ligand [$^{99/99m}$TcO(SNMeS)/L)] complexes **Tc1** and **Tc2** used for biodistribution studies in rats

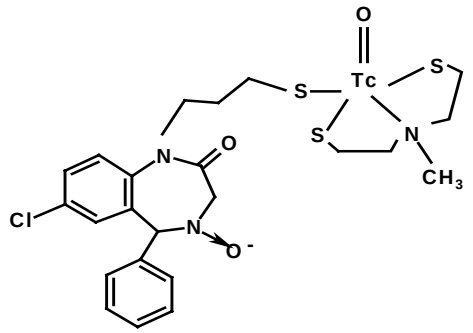 **Tc1**		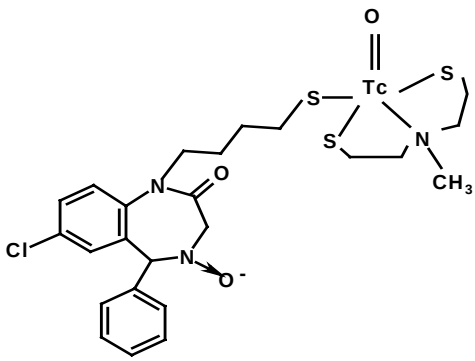 **Tc2**	
$logP_{O/W}$ 1.2		$logP_{O/W}$ 1.3	
c.a.yield: 20 %	n.c.a.yield: 70 - 80 %	c.a.yield: 30 %	n.c.a.yield: 50 – 60 %

Table 2. Biodistribution of the complexes **Tc1** and **Tc2** in Wistar rats as a percentage of the injected dose per gram of blood and per gram of tissue (mean ± SD ; n = 5).

Time [min] p.i.	Blood	Heart	Lung	Spleen	Kidney	Liver
Tc1						
5	0.5 ± 0.1	1.0 ± 0.2	0.9 ± 0.2	0.8 ± 0.1	2.8 ± 0.3	4.8 ± 0.7
120	0.15 ± 0.03	0.1 ± 0.02	0.2 ± 0.04	0.3 ± 0.1	3.0 ± 0.1	4.8 ± 0.8
Tc2						
5	0.4 ± 0.1	1.0 ± 0.1	0.9 ± 0.2	0.6 ± 0.1	3.3 ± 0.4	5.8 ± 0.5
120	0.2 ± 0.05	0.1 ± 0.01	0.2 ± 0.02	0.1 ± 0.03	3.7 ± 0.3	6.8 ± 0.9

As illustrated in Table 2, the biodistribution pattern of the two complexes is very similar. Both complexes showed a fast blood elimination. No brain uptake was observed in the rat brain (< 0.05 % ID up to 5 min post injection). After 120 min approx. 40% of the injected dose was found in the liver and 5% in the kidneys.

Conclusion

The first results of the combination of benzodiazepine derivatives with a technetium moiety according to the “3+1”mixed ligand concept did not meet the criteria of a CNS-receptor imaging agent in terms of an acceptable brain uptake and a high affinity to the target receptor.

References

[1] Bartenstein, P.; Koepp, M. Benzodiazepindarstellung mit Positronenemissionstomographie und Single-Photon-Emissionstomographie. Nervenarzt 66 (1995) 412-421.

[2] Abadie, P.; Rioux, P.; Scatton, B.; Zarifian, E.; Barré, L.; Patat, A.; Baron, J.-C. Central benzodiazepine receptor occupancy by zolpidem in the human brain as assessed by positron emission tomography. Eur. J. Pharmacol. 295 (1996) 35-44.

[3] Beer, H.-F.; Bläuenstein, P.A.; Hasler, P.H.; Delaloye, B.; Riccabona, G.; Bangerl, I.; Hunkeler, W.; Bonetti, E.P.; Pieri, L.; Grayson Richards, J.; Schubiger, A.P. In vitro and in vivo evaluation of iodine-123-Ro 16-0154: A new imaging agent for SPECT investigations of benzodiazepine receptors. J. Nucl. Med. 31 (1990) 1007-1014

[4] Marchi, A.; Marvelli, L.; Rossi, R.; Bertolasi, V.; Ferretti, V. Technetium and rhenium carbonyl complexes with 1,4-benzodiazepine derivatives: X-ray crystal structure. Inorg. Chim. Acta 272 (1998) 267-273

[5] Gringauz, A. Introduction to medicinal chemistry, How drugs act and why. Wiley-VCH (1997) 585.

[6] Richelson, E.; Nelson, A.; Neeper, R. Binding of benzodiazepines and some major metabolites at their sites in normal human frontal cortex in vitro. J. Pharmacol. Exp. Ther. 256 (1990), 897-901.

[7] Janssen, M.J.; Stegeman, M.; Ensing, K.; de Zeeuw, R.A. Solubilized benzodiazepine receptors for use in receptor assays. J. Pharm. Biomed. Analysis 14 (1996) 989-996.

[8] Drews, A.; Syhre, R.; Nudelman, A.; Pietzsch, H.-J.; Johannsen, B. Phenothiazine technetium complexes. *This Report*, pp. 60-61.

[9] Seifert, S.; Pietzsch, H.-J.; Scheunemann, M.; Spies, H.; Johannsen, B. Serotonin receptor binding technetium and rhenium complexes, 17. Different routes of n.c.a. preparation of “3+1“ ^{99m}Tc complexes. *Annual Report 1997*, Institute of Bioinorganic and Radiopharmaceutical Chemistry, FZR-200, pp.10-13.

[10] Seifert, S.; Pietzsch, H.-J.; Scheunemann, M.; Spies, H.; Syhre, R.; Johannsen, B. No carrier added preparations of “3+1“ mixed ligand ^{99m}Tc complexes. Appl. Radiat. Isot. 49 (1998) 5-11.

[11] Pietzsch, H.-J.; Scheunemann, M.; Brust, P.; Wober, J.; Spies, H.; Johannsen, B. *Annual Report 1996*, Institute of Bioinorganic and Radiopharmaceutical Chemistry, FZR-165, pp.9-12.

[12] Lowry, O. H.; Rosebrough, N.J.; Farr, A. L.; Randall, R.J. Protein measurement with the folin phenol reagent. J. Biol. Chem. 193 (1951) 265-275.

21. Phenothiazine Technetium Complexes

A. Drews, R. Syhre, A. Nudelman[1], H.- J. Pietzsch, B. Johannsen
[1]Bar Ilan Universität, Ramat Gan, Israel

Introduction

Phenothiazine derivatives have been discussed as affine ligands for central dopamine receptors [1 - 4] and are therefore of interest for labelling with technetium-99m [5]. Our concept of labelling involves thiol functionalized monodentate phenothiazine derivatives (2-trifluoromethyl-N-(4-butylthiol)-phenothiazine) (**L1**) or (2-chloro-N-(4-butylthiol)-phenothiazine) (**L2**) and a tridentate ligand (3-methyl-azapentane-1,5-dithiol) (**SNMeS**). Such "3+1" mixed ligand complexes were prepared according to Seifert *et al.* [6, 7]. The technetium phenothiazine complexes (**Tc1** and **Tc2**) were investigated with regard to their biodistribution in rats.

Experimental

C.a. labelling
Labelling of the ^{99}Tc reference compounds was performed by transchelation from [^{99}Tc]technetium gluconate, adding monodentate thiol ligand (L1 or L2), tridentate ligand (SNMeS) and stannous chloride dissolved in methanol/acetonitrile. The complexes were stirred at 50 °C for 5 h and purified by HPLC on a semipreparative Hypersil ODS column.

N.c.a. labelling
The ^{99m}Tc complexes were synthesized as described by Seifert *et al.* [6, 7]. The compounds were purified, using a semipreparative Hypersil ODS column.

The ^{99}Tc reference compounds were characterized by mass spectrometry on a Micromass Tandem Quadrupole Mass Spectrometer (Quattro LC) operating in the MS mode. Mass spectral data were recorded in a the positive ESI mode, using a cone voltage of 30 V. A solution of about 0.1 mg of the ^{99}Tc complex in 1 ml chloroform and 0.05 % formic acid was injected at a flow rate of 5 µl/min.
The values confirmed the assumed composition:

MS-**Tc1** ES+: m/z (found) 619 (M+) m/z (calc.) 618 for [^{99}TcO(SNMeS)/L1]

MS-**Tc2** ES+: m/z (found) 585 (M+), m/z (calc.) 584 for [^{99}TcO(SNMeS)/L2]

The partition coefficient was measured by the shake-flask method.

Biodistribution
The animal studies in male Wistar rats (5 - 6 weeks old) were carried out according to the relevant national regulations. 500 µl of [^{99m}Tc]technetium complex solution (500 kBq; saline propylene glycol 15 %) were injected into the tail vein. After the injection the rats were sacrificed by heart puncture under ether anaesthesia 5 - 120 min post injection (p.i.). The selected organs were isolated for weighting and counting.

Results and Discussion

^{99}Tc complexes were obtained in yields of 30 – 45 % after HPLC purification as shown in Table 1. The ^{99m}Tc complexes were obtained in 70 – 90 % yields. The radiochemical purity was > 95 %. The partition coefficients (log $P_{O/W}$) did not reflect the small structure differences of Tc1 and Tc2. The complexes were stable in aqueous solutions.
Accumulation of both complexes was mostly observed in the liver as illustrated in Table 2. More than 80 % of the radioactivity accumulated in the liver within 5 - 120 min post injectionem without any significant biliary clearance. A high initial uptake was also found in the lungs after administration of the complex **Tc1**, whereas complex **Tc2** was more extracted by the spleen. The preliminary data suggest that these neutral, lipophilic complexes are not able to cross the blood-brain barrier. Less than 0.1 % of the injected dose was found in the whole rat brain up to 5 minutes after the injection. The complexes were fast eliminated from the blood pool of rats.
From the biodistribution studies it can be concluded that this type of mixed-ligand ^{99m}Tc complexes containing a phenothiazine moiety is not suitable for the design of new CNS radiotracers.

Table 1. 3+1 mixed-ligand [$^{99/99m}$TcO(SNMeS)/L)] complexes **Tc1** and **Tc2** used for biodistribution studies in rats

Tc1		**Tc2**	
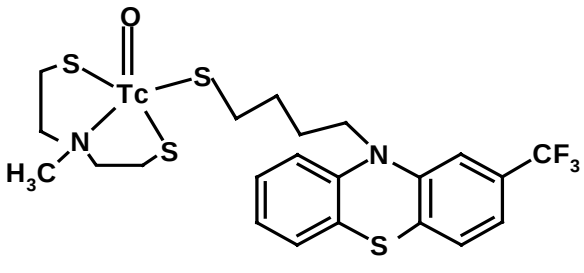		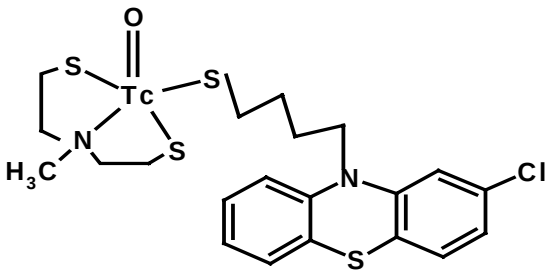	
$logP_{O/W}$ 1.5		$logP_{O/W}$ 1.3	
c.a.yield: 30 %	n.c.a. yield: 90 %	c.a. yield: 45 %	n.c.a. yield: 70 %

Table 2. Biodistribution of the complexes **Tc1** and **Tc2** in Wistar rats as a percentage of the injected dose per gram of blood and per gram of tissue (mean ± SD ; n = 5)

Time [min] p.i.	Blood	Heart	Lung	Spleen	Kidney	Liver
Tc1						
5	0.8 ± *0.1*	0.7 ± *0.1*	18.3 ±*1.6*	4.1 ± *0.8*	1.5 ± *0.2*	13.9 ± *1.9*
120	0.5 ± *0.1*	0.4 ± *0.1*	4.8 ± *1.1*	3.1 ± *0.7*	3.5 ± *0.3*	12.8 ± *1.6*
Tc2						
5	0.6 ± *0.2*	0.6 ± *0.1*	1.4 ± *0.2*	11.4 ± *2.0*	0.6 ± *0.1*	11.3 ± *0.5*
120	0.2 ± *0.1*	0.2 ± *0.1*	0.4 ± *0.1*	8.1 ± *1.7*	1.0 ± *0.1*	9.4 ± *0.7*

References

[1] Soskic, V.; Maelicke, A.; Petrovic, G.; Ristic, B. ; Petrovic, J. Synthesis of some phenothiazine derivatives as potential affinity ligands for the central dopamine receptors. J. Pharm. Pharmacol. 43 (1991) 27-31.

[2] Gordon, A.; Jamieson, Jr.; Vanaman, T.C. Calcium-dependent affinity chromatography of calmodulin on an immobilized phenothiazine. Biochem. Biophys. Res. Commun. 90 (1979) No 3.

[3] Savelyeva, M.V.; Baldenkov, G.N.; Kaverina, N.V. Receptor binding potencies of chloropromazine, trifluorazine, fluphenazine and their 10-N-substituted analogues. Biomed. Biochim. Acta 47 (1988) 1085-1087.

[4] Oelssner, W. jr.; Peinhardt, G.; Büge, A. Untersuchungen zur Affinität kernfluorierter Derivate von Phenothiazin-Neuroleptica zur ^{3}H-Spiroperidol-Bindungsstelle des Dopaminrezeptors mittels Radioligandtechnik in vitro. Pharmazie 40 (1985) 341-342.

[5] Hyttel, J. Receptor pharmacology. Ist use in neuroleptic research. Acta Psychiat. Belg. 87 (1987) 535-551.

[6] Seifert, S.; Pietzsch, H.-J.; Scheunemann, M.; Spies, H.; Syhre, R.; Johannsen, B. No carrier added preparations of "3+1" mixed ligand ^{99m}Tc complexes. Appl. Radiat. Isot. 49 (1998) 5-11.

[7] Seifert, S.; Pietzsch, H.-J.; Scheunemann, M.; Spies, H.; Johannsen, B. Serotonin receptor binding technetium and rhenium complexes, 17. Different routes of n.c.a. preparation of "3+1" ^{99m}Tc complexes. *Annual Report 1997*, Institute of Bioinorganic and Radiopharmaceutical Chemistry, FZR-200, pp.10-13.

22. '3+1' Mixed-Ligand Oxorhenium (V) Complexes Bearing 1,2,3,4-Tetrahydro-quinoline and Quinoline

A. Zablotskaya[1], I. Segal[1], E. Lukevics[1], A. Drews, T. Kniess, H. Spies
[1]Latvian Institute of Organic Synthesis, Aizkraukles str. 21, Riga, LV-1006, Latvia

To continue our investigations of '3+1' mixed-ligand oxorhenium(V) complexes containing quinoline and tetrahydro(sila,iso)quinoline as monodentate ligands [1], we synthesized [2-(N-tetrahydro-quinolyl)ethanethiolato](3-thiapentane-1,5-dithiolato)- **1** and (2-quinolylthiolato)(3-thiapent-ane-1,5-dithiolato)oxorhenium(V) **2** (Scheme 1).

Scheme 1. Reaction scheme for the synthesis of [2-(N-tetrahydroquinolyl)ethanethiolato](3-thiapent-ane-1,5-dithiolato)- **1** and (2-quinolylthiolato)(3-thiapentane-1,5-dithiolato)oxorhenium (V) **2**

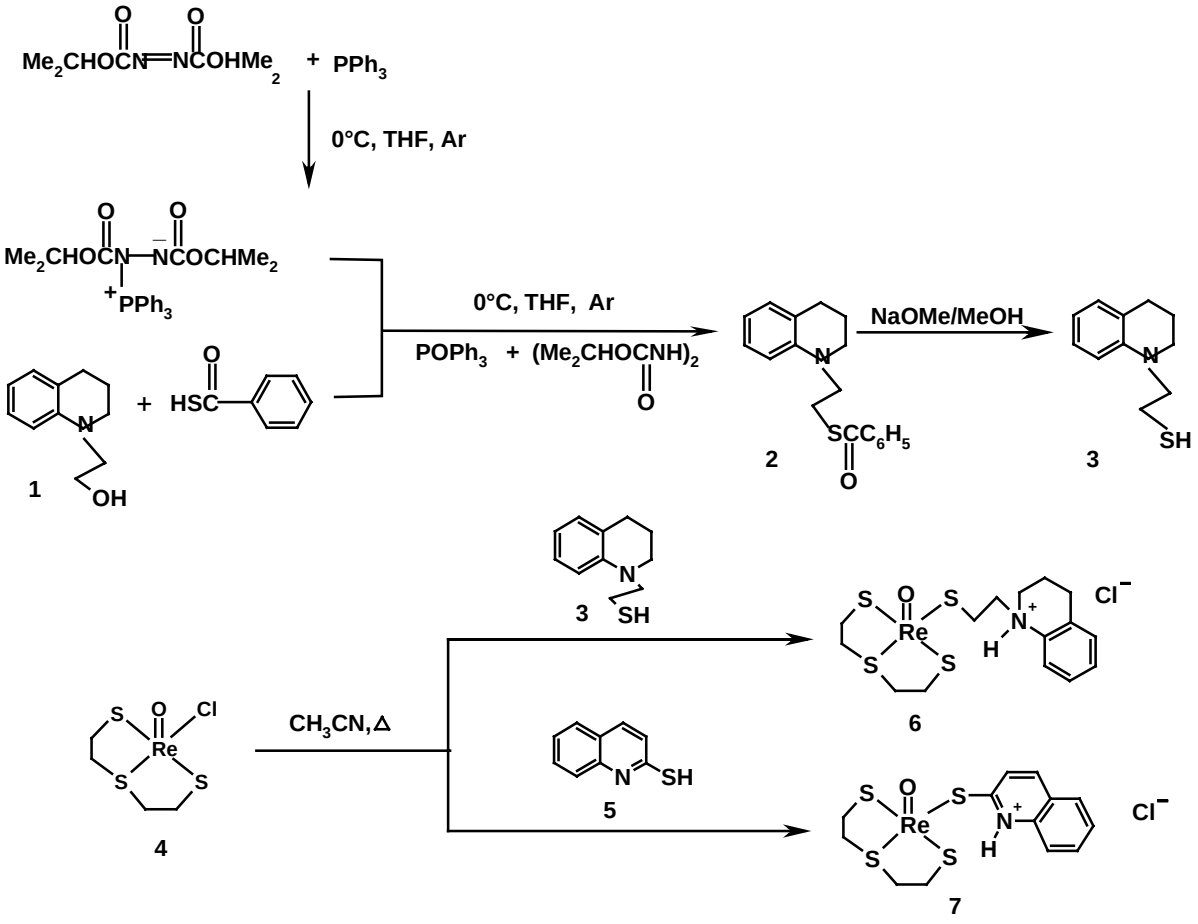

N-(2-Hydroxyethyl)-1,2,3,4-tetrahydroquinoline **1** obtained by condensation of 1,2,3,4-tetrahydro-quinoline with 2-iodoethanol in the presence of triethylamine was further converted into N-(2-mercaptoethyl)-1,2,3,4-tetrahydroquinoline **3** suitable for complexation. The introduction of a thiol group into the tetrahydroquinoline molecule was possible via thiobenzoate by the Mitsunobu proce-dure [2, 3]. This reaction is the method of choice for the introduction of a sulphur moiety under mild conditions in a high yield. By treating the alcohol **1** with the system of triphenylphosphine/ diisopro-pylazodicarboxylate/benzoic acid the thiobenzoate **2** was obtained in a satisfactory yield of 90 %. The saponification of **2** by sodium methoxide in MeOH produced the desired thiol **3**.
Thiols **3** and **5** were transformed into the corresponding '3+1' mixed-ligand complexes **6** and **7** by the oxorhenium (V) precursor **4** [4]. The newly prepared complexes were characterized by elemental analysis, ^{1}H and ^{13}C NMR and IR spectroscopy.
The brain-receptor-binding test *in vitro* reveals that the complexes **6** and **7** have very low affinities to the serotonin 5-HT_{1A} and 5-HT_{2A} receptors. But **6** was found to have a higher selectivity for the 5-HT_{1A} subtype and **7** for 5-HT_{2A} .

The psychotropic activity and acute toxicity *in vivo* and antitumour activity *in vitro* of compounds **6** and **7** are under investigation. The results will be published in the subsequent paper.

Acknowledgement

We are grateful to “Internationales Büro des BMBF” for the financial support of the project LET-008-97.

References

[1] Zablotska, A.; Segal, I.; Lukevics, E.; Pietzsch, H.-J.; Kniess, T.; Spies, H. ‘3+1’ Mixed-ligand oxorhenium (V) complex with 1,2,3,4-tetrahydroisoquinoline. *Report January 1998 – June 1999*, Institute of Bioinorganic and Radiopharmaceutical Chemistry, FZR-270, pp. 143-144.

[2] Mitsunobu, O. The use of diethyl azodicarboxylate and triphenylphosphine in synthesis and transformation of natural products. Synthesis (1981) 1-28.

[3] Corey, E.J.; Cimprich, K.A. Enantioselective routes to chiral benzylic thiols, sulfonic esters and sulfonic acids illustrated by the 1-phenylethyl series. Tetrahedron Lett. 33 (1992) 4099-4102.

[4] Fietz, T.; Spies, H.; Pietzsch, H.-J.; Leibnitz, P. Synthesis and crystal structure of (3-thiapentane-1,5-dithiolato)chlorooxorhenium (V). Inorg. Chim. Acta 321 (1995) 233-236.

23. Biological Study of '3+1' Mixed-Ligand Oxorhenium(V) Complex Bearing 1,2,3,4-Tetrahydroisoquinoline in the Monodentate Ligand

A. Zablotskaya[1], I. Segal[1], S. Germane[1], I. Shestakova[1], E. Lukevics[1], A. Drews, H. Spies
[1]Latvian Institute of Organic Synthesis, Aizkraukles str. 21, Riga, LV-1006, Latvia

Prompted by the fact that some alkaloids with opiate activity contain hydrogenated moieties of quinoline or isoquinoline and by the literature data that tetrahydro(iso)quinoline containing ligands display affinity to serotonin (5-HT_{1A}) and dopamine receptors [1,2], we studied the synthesis of a '3+1' mixed-ligand oxorhenium(V) complex with a 1,2,3,4-tetrahydro-isoquinoline-containing monodentate ligand to investigate its pharmacological properties [3].
The results of the *in vivo* study of the neurotropic activity and acute toxicity of [2-(N-tetrahydro-isoquinolyl)ethanethiolato](3-thiapentane-1,5-dithiolato)oxorhenium(V) hydrochloride are presented in Table 1.

Table 1. Neurotropic activity of [2-(N-tetrahydroisoquinolyl)ethanethiolato](3-thiapentane-1,5-dithiolato)oxorhenium(V) hydrochloride *in vivo*

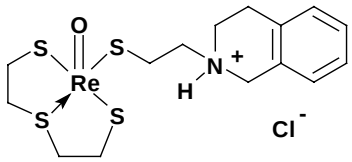

1	LD_{50}, mg/kg	> 500
2	Hypoxic hypoxia, %*	120
3	Phenamine hyperthermia, ^{o}C	-0.8(30')
4	Phenamine induced hyperactivity, %*	110
5	Hexenal induced narcosis, %*	113
6	Ethanol induced narcosis, %*	82
7	Electroshock, %	> 50
8	Corazol induced convulsions (clonic/tonic), %*	128/212
9	Retrograde amnesia, %*	40

%* - % to control (100%)

The investigated compound possesses antihypoxic activity and increases the life span of mice by 20%. In the test of Corazol induced convulsions it shows anticonvulsive properties, increasing the threshold of Corazol convulsions 1.3 times in the clonic phase and more than 2 times in the tonic one. Concerning the pharmacological effects of phenamine, hexenal and ethanol, the expressed biological properties are low. The investigated complex is slightly toxic.
[2-(N-Tetrahydroisoquinolyl)ethanethiolato](3-thiapentane-1,5-dithiolato)oxorhenium(V) was used in receptor binding assays to determine the affinity and selectivity of this ligand for serotonin 5-HT_{1A} and 5-HT_{2A} receptors *in vitro* (Table 2). The affinity (IC_{50} values) to receptor subtypes is relatively low but it reveals a higher selectivity for the 5-HT_{1A} subtype (389 nM) than for 5-HT_{2A} (1258 nM) .

Table 2. *In vitro* binding data of [2-(N-Tetrahydroisoquinolyl)ethanethiolato](3-thiapentane-1,5-dithiolato) oxorhenium(V) hydrochloride to serotonin receptors (5-HT_{1A}, 5-HT_{2A})

Formula	IC_{50} (nM)	
	5-HT_{1A} competitor [^{3}H]8-OH-DPAT	5-HT_{2A} competitor [^{3}H]ketanserin
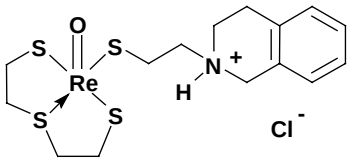	389.5 ± 4.86	1258.6 ± 14.7

The antitumour activity of [2-(N-tetrahydroisoquinolyl)ethanethiolato](3-thiapentane-1,5-dithiolato) oxorhenium(V) was tested *in vitro* on four monolayer tumour cell lines: MG-22A (mouse hepatoma), HT-1080 (human fibrosarcoma), Neuro 2A (mouse neuroblastoma) and B16 (mouse melanoma). The experimental evaluation of cytotoxicity properties is presented in Table 3. The studied compound possesses a good antitumour activity and NO-induction ability. It has a high cytotoxic effect on MG-22A and B16 cell lines and a high NO-generation activity, being the most active (500 %) in the B16 test. This compound was recommended for antitumour activity testing *in vivo.*

Table 3. *In vitro* cell cytotoxicity and the ability of intracellular NO generation caused by [2-(N-tetrahydroisoquinolyl)ethanethiolato](3-thiapentane-1,5-dithiolato)oxorhenium(V) hydrochloride

Cell lines											
HT-1080			MG-22A			Neuro2A			B16		
IC_{50} CV[a]	IC_{50} MTT[b]	NO% CV[c]	IC_{50} CV	IC_{50} MTT	NO% CV	IC_{50} CV	IC_{50} MTT	NO% CV	IC_{50} CV	IC_{50} MTT	NO% CV
5	6	150	0.5	0.9	200	7.7	9	250	3	4.5	500

[a] Concentration (μg/ml) providing 50% cell killing effect (CV: coloration)

[b] Concentration (μg/ml) providing 50% cell killing effect (MTT: coloration)

[c] NO concentration (%) (CV: coloration)

Acknowledgement

We are grateful to "Internationales Büro des BMBF" for financial support to the project LET-008-97.

References

[1] Heier, R.F.; Dolak, L.A.; Duncan, J.N.; Hyslop, D.K.; Lipton, M.F.; Martin, I.J.; Mouragis, M.A., Piercey, M.F.; Nichols, N.F.; Schreur, P.J.K.D.; Smith, M.W. ; Moon, M.W. Synthesis and biological activity of (R)-5,6-dihydro-N,N-dimethyl-4H-imidazo[4,5,1-ij]quinoline-5-amine and its metabolites. J. Med. Chem. 40 (1997) 639-646.

[2] Mokrosz, M.J.; Bojarski, A.J.; Duszynska, B.; Tatarczynska, E.; Klodzinska, A.; Deren-Wesolek, A.; Charakchieva-Minol, S.; Chojnacka-Wojcik; E. 1,2,3,4- Tetrahydroiso-quinoline derivatives: a new class of 5-HT_{1A} receptor ligands. Bioorg. Med. Chem. 7 (1997) 287-295.

[3] Zablotska, A.; Segal, I.; Lukevics, E.; Pietzsch, H.-J.; Kniess, T.; Spies, H. '3+1' Mixed-ligand oxorhenium (V) complex with 1,2,3,4-tetrahydroisoquinoline. *Report January 1998 – June 1999,* Institute of Bioinorganic and Radiopharmaceutical Chemistry FZR-270, pp. 143-144.

24. Psychotropic Activity of O-Organosilicon Containing 3-Thia, 3-Oxa and 3-Methyl-azapentane-1,5-Dithiolato-Oxorhenium(V)

A. Zablotskaya[1], I. Segal[1], S. Germane[1], E. Lukevics[1], H. Spies
[1]Latvian Institute of Organic Synthesis, Riga

Earlier we reported on the synthesis and a physico-chemical study of organosilicon rhenium complexes, where the oxorhenium(V) core ReO^{3+} was coordinated by a tridentate 3-thia, 3-oxa or 3-methylazapentane-1,5-dithiolate and additionally by an organosilicon containing monodentate thiolate with various organosilicon substituents [1 – 3].
The newly prepared complexes were tested on mice for their psychotropic activity and acute toxicity *in-vivo* being administered within the peritoneal cavity in doses of 5 mg/kg in comparison with their precursors. The action on the CNS was evaluated by indicators of hypoxia, hexenal and ethanol-induced narcosis, phenamine hyperactivity, corazol-induced convulsions, electroshock and retrograde amnesia. The results of the biological investigation are presented in Table 1.

Table 1. *In vivo* neurotropic activity of oxorhenium(V) complexes

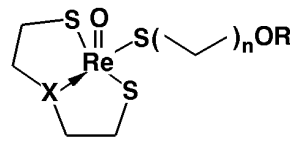				M ± m, % to control (100 %)					
				Test					
N	X	n	R	Hypoxic hypoxia	Hexenal anaes-thesia	Ethanol narcosis	Phena-mine hyper-activity	Corazol convulsions clonic/tonic	Retro-grade amnesia
I	S	2	H	113*	97	113	77*	134*/178*	80*
2	S	3	H	134*	118*	91	80	119*/157*	40
3	O	2	H	132*	103	60*	72*	135*/216*	60
4	O	3	H	146*	76*	62*	22*	134*/173*	80*
5	N	2	H	150*	89	96	2*	120/318*	80*
6	S	2	$SiMe_3$	95	92	73	111	125*/165*	60
7	S	2	$SiPh_3$	95	148*	84	183*	133*/178*	17
8	S	3	$SiPh_3$	150*	89	60*	48*	138*/213*	20
9	N	2	$SiMe_3$	126*	81*	104	22*	131*/301*	60

* Differences in relation to the control are statistically reliable at $P < 0.05$

All the investigated compounds exhibited the antihypoxic action; prolonging the life of mice under hypoxia by 13 – 50 %.
With respect to hexenal and ethanol narcosis, nearly all the compounds have only a slight influence. Nevertheless, the introduction of the triphenylsilyl-group into these compounds resulted in a 48 % prolongation of the hexenal anaesthesia for (2-hydroxyethanethiolato)- 7 and a 40 % reduction in the ethanol-induced narcosis for (3-hydroxypropanethiolato)(3-thiapentane-1,5-dithiolato)-oxorhenium(V) 8. An antagonistic action to ethanol was established for 3-oxapentane-1,5-dithiolato complexes 3 and 4.
The pharmacological effect of the interaction with phenamine for all investigated compounds is highly expressed. Almost all of them are phenamine antagonists, reducing its action by 23 – 98 %. The phenamine antagonistic action is expressed most for (2-hydroxyethanethiolato)[3-(N-methylaza-pentane-1,5-dithiolato)oxorhenium(V) 5, which fully depresses the phenamine action (by 98 %). (2-Tri-

phenylsiloxyethanethiolato)(3-thiapentane-1,5-dithiolato)oxorhenium (V) 7 is the only compound which definitly increases the phenamine action by 83 %.
For both silylated and unsilylated complexes the tendency to antiphenamine action decreases, depending on the heteroatom of the tridentate ligand (from aza to oxa and further to thia-): **5** (98%) >> **3** (28 %) > **1** (23 %), **4** (78 %) >> **2** (20 %), **9** (78 %) >> **6** (increases the action of phenamine by 11 %), and with silylation of complexes containing the 2-hydroxyethanethiolato-monodentate ligand: **5** (98 %) > **9** (78 %), **1** (23 %) > **6** > **7** (compounds **6** and **7** increase the phenamine action by 11 and 83 %).
For complexes containing the 3-hydroxypropanethiolato monodentate ligands **2** and **8**, the opposite effect was occured: the antagonistic action to phenamine increased with triphenylsilylation of the monodentate ligand.
Contrary to the test with the maximal electroshock in which no protective properties were found, in the test with Corazol-induced convulsions (clonic and tonic) all the synthesized compounds showed anticonvulsive activity. Here, as in the study of phenamine hyperactivity, the decisive part was played by the heteroatom of the tridentate ligand. The increase in the threshold of Corazol convulsions along the thia, oxa, methylaza sequence of tridentate ligands was observed for hydroxyalkylthiolato as well as for trimethylsiloxy-ethanethiolato complexes:

1 (134/178) << **3** (135/216) << **5** (120/318);

2 (119/157) < **4** (134/173); **6** (125/165) << **9** (131/301).

It was established that the strongest anticonvulsive activity was exhibited by the (3-methylazapentane-1,5-dithiolato) complexes **5** and **9**, which increase the corazole dose, leading to a lethal outcome in more than 3 times as many mice. The introduction of the organosilicon substituent into the molecule has little influence on anticonvulsive properties, except in the case of (3-triphenylsiloxypropanethiolato)(3-thiapentane-1,5-dithiolato)oxorhenium(V) **8**, whose protective properties are essentially higher than those of the unsilylated precursor **2** (by 20 % in clonic and by 60 % in tonic phases).
The data obtained indicate that, unlike the trimethylsilyl group, the introduction of the bulkier triphenylsilyl group, which is more stable to hydrolysis (lipophilicity, log P, increase up to 5.37 [3]) results in an essential increase in the sedative properties of the complex containing the parent hydroxyl group. **7** is thus the only compound by which the hexenal action is maximally prolonged (in 1.5 times), but **8** possesses strong antihypoxic and anticonvulsive action in comparison with its unsilylated precursor **2**, and at the same time shortens the ethanol narcosis.

Acknowledgement

We are grateful to “Internationales Büro des BMBF” for the financial support of the project LET-008-97.

References

[1] Fietz, T.; Spies, H.; Zablotskaya, A. ; Scheller, D. Reactions of hydroxygroup containing ”3 + 1” mixed-ligand rhenium(V) compounds. Part 1: Silylation of ”3 + 1” mixed-ligand complexes. *Annual Report 1997*, Institute of Bioinorganic and Radiopharmaceutical Chemistry, FZR-200, pp. 113–116.

[2] Spies, H.; Fietz, T.; Zablotskaya, A.; Belyakov, S.; Lukevics, E. Organosilicon containing rhenium(V) complexes with mixed ligands. Chem. Heterocycl. Comp. 35 (1999) 116–125.

[3] Zablotska, A.; Segal, I.; Kemme, A.; Lukevics, E.; Berger, R.; Spies, H. Reactions of hydroxygroup containing ”3 + 1” mixed-ligand oxorhenium(V) complexes. Part 3: Synthesis and physicochemical investigation of O-organosilicon containing 3-thia-, 3-oxa- and 3-methyl- azapentane-1,5-dithiolato-oxorhenium(V). *Report January 1998 – June 1999*, Institute of Bioinorganic and Radiopharmaceutical Chemistry, FZR-270, pp. 156–158.

25. Substrates of the Herpes-Simplex-Virus 1 Thymidine Kinase and Escherichia Coli Cytosine Deaminase for Monitoring Gene Expression.

Part 1: Syntheses of New Modified Acyclic Purine and Pyrimidine Nucleosides

St. Noll, M. Grote, B. Große, B. Noll

Suicide gene therapy with the herpes simplex virus type 1 thymidine kinase gene (HSV1-tk) is considered to be one of the most promising approaches to the treatment of cancer. The HSV1-tk gene expresses the enzyme thymidine kinase HSV1-TK in virus-infected cells. Unlike the host thymidine kinase, this enzyme of low substrate specificity phosphorylates numerous nucleosides or nucleoside analogues into monophosphates. The substrates were further phosphorylated by host cellular kinases into di- and triphosphates, which inhibit DNA polymerase and induce cell death.
As the phosphorylated metabolites are negatively charged and remain trapped in the cell, radiolabelling these antiviral agents with a positron-emitting isotope may make it possible to monitor the viral kinase enzyme activity by positron emission tomography (PET) [1, 2, 3]. PET with a suitable radiotracer represents a potential tool for determining the level of HSV-tk expression and establishing the optimal protocol of gene and prodrug administration in humans. Promising candidate radiotracers were recently described for this purpose [4 - 15], but an optimal tracer has not yet been developed.
Suicide gene therapy also seeks to make use of the bacterial cytosine deaminase / 5-fluorocytosine system. The Escherichia coli CD gene in transfected cancer cells expresses the enzyme cytosine deaminase. This enzyme converts the nontoxic prodrug 5-fluorocytosine into the toxic metabolite 5-fluorouracil, which induces cell death. However, 5-fluorouracil is not significantly accumulated in the transduced cells as it freely diffuses out (high bystander effect) is therefore not suitable for monitoring [16, 17, 18]. The aim of our investigations in this context is the search for new ^{18}F–labelled tracers which are substrates of the CD and will be trapped in the cell.
As for the herpes simplex virus 1 thymidine kinase system (HSV1-tk), our activities are focused on finding a new substrate for monitoring gene expression. Thus, we synthesized the adenine derivative N^6-methyl-9-[(1,3-dihydroxy-2-propoxy)methyl]adenine (metacycad) (I) and the uracil derivatives 5-hydroxy-1-[(1,3-dihydroxy-2-propoxy)methyl]uracil (hydracyclur) (II) and 6-methyl-1-[(1,3-dihydroxy-2-propoxy)methyl]uracil (metacyclur) (III). Because 6-methyl-1-[(1-hydroxy-3-fluoro-2-propoxy)methyl]-uracil (IV) was found to have a high affinity to HSV 1-TK comparable to ganciclovir [19], this compound seemed to us worth being labelled with ^{18}F and so we prepared the precursor for ^{18}F labelling and the nonradioactive reference compound. At last we synthesized N^1-methyl-9-[(4-hydroxy)-3-hydroxy-methylbutyl]guanine (V) as a representative of the penciclovir analogues.

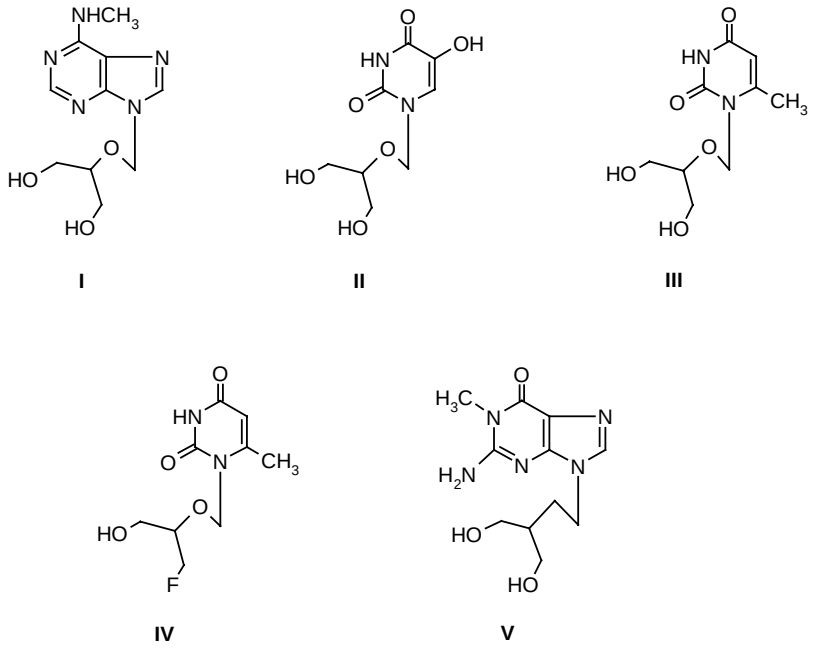

Fig. 1. Novel modified acyclic purine and pyrimidine nucleosides

The synthesis of the acyclic part of the compounds (**I**), (**II**) and (**III**) was modified according to a procedure described in [20, 21] and follows the route shown in Fig. 2.

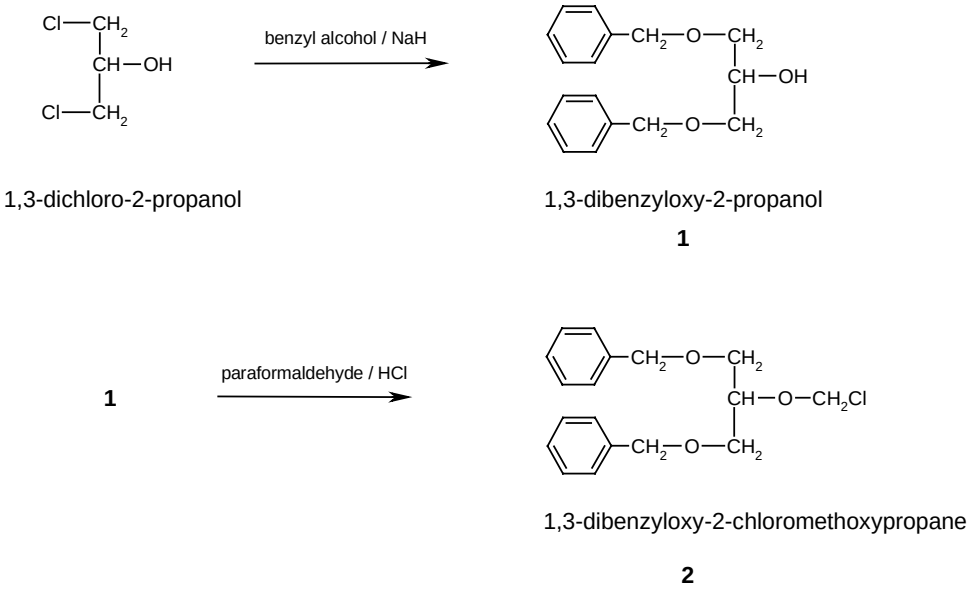

Fig. 2. The synthesis of 1,3-dibenzyloxy-2-chloromethoxypropane

Benzyl alcohol and sodium hydride were stirred at room temperature in dry hexane. 1,3-Dichloro-2-propanol was added and stirring was continued for 8 hours under nitrogen at 100 °C to produce 1,3-dibenzyloxy-2-propanol (**1**) in a yield of 64 %. (**1**) was added to 1,2-dichloroethane followed by paraformaldehyde and with bubbling of dry HCl gas through the reaction mixture 1,3-dibenzyloxy-2-chloromethoxypropane (**2**) was obtained (82 %).

The bases N^6-methyladenine, 5-hydroxyuracil and 6-methyluracil were coupled to 1,3-dibenzyloxy-2-chloromethoxypropane (**2**) in dry dimethyl formamide with triethyl amine to produce N^6-methyl-9-[(1,3-dibenzyloxy-2-propoxy)methyl]adenine (**3**), 5-hydroxy-1-[(1,3-dibenzyloxy-2-propoxy)-methyl]uracil (**4**) and 6-methyl-1-[(1,3-dibenzyloxy-2-propoxy)methyl]uracil (**5**). Splitting off the protection group resulted in N^6-methyl-9-[(1,3-dihydroxy-2-propoxy)methyl]adenine (metacycad) (**I**), 5-hydroxy-1-[(1,3-dihydroxy-2-propoxy)methyl]uracil (hydracyclur) (**II**) and 6-methyl-1-[(1,3-dihydroxy-2-propoxy)-methyl]uracil (metacyclur) (**III**) (Fig. 3).

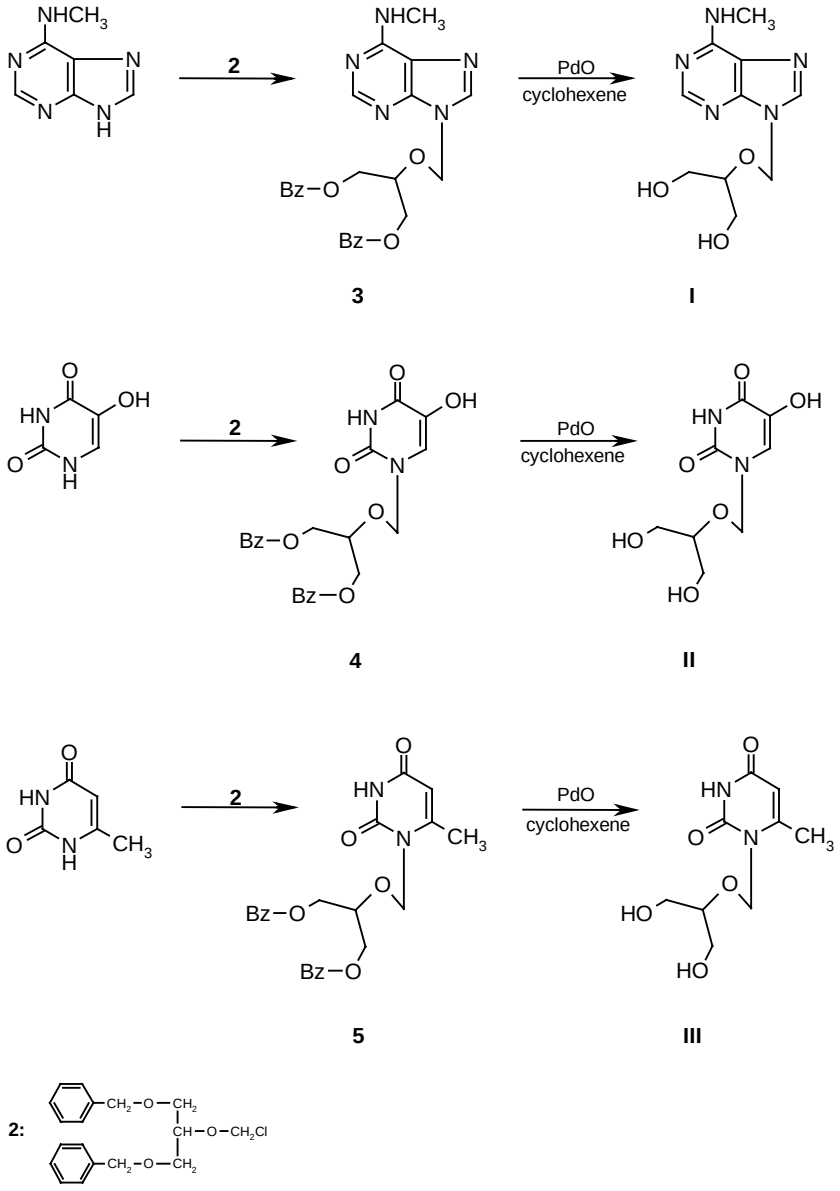

Fig. 3. The syntheses of metacycad (**I**), hydracyclur (**II**) and metacyclur (**III**)

The preparation of fluor-substituted metacyclur involved the protection of the hydroxylic group in position 1‘, followed by introduction of a leaving group for fluorination in 3‘. The precursor 6-methyl-1-[[1-(p-anisyldiphenylmethoxy)-3-(p-toluenesulphonyloxy)-2-propoxy]methyl]uracil (**7**) was obtained from 6-methyl-1-[(1,3-dihydroxy-2-propoxy)methyl]uracil (**III**) by treatment with p-anisychloro-diphenylmethane in dimethyl formamide and with a trace of dimethylamino pyridine to produce 6-methyl-1-[[1-(p-anisyldiphenylmethoxy)-3-hydroxy)-2-propoxy]methyl]-uracil (**6**) in a 47 % yield, followed by tosylation with tosyl chloride in anhydrous pyridine (63 %).

Fluorination occurred with potassium fluoride and kryptofix 2.2.2. in acetonitrile at 120 °C, forming 6-methyl-1-[[1-(p-anisyldiphenylmethoxy)-3-fluoro 2-propoxy]methyl]uracil (**8**) in a yield of 23 %. Finally the protection group was split off, yielding the fluorinated compound 6-methyl-1-[(1-hydroxy-3-fluoro 2-propoxy)methyl]uracil (**IV**) (63 %) (Fig. 4).

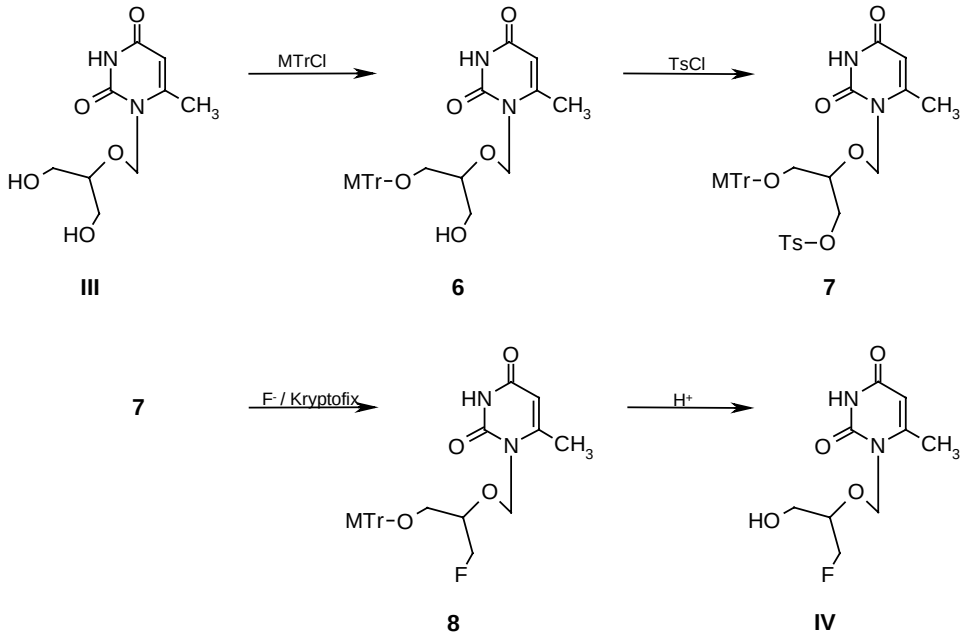

Fig. 4. Synthesis of 6-methyl-1-[(1-hydroxy-3-fluoro-2-propoxy)methyl]uracil (**IV**)

The synthesis of penciclovir (**14**) was carried out according to a modified procedure described in [22]. The reaction scheme is illustrated in Fig. 5.

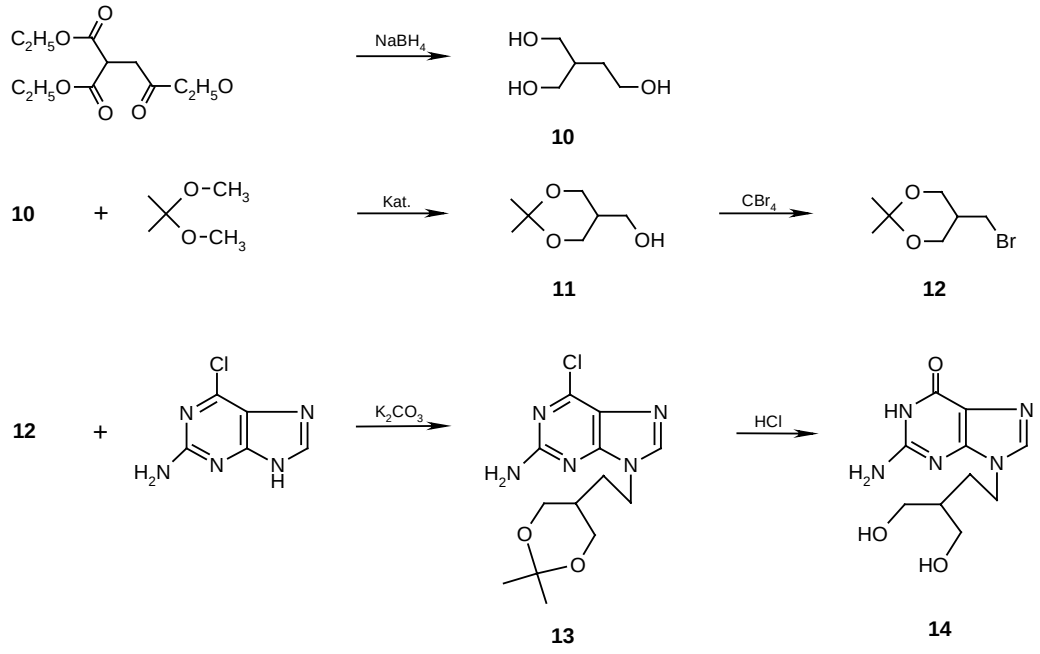

Fig. 5. The synthesis of penciclovir

2-(Hydroxymethyl)butane-1,4-diol (**10**) was prepared in a yield of 94 % from triethyl-1,1,2-ethane-tricarboxylate by heating in tert. butanol with sodium borhydride. (**10**) was isolated as a colourless oil which reacted with 2,2-dimethoxypropane and a trace of toluenesulphonic acid in tetrahydrofurane under mild conditions to yield 5-(2-hydroxyethyl)-2,2-dimethyl-1,3-dioxane (**11**) (34 %). Treatment of (**11**) with carbon tetrabromide in dimethyl formamide at low temperature provided 5-(2-bromoethyl)-2,2-dimethyl-1,3-dioxane (**12**). The yield of the bromination reaction was (83 %). Reaction of (**12**) with 2-amino-6-chloropurine and anhydrous potassium carbonate afforded a 31 % yield of 2-amino-6-chloro-9-[2-(2,2-dimethyl-1,3-dioxane-5-yl)-ethyl]purine (**13**). In order to obtain the desired penciclovir

(**14**), deprotection of (**13**) in refluxing hydrochloric acid was required. This reaction was carried out in a yield of 90 %.
We decided to optimize the substrate properties of penciclovir to TK by introducing a methyl group into the molecule in order to change the lipophilicity of the compound, referring to [23, 24] where the change in antiviral activities depending on a methyl group in the acyclovir molecule is described (Fig. 6).

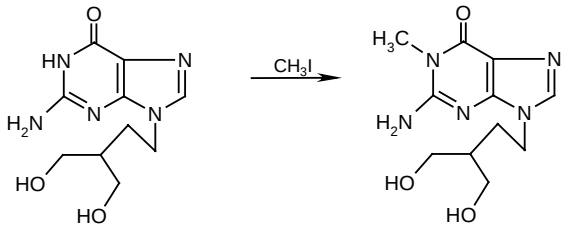

14 **V**

Fig. 6. Methylation of penciclovir

The desired product (**V**) was obtained from penciclovir (**14**) by treatment with methyl iodide in dimethyl formamide followed by an extensive preparative column chromatography.
All substances were identified by elemental analysis and structures were proved by ^{1}H NMR spectroscopy. The content of fluorine was determined by ^{19}F NMR spectroscopy. The compounds (**I**)-(**IV**) were evaluated by an isolated nucleoside kinase essay for their enzyme affinity to HSV-1TK and (**IV**) was found to have a high affinity to HSV-1 TK in comparison with ganciclovir [18].

References

[1] Morin, K.W.; Knaus, E.E.; Wiebe, L.I. Non-invasive scintigraphic monitoring of gene expression in a HSV-1 thymidine kinase gene therapy model. Nucl. Med. Commun. 18 (1997) 599-605.
[2] Blasberg, R.G.; Tjuvajev, J.G. Herpes simplex virus thymidine kinase as a marker / reporter gene for PET imaging of gene therapy. Q. J. Nucl. Med. 43 (1999) 163-169.
[3] Gambhir, S.S.; Barrio, J.R.; Herschman, H.R.; Phelps, M.E. Assays for noninvasive imaging of reporter gene expression. Nucl. Med. Biol. 26 (1999) 481-490
[4] Alauddin, M.M.; Conti, P.S.; Mazza, S.M.; Hamzeh, F.M.; Lever, J.R. 9-[(3-[^{18}F]-fluoro-1-hydroxy-2-propoxy)methyl]guanine ([^{18}F]-FHPG): a potential imaging agent of viral infection and gene therapy using PET. Nucl. Med. Biol. 23 (1996) 787-792.
[5] Shields, A.F.; Grierson, J.R.; Kozawa, S.M.; Zheng, M. Development of labeled thymidine analogs for imaging tumor proliferation. Nucl. Med. Biol. 23 (1996) 17-22.
[6] Morin, K.W.; Atrazheva, E.D.; Knaus, E.E.; Wiebe, L.I. Synthesis and cellular uptake of 2'-substituted analogues of (E)-5-(2-[^{125}I]iodovinyl)-2'-deoxyuridine in tumor cells transduced with the herpes simplex type-1 thymidine kinase gene. Evaluation as probes for monitoring gene therapy. J. Med. Chem. 40 (1997) 2184-2190.
[7] Alauddin, M.M.; Conti, P.S. Synthesis and preliminary evaluation of 9-[(4-[^{18}F]-fluoro-3-hydroxymethylbutyl]guanine ([^{18}F]-FHBG): a new potential imaging agent for viral infection and gene therapy using PET. Nucl. Med. Biol. 25 (1998) 175-180.
[8] Gambhir, S.S.; Barrio, J.R.; Wu, L.; Iyer, M.; Namavari, M.; Satyamurthy, N.; Bauer, E.; Parrish, C.; MacLaren, D.C.; Borghei, A.R.; Green, L.A.; Sharfstein, S.; Berk, A.J.; Cherry, S.R.; Phelps, M.E.; Herschman, H.R. Imaging of adenoviral-directed herpes simplex virus type 1 thymidine kinase reporter gene expression in mice with radiolabeled ganciclovir. J. Nucl. Med. 39 (1998) 2003-2011.
[9] Germann, C.; Shields, A.F.; Grierson, J.R.; Morr, I.; Haberkorn, U. 5-Fluoro-1-(2'-deoxy-2'-fluoro-beta-D-ribofuranosyl) uracil trapping in Morris hepatoma cells expressing the herpes simplex virus thymidine kinase gene. J. Nucl. Med. 39 (1998) 1418-1423.
[10] Alauddin, M.M.; Conti, P.S.; Mazza, S.M.; Hamzeh, F.M.; Lever, J.R. Evaluation of 9-[(3-[^{18}F]-fluoro-1-hydroxy-2-propoxy)methyl]guanine ([^{18}F]-FHPG) *in vitro* and *in vivo* as a probe for PET imaging of gene incorporation and expression in tumors. Nucl. Med. Biol. 26 (1999) 371-376.
[11] Gambhir, S.S.; Barrio, J.R.; Phelps, M.E.; Iyer, M.; Namavari, M.; Satyamurthy, N.; Wu, L.; Green, L.A.; Bauer, E.; MacLaren, D.C.; Nguyen, K.; Berk, A.J.; Cherry, S.R.; Herschman, H.R. Imaging

adenoviral-directed reporter gene expression in living animals with positron emission tomography. Proc. Natl. Acad. Sci. U S A. 96 (1999) 2333-2338.
[12] Tjuvajev, J.G.; Avril, N.; Oku, T.; Sasajima, T.; Miyagawa, T.; Joshi, R.; Safer, M.; Beattie, B.; DiResta, G.; Daghighian, F., Augensen F.; Koutcher, J.; Zweit, J.; Humm, J.; Larson, S.M.; Finn, R.; Blasberg, R. Imaging herpes virus thymidine kinase gene transfer and expression by positron emission tomography. Cancer Res. 58 (1998) 4333-4341.
[13] Devries, E.F.J.; Vanwaarde, A.; Harmsen, M.C.; Mulder, N.H.; Vaalburg, W.; Hospers, G.A.P. [C-11]FMAU and [F-18]FHPG as PET tracers for herpes simplex virus thymidine kinase enzyme activity and human cytomegalovirus infections. Nucl. Med. Biol. 27 (2000) 113-119.
[14] Gambhir, S.S.; Herschman, H.R.; Cherry, S.R.; Barrio, J.R.; Satyamurthy, N.; Toyokuni, T.; Phelps, M.E.; Larson, S.M.; Balatoni, J.; Finn, R.; Sadelain, M.; Tjuvajev, J.; Blasberg, R. Imaging transgene expression with radionuclide imaging technologies. Neoplasia 2 (2000) 118-138.
[15] Varagnolo, L.; Stokkel, M.P.M.; Mazzi, U.; Pauwels, E.K.J. ^{18}F-labeled radiopharmaceuticals for PET in oncology, excluding FDG. Nucl. Med. Biol. 27 (2000) 103-112.
[16] Larson, S.M.; Tjuvajev, J.; Blasberg, R. Triumph over mischance: a role for nuclear medicine in gene therapy. J. Nucl. Med. 38 (1997) 1230-1233.
[17] Haberkorn, U.; Oberdorfer, F.; Gebert, J.; Morr, I.; Vankaick, G.; Schackert, H.K.; Monitoring of gene therapy with cytosine deaminase - 5-fluorcytosine uptake in glioblastoma cells. Radiology 197 (1995) 320-320.
[18] Ichikawa, T.; Tamiya, T.; Adachi, Y.; Ono, Y.; Matsumoto, K.; Furuta, T.; Yoshida, Y.; Hamada, H.; Ohmoto, T. In vivo efficacy and toxicity of 5-fluorocytosine/cytosine deaminase gene therapy for malignant gliomas mediated by adenovirus Cancer Gene Therapy 7 (2000) 74-82.
[19] Grote, M.; Gupta, A.; Noll, St.; Kniess, T.; Noll, B.; Schackert, H.K.; Hauses, M. Substrates of the herpes-simplex virus 1 thymidine kinase and Escherichia Coli cytosine deaminase for monitoring gene expression. Part 7: exploiting cytosine deaminase from Escherichia Coli for suicide gene therapy. *This Report*, pp. 88-89.
[20] Ogilvie, K.K.; Hamilton, R.G.; Gillen, M.F.; Radatus, B.K.; Smith, K.O.; Galloway, K.S. Uracil analogues of the acyclonucleoside 9-[[2-hydroxy-1-(hydroxymethyl)ethoxy]-methylguanine (BIOLF-62). Can. J. Chem. 62 (1984) 16-21.
[21] Ogilvie, K.K.; Nguyen-ba, N.; Gillen, M.F.; Radatus, B.K.; Cheriyan, U.O.; Hanna, H.R.; Smith, K.O.; Galloway, K.S. Synthesis of a purine acyclonucleoside series having pronounced antiviral activity. The glyceropurines. Can. J. Chem. 62 (1984) 241-252.
[22] Harnden, M.R.; Jarvest, R.L.; Bacon, T.H.; Boyd, M.R. Synthesis and antiviral activity of 9-[4-hydroxy-3-(hydroxymethyl)but-1-yl]purines. J. Med.Chem. 30 (1987) 1636-1642.
[23] Boryski, J.; Golankiewicz, B.; De Clercq, E. Synthesis and antiviral activity of novel N-substituted derivatives of acyclovir. J. Med. Chem., 31 (1988) 1351-1355.
[24] Wilson, A.A.; Conti, P.S.; Dannals, R.F.; Ravert, H.T.; Wagner, Jr. H.N. Radiosynthesis of [^{11}C]-N-methylacyclovir. J. Labelled. Compd. Radiopharm. 7 (1991) 765-768.

26. Substrates of the Herpes-Simplex-Virus 1 Thymidine Kinase and Escherichia Coli Cytosine Deaminase for Monitoring Gene Expression
Part 2: Synthesis of New IVFRU Derived Nucleosides

T. Kniess, B. Noll

Introduction

(E)-5-(2-iodovinyl)-2'-fluoro-2'-deoxyuridine (IVFRU), a nucleoside analogue that displays potent and selective anti-HSV-1 activity in vitro, is an effective substrate for herpes simplex virus type-1 thymidine kinase (HSV-1 Tk) [1, 2]. Bearing a fluorine substituent at the 2'-position, IVFRU is also resistant to phosphorylase–mediated deglycosation [3]. The facile noninvasive scintigraphic detection of HSV-1 Tk gene expression in tumour cell lines, using [^{125}I] and [^{131}I] iodo labelled IVFRU, was reported [4, 5].
It seems to be worthwhile developing an IVFRU derivative labelled with the positron emitter [^{18}F]fluorine for utilization of the nucleoside to monitor gene expression by PET. Early attempts to introduce a [^{18}F]fluorine into the 2'-position of uridine produced very low yields [6]. Our approach started with the synthesis of new nonradioactive nucleosides derived from the IVFRU structure.

Experimental

General
2'-Fluoro-2'-deoxy-uridine **1** and 2'-chloro-3',5'-diacetyl-uridine **3** were synthesized as described in the literature [6, 7]. Preparative HPLC separation was performed with an RP 18 column (16 mm diameter) at a flow rate of 5 ml/min, isocratic mixtures of acetonitrile and water as eluents and UV detection at 254 nm. The melting points and ^{1}H NMR spectroscopic data of the new compounds were given as follows:

2'-Fluoro-2'-deoxy-3',5'-diacetyl-uridine **2**: colourless crystals; melting point: 172 – 173 °C
^{1}H NMR-data (ppm, DMSO-d_6): 2.02 (s, 3H, -OCH_3); 2.10 (s, 3H, -OCH_3); 4.17/4.35 (m, 1H, 5'-H); 4.26 (m, 1H, 4'-H); 5.22 (m, 1H, 3'-H); 5.47/5.60 (dd, 1H, 2'-H); 5.68 (d, 1H, 5-H), 5.89 (d, 1H, 1'-H), 7.72 (d, 1H, 6-H); 11.46, (s, 1H, -NH).

5-Iodo-2'-fluoro-2'-deoxy-uridine **4**: light yellow crystals; melting point: 210 – 213 °C
^{1}H NMR-data (ppm, DMSO-d_6): 3.59/3.80 (dd, 2H, 5'-H); 3.88 (d, 1H, 4'-H); 4.17 (d, 1H, 3'-H); 4.94 / 5.07 (dd, 1H, 2'-H); 5.38 (t, 1H, 5'-OH); 5.60 (d, 1H, 3'-OH); 5.85 (d, 1H, 1'-H); 8.49 (s, 1H, 6-H); 11.71 (s, 1H, -NH).

5-Iodo-2'-fluoro-2'-deoxy-3',5'-diacetyl-uridine **5**: yellow foam; melting point: 71 – 73 °C
^{1}H NMR-data (ppm, $CDCl_3$): 2.13 (s, 3H, -OCH_3); 2.19 (s, 3H, -OCH_3); 4.35 (m, 1H, 4'-H); 4.43 (d, 2H, 5'-H); 5,13 (m, 1H, 3'-H); 5.24/5.37 (dd, 1H, 2'-H); 5.89 (d, 1H, 1'-H); 7.88 (s, 1H, 6-H); 9.93 (s, 1H, -NH).

5-Iodo-2'-chloro-2'-deoxy-3',5'-diacetyl-uridine **6**: white foam; melting point: 62 - 66 °C
^{1}H NMR-data (ppm, $CDCl_3$): 2.18 (s, 3H, -OCH_3); 2.24 (s, 3H, -OCH_3); 4.39 (s, 2H, 5'-H); 4.46 (m, 1H, 4'-H); 4.57 (t, 1H, 3'-H); 5.19 (t, 1H, 2'-H); 6.10 (d, 1H, 1'-H); 7.92 (s, 1H, 6-H); 9.42 (s, 1H, -NH).

5-Iodo-2'-chloro-2'-deoxy-uridine **7**: white solid; melting point: >230 °C (decomp.)
^{1}H NMR-data (ppm, DMSO-d_6): 3.60/3.75 (dd, 2H, 5'-H); 3.94 (m, 1H, 4'-H); 4.23 (m, 1H, 3'-H); 4.58 (t, 1H, 2'-H); 5.44 (t, 1H, 5'-OH); 5.89 (d, 1H, 1'-H); 5.92 (d, 1H, 3'-OH); 8.52 (s, 1H, 6-H); 11.75 (s, 1H, -NH).

5-(3-Hydroxy-1(E)-propenyl)-2'-fluoro-2'-deoxy-uridine **8**: white solid; melting point: 180 - 183 °C
^{1}H NMR-data (ppm, DMSO-d_6): 3.60/3.77 (dd, 2H, 5'-H); 3.83 (d, 1H, 4'-H); 3,97 (d, 2H, propenyl-CH_2); 4.20 (m, 1H, 3'-H); 4.70 (t, 1H, propenyl-OH); 4.87/5.01 (dd, 1H, 2'-H); 5.37 (t, 1H, 5'-OH); 5.62 (d, 1H, 3'-OH); 5.91 (d, 1H, 1'-H); 6.19 (d, 1H, =CH-); 6.47 (dt, 1H, =CH-); 7.88 (s, 1H, 6-H); 11.46 (s, 1H, -NH).

5-(3-Hydroxy-1(E)-propenyl)-2'-fluoro-2'-deoxy-3',5'-diacetyl-uridine **9**: light yellow foam; melting point: 62 - 64 °C
^{1}H NMR-data (ppm, DMSO-d_6): 2.02 (s, 3H, -OCH_3); 2.09 (s, 3H, -OCH_3); 4.02 (t, 2H, propenyl-CH_2), 4.14/4.35 (dd, 2H, 5'-H); 4.27 (t, 1H, 4'-H); 4.81 (t, 1H; propenyl-OH); 5.28 (m, 1H, 3'-H);5.49/5.62 (dd, 1H, 2'-H); 5.91 (dd, 1H, 1'-H); 6.23 (d, 1H, =CH-); 6.59 (dt, 1H, =CH-); 7.80 (s, 1H, 6-H); 11.56 (s, 1H, -NH).

5-(3-Hydroxy-1(E)-propenyl)-2'-chloro-2'-deoxy-uridine **10**: oil
^{1}H NMR-data (ppm, DMSO-d_6): 3.24/3.29 (m, 2H, 5'-H); 4.02 (t, 2H, propenyl-CH_2); 4.07 (t, 1H, 4'-H); 4.38 (m, 1H, 3'-H); 5.19 (m, 1H, 2'-H); 5.90 (s, 1H, -OH); 6.29 (d, 1H, 1'-H); 6.31 (d, 1H, =CH-); 6.68 (dt, 1H, =CH-); 8.01 (s, 1H, 6-H); 11.42 (s, 1H, -NH).

5-(3-Methoxy-1(E)-propenyl)-2'-fluoro-2'-deoxy-3',5'-diacetyl-uridine **11**: oil
^{1}H NMR-data (ppm, DMSO-d_6) : 2.02 (s, 3H, -$COOCH_3$); 2.10 (s, 3H, -$COOCH_3$); 3.23 (s, 3H, -OCH_3); 3.94 (d, 2H, propenyl-CH_2); 4.20/4.32 (m, 2H, 5'-H); 4.27 (t, 1H, 4'-H); 5.29 (m, 1H, 3'-H); 5.49/5.62 (dd, 1H, 2'-H); 5.90 (d, 1H, 1'-H); 6.26 (d, 1H, =CH-); 6.55 (dt, 1H, =CH-); 7.84 (s, 1H, 6-H); 11.60 (s, 1H, -NH).
5-(3-Methoxy-1(E)-propenyl)-2'-fluoro-2'-deoxy-uridine **12**: white solid; melting point: 73 - 77°C
^{1}H NMR-data (ppm, DMSO-d_6) : 3.31 (s, 3H, -OCH_3); 3,62/3.79 (dd, 2H, 5'-H); 3.88 (d, 1H, 4'-H); 3.92 (d, 2H, propenyl-CH_2); 4.20 (m, 1H, 3'-H); 4.97/5.10 (dd, 1H, 2'-H); 5.38 (t, 1H, 5'-OH); 5.62 (d, 1H, 3'-OH); 5.92 (d, 1H, 1'-H); 6.24 (d, 1H, =CH-); 6.43 (dt, 1H, =CH-); 8.17 (s, 1H, 6-H); 11.49 (s, 1H, -NH).

Results and Discussion

The synthesis strategy was based on the introduction of an alkenyl side chain to 5-iodo-2'-halogeno-uridines. This chain was to bear a formal functional group, primarily hydroxyl, to facilitate a further modification with a view to [^{18}F]fluorine labelling.
The scheme of synthesis is outlined in Fig. 1. 2,2'-Anhydrouridine was the general starting material. Ring cleavage with hydrogen fluoride in dioxane under anhydrous conditions produced 2'-fluoro-2'-deoxy-uridine **1** .By reacting 2,2'-anhydrouridine with an excess of acetyl chloride in acetonitrile, a chlorine atom was introduced at the 2'-position with simultaneous acetylation of the 3'- and 5'-position to yield 2'-chloro-2'-deoxy3',5'-diacetyl-uridine **3**.

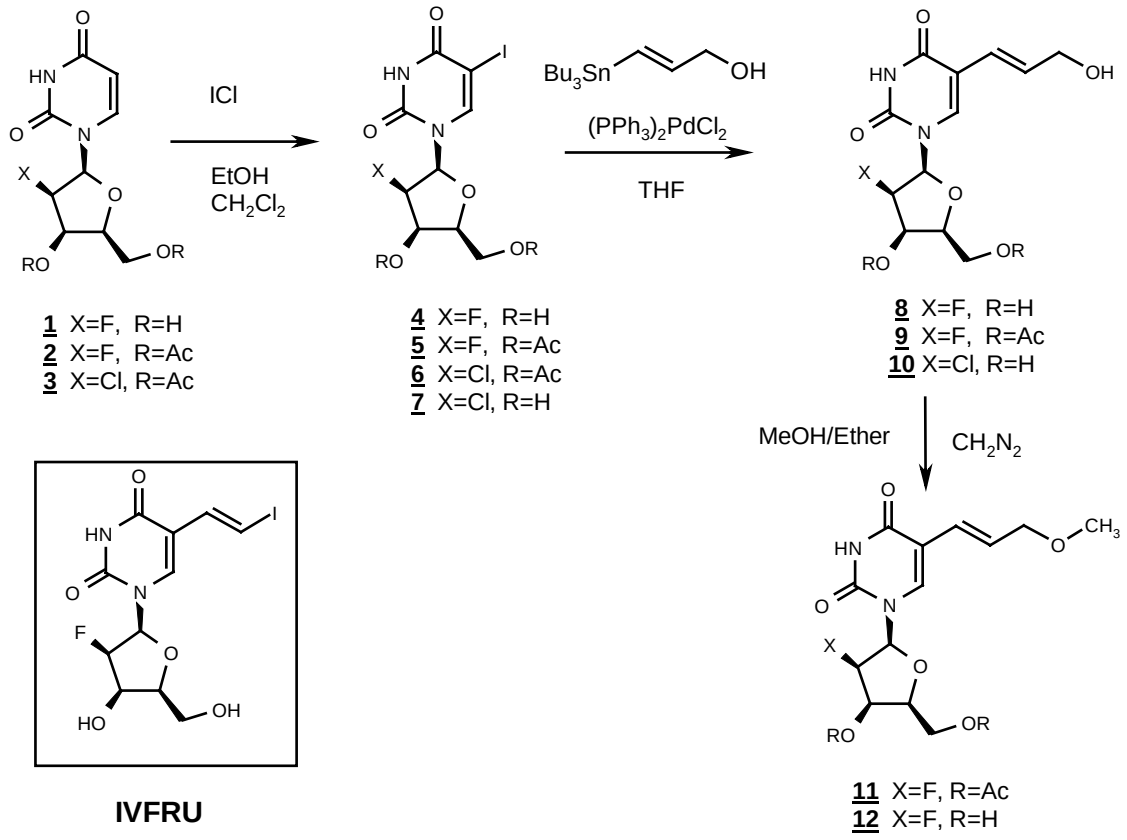

Fig. 1. Scheme of synthesis of nucleosides derived from IVFRU

Compound **2** was synthesized in a 62 % yield by reaction of **1** with acetic anhydride in the classical manner. For the introduction of the side chain at the 5-position of the uridine, this point had to be activated by a iodine substituent. So 5-iodo-2'-fluoro-2'-deoxy-uridine **4** was produced by iodination of **1** with iodine monochloride in methanol at 80 °C, which produced good results (a 67 % yield). This seems to be a simpler procedure than iodination of **1** with sodium iodide and nitric acid as described in the literature [9]. For iodination of **2** and **3** an aprotic solvent such as dichloromethane was required to prevent complete deprotection of the hydroxyl groups. For **5** the yield of this reaction came to 88 %

and for **6** it was 93 %. 5-Iodo-2'-chloro-2'-deoxy-uridine **7** was synthesized by removing the acetyl protective groups in **6** with potassium carbonate in water.
Furthermore, we focused on having a hydroxyl group at the end of the side chain. The preparation of a protected tributylstannylated unsaturated alcohol seemed to be difficult, so we tried coupling it with E-(1-tributylstannyl)-propene-1-ol. By reaction of **5** and E-(1-tributylstannyl)-propene-1-ol with $(PPh_3)_2PdCl_2$ in dry tetrahydrofurane the 5-alkylated nucleoside **9** was obtained in a 49 % yield. Using the nonprotected nucleosides **4** or **7** as starting compounds, the yields of the products were small (8 to 26 %).
To modify the free hydroxyl group of the side chain **9** was methylated with diazomethane. The structure of the resulting methyl ether **11** was identified by the appearance of a new methyl group in the ^{1}H-NMR spectrum at 3.23 ppm, while the signal of the former hydroxyl group at 4.81 ppm was no longer detected. Compound **11** was also deprotected with potassium carbonate to obtain the nucleoside **12** in a 32 % yield.
To sum up, alkenylation of the 5-position of 2'-fluoro-2'-deoxy-uridine with a stannylated 3-hydroxy-(E)-1-propenyl side chain opened the way to synthesizing new 3-hydroxy-(E)-1-propenyl substituted uridine derivatives similar to IVFRU.

References

[1] Iwashina, T.; Tovell, D.R.; Xu, L.; Tyrrell, D.L..; Knaus, E.E.; Wiebe, L.I. Synthesis and antiviral activity of IVFRU, a potential probe for the non-invasive diagnosis of herpes simplex encephalitis. Drug Des. Deliv. 3 (1988) 309-321.

[2] Balzarini, J.; Morin, K.W.; Knaus, E.E.; Wiebe, L.I.; De Clercq, E. Novel (E)-5-(2-iodovinyl)-2'-deoxyuridine derivatives as potential cytostatic agents against herpes simplex virus thymidine kinase gene transfected tumors. Gene Therapy 2 (1995) 317-322.

[3] Samuel, J.; Gill, M.J.; Iwashina, T.; Tovell, D.R.; Tyrrell, D.L.; Knaus, E.E.; Wiebe, L.I. Pharmacokinetic and metabolism of E-5-(2[^{131}I]iodovinyl)-2'-deoxy-uridine in dogs. Antimicrob. Agents Chemother. 29 (1986) 320-324.

[4] Morin, K.W.; Atrazheva, E.D.; Knaus, E.E.; Wiebe, L.I. Synthesis and cellular uptake of 2'-substituted analogues of (E)-5-(2-[^{125}I]iodovinyl)-2'-deoxyuridine in tumor cells transducted with the herpex simplex type-1 thymidine kinase gene. Evaluation as probes for monitoring gene therapy., J. Med. Chem. 40 (1997) 2184-2190.

[5] Morin, K. W.; Knaus, E.E.; Wiebe, L.I.; Non-invasive scintigraphic monitoring of gene expression in a HSV-1 thymidine kinase gene therapy model. Nucl. Medicine Commun. 18 (1997) 599-605.

[6] Abrams, D.N.; Mercer, J.R.; Knaus, E.E.; Wiebe, L.I. The synthesis of radiolabelled 1-(2'-fluoro-2'-deoxy-β-D-ribofuranosyl)-uracil and 1-(2'-chloro-2'-deoxy-β-D-ribofuranosyl)-uracil. J. Appl. Radiat. Isot. 3 (1985) 233-238.

[7] Marumoto, R.; Honjo, M. One-step halogenation at the 2'-position of uridine and related reactions of cytidine and N^4-acetylcytidine. Chem. Pharm. Bull. 22 (1974) 128-134.

[8] Jung, M.E.; Light, L.A.. Preparation of iodoallylic alcohols via hydrostannylation: spectroscopic proof of structures. Tetrahedron Lett. 38 (1982) 3851-3854.

[9] Mercer, J.R.; Xu, L.H.; Knaus, E.E.; Wiebe, L.I. Synthesis and tumor uptake of 5-[^{85}Br]- and 5-[^{131}I]-labeled 5-halo-1-(2-fluoro-2-deoxy-β-D-ribofuranosyl)uracils. J. Med. Chem. 32 (1989) 1289-1294.

27. Substrates of the Herpes-Simplex-Virus 1 Thymidine Kinase and Escherichia Coli Cytosine Deaminase for Monitoring Gene Expression

Part 3: Synthesis of a Precursor for Labelling of 5-Iodo-2'-fluoro-2'-deoxy-uridine (FIRU) with [^{18}F]Fluorine

T. Kniess, St. Noll, B. Noll

Introduction

Imaging by gamma scintigraphy has been of increasing interest for the detection of HSV-1 Tk expression. For that purpose 5-Iodo-2'-fluoro-2-deoxy-uridine (FIRU), a substrate of HSV-1 Tk was labelled with the isotopes [^{131}I] and [^{125}I]iodine and the *in-vitro* uptake of the radioiodinated compounds was determined in tumour cells transducted with a retroviral vector possessing the HSV-1 Tk-gene [1, 2]. In a comparative study between [^{123}I]IVFRU and [^{125}I]FIAU, the [^{125}I]FIRU provided optimal performance in terms of selectivity for HSV-1 Tk expressing cells and with 14 % of the injected dose/gram of tumour the highest uptake [3].
To make use of the advantages of PET we were looking for a method to introduce [^{18}F]fluorine into FIRU. Previous attempts at labelling 2'-fluoro-2'-deoxy-uridine with [^{18}F]fluorine in the 2'-position were thwarted by very low yields [4]. Our approach consisted in labeling FIRU in the 3'-position, for which we needed a suitable precursor. This paper reports the synthesis of a FIRU derivative which is methylsulphonylated in the 3'-position and methoxy-tritylated in the 5'-position and may serve as a precursor for [^{18}F]fluorine labelling.

Experimental

5-Iodo-2'-fluoro-2'-deoxy-5'-(p-methoxy-triphenylmethyl)-uridine **2**: melting point: 96 - 100 °C
^{1}H NMR data (ppm, DMSO-d_6): 3.23 (s, 2H, 5'-H); 3.73 (s, 3H, -OCH_3); 4.01 (m, 1H, 4'-H); 4.33 (m , 1H, 3'-H); 5.09/5.23 (dd, 1H, 2'-H); 5.59 (d, 1H, 3'-OH); 5.84 (d, 1H, 1'-H); 6.90-7.42 (m, 14H, H_{arom}); 8.06 (s, 1H, 6-H); 11.79 (s, 1H, -NH).
5-Iodo-2'-fluoro-2'-deoxy-5'-(p-methoxy-triphenylmethyl)-3'-methylsulfonyl-chloride **3**: melting point : 122 – 126 °C
^{1}H NMR-data (ppm, DMSO-d_6): 3.18 (s, 3H, SO_2CH_3); 3.23/3.37 (dd, 2H, 5'-H); 3.72 (s, 3H, -OCH_3); 4.20 (s, 1H, 4'-H); 5.47 (m, 1H, 3'-H); 5.56/5.69 (dd, 1H, 2'-H); 5.90 (d, 1H, 1'-H); 6.87-7.41 (m, 14H, H_{arom}); 8.21 (s, 1H, 6-H); 11.91 (s, 1H, -NH).

Results and Discussion

The synthesis of the precursor **3** is illustrated in Fig. 1. FIRU **1** [2] was reacted with p-methoxy-triphenylmethyl chloride and 4-dimethylamino-pyridine in acetonitrile at 40 °C. After purification by column chromatography the p-methoxy-tritylated product **2** was obtained in a 64 % yield. Although we used a twofold excess of p-methoxy-triphenylmethyl chloride, no tritylation in the 3'-position was observed, as was proved by ^{1}H NMR spectroscopy with the appearance of the –OH signal at 5.59 ppm. This is consistent with the literature where the protecting reagent is described as being selective for the 5'-position of nucleosides.

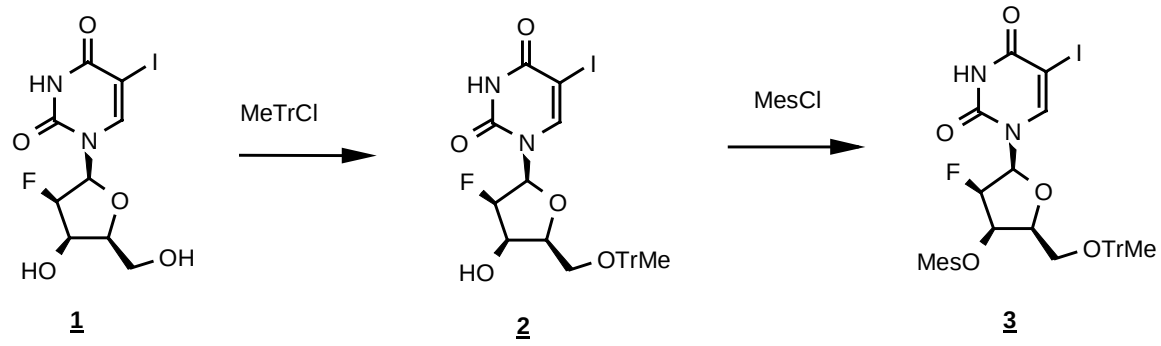

1 **2** **3**

Fig. 1. Methoxytritylation and mesylation of FIRU

Mesylation was carried out by reacting **2** with methanesulphonyl chloride in dry dichloromethane and triethylamine at room temperature. For separation of **3** from unreacted starting material we had to carry out a preparative HPLC on a RP 18 column with an isocratic mixture of acetonitrile/water. In this way **3** was obtained as a white foam in a 60 % yield. In the ^{1}H NMR spectrum of **3** the mesyl group is detectable as a new signal at 3.18 ppm while the signal of the 3'-proton is shifted by the new substituent to 5.47 ppm compared from 4.33 ppm in the starting compound **2**.
The mesylated product **3** will be used as a precursor for fluorination with potassium fluoride and kryptofix-2.2.2 in acetonitrile to obtain the inactive 2',3'-difluorinated nucleoside needed after deprotection as reference compound for the labelling with [^{18}F]fluorine.
Efforts to synthesize a 3'-tosylated precursor by reaction of **2** with p-toluenesulphonyl chloride in dry pyridine resulted in the loss of the methoxytrityl group during this reaction so that only the 5'-iodo-2'-fluoro-2'-deoxy-3'-(p-tolylsulfonyl)-uridine was isolated.

References

[1] Tovell, D.R.; Samuel, J.; Mercer, J.R.; Misra, H.K.; Xu, L.; Wiebe, L.I.; Tyrrell, D.L.; Knaus, E.E. The in vitro evaluation of nucleoside analogues as probes for use in the non-invasive diagnosis of herpes simplex encephalitis. Drug Des. Deliv. 3 (1988) 213-221.

[2] Mercer, J.R.; Xu, L.H.; Knaus, E.E.; Wiebe, L.I. Synthesis and tumor uptake of 5-[^{82}Br]- and 5-[^{131}I]-labelled 5-halo-1-(2-fluoro-2-deoxy-β-D-ribofuranosyl)uracils. J. Med. Chem. 32 (1989) 1289-1294.

[3] Wiebe, L.I.; Knaus, E.E.; Morin, K.W. Radiolabelled pyrimidine nucleosides to monitor the expression of HSV-1 thymidine kinase in gene therapy. Nucleosides Nucleotides 18 (1999) 1065-1066.

[4] Abrams, D.N.; Mercer, J.R.; Knaus, E.E.; Wiebe, L.I. The synthesis of radiolabelled 1-(2'-fluoro-2'-deoxy-β-D-ribofuranosyl)-uracil and 1-(2'-chloro-2'-deoxy-β-D-ribofuranosyl)-uracil. J. Appl. Radiat. Isot. 3 (1985) 233-238.

28. Substrates of the Herpes-Simplex-Virus 1 Thymidine Kinase and Escherichia Coli Cytosine Deaminase for Monitoring Gene Expression.
Part 4: Synthesis and Tosylation of 5-Hydroxymethyl-Cytosine

T. Kniess, St. Noll, B. Noll

Introduction

The cytosine deaminase gene of Escherichia coli is one of the suicide genes used in gene therapy. For monitoring the gene expression by PET, a cytosine derivative labelled with the positron emitting element [^{18}F]fluorine is obligatory. 5-[^{18}F]Fluoro-cytosine, synthesized some years ago [1] is unlikely to be suitable since the resulting 5-[^{18}F]fluoro-uracil is not accumulated in the cell which results in an unfavourable target/nontarget ratio.
Looking for other substrates of cytosine deaminase usable for development of a [^{18}F]fluorine labelled imaging agent, we considered 5-hydroxymethyl-cytosine .The synthesis and tosylation are described in this report.

Experimental

The structures and purity of the synthesized compounds were confirmed by elemental analysis and ^{1}H NMR spectroscopy.

4-Amino-5-carbethoxy-2-mercaptopyrimidine **1**: white solid; melting point: 261 - 265 °C
^{1}H NMR data (ppm, DMSO-d_6): 1.25 (3H, t, -CH_3); 4.22 (2H, q, -CH_2-); 7.86 (1H, s, -NH), 8.01 (1H, s, -=CH-); 8.50 (1H, s, -NH); 12.65 (1H, s, -SH).

4-Amino-5-carbethoxy-2-methylthiopyrimidine **2**: white crystals; melting point: 125 – 127 °C
^{1}H NMR-data (ppm, DMSO-d_6): 1.27 (3H, t, -CH_3); 2,45 (3H, s, -SCH_3), 4,24 (2H, q, -CH_2-), 7.64(1H, s, -NH); 8.01 (1H, s, -NH); 8.55 (1H, s, =CH-).

4-Amino-5-hydroxymethyl-2-methylthio-pyrimidine **3**: white cristals; melting point: 121 - 123 °C
^{1}H NMR-data (ppm, DMSO-d_6): 2.37 (3H, s, -SCH_3); 4.27 (2H, d, -CH_2-); 5.28 (1H, s, -OH); 6.74 (2H, s, -NH_2); 7.87 (1H, s, =CH-).

5-Hydroxymethyl-cytosine **4**: white solid, melting point: > 300 °C (decomp.)
^{1}H NMR-data (ppm, DMSO-d_6): 4.13 (2H, d, -CH_2-); 4.94 (1H, t, =CH-); 6.48 (1H, s, -OH), 7.25 (2H, s, -NH_2); 10.47 (1H, s, -NH-).

N^4-Tosyl-5-hydroxymethyl-cytosine **5**: white solid, melting point: 190 - 192°C
^{1}H NMR-data (ppm, DMSO-d_6): 2.39 (3H, s, -CH_3); 4.25 (2H, d, -CH_2-); 5.26 (1H, t, -OH); 7.33 (1H, s -NH-); 7,44 (2H, d, Ar); 7.82(2H, d, Ar); 8.00 (1H, s, =CH-); 8,10 (1H, s, -NH-).

Results and Discussion

The synthesis of 5-hydroxymethyl-cytosine was adapted from the literature [2]. The scheme of reaction is illustrated in Fig. 1. 4-Amino-5-carbethoxy-*2*-mercaptopyrimidine **1** was synthesized in a 56 % yield by cyclization of ethyl-ethoxymethylene-cyanoacetate with thiourea. The methylation of **1** was a crucial step in the course of the reaction. Despite using an excess of dimethyl sulphate, large amounts of unreacted starting material remained. An effective separation of product **2** was required, which was only possible by Soxhlet extraction with 20 % acetic acid. In this way the pure **2** was isolated only in a 37 % yield. The reduction of the carboxylic group of **2** with $LiAlH_4$ went without problems to supply the hydroxyl compound **3** in a 68 % yield. The desired 5-hydroxymethyl-cytosine **4** was obtained by desulphuration of **3** with hydrochloric acid, the yield in this step was 39 %. Summing up, we find the overall yield of this 4-step synthesis to be only 5.4 % compared with 36 % described in the literature.

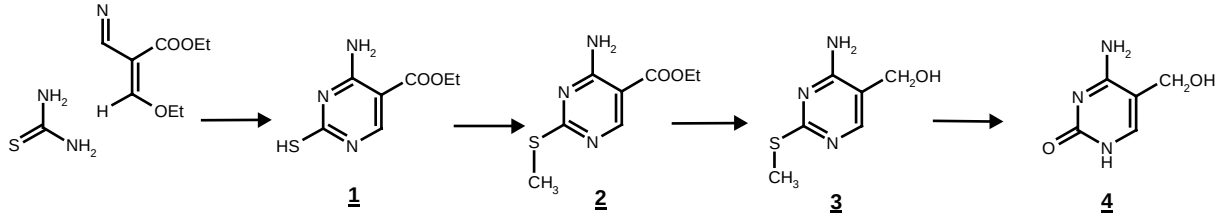

Fig. 1. Scheme of synthesis of 5-hydroxymethyl-cytosine **4**

To label 5-hydroxymethyl-cytosine with [^{18}F]fluorine, a precursor bearing an activated leaving group is required. Tosylate and triflate, the most often used leaving groups, were introduced by reaction of a hydroxyl group with p-toluenesulphonyl chloride or trifluoromethanesulphonic anhydride. In the reaction of 5-hydroxymethyl-cytosine **4** with tosyl chloride in dry pyridine, tosylation was expected at the hydroxyl or at the amino group. The product we isolated was identified as N^4-tosyl-5-hydroxymethyl-cytosine **5** (Fig. 2). The structure was confirmed by ^{1}H NMR where a free unsubstituted hydroxyl group occurred at 5.26 ppm. So the amino group was found to be the preferred position for tosylation. When tosylation at the 5-position is intended, the amino group has to be protected, for instance by a BOC group.
The usefulness of the N-tosylated compound **5** as a precursor for fluorination with fluorine gas to yield an N-fluorinated cytosine derivative will be investigated.

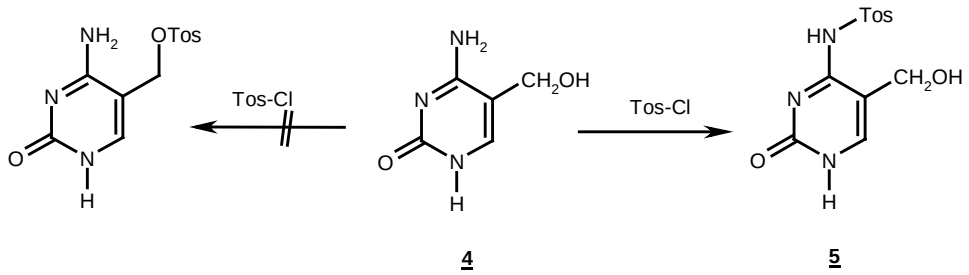

4 **5**

Fig. 2. Tosylation of 5-hydroxymethyl-cytosine **4**

References

[1] Visser, G.W.M.; Boele, S.; Knops, G.H.J.N.; Herscheid, J.D.M.; Hoekstra, A. Synthesis and biodistribution of [^{18}F]-5-fluorocytosine. Nucl. Med. Commun. 6 (1985) 455-459.

[2] Ulbricht, T.L.V.; Price, C.C. The synthesis of some pyrimidine metabolite analogs. J. Org. Chem. 21 (1956) 567-571.

29. Substrates of the Herpes-Simplex-Virus 1 Thymidine Kinase and Escherichia Coli Cytosine Deaminase for Monitoring Gene Expression.

Part 5: Efficiency Study to Improve the ^{18}F-labelling of N^1-Methyl-9-[(1-hydroxy-3-[^{18}F]fluoro-2-propoxy)methyl]guanine by HPLC Detailed Control

B. Noll, M. Scheunemann, M. Grote, St. Noll

The ^{18}F-labelled derivative of Ganciclovir 9-[(1-hydroxy-3-[^{18}F]fluoro-2-propoxy)methyl]guanine ([^{18}F]FHPG) is an useful substrate of the Herpes-Simplex-Virus 1 Thymidine Kinase (HSV1-TK) for monitoring the expression of the therapeutic gene.
The predominant elimination for the tracer is via the renal excretion pathway. Although, significant tracer amounts of [^{18}F]FHPG were found in the intestine [1]. To increase the renal excretion pathway we intended to vary the lipophilicity of [^{18}F]FHPG by introduction of a methyl group into the N^1-position of ganciclovir to get N^1-Methyl-9-[(1-hydroxy-3-[^{18}F]fluoro-2-propoxy)methyl]guanine **3** [1]. Attempts to label the corresponding precursor according to the procedure described in [2] for [^{18}F]FHPG synthesis failed. However we succeeded in modifying the procedure so that the labelling product **3** results to >25 % yield.

^{18}F-Labelling Procedure

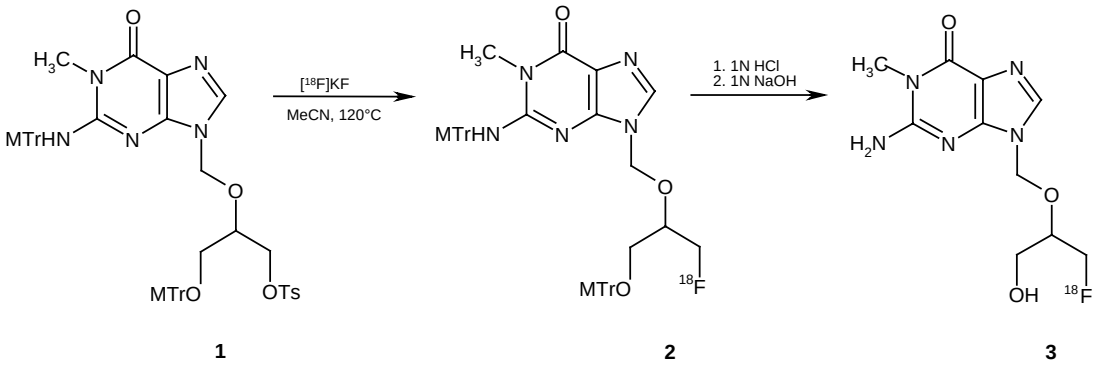

Fig.1. [^{18}F] labelling of the precursor (**1**) containing methoxy trityl (MTr) protecting groups and a tosyl leaving group (Ts).

The modified procedure involves the azeotropic destillation of the ^{18}F containing mixture of kryptofix 2.2.2 and K_2CO_3 with acetonitrile and evacuation of the reaction vial under vacuum. To this anhydrous fluoride / kryptofix complex a solution of the precursor **1** in dry acetonitrile was added and heated at 140 °C. After cooling, first HPLC analysis was performed to investigate the formation of the intermediate compound **2**. Subsequently, the reaction mixture was passed through a Sep-Pak silica gel cartridge (LiChrolut Si, MERCK). It was pretreated with methanol and dried before use. The cartridge was eluted with 15 % MeOH in CH_2Cl_2 and in a further HPLC analysis the eluate was investigated. The methylene chloride was removed in a continuous flow of nitrogen. To split off the protecting groups 1 N HCl was added and the closed vial heated. The completeness of the reaction was checked after 2 min and 5 min. The mixture was neutralised by adding of NaOH and purified by semipreparative HPLC (eluent: 5 % acetonitrile / water, flow rate 5 ml/min, column: Knauer Hypersil-ODS, 10 µm, 250 × 8 mm).
The isolated fraction was diluted with water and passed through an activated polystyrene cartridge (LiChrolut EN, Merck). The cartridge was washed with 2 ml water and finally the product eluted with ethanol. HPLC analysis reveals that the "cold" reference compound co-elutes with the [^{18}F] labelled product.

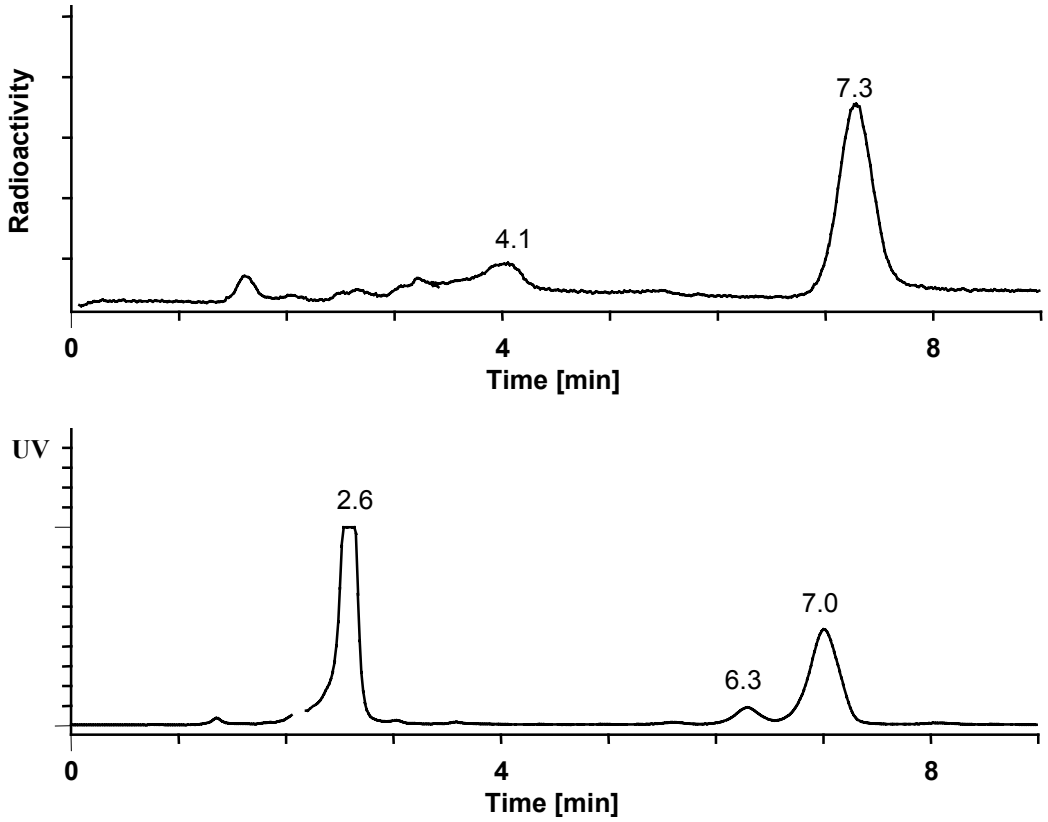

Fig. 2. HPLC chromatograms of the intermediate **2** after adding the inactive reference compound; column: Nucleosil C 8 25 x 4 mm, Knauer, eluent (isocratic): 30 % H_2O / 70 % MeCN, flow: 1 ml/min

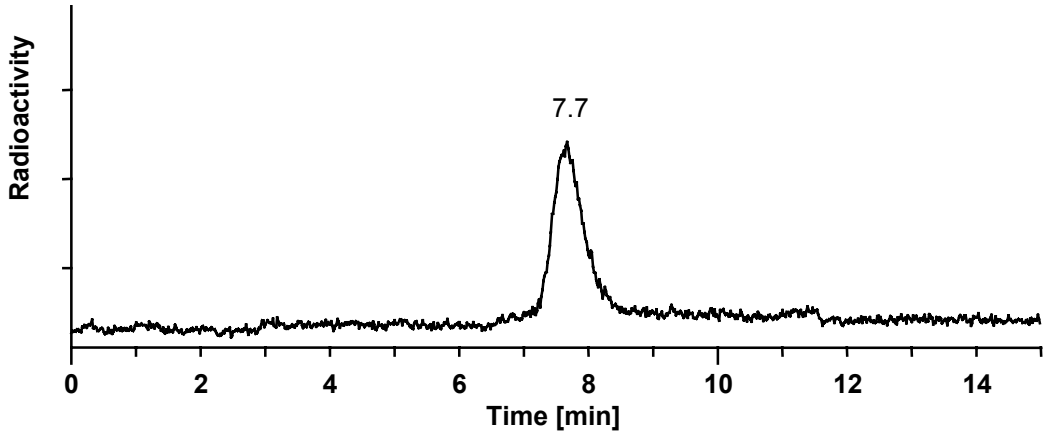

Fig. 3. HPLC chromatogram of the ^{18}F labelled final product **3**; (column: Eurospher-100 C18, 250x 4mm, eluent A: H_2O, eluent B: MeCN; 5 min 92% A/ 8 % B; 15 min from 92% A/8 % B to 0 % A/100 % B; 5 min 0 % A/100 % B).

Discussion

We found that **1** can be converted in the fluorinated product **2** in about 75 % yield showing that the tosyl leaving group is well appropiated for this labelling step (Fig. 1). Several inactive substances in the reaction mixture (unreacted precursor **1** (R_t = 9.7 min), p-toluenesulfonic acid (R_t = 2.1 min) and some unidentified species (R_t = 3.2 min) and additionally some radioactive impurities (Fig. 2) were successfully removed by a Sep Pak cartridge purification. A reaction time of 5 min was sufficient to remove the methoxytrityl protecting groups.

Whereas the radiochemical yield of the labelling method described in [2] was approximately 10 % (decay corrected), the yield in our preparation amounts to >20 % with a radiochemical purity >95 %. The preparation time was not optimized but does not exceed, in sum, 175 min. This modified method of the ^{18}F labelling of precursors having tosyl as leaving group can successfully be transferred to a series of precursors with acyclic sugar derivatives.

References

[1] Noll, B; Noll, St; Scheunemann, M.; Brust, P.; Jordanova, A.; Friedrich, A.; Koufaki, O.; Schackert, G.; Schackert, H.K.; Johannsen, ;Synthesisb. Preliminary evaluation of N^1-methyl-9-[(3-[^{18}F]fluoro-1-hydroxy-2-propoxy)methyl]guanine [^{18}F]MFHPG in rats. Publication in preparation.

[2] Alauddin, M.M.; Conti, P.S.; Mazza, S.M.; Hamzeh, F.M.; Lever, J.R. 9-[(3-[^{18}F]-fluoro-1-hydroxy-2-propoxy)methyl]guanine ([18F]-FHPG): a potential imaging agent of viral infection and gene therapy using PET Nucl. Med. Biol. 23 (1996) 787-792.

30. Substrates of the Herpes-Simplex-Virus 1 Thymidine Kinase and Escherichia Coli Cytosine Deaminase for Monitoring Gene Expression.

Part 6: Results of a Fast and Simple Screening Method to Determine Possible Substrates for the Herpes-Simplex-Virus 1 Thymidine Kinase

M. Grote, B. Noll, St. Noll, T. Kniess, L. Scapozza[1]
[1]Department Pharmacy, ETH Zurich

As explained in the editorial, the Herpes Simplex Virus Type-1 Thymidine Kinase (HSV1-TK) is characterized by a broad substrate diversity. It phosphorylates several pyrimidine and purine nucleoside analogues into their corresponding monophosphates. Because of the low stereochemical demands for the sugar moiety, ribofuranosyl and arabinofuranosyl derivatives of these bases as well as molecules with open-chain side groups are accepted. The knowledge as to whether a compound is a suitable substrate for the HSV-1-TK or not is important for the use of radiolabelled derivatives for monitoring. A modified version of a previously published method [1] was used for this purpose.

Experimental Procedures

Materials: [*Methyl*-^{3}H]thymidine (185 GBq/mmol), adenosine-triphosphate (ATP) and bovine serum albumin (BSA) were obtained from Sigma. 5-Iodo-2'-fluoro-2'-deoxy-β-D-arabinofuranosyl-uridine (FIAU) **24** was purchased from Hartmann Analytic and 2'- fluoro 2'-deoxy-β-D-arabinofuranosyl-uridine **23** from ABX. Compounds **13** –**16**, **25** – **29** were commercially available (Aldrich), all others were prepared in our laboratories. Analysis was performed by RP-HPLC using Eurospher RP-18 (Knauer) columns (25 x 4 mm).
The viral TK was selected as previously described [1].

Nucleoside kinase assay: Standard assay conditions [2] were 50 mM tris buffer solution pH 7.5, 5 mM $MgCl_2$, 5 mM ATP, 0.5 mg/ml BSA and 1 μM [*methyl*- ^{3}H]thymidine in a final volume of 50 μl. Assays were incubated at 37 °C for 15 min. Fractions obtained by HPLC separation were collected and the radioactivity was determined by liquid scintillation measurement. 90 units/mg enzyme were determined, but one enzyme unit is defined as the amount of enzyme catalysing the formation of 1nm thymidine monophosphate / min. This correlates with previously published data.[3]

HPLC assay: In order to predict wether a compound is a substrate for the viral TK or not, the formation of ADP and the corresponding monophosphate was quantitatively monitored by ion-pair HPLC with NaH_2PO_4-buffer, tetrabutylammonium hydrogensulfate and varying amounts of methanol as the eluent. The ratio ADP / ATP provided information about the possible substrate affinity. The formation of the nucleoside monophosphate was qualitatively checked. A typical assay was carried out at 37 °C and contained 50 mM tris, pH 7.5, 5 mM $MgCl_2$, 5 mM ATP, 1 – 5 μg enzyme (HSV-1 TK) and 1 mM substrate. Samples were taken after 1 h, 4 h and 8 h and diluted with water to stop the reaction. Every assay was repeated at least three times. Two blank reactions (no enzyme or no substrate) were run concurrently to determine the minimal reaction. ATP hydrolysis was not taken into account.

Results

A series of nucleosides were tested to obtain information about a possible substrate affinity to the HSV-1 TK. The results are shown in Fig. 1 and Fig. 2.

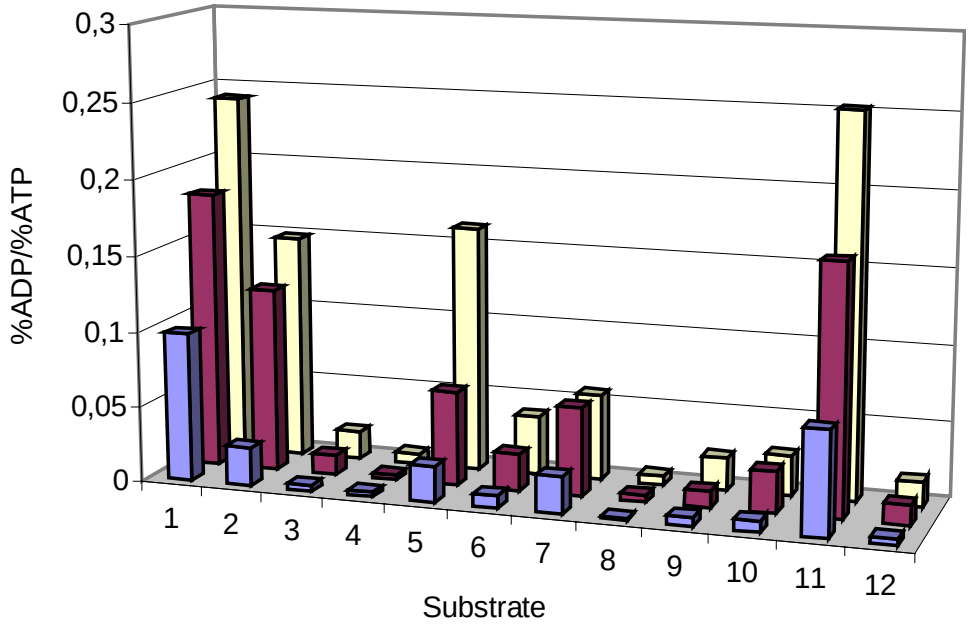

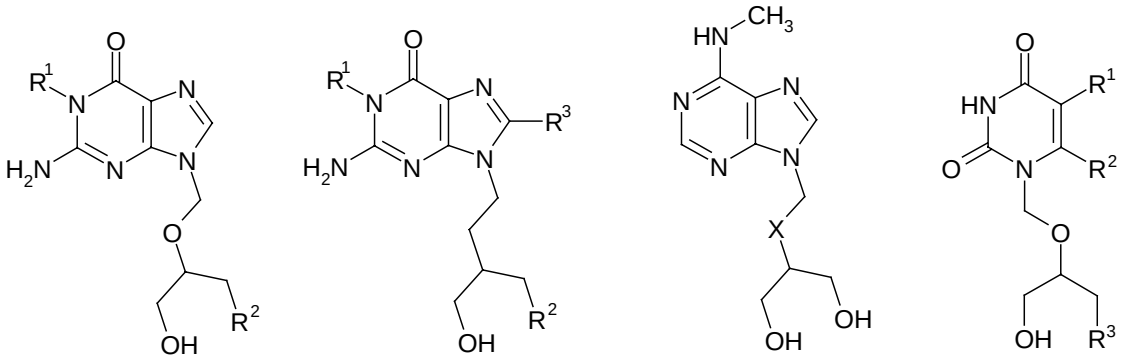

1 - **4** **5** - **7** **8** + **9** **10** - **11**

1. R^1 = H, R^2 = OH
2. R^1 = H, R^2 = F
3. R^1 = CH_3, R^2 = OH
4. R^1 = CH_3, R^2 = F
5. R^1 = H, R^2 = OH, R^3 = H
6. R^1 = CH_3, R^2 = OH, R^3 = H
7. R^1 = H, R^2 = OH, R^3 = Br
8. X = O
9. X = CH_2
10. R^1 = H, R^2 = CH_3, R^3 = OH
11. R^1 = H, R^2 = CH_3, R^3 = F
12. R^1 = OH, R^2 = H, R^3 = OH

Fig.1. ADP/ATP ratio of tested acyclopurines and -pyrimidines

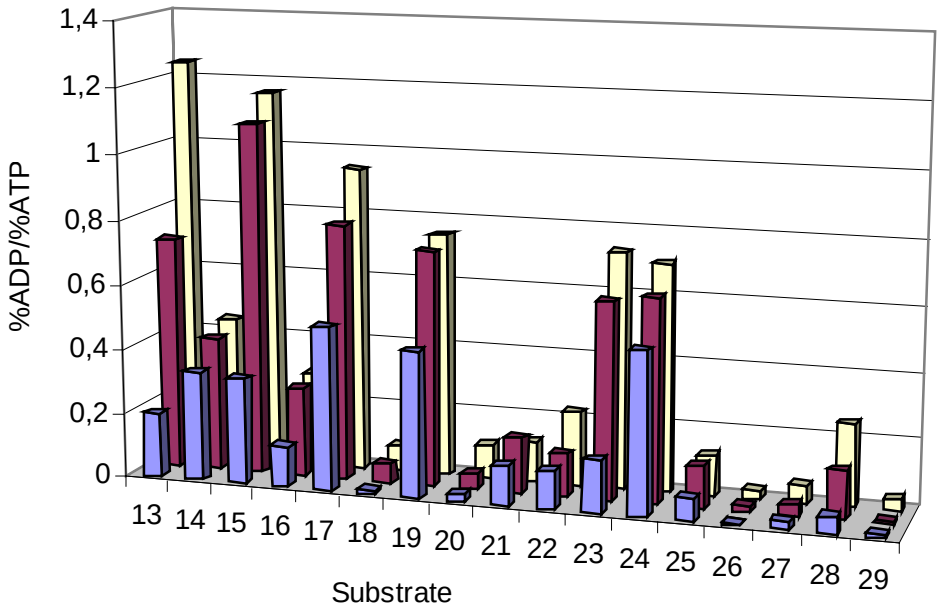

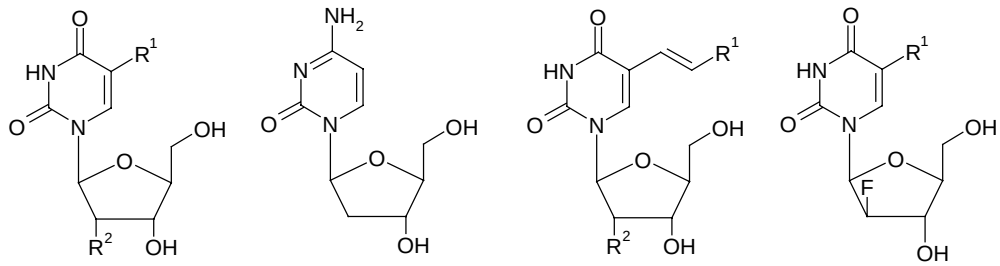

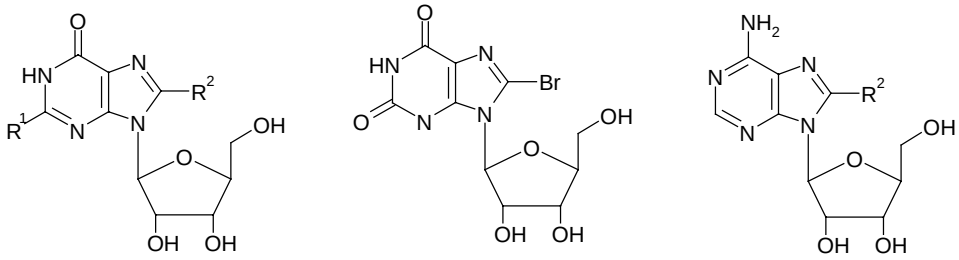

13. $R^1 = CH_3$, $R^2 = H$
14. $R^1 = H$, $R^2 = OH$
15. $R^1 = Br$, $R^2 = OH$
17. $R^1 = H$, $R^2 = F$
18. $R^1 = H$, $R^2 = Cl$
19. $R^1 = I$, $R^2 = F$
20. $R^1 = CH_2OH$, $R^2 = F$
21. $R^1 = I$, $R^2 = F$
22. $R^1 = CH_2OCH_3$, $R^2 = F$
23. $R^1 = H$, $R^2 = F$
24. $R^1 = I$, $R^2 = F$
25. $R^1 = H$, $R^2 = H$
27. $R^1 = NH_2$, $R^2 = H$
28. $R^1 = NH_2$, $R^2 = Br$

Fig. 2. ADP/ATP ratio of tested ribofuranosyl and arabinofuranosyl derivates

Discussion

The ion-pair HPLC allows quick screening of substances for their substrate activity in response to the HSV-1-TK enzyme. The retention times of ADP (5.8 min) and ATP (11.5 min) under standard conditions show a high reproducibility and permit a quantitative evaluation of the enzymatic conversion rate. Substances with an acyclic sugar moiety (**1**-**12**) generally have a lower conversion rate compared to those with cyclic sugar moiety (**13**-**18**) (Figs.1, 2).

A comparison of purines with an acyclic sugar moiety (**1** with **2** and **3** with **4**, Fig.1) shows that the substitution of a hydroxy group by fluorine results in a lower substrate affinity. An exception are the pyrimidine derivatives **10** and **11** where the fluorinated compound **11** shows a higher ADP formation rate than the non-fluorinated **10**. This phenomenon will be studied in further investigations. The carba analogue **5** (penciclovir) of **1** (ganciclovir) shows a similarly good ADP / ATP ratio as **1**. Against that, alkylation of the 1-NH group (**3**, **6**) or the N-methyl derivative of adenine (**8**, **9**) instead of guanine leads to a drastic decrease in the ADP / ATP ratio (Fig. 1).

Ribofuranosyl and arabinofuranosyl derivatives with a pyrimidine moiety show good ratios compared with thymidine (Fig. 2). By contrast, the affinity of derivatives with a purine base (**25**-**28**) is reduced. The substitution of the methyl group in 6-position of the uracil ring against bromine (**15**) or iodine (**19**), or of hydrogen respectively a hydroxy group in the 2'-position by fluorine (**17**, **19**, **23**, **24**) does not show great differences. But the introduction of a longer side chain (**20** – **22**) reduces the conversion rate. No differences worth mentioning were observed between furanosyl and arabinofuranosyl derivatives (**17**, **19**, **23**, **24**).

However, several ribofuranosyl pyrimidines (**13**-**16**, **23**) are also substrates for the mammalian thymidine host kinase and therefore not suitable for gene therapy nor, possibly, for monitoring.[**4**, **5**]

References

[1] Pilgert, B.D.; Perozzo, R.; Albers, F.; Wurth, C.; Folkers, G.; Scapozza, L. Substrate diversity of herpes simplex virus thymidine kinase. J. Biol. Chem. 274 (1999) 31967-31973.

[2] Balzarini, J.; Bohmann, C.; Walker, R.T.; de Clerq, E. Comparative Cytostatic Activity of different antiherpic drugs against herpes simplex virus thymidine kinase gene-transfected tumor cells. Mol. Pharm. 45 (1994) 1253-1258.

[3] Fetzer, J.; Michael, M.; Bohner, T.; Hofbauer, R.; Folkers, G. A fast method for obtaining highly pure recombinant herpes simplex virus type 1 thymidine kinase. Protein Expres. Purif. 5 (1994) 432-441.

[4] Conti, P.S. Synthesis of 2'-fluoro-5-[^{11}C]-metyl-1-ß-D-arabinofuranosyluracyl. Nucl. Med. Biol. 22 (1995) 783-789.

[5] Haberkorn, U.; Altmann, A.; Morr, I.; Knopf, K. W.; Germann, C.; Haeckel, R.; Oberdorfer, F.; van Kaick, G. Monitoring gene therapy with herpes simplex virus thymidine kinase in heptoma cells: uptake of specific substrates. J. Nucl. Med. 38 (1997) 287-294.

31. Substrates of the Herpes-Simplex-Virus 1 Thymidine Kinase and Escherichia Coli Cytosine Deaminase for Monitoring Gene Expression.
Part 7: Preparation of Cytosine Deaminase from Escherichia Coli

M. Grote, A. Gupta, St. Noll, T. Kniess, B. Noll, H. K. Schackert[1], M.Hauses[1]
[1]Abt. Chirurgische Forschung, Uniklinikum der TU Dresden

Introduction

Cytosine deaminase (CD), an enzyme which catalyses hydrolytic deamination of cytosine **1** to uracil **3**, originates in lower organisms such as Escherichia Coli and yeast's but not in mammalian cells [1]. The ability to convert 5-fluoro-cytosine **2** into cell-toxic 5-fluoro-uracil **4** makes it suitable for use in several suicide gene therapy protocols [2]. A suitable radiolabelled cytosine derivative would make it possible to monitor the transfection and expression of the suicide gene in tumor cells by positron emission tomography (PET), provided that a sufficient amount of the radiotracer is trapped in the tumor cells. The first step to developing such compounds is to prove their substrate affinity to cytosine deaminase in vitro. For that purpose the isolated enzyme was obtained by over-expression and purification from transformed Escherichia Coli bacteria. This paper describes the isolation of the CD and the determination of enzymatic activity by measuring the enzyme units, K_M and K_{kat} of the substrates cytosine and 5-fluorocytosine.

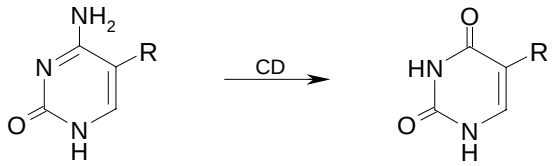

R = H (**1**) R = H (**3**)
R = F (**2**) R = F (**4**)

Fig.1. CD catalysis the deamination of cytosine **1** and 5-fluoro-cytosine **2**

Materials and Methods

Bacterial strain: Escherichia coli S∅113(CSH01 codA) with the expression vector pTrcHisCD were gifts from Dr. J. Gebert, Ruprecht-Karls-University, Heidelberg. Isopropyl β-D-thiogalactopyranoside (IPTG), imidazole, lysozyme, cytosine and 5-fluorocytosine were obtained from Sigma, purification was carried out using a standard kit (Quiagen). Pall Filtron Microsept Centrifugal Devices were used for concentration of the enzyme.
Media and growth conditions: The growth medium was LB medium (bacto-tryptone, bacto-yeast extract and NaCl in H_2O) containing 100 mM $MgCl_2$ and 100 mM $CaCl_2$.
Over-expression and purification: 200 ml LB liquid media (containing 400µl ampicilin) were inoculated with 5 ml of an overnight culture (LB/ampicilin) and grown at 37 °C until the OD_{600} was 0.5 (140min). Expression was induced by adding IPTG up to a final concentration of 1 mM, followed by cultivation for another of 4 hours, centrifugation and freezing of the cell pellets at –70 °C. To prove the expression of the CD, a Coomassie-stained SDS-PAGE analysis was performed which showed a clear induction tag in contrast to the noninduced sample. The cell pellets were resuspended in lysis buffer, lysozyme (1mg/ml) was added and the probes incubated on ice for 30 min. After ultrasonic treatment the lysate was centrifuged, the supernatant decanted and saved on ice until purification using a Ni-NTA Spin Kit under native protein conditions as described by Quiagen and analysed for purity by SDS-PAGE. Subsequently the purified protein was concentrated with Pall Filtron Microsept Centrifugal Devices followed and finally the enzyme was stored at –70 °C prior to being used.
Enzyme assay: Various amounts (up to 2 µg) of cytosine deaminase were added to quartz cuvette with 0.2 cm length of path containing 1 mM cytosine or 5-fluoro-cytosine dissolved in tris-buffer pH 7.5. The cuvette was shaken up once and than the absorbance at 286 nm was continuously measured by an uv/vis spectrometer for 5 min. One unit of activity is the amount of enzyme catalysing the deamination of 1.0 µmole of substrate per minute at 25 °C. Specific activity is given in units per milligram protein [3].

For each substrate the initial rates were measured with various substrate concentrations ranging from 0.1 mM to 3.0 mM as described above and the K_M, V_{max} and turnover number *k* of the protein was determined. The data were fitted, using a Lineweaver-Burk plot (Figs. 2, 3).

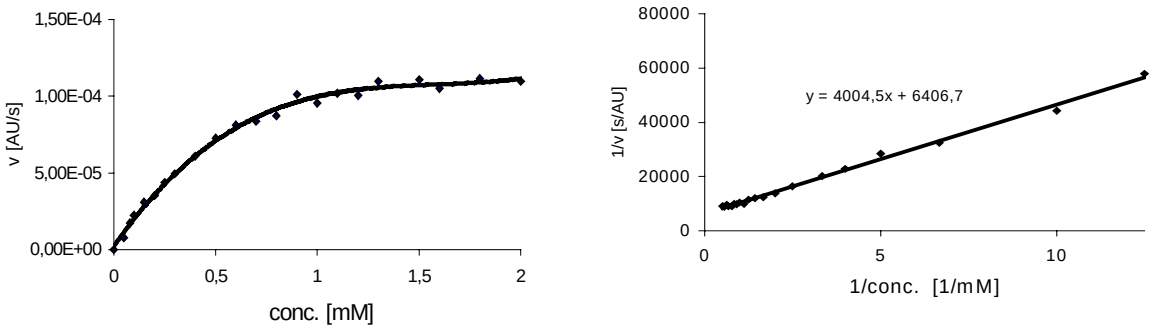

Fig.2. left: Direct plot of initial rate vs concentration of cytosine, right: Lineweaver-Burk plot of cytosine

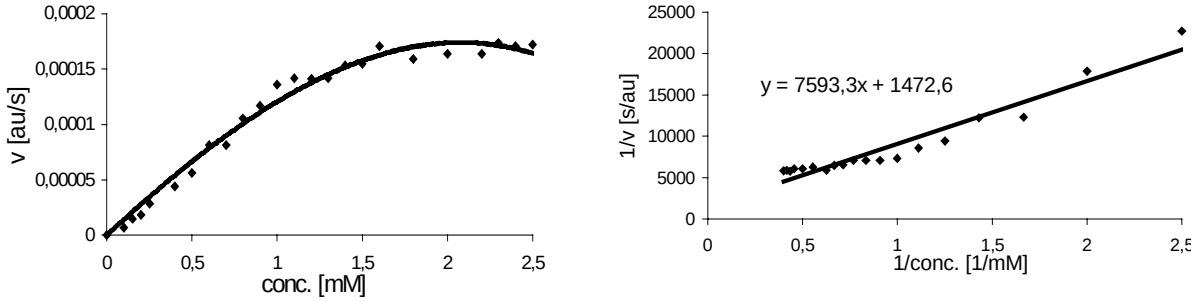

Fig.3. left: Direct plot of initial rate vs concentration of 5-fluorocytosine, right: Lineweaver-Burk plot of 5-fluorocytosine

Results and Discussion

The expression and purification of cytosine deaminase, followed by ist concentration using Pall Filtron Microsept Centrifugal Devices, result in a concentrated enzyme (up to 50 mg CD/ml) of high specific activity in a good yield. It is stable and can be stored at –70 °C for several weeks. The enzyme unit, specific activity and the K_M value were determined for two substrates by kinetic measurements. The results are given in Table 1.

Table 1. Results of kinetic measurements and specific activity of the CD

Substrate	Enzyme Unit [µmole/min]	Specific activity [U/mg protein]	K_M [mM]	V_{max} [mM/s]	k [1/s]
Cytosine	$16 \cdot 10^{-3}$	38	0.63	$9.5\ 10^{-4}$	0.127
5-Fluorocytosine	$4.3\ 10^{-3}$	2.1	5.2	$8.4\ 10^{-4}$	0.026

For cytosine a K_M of 0.63 mM falls in the range of further data published, ranging from 0.2 mM to 2.5 mM [3]. The decrease in specific activity and the increase in K_M of one dimension by using 5-fluoro-cytosine as substrate is also in good agreement with published data. The highly concentrated enzyme obtained can be used now for screening of new substances of lower substrate affinity.

[1] Rowley, S.; Lindauer, M.; Gebert, J.F.; Haberkorn, U.; Oberdorfer, F.; Moebius, U.; Herfarth, C.; Schackert H.K. Cytosine deaminase gene as a potential tool for the genetic therapy of colorectal cancer, J. Surg. Onc. 61 (1996) 42-48.

[2] Haberkorn, U.; Oberdorfer, F.; Gebert, J.; Morr, I.; Haack, K.; Weber, K.; Lindauer, M.; van Kaick, G.; Schackert, H.K. Monitoring gene therapy with cytosine deaminase: In vitro studies using tritiated 5-fluoro-cytosine. J. Nucl. Med. 37 (1996) 87-94.

[3] Ipata, P.L.; Cercignani, G. Cytosine and cytidine deaminase from yeast. Methods. Enzymol. 51 (1978) 394-399.

32. Synthesis of S-([^{18}F]Fluoromethyl)-(+)-McN5652 - A Potential Radiotracer for Imaging the Serotonin Transporter

J. Zessin, O. Eskola[1], P. Brust, J. Bergman[1], J. Steinbach, P. Lehikoinen[1], O. Solin[1], B. Johannsen
[1]Turku PET Centre, Radiochemistry Laboratory, Porthaninkatu 3-5, FIN-20500 Turku, Finland

Introduction

The radioligand (+)-[^{11}C]McN5652 ([^{11}C]**1**) is the most promising PET tracer for noninvasive investigations of the serotonin transporter (SERT) in the living organism. However, the kinetics of this radiotracer in the human brain is to slow in relation to the half-life of carbon-11 (t½ = 20.4 min). A satisfactory ratio of 1.8 between specific (midbrain) and nonspecific binding (cerebellum) was reached after 115 min [1].
Suehiro *et al.* [2] therefore made an effort to label (+)-McN5652 with fluorine-18 (t½ = 110 min) by synthesis of the [^{18}F]fluoroethyl analogue [^{18}F]**2**. Replacement of the original S-methyl group by the S-fluoroethyl moiety led to a considerable decrease in affinity and selectivity for the SERT. The penetration of [^{18}F]**2** into the brain of mice and the ratios between specific and nonspecific binding are lower than with [^{11}C]**1**.

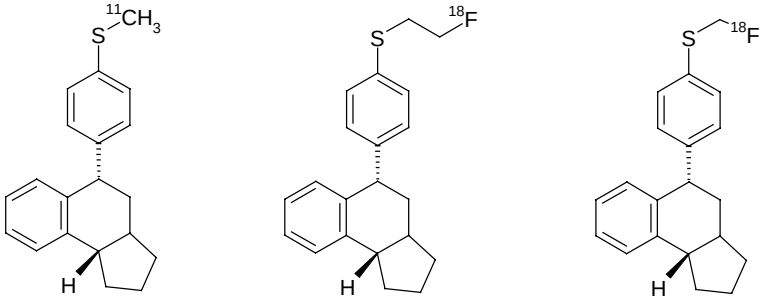

Fig. 1. Structure of serotonin transporter radioligands based on (+)-McN5652

Alternatively, the fluoromethyl analogue **3** of (+)-McN5652 (FMe-McN) is also of interest as its structure is close to the original structure of McN5652. The affinity to the SERT of this new compound is similar to that of **1**. The ^{18}F-labelled **3** can be synthesized by reaction of demethylated **1** with [^{18}F]bromofluoromethane, which was introduced in the late eighties by Coenen and co-workers [3].
In this paper we describe the preparation of the nonradioactive FMe-McN, its preliminary biological evaluation as well as the synthesis of [^{18}F]FMe-McN.

Experimental

General
All reagents and solvents were of analytical or HPLC grade and used without further purification. (+)-McN5652 and the thioester precursor **4** were synthesized as described in an earlier report [4]. The [^{18}F]fluoromethylation reagent [^{18}F]bromofluoromethane was prepared from dibromomethane by nucleophilic substitution of bromine by [^{18}F]fluoride according to Eskola *et al.* [5].
NMR spectra were recorded on a Varian INOVA 400 spectrometer. ^{1}H and ^{13}C NMR spectra were obtained, using $CDCl_3$ as a solvent and internal standard. Mass spectrometric analyses were performed on a Perkin Elmer mass spectrometer PE SCIEX API 150 EX, using the positive ion mode with a turbo ion spray as an ion source.
The chemical and radiochemical purity was determined by high pressure liquid chromatography (HPLC) with a Purospher RP18 column (Merck) isocratically eluted with water/acetonitrile (50/50) containing 0.1M ammonium formate. Semipreparative HPLC purification was carried out with a Kromasil RP18 column (7 µm, 300 mm x 8 mm) isocratically eluted with water/acetonitrile (60/40) containing 0.1M ammonium formate at a flow rate of 4 ml/min. The enantiomeric purity of [^{18}F]FMe-McN was determined by chiral HPLC or by ^{1}H NMR of the complexes of **3** with R-(+)-α-methoxy-α-trifluoromethylphenylacetic acid ((+)-MTPA, Mosher's acid) as described in [4].

*Synthesis of (+)-trans-1,2,3,5,6,10b-hexahydro-6-[4-(fluoromethylthio)phenyl]-pyrollo-[2,1-a]-isoquinoline (FMe-McN, **3**)*

Normethyl-(+)-McN5652 was prepared by hydrolysis of the thioester **4** (100 mg, 0.34 mmol) by 1 M tetrabutylammonium hydroxide solution in methanol (TBAH, 600 µl, 0.6 mmol). The resulting solution was diluted with dimethyl formamide (4 ml), placed in a sealed reaction vessel and cooled down with methanol/dry ice.

Bromofluoromethane (200 mg, 1.8 mmol) was trapped in this solution at -78 °C. The reaction mixture was warmed up to room temperature and stirred for 5 min at this temperature.

After dilution with water (10 ml), the product was extracted with dichloromethane (3 x 25 ml). The combined organic extracts were washed with water (2 x 30 ml), dried with magnesium sulphate and evaporated in vacuum.

The crude product was purified by flash chromatography and converted into the (+)-O-di-p-toluoyltartrate.

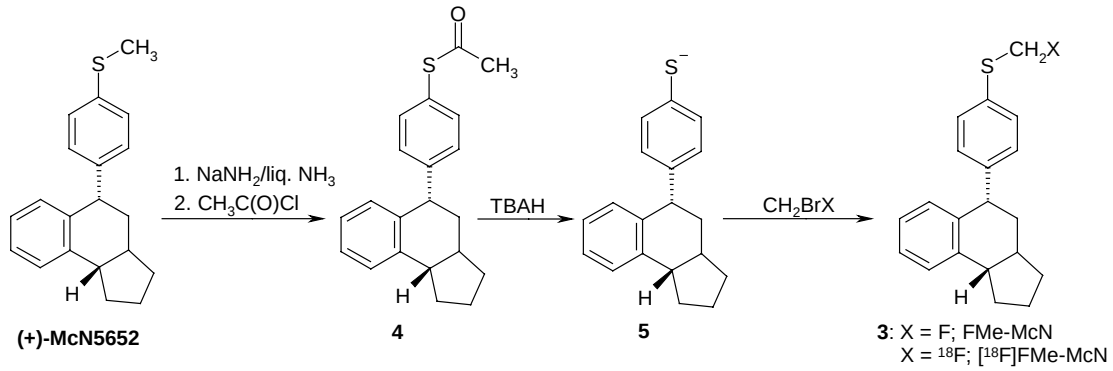

Fig. 2. Synthesis of the thioester precursor, FMe-McN, and [^{18}F]FMe-McN

*Synthesis of (+)-trans-1,2,3,5,6,10b-hexahydro-6-[4-([^{18}F]fluoromethylthio)phenyl]-pyrollo-[2,1-a]-isoquinoline ([^{18}F]FMe-McN, [^{18}F]**3**)*

The thioester precursor **4** (0.5 mg, 1.5 µmol) was treated with a 0.3 M TBAH solution in methanol (60 µl, 18 µmol) for 10 min at room temperature. The reaction mixture was then diluted with DMF (200 µl). [^{18}F]Bromofluoromethane was trapped in this solution at room temperature. After trapping [^{18}F]bromofluoromethane, the reaction vessel was heated at 40 °C for 1 min. The reaction mixture was then diluted with water/acetonitrile (50/50, 400 µl). [^{18}F]FMe-McN was separated by semipreparative HPLC using the system described above. The product fraction was diluted with water (20 ml) and pressed through an activated Chromafix RP18 cartridge. The cartridge was washed with water (5 ml) and [^{18}F]FMe-McN was eluted with absolute ethanol (1 ml).

Radioligand binding assays

The affinity of FMe-McN to the serotonin, dopamine (DAT), and norepinephrine transporter (NET) was tested, using the radioligand binding assays summarized in Table 1.

Results and Discussion

Synthesis of FMe-McN

The synthesis of the fluoromethyl analogue of (+)-McN5652 **2** (FMe-McN) was prepapred by fluoromethylation of demethylated (+)-McN5652 with bromofluoromethane. The structure of the resulting product was confirmed by mass spectrometric and NMR spectrometric analyses. The ^{1}H NMR spectrum is characterized by a doublet for the thiofluoromethyl moiety at 5.7 ppm with a H-F coupling constant of 53.1 Hz. The ^{13}C NMR spectrum has a doublet for the thiofluoromethyl group at 88.8 ppm with a C-F coupling constant of 216 Hz.

In vitro binding studies

FMe-McN was used for *in vitro* binding studies to determine its affinity to the 5-HT, dopamine, and norepinephrine transporter in comparison with (+)-McN5652 (Table 2).The affinity of FMe-McN to the 5-HT transporter was compared with other inhibitors (Table 3).

The replacement of hydrogen by fluorine at the S-methyl group of McN5652 slightly reduces the affinity to the 5-HT transporter. However, it is still better by a factor of 3 than the affinity of citalopram, the most selective 5-HT uptake inhibitor kwnon so far. The affinity of FMe-McN to the dopamine and norepinephrine transporter is similar to that of (+)-McN5652.

We therefore expect [^{18}F]FMe-McN to be a suitable radiotracer for *in vivo* imaging of the 5-HT transporter.

Table 1. Radioligand binding assays

Transporter	Membran preparation	Radioligand	Buffer	Incubation	Nonspecific binding
SERT	Caudate nucleus from porcine brain	[^{3}H]Paroxetine (17.1 Ci/mmol)	50 mM TRIS-HCl, 100mM NaCl, 5 mM KCl, pH 7.4	60 min, 20 °C	10 µM clomipramine
DAT	Cloned human transporter	[^{3}H]WIN 35,428 (83.5 Ci/mmol)	50 mM TRIS-HCl, 100mM NaCl, 5 mM KCl, pH 7.4	120 min, 4 °C	1 µM GBR-12909
NET	Rat cortex pre-paration	[^{3}H]Nisoxetine (80.6 Ci/mmol)	50 mM TRIS-HCl, 100mM NaCl, 5 mM KCl, pH 7.4	120 min, 4 °C	10 µM protriptylin

Table 2. Inhibition constants (K_i) of FMe-McN and (+)-McN5652 for the 5-HT (SERT), dopamine (DAT), and norepinephrine transporter (NET)

Transporter	FMe-McN	(+)-McN5652
SERT	2.3 nM	0.72 nM
DAT	9.6 nM	9.4 nM
NET	9.3 nM	6.6 nM

Radiochemistry

[^{18}F]Bromofluoromethane was prepared, starting from dibromomethane, by nucleophilic substitution of bromine by [^{18}F]fluoride. The product was reacted with normethyl-McN5652 to yield [^{18}F]FMe-McN. After separation by semipreparative HPLC and solid phase extraction, [^{18}F]FMe-McN was obtained in a radiochemical purity > 97 %. The decay-corrected radiochemical yield (based on [^{18}F]fluoride, calculated at the end of bombardment) was 5 ± 1 %. The total synthesis time was about 65 min. The specific radioactivity was 200 - 2,000 GBq/µmol (5.4 - 54 Ci/µmol) at the end of synthesis.

The reaction mixture resulting from the fluoromethylation step contained [^{18}F]FMe-McN (50 %), a polar by-product (45 %) and unreacted [^{18}F]bromofluoromethane (< 5 %). The composition of the reaction mixture was not dependent on the reaction temperature in the range from 25 to 60 °C. Prolongation of the reaction time to up to 10 min did not significantly change the product ratio.

The incomplete conversion of [^{18}F]bromofluoromethane is an indication of the lower reactivity of this fluoromethylation agent in comparison with [^{11}C]methyl iodide. Under similar reaction conditions [^{11}C]methyl iodide completely reacted with thiol **5**.

Table 3. Inhibition constants (K_i) of FMe-McN and other ligands for the 5-HT transporter

Inhibitor	K_i (nM)
Paroxetine	0.19 ± 0.05
Clomipramine	0.19 ± 0.04
(+)-McN5652	0.72 ± 0.20
Fluoxetine	0.89 ± 0.12
FMe-McN	**2.30 ± 0.05**
Imipramine	2.90 ± 0.49
Citalopram	6.61 ± 0.64
Venlafaxin	35.0 ± 5.0
Protryptiline	35.9 ± 7.1
Nisoxetine	57.9 ± 14.0
Serotonin	592 ± 98

Conclusion

After demonstration of the high *in vitro* affinity to the serotonin transporter, the [^{18}F]fluoromethyl analogue of (+)-McN5652 was synthesized as a potential radiotracer for imaging of the serotonin transporter. Satisfactory radiochemical yields were achieved by fluoromethylation of S-demethylated (+)-McN5652 with [^{18}F]bromofluoromethane.

Acknowledgements

We would like to thank the cyclotron staff of the Turku PET Centre for providing [^{18}F]fluoride. Thanks are also due to R. Herrlich, H. Kasper, and S. Lehnert for technical assistance.

References

[1] Szabo, Z.; Kao, P. F.; Scheffel, U.; Suehiro, M.; Mathwes, W. B.; Ravert, H. T.; Musachio, J. L.; Marenco, S.; Kim, S. E.; Ricaurte, G. A.; Wong, D. F.; Wagner Jr., H. N.; Dannals, R. F. Positron emission tomography imaging of serotonin transporters in the human brain using [^{11}C](+)-McN5652. Synapse 20 (1995) 37-43

[2] Suehiro, M.; Greenberg, J. H.; Shiue, C. Y.; Gonzalez, C.; Dembowski, B.; Reivich M. Radiosynthesis and biodistribution of the S-[^{18}F]fluoroethyl analog of McN5652. Nucl. Med. Biol. 23 (1996) 407-412.

[3] Coenen, H. H.; Colosimo, M.; Schüller, M.; Stöcklin, G. Preparation of n.c.a. [^{18}F]CH_2BrF via aminopolyether supported nucleophilic substitution. J. Labelled Compd. Radiopharm. 23 (1986) 587-595.

[4] Zessin, J.; Gucker, P.; Ametamey, S. M.; Steinbach, J.; Brust, P.; Vollenweider, F. X.; Johannsen, B.; and Schubiger, P. A. Efficient synthesis of enantiomerically pure thioester precursors of [^{11}C]McN-5652 from racemic McN-5652. J. Labelled Compd. Radiopharm. 42 (1999) 1301-1312.

[5] Eskola, O.; Bergman, J.; Lehikoinen, P.; Ögren, M.; Långström, B.; Solin, O. Synthesis of ^{18}F-bromofluoromethane [^{18}F]FCH_2Br; Fluoromethylation reagent with high specific radioactivity. J. Labelled Compd. Radiopharm. 42 (Suppl. 1) (1999) 543-545.

33. Chemical Stability of S-([^{18}F]Fluoromethyl)-(+)-McN5652

J. Zessin, O. Eskola[1], J. Bergman[1], J. Steinbach, P. Lehikoinen[1], P. Brust, O. Solin[1]
[1]Turku PET Centre, Radiochemistry Laboratory, Porthaninkatu 3-5, FIN-20500 Turku, Finland

Introduction

Several ^{11}C- and ^{18}F-labelled tracers are known for investigating the serotonin transporter, but only (+)-[^{11}C]McN5652 was recently demonstrated to be suitable for clinical use. Satisfactory ratios between specific and nonspecific binding were reached In the human brain after 115 min [1]. By that time the total amount of radioactivity in the brain is quite low due to the half-life of ^{11}C (20.4 min).
In view of the slow washout of the unspecifically bound tracer, we expected an improvement in the target-to-nontarget ratios by prolonging the investigation time. We therefore synthesized the [^{18}F]fluoromethyl analogue of (+)-McN5652 ([^{18}F]FMe-McN) [2]. With a comparable affinity to the serotonin transporter, this new radioligand allows longer investigation times.
Several authors described solvolysis of [^{18}F]fluoromethyl compounds [3, 4]. We therefore have the stability of FMe-McN and [^{18}F]FMe-McN in various solvents.

Experimental

General
All reagents and solvents were of analytical or HPLC grade and were used without further purification. FMe-McN and [^{18}F]FMe-McN were prepared as described in an earlier report [2].
Radio thin layer chromatography (radio TLC) was performed, using Merck silica gel 60 F_{254} plates eluted with ethyl acetate/hexane/methanol (5/5/1). The compounds were detected, using a radio TLC scanner [5].
Mass spectrometric analysis of the decomposition of FMe-McN
(+)-FMe-McN (1 mg) was dissolved in a water/methanol mixture (80/20) containing 0.01 M ammonium formate. This solution was kept at room temperature. In order to follow the course of the decomposition reaction, samples of the solution were analysed with the LC-MS system according to [2] after 0, 15, and 38 min.
Stability of [^{18}F]FMe-McN
The stability of [^{18}F]FMe-McN was analysed in ethanol, propylene glycol, water containing 0.9 % sodium bicarbonate, and mixtures of ethanol or propylene glycol with sodium bicarbonate solution.
The ethanolic solution of [^{18}F]FMe-McN resulted from solid phase extraction after synthesis and purification of the labelled compound as described in [2]. Parts of this solution were diluted with various volumes of sodium bicarbaonate solution (0.9 %).
The solution of [^{18}F]**1** in propylene glycol was prepared by evaporating the starting ethanolic solution almost to dryness. The residue was diluted in propylene glycol and diluted with appropriate amounts of sodium bicarbonate solution (0.9 %).
The solution of [^{18}F]FMe-McN in water containing sodium bicarbonate (0.9 %) was prepared in a similar manner.
The decomposition was monitored by radio TLC as described above.

Results and Discussion

We studied the stability of FMe-McN and [^{18}F]FMe-McN in various solvents and solvent mixtures. Solvolysis of FMe-McN in a water/methanol mixture (80/20) at pH 7 yielded a product with a molecular mass of 281 g/mol, which corresponds to normethyl-McN5652. These findings indicated, that the sulphur-fluoromethyl bond was cleaved in the course of the decomposition reaction.
The stability of [^{18}F]FMe-McN was analysed in solutions with various contents of ethanol or propylene glycol at room temperature. In ethanol or propylene glycol no solvolysis was observed within 180 min. In ethanol or propylene glycol solutions containing 50 % of a sodium bicarbonate solution (0.9 %) 10 % of [^{18}F]FMe-McN was converted into a polar product within 180 min. The rate of solvolysis increased with increasing proportions of the sodium bicarbonate solution as shown in Table 1.

[^{18}F]FMe-McN is stable in solutions containing 50 % ore more ethanol. Such solutions cannot be administered to animals or humans. Our observations suggest that [^{18}F]FMe-McN possesses a satisfactory stability in solutions containing 50 % propylene glycol. Solutions with this amount of propylene glycol are acceptable for intravenous injection. Preliminary *in vivo* studies in rats demonstrate the stability of [^{18}F]FMe-McN under these conditions.

Table 1. Stability of [^{18}F]FMe-McN

Solvent	Solvent composition	Time [min]	Amount of [^{18}F]FMe-McN [%]
propylene glycol	-	200	96
propylene glycol/$NaHCO_3$ (0.9 %)	50:50	120	86
ethanol/ $NaHCO_3$ (0.9 %)	50:50	120	95
propylene glycol/ $NaHCO_3$ (0.9 %)	25:75	30	76
ethanol/ $NaHCO_3$ (0.9 %)	25:75	30	80
ethanol/ $NaHCO_3$ (0.9 %)	10:90	30	55
$NaHCO_3$ (0.9 %)	-	10	55

References

[1] Szabo, Z.; Kao, P. F.; Scheffel, U.; Suehiro, M.; Mathwes, W. B.; Ravert, H. T.; Musachio, J. L.; Marenco, S.; Kim, S. E.; Ricaurte, G. A.; Wong, D. F.; Wagner Jr., H. N.; Dannals, R. F. Positron emission tomography imaging of serotonin transporters in the human brain using [^{11}C](+)-McN5652. Synapse 20 (1995) 37-43.

[2] Zessin, J.; Eskola, O.; Brust, P.; Bergman, J.; Steinbach, J.; Lehikoinen, P.; Solin, O.; Johannsen, B. Synthesis of S-([^{18}F]Fluoromethyl-(+)-McN5652 - A Potential Radiotracer for Imaging the Serotonin Transporter. This *Report,* pp. 90-93.

[3] Coenen, H. H.; Colosimo, M.; Schüller, M.; Stöcklin, G. Preparation of n.c.a. [^{18}F]CH_2BrF via aminopolyether supported nucleophilic substitution. J. Labelled Compd. Radiopharm. 23 (1986) 587-595.

[4] Petric, A.; Barrio, J. R.; Namavari, M.; Huang, S.-C.; Sathyamurthy, N. Synthesis of 3β-(4-[^{18}F]fluoromethylphenyl)- and 3β-(2-[^{18}F]fluoromethylphenyl)tropane-2β-carboxylic acid methyl esters: New ligands for mapping brain dopamine transporter with positron emission tomography. Nucl. Med. Biol. 26 (1999) 529-535.

[5] Solin O. Counting of Positron- Emitting Radionuclides on Thin Layer Chromatograms. Int. J. Appl. Radiat. Isot. 34 (1983) 1653.

34. Self-Condensation Reaction of Pentamethinium Salts under Basic Conditions

B. Pawelke, P. Mäding, J. Steinbach, R. Schlecker[1]
[1]BASF AG Ludwigshafen

Introduction

Pentamethinium salts, belonging to the extensive class of polymethines, are of great interest because of their electronic properties, which make them attractive for theoretical investigations as well as for synthetic purposes.
The structure-property relationships of polymethines have been widely examined, especially in terms of their suitability as dyestuffs [1]. In addition, their reactivity towards various classes of compounds (e.g. oxidants, reductants [1], nucleophiles [2]) as well as their thermal behaviour [1, 3] have been described.
We applied pentamethinium salts as precursors in labelling reactions to synthesize ^{11}C-ring labelled benzenoid aromatics [4]. In various reactions starting from 5-dimethylamino-1-methyl-penta-2,4-dienylidene-1-dimethylammonium perchlorate (**1**), the occurrence of typical by-products was observed.
Our intention was now to identify the nature of these substances as well as the pathway of their formation.

Results and Discussion

In our condensation experiments to obtain ^{11}C-labelled compounds, 5-dimethylamino-1-methyl-penta-2,4-dienylidene-1-dimethylammonium perchlorate (pentamethinium salt **1**) was found to give N,N-dimethylaniline (**3**) in the presence of a base (Scheme 1). Yields of **3** are found to range between about 20 % and a nearly quantitative yield (determined by HPLC), depending on the reaction conditions and the compounds reacting.

Scheme 1. Formation of N,N-dimethylaniline starting from compound **1**

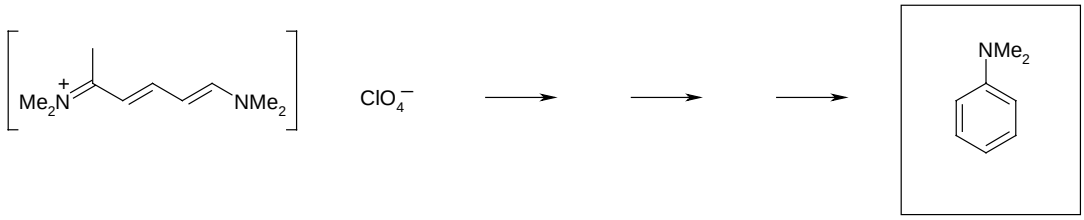

1 **3**

This finding can be explained by means of a base-catalysed intramolecular condensation reaction of compound **1** (Scheme 2). Obviously, the pentamethinium salt itself has a considerable inherent CH acidity leading to deprotonation of the 1-methyl group by the auxiliary base, resulting in the formation of a hexatriene system (**2a/2b**) as shown in Scheme 2. At higher temperatures, those hexatriene systems are known to undergo a cyclisation reaction (synchronous six-electron cyclisation) into cyclohexadienes, followed by elimination and thus aromatisation, provided that they bear a suitable leaving group [5].

Scheme 2. Base-catalysed intramolecular condensation reaction of pentamethinium salt **1**

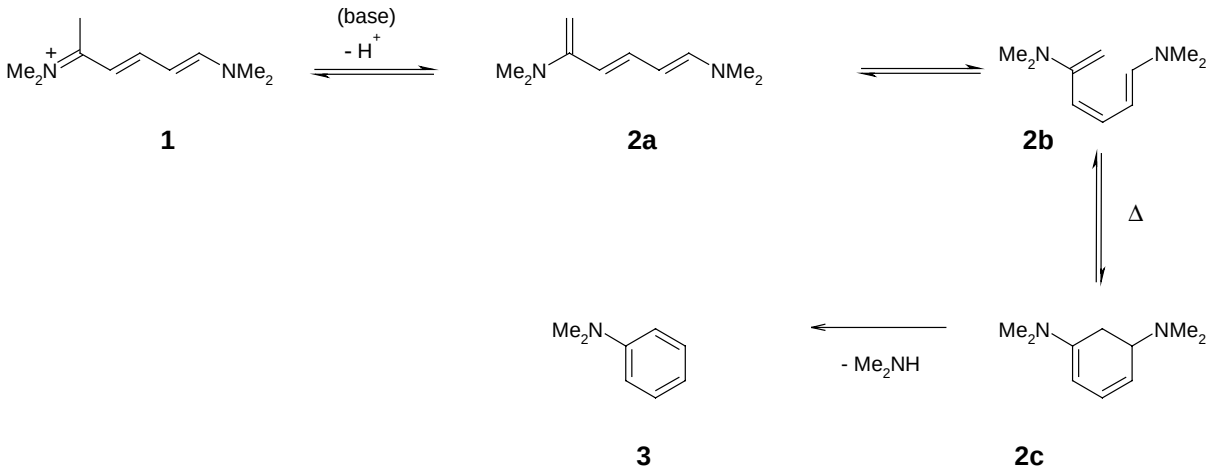

According to [5], compounds **2a**, **2b** and **2c** (Scheme 2) are postulated to be intermediates of the reaction, although they were neither isolated nor characterised.
N,N-dimethylaniline was identified by HPLC, corresponding to an authentic sample in retention time and UV spectrum.

Depending on the strength of the CH acidity of the compound to be reacted, the described intramolecular cyclisation reaction of the pentamethinium salt may occur as a competitive reaction or even become the main process. In those cases the suitability of the precursor **1** for the synthesis of ^{11}C-labelled aromatic compounds in the described way [4] seems to be limited.

References

[1] Berlin, L.; Riester, O. Cyanine. in: Methoden der Organischen Chemie (Houben-Weyl)-5/1d, 4.Aufl., 1972, 227-299.

[2] Viteva, L.; Stefanovski, Y.; Gospodova, T.; Mazières, M.R.; Wolf, J.G. Lithium reagents addition in cyanine dyes series. Tetrahedron Lett. 41 (2000) 2541-2544.

[3] Schedler, U.; Bendig, J.; Dähne, L. Solid state chemistry of polymethines. Mol. Cryst. Liq. Cryst. Sci. Technol. Sect.A 264 (1995) 11-22.

[4] Steinbach, J.; Mäding, P.; Füchtner, F.; Johannsen B. N.c.a. ^{11}C-labelling of benzenoid compounds in ring positions: Synthesis of nitro-[1-^{11}C-]benzene and [1-^{11}C-]aniline. J. Labelled Compd. Radiopharm. 36 (1995) 33-41.

[5] Mäding, P.; Steinbach, J.; Johannsen B. N.c.a. ^{11}C-labelling of benzenoid compounds in ring positions: [^{11}C]Anisole derivatives. J. Labelled Compd. Radiopharm. 39 (1997) 585-599.

[6] Mäding, P.; Steinbach, J. N.c.a. ^{11}C-labelling of benzenoid compounds in ring positions: Synthesis of 3-nitro-[3-^{11}C-]toluene and 4-nitro-[4-^{11}C-]toluene and their corresponding toluidines. J. Labelled Compd. Radiopharm. 41 (1998) 647-656.

[7] Jutz, C.; Wagner, R.M. Die synchrone Sechs-Elektronen-Cyclisierung von Hexatriensystemen. Angew. Chem. 84 (1972) 299-302.

35. Simultaneous Preparation of 16α-[^{18}F]Fluoroestradiol-Sulphamates in an Automated Module. A High-Yield Procedure for 16α-[^{18}F]Fluoro-Estradiol-17β-Sulphamate

J. Römer, F. Füchtner, J. Steinbach, R. Lücke, C. Smuda, H. Kasch [1]
[1] id pharma, Jena

Introduction

Our efforts to produce 16α-[^{18}F]fluoroestradiol ([^{18}F]FES) in a high radioactivity level has resulted in a module-assisted procedure [1] applied for breast cancer diagnosis in our PET centre since that time. Later, we were able to convert [^{18}F]FES in the same module into 16α-[^{18}F]fluoroestradiol-3,17β-disulphamate ([^{18}F]FESDS) [2]. We were further able to produce [^{18}F]FESDS in a module-assisted one-pot procedure [3] within 90 min.
After the discovery that 16α-halogen-estradiol-3,17β-disulphamates are highly active steroid sulphatase inhibitors [4, 5], it was supposed that steroids as 16α-fluoro-estradiol-3,17β-disulphamate (FESDS) should be suitable for chemotherapeutic intervention in breast cancer because the breast cancer tissue contains steroid sulphatase in high activity. On the other hand, [^{18}F]FESDS should be applicable in PET investigations to image such sites of high steroid sulphatase activity.
The conditions for producing sulphamates were exactly studied. When estradiol was subjected to sulphamoylation with excess sulphamoyl chloride (H_2N-SO_2Cl, SCl) in anhydrous acetonitrile and in the presence of solid sodium carbonate as a base, three sulphamates were formed: estradiol-3-sulphamate, estradiol-17β-sulphamate, and estradiol-3,17β-disulphamate. The same result was found for substituted estradiols. Thus, using 16α-fluoroestradiol (FES) as the starting compound, a procedure for producing 16α-fluoroestradiol-3-sulphamate (FES3S), 16α-fluoroestradiol-17β-sulphamate (FES17S), and 16α-fluoroestradiol-3,17β-disulphamate (FESDS), and for purifying them by HPL chromatography was elaborated [6].
In the module-assisted procedure [3], SCl was applied in high excess related to n.c.a. [^{18}F]FES. The primary product was [^{18}F]FESDS, as expected. 16α-[^{18}F]fluoro-estradiol-3-sulphamate ([^{18}F]FES3S) and 16α-[^{18}F]fluoroestradiol-17β-sulphamate ([^{18}F]FES17S) were obtained with a very low radioactivity level.
In the first animal experiments [^{18}F]FESDS was found to bind strongly to the erythrocytes [7]. Thus, the blood vessels were primarily imaged. The questions whether this applies to both monosulphamates and whether there were also other targets are still unanswered. We therefore carried out modified module-assisted experiments to produce [^{18}F]FES3S and [^{18}F]FES17S with an appreciable radio-activity level.

Experimental

Materials and methods
The experiments were carried out in an automatically operating module which was also used to produce [^{18}F]FES and [^{18}F]FESDS . Module and procedure were described in detail [3]. The necessary precursor, 3-O-methoxymethyl-16,17-O-sulphuryl-estra-1,3,5(10)-triene-3,16β,17β-triol (cyclic sulphate), was prepared according to a given formula [8]. Sulphamoyl chloride (SCl) was prepared from commercially available N-carbonylsulphamoyl chloride [9] and stored at 5 °C under nitrogen. Solvents and reagents (Sigma-Aldrich) were used as supplied. Kryptofix 2.2.2 (K222) was purchased from Merck. [^{18}F]HF was produced in an IBA CYCLONE 18/9 cyclotron using enriched [^{18}O]H_2O (1.5 ml, 94 %) from Chemotrade (Leipzig, Germany). After 60 min irradiation time, the radioactivity at end of bombardment (EOB) was between 40 and 60 GBq. To separate the final products, an HPLC system (JASCO) was used. It consisted of an injection loop (10 ml), a semipreparative RP column (SP 250/10 Nucleosil 120-7 C_{18}, Macherey & Nagel, Germany), a UV/VIS detector and a radioactivity detector. 45 % EtOH was used as the eluant at a flow of 1.5 ml/min. To keep check of the purity of the final products, an HPLC system (Hewlett Packard) with a diode array detector, a radioactivity detector and an analytical column (ET 125/8/4 Nucleosil 120-5 C_{18} Macherey & Nagel) were used.
Before the synthesis the following solutions were prepared:

Solution I	K222 (10 mg) and K_2CO_3 (1.85 mg) per ml 86 % aqueous MeCN (3 ml)
Solution II	Cyclic sulphate (2 mg) in 1 ml absolute MeCN (freshly prepared solution)
Solution III	0.1 M hydrochloric MeCN (6 ml), freshly prepared by mixing 9 parts of MeCN and 1 part of 1 M HCl
Solution IV	SCl (10 – 25 mg) in 1.5 ml absolute MeCN (freshly prepared solution)
Solution V	22.5 % EtOH (4 ml)

Before each synthesis, the module was washed with acetone and dried by an air stream (cleaning program). Five storage vials of the module were filled with solutions I - V, a sixth vial with absolute MeCN (12 ml). Then the starting [^{18}F]HF solution was transferred from the cyclotron into the module. After measuring the starting radioactivity A_0 at $t = t_0$, the synthesis program was started.

Simultaneous synthesis of [^{18}F]FES3S and [^{18}F]FES17S

After starting the synthesis program, the following operating steps were automatically carried out:

1. ***Careful drying of the reaction mixture before fluorination***. – Addition of solution I (1.5 ml) and MeCN (3 ml) and removing the solvent at 100 °C for 4 min. Addition of MeCN (3 ml) alone. Repeat of the drying process.
2. ***Nucleophilic fluorination.*** – Addition of solution II. Closing the reaction vessel and heating the reaction mixture to 100 °C. After 10 min the reaction mixture was cooled and dried.
3. ***Acidic hydrolysis to remove the protective groups.*** – Addition of a third of solution III and removing the solvent at 100 °C for 3 min. Repeat of the process twice.
4. ***Careful drying of the reaction mixture before sulphamoylation.*** – Addition of solution I (1.5 ml) and MeCN (2 ml) and removing the solvent at 100 °C for 4 min. Addition of MeCN (2 ml) and removing the solvent at 100 °C for 4 min. Repeat of the latter process. The temperature was reduced to 30 °C.
5. ***Sulphamoylation of the reaction mixture at 30 °C .*** – Addition of solution IV. The temperature was kept at 30 °C for 5 min. The reaction mixture was dried.
6. ***Destruction of the excess SCl.*** – Addition of solution V (1 ml). The reaction mixture was dried.
7. ***Preparation of the HPLC purification.*** – Addition of solution V (3 ml). After 1 min the solution was transferred into the injection loop.
8. ***HPLC purification.*** - The solution was injected into the column. The radiochromatogram was observed, and the eluate was fractionated according to the peaks being eluted. The radioactivity of the peaks was measured.

Synthesis of [^{18}F]FES17S from [^{18}F]FESDS

Before synthesis an additional hose pipe was installed for adding further solutions through the MeCN vial into the reaction vessel. 0.1 M HCl was ready to hand. After starting the synthesis program, the operating steps 1 - 4 were carried out as before, but the temperature was reduced to only 70 °C. The synthesis was continued as follows:

5. ***Sulphamoylation of the reaction mixture at 70 °C. –*** Addition of solution IV. The temperature was kept at 70 °C for 5 min. The reaction mixture was dried.
6. ***Destruction of the excess SCl. –*** Addition of solution V (1 ml). The reaction mixture was dried.
7. ***Alkaline treatment of the reaction mixture*** . **–** Addition of solution I (1.5 ml) and MeCN (3 ml) through the additional supply pipe into the reaction vessel. The temperature was kept at 70 °C for 5 min. The reaction mixture was dried.
8. ***Ensuring an acidic medium for HPLC and preparation of HPLC purification***. – Addition of solution V (3 ml) and 1 ml of 0.1 M HCl through the additional supply pipe into the reaction vessel. Then the solution was transferred into the injection loop.
9. ***HPLC purification.*** – The solution was injected into the column. The radiochromatogram was observed, and the eluate was fractionated according to the peaks being eluted. The radioactivity of the peaks was measured.

Results and Discussion

Synthesis of [^{18}F]FES-monosulphamates

In non-radioactive experiments we succeeded in preparation of FES-monosulphamates by stirring FES in an anhydrous solvent in the presence of a base and excess SCl only at room temperature. The yields increased with the stirring time [6]. The sulphamates were formed in the following descending order: m(FESDS) > m(FES17S) > m(FES3S). On average 25 % FES17S and 15 % FES3S were obtained. At higher temperatures, the monosulphamates were not obtained in noticeable amounts. Numerous radioactive module-assisted experiments [3] which were performed at 70 °C confirmed this result.

The module allowed to work with 30 °C as the lowest temperature. All the experiments described here were therefore carried out at this temperature.

The results of 10 experiments are compiled in Table 1. The sulphamoylation reaction was carried out while stirring in absolute acetonitrile, using 10 - 20 mg SCl within 5 min. Only the base for deprotonating the hydroxy groups (Table 1, column 2) was modified.
Similar to the experiments at 70 °C [2], the highest radioactivity (up to 50 %) was again found in the polar products . The highest radioactivity for [^{18}F]FES-monosulphamates was found when the sulphamoylation was carried out in the presence of a reduced potassium carbonate concentration (condition B in Table 1). Nevertheless, it did not exceed 25 %. Experiments without a base (condition C) or without a base and Kryptofix 2.2.2 (condition D) produced even worse results.
The Expts. 5, 6, and 7 of Table 1 started with a high radioactivity level from a 60 min irradiation. The radioactivities of [^{18}F]FESDS, [^{18}F]FES3S, and [^{18}F]FES17S found at the end of synthesis (EOS, about 90 min after EOB) are summarized in Table 2. By starting with a high radioactivity (A_0 = 40 - 60 GBq) and carrying out the following sulphamoylation reaction under condition B of Table 1, the accessible amounts of radioactivity of [^{18}F]FES3S and [^{18}F]FES17S were about 3 GBq and 1 GBq.
Expt. 4 of Table 1 showed the highest proportions of both [^{18}F]FES-monosulphamates. The radiochromatogram of Expt. 4 is illustrated in Fig. 1. The retention times found for [^{18}F]FESDS, [^{18}F]FES17S, [^{18}F]FES3S, and for the remaining [^{18}F]FES were: 28.2 min, 34.3 min, 37.2 min, and 46.4 min.

Table 1. Distribution of the radioactivity after sulphamoylation of [^{18}F]FES with sulphamoyl chloride under miscellaneous conditions. Solvent: acetonitrile (1.5 ml); reagent applied: 10 - 20 mg; reaction temperature : 30 °C; stirring time: 5 min.

Expt.	Conditions a)	Distribution of radioactivity % b)				
		Polar products	[^{18}F]FESDS	[^{18}F]FES3S	[^{18}F]FES17S	[^{18}F]FES c)
1	A	45	36	6	2	11
2	A	47	31	7	2	13
3	A	48	35	9	4	4
4	B	40	13	16	9	22
5	B	41	18	15	7	19
6	B	46	21	16	6	11
7	B d)	37	27	14	6	16
8	C e)	56	9	8	5	22
9	C	46	15	9	5	25
10	D	43	2	12	4	39

a) A - Sulphamoylation in presence of 15 mg K222 and 2,77 mg K_2CO_3 ; B - Sulphamoylation in presence of 15 mg K222 and 0,46 mg K_2CO_3 ; C - Sulphamoylation in presence of 15 mg K222 alone; D –Sulphamoylation in absence of any base
b) Radioactivity of the peaks eluted from the column was measured, time-corrected and related to the sum of all
c) Unconverted [^{18}F]FES
d) Instead of 0.46 mg K_2CO_3 only 0.18 mg had been used
e) Instead of 15 mg K222 only 7 mg K222 had been used

Table 2. Radioactivities of [^{18}F]FES3S and [^{18}F]FES17S available at EOS after starting the synthesis with [^{18}F]fluoride from a 60 min irradiation

Expt. a)	A_0 [MBq]	Radioactivity obtained [MBq] at EOS		
		[^{18}F]FESDS	[^{18}F]FES3S	[^{18}F]FES17S
5	52000	3980	3080	1110
6	58000	4070	3000	1070
7	46200	4360	2350	1000

a) Experiment number as in Table 1

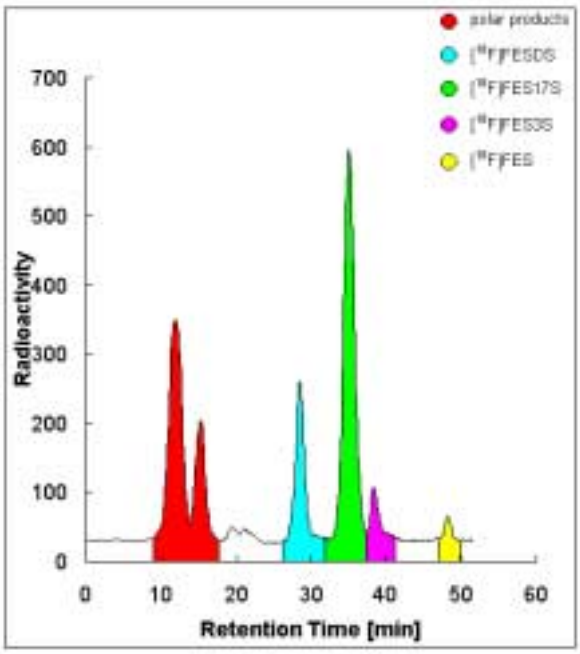

Fig. 1. Radiochromatogram of Expt. 4 of Table 1

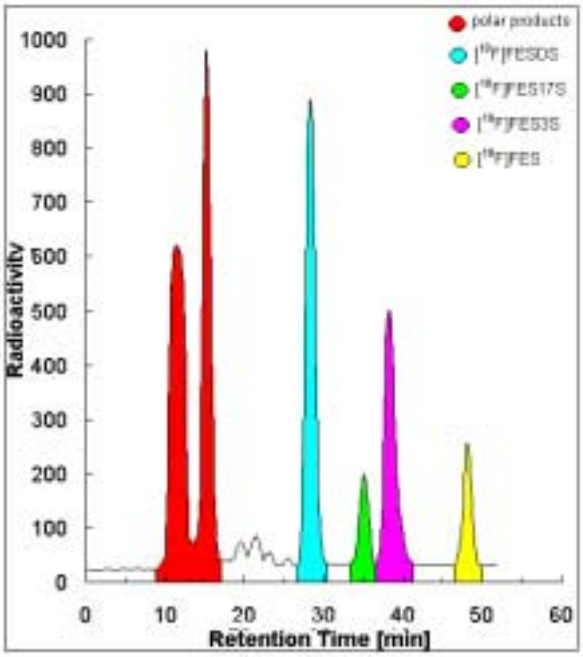

Fig. 2. Radiochromatogram of Expt. 3 of Table 2

Different results of radioactive and non-radioactive reactions

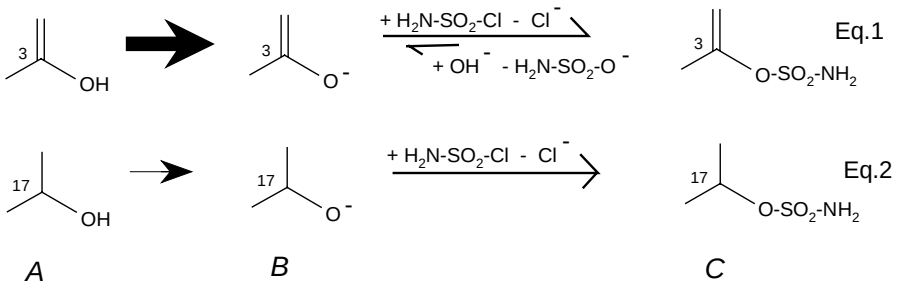

Scheme 1 : Equilibriums between hydroxysteroid A , deprotonated hydroxysteroid B, and amidosulphonyloxysteroid C

Eq.1 - Substitution of the proton of the phenolic 3-hydroxy group

Eq.2 - Substitution of the proton of the aliphatic 17β-hydroxy group

At first sight, it seemed surprisingly that the radioactivity proportion of [^{18}F]FES3S was greater than that of [^{18}F]FES17S in all experiments of Table 1, while former non-radioactive sulphamoylation experiments [6] had produced more of the corresponding 17-monosulphamate. But this is not contradictory as several reactions proceed side by side, depending on the existing equilibrium (see the reactions in Scheme 1). The more acidic proton of the phenolic hydroxy group is easily deprotonated and hence 3-monosulphamate is preferentially formed by sulphamoylation (Scheme 1, Eq. 1, A→B→C). This is the case in the rapid radioactive reactions with a high excess of SCl. However, the non-radioactive experiments were carried out in the presence of solid sodium carbonate as a base for several hours. During this time the base split off the 3-amidosulphonyloxy group from FES3S and FESDS (Scheme 1, Eq. 1, C → A). Because the 17-amidosulphonyloxy group is less sensitive to sodium carbonate (Scheme 1, Eq. 2, C –□–> A), FES17S outweighed FES3S in the non-radioactive reactions due to the long contact time.

Synthesis of [^{18}F]FES17S from [^{18}F]FESDS

The high sensitivity of the 3-amidosulphonyloxy group to a base was confirmed in non-radioactive experiments. FESDS was shown to be quantitatively converted into FES17S, and likewise FES3S into FES. This fact should open a new approach to [^{18}F]FES17S at a higher radioactivity level. In order to

prove this, we carried out three experiments in which a reaction mixture from the module-assisted procedure [3] was subjected to an additional alkaline treatment before HPL-chromatographic separation. Only the alkaline conditions were modified to a slight degree in these three experiments. The results are summarized in Table 3. In two cases (Expt. 1 and 2) the alkaline reaction mixture was carefully dried, then heated and stirred. A moderate conversion of [^{18}F]FESDS into [^{18}F]FES17S took place. But the highest conversion was observed when the careful drying of the alkaline reaction mixture was left out (Expt. 3). A radiochromatogram of Expt. 3 is illustrated in Fig. 2.

Table 3. Distribution of the radioactivity after alkaline treatment of [^{18}F]FESDS. Solvent: acetonitrile; reagent: 15 mg K222 and 2.77 mg K_2CO_3; stirring time: 5 min.

Expt.	Conditions a)	A_0 [MBq]	[^{18}F]FES17S at EOS b) [MBq]	Distribution of radioactivity [%] c)			
				Polar products	[^{18}F]FESDS d)	[^{18}F]FES17S	[^{18}F]FES
1	A	46200	1160	47.5	25.0	27.4	0
2	B	59000	1650	44.5	23.7	19.5	12.3
3	C	58000	2580	26.1	22.7	44.5	6.5

a) A – Alkaline treatment as described in Experimental. B – Alkaline treatment as described in Experimental, but 90 °C in place of 70 °C. C – Reaction mixture was not carefully dried as done in A or B.
b) EOS was 100 min after starting the synthesis.
c) Radioactivity of the peaks eluted from the column were measured, time-corrected and related to the sum of radioactivity.
d) Unconverted [^{18}F]FESDS

Different from the non-radioactive experiments, Fig. 2 shows that [^{18}F]FESDS was not completely converted into [^{18}F]FES17S by the additional alkaline treatment. But the peak of [^{18}F]FES17S was the highest. The radioactivity proportion of the remaining [^{18}F]FES was small, as expected. Because the starting radioactivity was high (A_0 = 52 GBq) the radioactivity of [^{18}F]FES17S obtained at EOS was also high (2.6 GBq). In this way [^{18}F]FES17S can be made accessible for biological experiments on a large scale.

References

[1] Römer, J.; Füchtner, F.; Steinbach, J.; Johannsen, B. Automated production of 16α-[^{18}F]fluoroestradiol for breast cancer imaging. Nucl. Med. Biol. 26 (1999) 473-479.

[2] Römer, J.; Füchtner, F.; Steinbach, J. Synthesis of 16α-[^{18}F]fluoroestradiol-3,17β-disulphamate. J. Labelled Compds. Radiopharm. 43 (2000) 425-436.

[3] Römer, J.; Füchtner, F.; Steinbach, J.; Kasch, H. Automated Synthesis of 16α-[^{18}F]Fluoroestradiol-3,17β-disulphamate. Appl. Radiat. Isot. 52 (2001) in press.

[4] Kasch, H.; Schumann, W.; Römer, J.; Steinbach, J. Steroid sulphamates, methods for preparation and use thereof. Patent PCT/DE 98/00813 (1998).

[5] Kasch, H.; Dintner, U.; Härtl, A.; Römer, J.; Steinbach, J. ^{18}F-PET tracer - effective tools for disclosing ways of signal transduction. Annual Report of Hans-Knöll-Institute for Natural Products Research (1998) pp. 33-36.

[6] Römer, J.; Kasch, H.; Steinbach, J.; Scheller, D. Herstellung und Charakterisierung der Sulfamate von Estra-3,17ξ-diolen. Schnelle Umsetzung von 16α-Fluorestradiol zum 16α-Fluorestradiol-3,17β-disulfamat. J. prakt. Chem. 341 (1999) 574-587.

[7] Brust, P.; Rodig, H.; Bergmann, R.; Römer, J.; Baumann, M.; Kasch, H.; Füchtner, F.; Steinbach, J. Distribution of 16α-[^{18}F]fluoro-estradiol-3,17-β-disulphamate (FESDS) in rats and tumour-bearing nude mice. *This Report,* pp. 144-148.

[8] Römer, J.; Steinbach, J.; Kasch, H. Studies on the synthesis of 16α-[^{18}F]fluoroestradiol. Appl. Radiat. Isot. 47 (1996) 395-399.

[9] Appel, R.; Berger, G. Über das Hydrazodisulfamid. Chem. Ber. 91 (1958) 1339-41.

36. Mass Spectroscopic Investigations of By-Products in the Synthesis of 16α-[^{18}F]Fluoro-Estradiol-3,17β-Disulphamate

K. Fischer, J. Römer

Introduction

In the radioactive synthesis of 16α-[^{18}F]fluoroestradiol-3,17β-disulphamate ([^{18}F]FESDS) [1], some polar by-products are formed which are eluted in the following RP HPLC purification process before [^{18}F]FESDS (see Fig. 1). They contain almost half the total amount of radioactivity. Optimization experiments to reduce this percentage of radioactive by-products failed. However, if the composition of these polar products and the conditions of their formation were known, successful optimization experiments should be possible. The by-products were therefore investigated by mass spectroscopy.
Surprisingly, highly radioactive polar products were also formed when pure [^{18}F]FESDS was treated in an alkaline medium. Alkaline treatment of [^{18}F]FESDS is a new method of producing 16α-[^{18}F]fluoroestradiol-17β-sulphamate [2], which was not otherwise available in a high yield. The polar products were also investigated by mass spectroscopy.

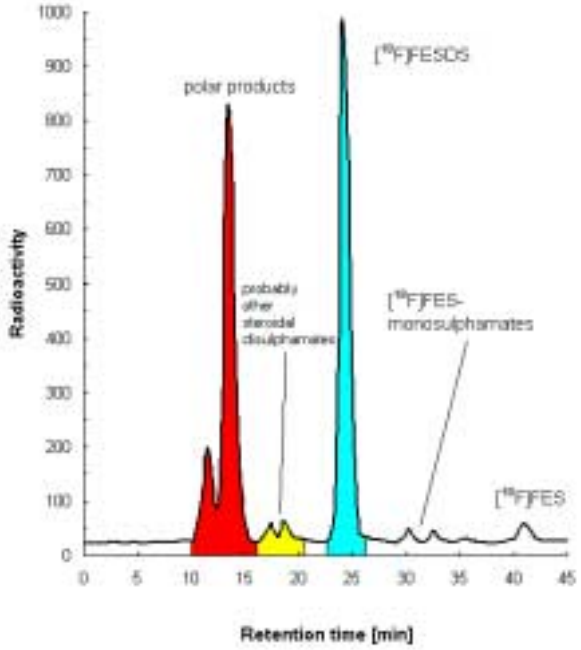

Fig. 1. Typical column radiochromatogram after synthesis of 16α-[^{18}F]fluoro-estradiol-3,17βdisulphamate

Experimental

General
Mass spectrometric analyses were carried out on a Micromass tandem quadrupole mass spectrometer (Quattro LC) operated in the MS mode and combined with an HPLC system of the 1100 series (Hewlett Packard). The LC-MS method used a Macherey-Nagel NUCLEOSIL 120 C-18 column (10 mm x 4 mm) and 50 % ethanol as the mobile phase at 0.25 ml/min. The UV absorption of the column eluate was recorded at 216 nm.
The MS parameters:

Detection mode	positive and negative API
Cone	40 V
Capillary	3.5 kV
Desolvation gas flow	763 L/h
Nebulizer gas flow	53 L/h
Mass range	50-800 amu

Products to be investigated
The products to be investigated were eluted as the red and yellow peaks, which were collected in single fractions and lyophilized (Fig. 1). Before measurement the residue of each fraction was dissolved in 1 ml 50 % EtOH.

Strategy
The following test series were carried out:
Investigation of the eluate of the (yellow) peaks between 15 and 20 min.
Investigation of the eluate of the (red) peaks between 10 and 15 min.
Investigation of the eluate of the polar products formed by alkaline treatment of column-purified [^{18}F]FESDS with Kryptofix 2.2.2/K_2CO_3.

Results and Discussion

Investigation of the eluate of the (yellow) peaks between 15 and 20 min
The tests produced mass spectra which contained m/z 524 and m/z 445. The difference Δ m = 79 indicates the presence of NH-SO_2 as a fragment. If this is true, the mol peak M^+ = 524 should originate from a substituted fluoroestradioldisulphamate, e.g. 3-(N-amidosulphonyl)fluoroestradiol-3,17β-disulphamate (M = 526 g/mol, N-amidosulphonyl-FESDS). Such a compound would be more polar than fluoroestradiol-3,17β-disulphamate (FESDS).

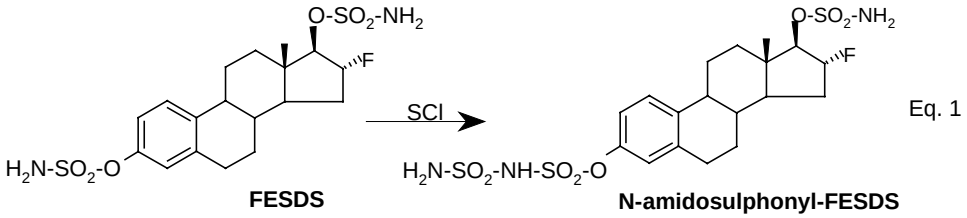

Eq. 1

In the sulphamoylation reaction, excess sulphamoyl chloride (SCl) is used to convert fluoroestradiol (FES) into FESDS. If excess SCl were also to substitute a proton of the NH_2-SO_2 group of just formed FESDS, N-amidosulphonyl-FESDS would be present as shown in Eq. 1.

But it is also possible that two SCl molecules react with each other to produce N-amidosulphonyl-sulphamoyl chloride (AS-SCl) as shown in Eq. 2. If AS-SCl were to substitute the favoured 3-OH of fluoroestradiol (FES) and SCl the 17β-OH of FES, the same substituted FESDS would be present (Eq. 3).

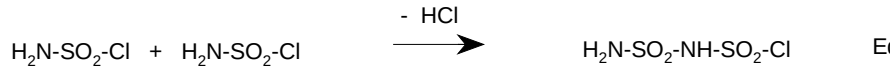

Eq. 2

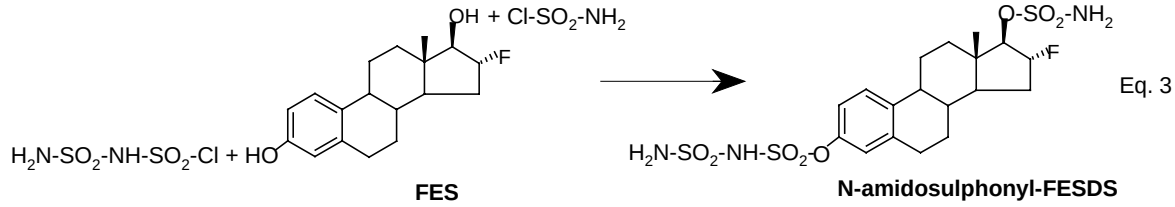

Eq. 3

Investigation of the eluate of the (red) peaks between 10 and 15 min
Since the development of the FESDS synthesis we have known that sulphamoyl acid and Kryptofix 2.2.2 (K222) are eluted from an RP column as the first compounds. But especially for K222, the exact analytical detection has not been previously reported. And we have been unable to explain why the polar products contained half the total radioactivity in a radioactive synthesis.

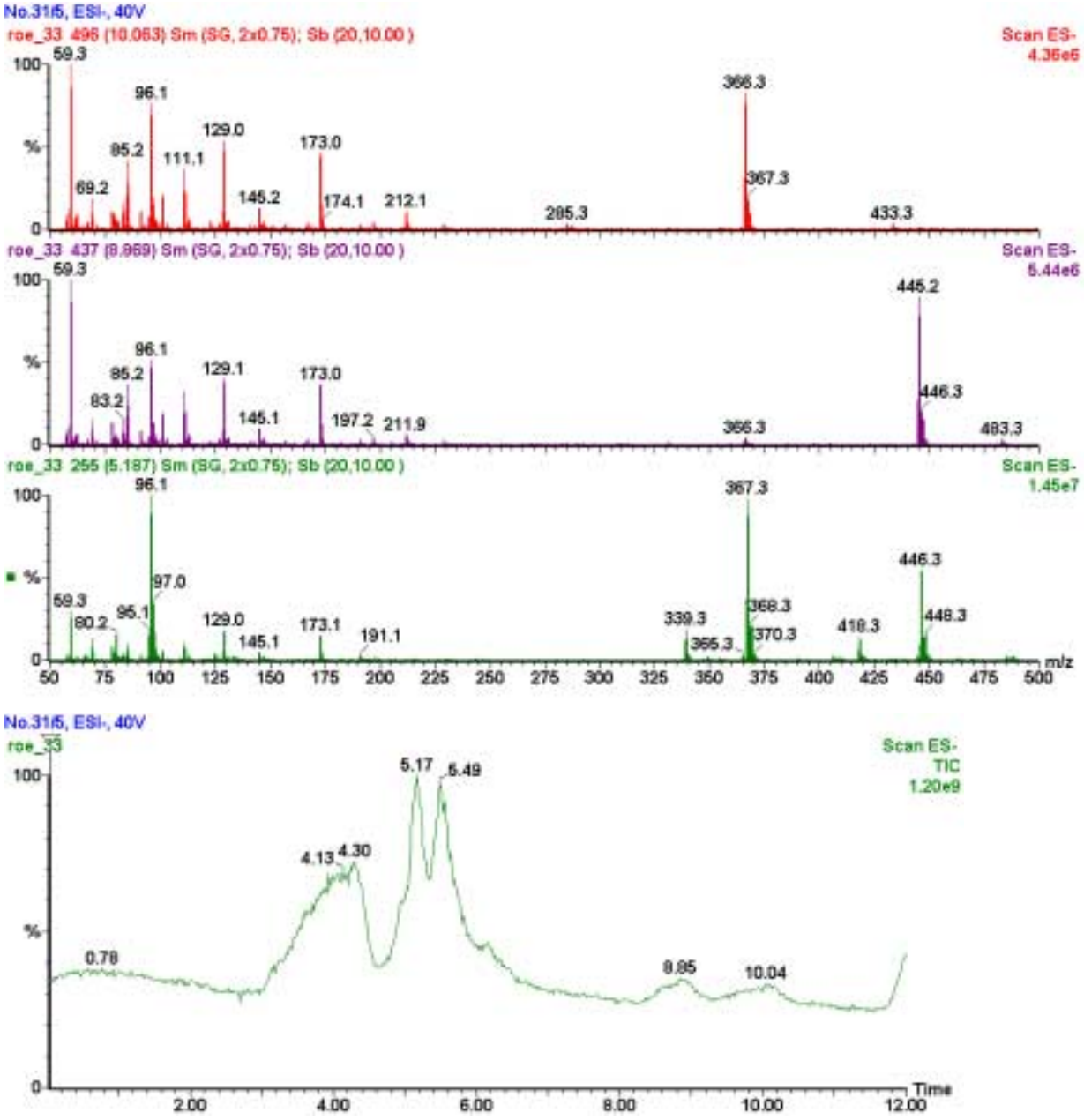

Fig. 2. Mass spectra of the polar products which were eluted as the red peaks in Fig. 1. Only the peaks at 5.17, 8.85 and 10.04 min in the TIC chromatogram (below) contained masses of N-amidosulphonyl derivatives of FESDS as shown in the mass spectra (above)

We recorded ESI^- and ESI^+ spectra of the polar products. The ESI^- spectra of these eluates showed m/z 96 due to the sulphamoyl acid (H_2H-SO_2-OH, M = 97 g/mol), which was formed from the decomposition of SCl in water. Analysis of the total-ion-current (TIC) chromatograms showed the appearance of m/z 366, 367 and m/z 445, 446, 448 in three TIC peaks (see Fig. 2). In another sample m/z 525, 527 and m/z 604 were found. The known difference Δ m = 79 again indicates the presence of NH-SO_2 as a fragment. This fragment is most likely due to the presence of FESDS, which is substituted by one or two sulphamoyl groups. Even molecules with more than two sulphamoyl groups are imaginable. Such substituted FESDS molecules can explain why the polar products contain a lot of radioactivity.
The ESI^+ spectra of all eluates of the red peaks showed m/z 377 and m/z 415. This is K222 (M = 376 g/mol) as $(M + H)^+$ and $(M + K)^+$. Further masses were 189, 158, 114 and 70. As the mass-spectral behaviour of a tertiary amine resembles that of a secondary amine, which often has m/z 70 at the end of its fragmentation pathway, we believe that the proposed pathway in Fig. 3 is plausible for K222 fragmentation. The occurrence of m/z 377 and m/z 415 shows that LC-MS (ESI^+) is a rather

important analytical method of detecting K222. The high proportion of radioactivity of the polar products can be explained by clusters $(M + K)^+F^-$.

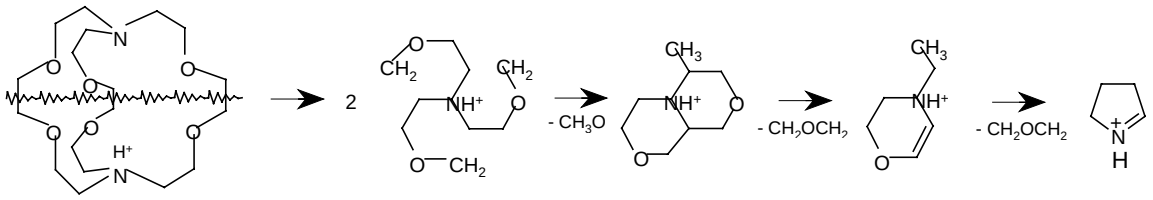

Fig. 3. Mass-spectral reactions after ES^+ ionization of Kryptofix 2.2.2 (M = 376) g/mol)

Investigation of the eluate of polar products formed by alkaline treatment of column-purified [^{18}F]FESDS with Kryptofix 2.2.2/K_2CO_3.

The mass spectra confirmed the results, i.e. we found sulphamoyl acid (ESI^-) and K222 (ESI^+). Another important result was the fact that the eluate of the polar products did not contain steroids, i.e. a reaction as given in Eq. 1 did not occur when [^{18}F]FES was sulphamoylated. However, as radioactivity is present in the eluate of these polar products , we have to conclude that [^{18}F]fluoride was split from [^{18}F]FESDS as a result of its alkaline treatment.

Conclusion

We made efforts to optimize the synthesis of [^{18}F]FESDS in order to reduce the losses of radioactivity bound in the polar products, but the experiments were not successful. The results obtained show that the sulphamoylation of [^{18}F]FES as well as the splitting of [^{18}F]fluoride from the labelled molecules are both due to the alkaline medium, i.e. that the automated procedure of the production of [^{18}F]FESDS already represents a compromise. There is little chance to improve it. Thus, the results of the present report can be summarized as follows:

1. The radioactivity of the polar products is due to (N-amidosulphonyl)$_n$ FESDS with n = 1,2,3,4 and [^{18}F]fluoride. The counterion of [^{18}F]F^- is $(K222 + K)^+$.
2. K222 is quantitatively eluted in the eluate of the polar products.

References

[1] Römer, J.; Füchtner, F.; Steinbach, J.; Kasch, H. Automated synthesis of 16α-[^{18}F]fluoroestradiol-3,17β-disulphamate. Appl. Radiat. Isot. 52 (2001), in press.

[2] Römer, J.; Füchtner, F.; Steinbach, J.; Lücke, R.; Smuda, C.; Kasch, H. Simultaneous preparation of 16α-[^{18}F]fluoro-estradiol-sulphamates in an automated module. A high-yield procedure for 16α-[^{18}F]fluoroestradiol-17β-sulphamate. *This Report*, pp. 98-102.

37. Steroidal 16,17-O-Sulphuryl Derivatives as Suitable Precursors for ^{18}F-Labelled *trans* 16,17-Fluoro Hydrines

J. Römer, F. Füchtner, J. Steinbach, H. Kasch[1]
[1] id pharma, Jena

Introduction

After the synthesis and successful application of 16α-[^{18}F]fluoroestradiol (**αFES**) [1] we were anxious to find out whether 16α-[^{18}F]fluoro-androst-5-ene-3β,17β-diol (**αFAD**) can be developed as a new PET tracer because androst-5-ene-3β,17β-diol was known as a compound with a high affinity to the estrogen receptor.
A general route to synthesize suitable precursors for **αFES** and **αFAD** was elaborated by Kasch *et al.* [2]. This route made it possible to synthesize 16α,17α-O-sulphuryl and 16β,17β-O-sulphuryl derivatives of 16,17-diols in the estrane as well as in the androstane series. Thus, the isomeric *trans* fluoro hydrines of **αFES** and **αFAD,** 16β-[^{18}F]fluoro-estra-1,3,5(10)-triene-3,17α-diol (**βFES**) and 16β-[^{18}F]fluoro-androst-5-ene-3β,17α-diol (**βFAD**), should also be accessible. The reactions of the *cis* 16,17-cyclic sulphates are illustrated in Scheme 1.

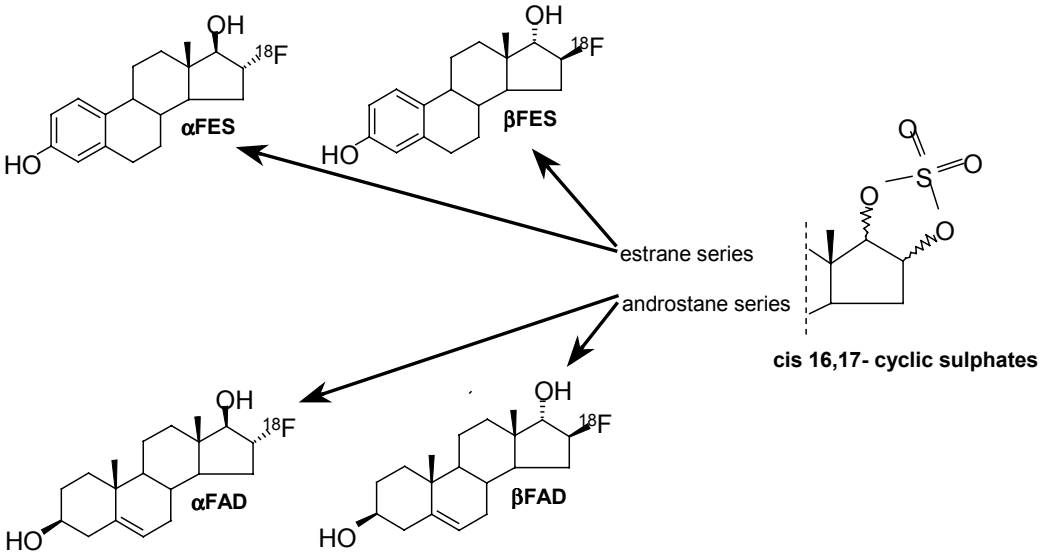

Scheme 1 .
***trans* 16,17- Fluoro hydrines of the estrane series (αFES, βFES) and androstane series (αFAD, βFAD) from *cis* 16,17- cyclic sulphates**

The first radioactive experiments are described in the present paper to produce **αFAD** , **βFES** , and **βFAD** .

Experimental

The experiments were carried out in a Nuclear Interface module, which was normally used for routine production of 16α-[^{18}F]fluoroestradiol (**αFES**). The procedure is described in detail elsewhere (see [1]). Irradiated [^{18}O]H_2O which contained either 1700 MBq (two experiments) or 3400 MBq (one experiment) of no-carrier-added (n.c.a.) [^{18}F]HF was used in the experiments. The complete procedure consisted of three parts: (1) nucleophilic fluorination of the cyclic sulphate as 3-methoxymethyl ether, (2) acid hydrolysis to remove the protective groups, (3) semipreparative HPLC purification, using an RP column and 50 % EtOH as solvent. The column was eluted at 1.5 ml/min. The following precursors were used:

3-O-Methoxymethyl-16,17-O-sulphuryl-androst-5-ene-3β,16β,17β-triol to synthesize **αFAD.**
3-O-Methoxymethyl-16,17-O-sulphuryl-estra-1,3,5(10)-triene-3,16α,17α-triol to synthesize **βFES**.
3-O-Methoxymethyl-16,17-O-sulphuryl-androst-5-ene-3β,16α,17α-triol to synthesize **βFAD**.

The non-radioactive analogues of **αFAD**, **βFAD** and **βFES** were prepared as reference substances also according to Scheme 1.

Results and Discussion

The most important result is the fact that we were able to prepare all the ^{18}F-labelled fluoro hydrines **αFAD**, **βFAD** and **βFES** according to the module-assisted procedure used for **αFES** [1]. The precursors were rapidly converted and produced the desired fluoro hydrines in yields of about 25 %. The results are compiled in Table 1. Berridge's opinion [3] that the cyclic sulphates were a useful synthetic tool was fully confirmed.

Table 1. Real yields of ^{18}F labelled *trans* 16,17-fluoro hydrines after nucleophilic fluorination of the corresponding *trans* 16,17-cyclic sulphates with no-carrier-added (n.c.a.) [^{18}F]HF

Expt.	A_0	EOS	^{18}F Labelled *trans* 16,17-fluoro hydrines		Real yield at EOS
	[MBq]	[min] after t_0	Compound	Radioactivity at EOS [MBq]	[%]
1	3480	87	**αFAD**	873	25.0
2	1720	88	**βFAD**	393	22.8
3	1740	80	**βFES**	466	26.8

Each ^{18}F labelled fluoro hydrine showed the same retention time as found for its non-radioactive analogue: **αFES** (30.0 min), **βFES** (34.6 min), **αFAD** (38.2 min), and **βFAD** (51.0 min). As can be seen, **βFES** was eluted later than **αFES**, **βFAD** was eluted later than **αFAD**. This means that the β-analogue is less polar than the α-compound, probably because of the interaction between the 13-methyl group and 16β-fluorine.
The radiochromatogram of each ^{18}F labelled fluoro hydrine revealed polar products, the radioactivity being almost 50 %. The degree of conversion of [^{18}F]fluoride into the fluoro hydrines investigated was: **αFAD** (50.9 %), **βFAD** (52.8 %), **βFES** (50.4 %). The radiochemical purity of the ^{18}F-labelled fluoro hydrines immediately after semipreparative HPLC separation was 99.9 % for **αFAD** and **βFAD,** but 99.5 % for **βFES**.

Conclusions

The first results are very promising. It should be possible to perform further reactions in the automated module. Our plans include especially oxidizing **αFAD** to 16α-[^{18}F]fluoro-dehydroepiandrosterone because the non-radioactive analogue is an anti-cancer drug.

References

[1] Römer, J.; Füchtner, F.; Steinbach, J.; Johannsen, B. Automated production of 16α-[^{18}F]fluoro-estradiol for breast cancer imaging. Nucl. Med. Biol. 26 (1999) 473-479.

[2] Kasch, H.; Dintner, U.; Römer, J.; Steinbach, J. Steroidal 16,17-cyclic carbonates as key products for cyclic sulphites and sulphates. *Report July - December 1999*, Institute of Bioinorganic and Radiopharmaceutical Chemistry, FZR-283, pp. 51 – 53.

[3] Berridge, M.S.; Franceschini, M.P.; Rosenfeld, E.; Tewson, T.J. Cyclic sulfates: Useful substrates for selective nucleophilic substitution. J. Org. Chem. 55 (1990) 1211 – 1217.

38. 16α-Fluoro-Estradiol-3-Monosulphamate (FESMS) and 16α-Fluoro-Estradiol-3,17ß-Disulphamate (FESDS)– New Carbonic Anhydrase Inhibitors of High Potency

H. Rodig, J. Gross[1], A. Müller[1], H. Kasch[2], P. Brust
[1]TU Dresden, [2]idPharma, Jena

Introduction

Recently the synthesis of 16α-[^{18}F]fluoroestradiol-3,17β-disulphamate ([^{18}F]FESDS) was described [1, 2] and the compound suggested as a potential PET tracer for imaging steroid-dependent breast tumours because it has a high affinity to the enzyme estrone sulphatase which is present in these tumours in high amounts [3]. However, as a result of in-vivo studies it was concluded that this tracer is not suitable for tumour imaging, irrespective of whether the tumours express estrone sulphatase or not [4]. Furthermore, evidence was obtained that the binding to estrone sulphatase seems to be negligible compared with the binding to another target: carbonic anhydrase. This is not surprising because the sulphonamides are well-known carbonic anhydrase inhibitors [5, 6].
Carbonic anhydrase (CA; EC 4.2.1.1) is a widespread enzyme whitch catalyses the hydration of carbon dioxide and the dehydration of bicarbonate [7]. At least seven, probably nine, distinct isoenzymes are known, designated CA I – CA IX [8]. They are localized in various compartments of the mammalian cell [7]. CA I, II, III, and VII are cytosolic, CA V is mitochondrial, CA IV and V are membrane-bound, CA VI is secreted outside the cell.
The sensitivity of the isoenzymes to the sulphonamides varies, CA II and CA V are the most sensitive isoenzymes, CA I, IV, and VI are somewhat sensitive and CA III is insensitive towards inhibition by sulphonamides [9, 19].
To test the hypothesis that [^{18}F]FESDS binds to the CA, we used purified enzyme preparations of human CA I and CA II (HCA I, HCA II) and bovine CA II (BCA II) and investigated the enzyme activity in the presence of well-known CA inhibitors (Table 1) and of FESDS and 16α-Fluorestradiol-3-monosulphamate (FESMS) (Fig. 1).

Table 1. Comparison of the K_i values of various carbonic anhydrase inhibitors

CA inhibitor	Formula	K_i value (nM)	Species, Isoenzyme	Reference
Acetazolamide	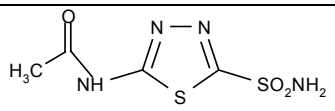	7 5 16	dog (25 °C) cattle, CA II human, CA II	[10] [11] [14]
Ethoxyzolamide	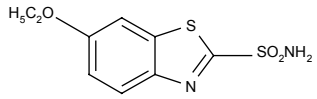	0.7 7.1 9.0 3.4	dog (25 °C) dog (25 °C) human, CA I human, CA II	[10] [13] [12] [12]
Furosemide	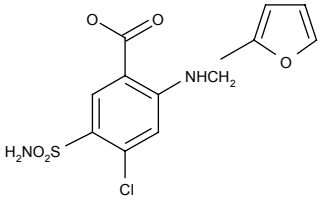	80	dog (25 °C)	[10]
Hydrochlorothiazide	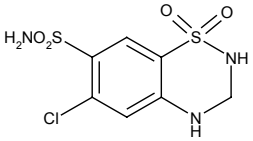	2350	dog (25 °C)	[10]

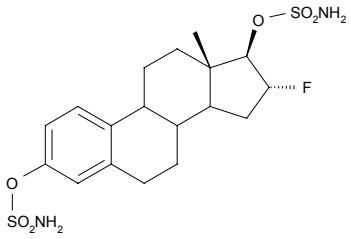

Fig. 1a. 16α-Fluorestradiol-3,17ß-disulphamate (FESDS)

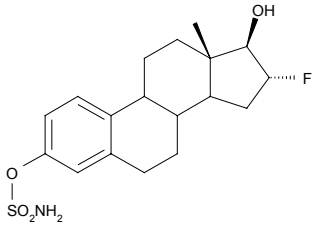

Fig. 1b. 16α-Fluorestradiol-3-monosulphamate (FESMS)

Experimental

Chemicals

Acetazolamide, hydrochlorothiazide, ethoxyzolamide, furosemide, p-nitrophenylacetate and p-nitrophenolate were purchased from Sigma (Steinheim, Germany). FESDS and FESMS were synthesized as previously described [2]. Human carbonic anhydrase I and II (HCA I and II) from erythrocytes was obtained from Sigma and bovine carbonic anhydrase II (BCA II) from Biochemika (Steinheim, Germany).

Enzyme assay

We used a CA assay according to Verpoorte *et al.* [15] to measure the esterase activity of CA. P-nitrophenylacetate was converted into p-nitrophenolate and acetate (Fig. 2). Because of the colour shift from white to yellow it was possible to measure the reaction by spectroscopy at a wavelength of 340 nm.

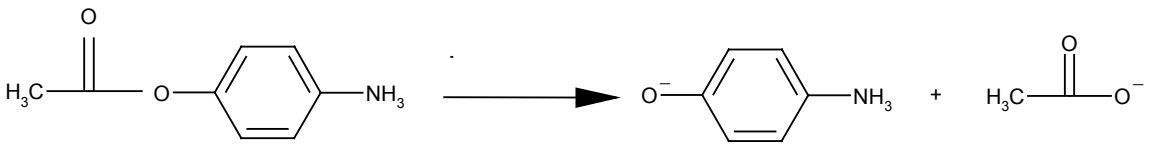

P-nitrophenyl acetate P-nitrophenolate Acetate

Fig. 2. Reaction scheme of measuring the esterase activity of carbonic anhydrase

The assay was performed in 2 ml reaction tubes (Eppendorf, Germany) containing 450 µl buffer (50 mM Tris-HCl, 50 mM Tris-aminomethane, or 50 mM Tris-sulphate, pH 7.4), 0.1 mg/ml human or bovine CA II or 0.2 mg/ml human CA I, between 0.07 and 0.7 mM p-nitrophenylacetate, and between 10^{-10} and 10^{-3} M inhibitor diluted in 50 µl water from 10 mM and 1 mM stock solutions (in 60 % DMSO). Blanks contained the same reagents without enzyme.

Various incubation temperatures (4, 25, 30, and 37 °C), incubation times (3, 5, 10, 20, and 30 minutes), and buffers (see above) were used to optimize the assay.

The absorption of p-nitrophenolate was measured at 340 nm with an anthos htII photometer (anthos labtec instruments, Salzburg, Austria). The substrate turnover was calculated from a standard curve. IC_{50} values were estimated from sigmoidal dose-response curves using the software Prism 3.0.

Results and Discussion

Fig. 3 shows the dependency of the CA activity on the incubation temperature. As expected the highest activity was found at 37 ^{o}C. At 25 °C the activity was reduced by more than 50%, which indicates the need to use the higher temperature in our study. In a direct assay of anhydrase activity of human CA I the reduction by decreasing the temperature was only 30 % [16]. The affinity of the sulphonamide binding was also found to decrease with increasing temperature [12]. For comparison an assay temperature of 37 ^{o}C is therefore recommended.

To optimize the conditions we performed the assay, using various buffers (50 mM Tris-sulphate, Tris-HCl, and Tris-aminomethane at pH 7.4). No major differences between the buffers were found (data

not shown). We therefore continued to use Tris-sulphate as described by Verpoorte *et al.* [15]. The esterase activity of carbonic anhydrase increased linearly with the incubation time (Fig. 4)so that the activity after 30 min was 4 times as high as after 5 min. For our experiments we chose an incubation time of 30 min for high measuring signals.

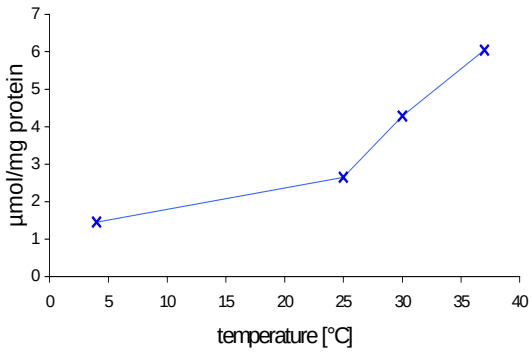

Fig. 3. Carbonic anhydrase activity at various incubation temperatures

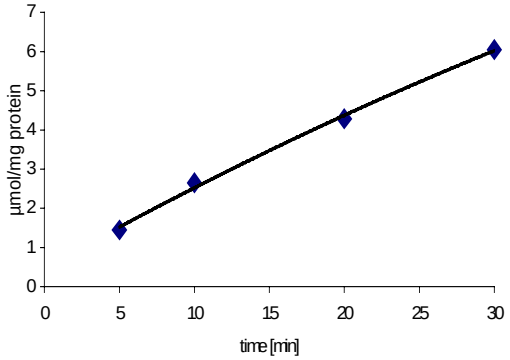

Fig. 4. Carbonic anhydrase activity at various incubation times

Various concentrations of FESDS and FESMS were used in the CA assay to obtain IC_{50} values for these compounds as a measure of their affinity towards carbonic anhydrase. For comparison inhibition experiments were also performed with acetazolamide, hydrochlorothiazide, ethoxyzolamide, and furosemide (Table 2).

Table 2. IC_{50} values (nM) of FESDS and FESMS in comparison with various carbonic anhydrase inhibitors

Ligand	HCA I	HCA II	BCA II
FESDS	288 ± 3	54 ± 1	271 ± 4
FESMS	1050 ± 12	53 ± 1	323 ± 3
Acetazolamide	219 ± 2	30 ± 1	100 ± 1
Ethoxyzolamide	655 ± 8	27 ± 1	337 ± 4
Furosemide	631 ± 1	1061 ± 8	795 ± 5
Hydrochlorothiazide	15200 ± 169	7654 ± 90	4304 ± 42

Both FESDS and FESMS have a high affinity towards the human CA II which is only slightly lower than the affinities of the clinically used CA inhibitors acetazolamide and ethoxyzolamide. FESDS and FESMS differ by about a factor of three in their affinities to human CA I. The affinity of FESDS is again similar to that of acetazolamide. It is known that human CA II is more sensitive to sulphonamides than human CA I [9]. This was confirmed by the present study.

The IC_{50} values determined in this paper correlate well with data from the literature which were obtained by direct measurement of anhydrase activity (Tab. 1). Generally, the values obtained by Maren [10], using dog red cells at 25 °C, are about one-tenth of those obtained from our measurements of esterase activity. However, as mentioned above, the affinity is inversely correlated to the incubation temperature. This may not be the only explanation. Another study, also performed at 25 °C, found a ten times increased K_i for ethoxyzolamide (7.1 nM) in dog erythrocytes compared with Maren [13]. We therefore conclude that FESDS has about the same potency as acetazolamide to inhibit the anhydrase activity of CA. an The IC_{50} for acetazolamide of 550 nM and 64 nM for human CA I and II is also close to our values [17]. Bayne *et al.* [18] studied the binding of acetazolamide to CA I and CA II in human erythrocytes and found inhibitory constants of 2.72 µM and 41 nM.

To sum up, we demonstrated that FESDS and FESMS are among the best carbonic anhydrase inhibitors described so far. It remains to be seen whether these compounds will gain clinical importance.

References

[1] Römer, J.; Füchtner, F.; Steinbach, J.; Kasch, H. Automated synthesis of 16α-[^{18}F]fluoroestradiol-3,17ß-disulphamate. Appl. Radiat. Isot. (in press).

[2] Römer, J; Steinbach, J. Herstellung und Charakterisierung der Sulfamate von Estra-3,17ß-diolen. Schnelle Umsetzung von 16α-Fluorestradiol zum 16α-Fluorestradiol-3,17ß-disulfamat. J. Prakt. Chem. 341 (1999) 574-583.

[3] Pasqualini, J.R.; Chetrite, G.; Nestour, E.L. Control and expression of oestrone sulphatase activities in human breast cancer. J. Endocrinol. 150 (Suppl) (1996) 99-105.

[4] Brust, P.; Rodig, H.; Bergmann, R.; Römer, J.; Baumann, M.; Kasch, H.; Füchtner, F.; Steinbach, J. Distribution of 16-α-[^{18}F]fluoro-estradiol-3,17-β-disulphamate (FESDS) in rats and tumour bearing nude mice. *This Report,* pp. 144-148.

[5] Lindskog, S.; Engberg, P.; Forsman, C.; Ibrahim, S.A.; Johansson, B.-H.; Simonsson, L.; Tibell, L. Kinetics and mechanism of carbonic anhydrase isoenzymes. Ann. N. Y. Acad. Sci. 429 (1984) 61.

[6] Hurvitz, L.M.; Kaufman, P.L.; Robin, A.L.; Weinreb, R.N.; Crawford. K.; Shaw, B. New developments in the drug treatment of glaucoma. Drugs 41 (1991) 514-32.

[7] Tashian, R. The carbonic anhydrase: widening perspectives on their evolution, expression and function. BioEssays 10 (1989) 186-192.

[8] Hewett-Emmett, D.; Tashian, R.E. Functional diversity, conservation, and convergence in the evolution of the alpha-, beta-, and gamma-carbonic anhydrase gene families. Mol. Phylogenet. Evol. 5 (1996) 50-77.

[9] Maren, T.H.; Conroy, C.W. A new class of carbonic anhydrase inhititor. J. Biol. Chem. 268 (1993) 26233-26239.

[10] Maren, T.H. Direct measurement of the rate constants of sulphonamides with carbonic anhydrase. Mol. Pharmacol. 41 (1992) 419-426.

[11] Sharier, M.; Pierce, W.M. Jr.; Chen, D.; Zimmerman, T.J. Pharmacokinetics, acid-base balance and intraocular pressure effects of ethyloxaloylazolamide - a novel topically active carbonic anhydrase inhibitor. Exp. Eye Res. 58 (1994) 107-116.

[12] Conroy, C.W.; Maren, T.H. The effect of temperature on the binding of sulphonamides to carbonic anhydrase isoenzymes I, II, and IV. Mol. Pharmacol. 48 (1995) 486-491.

[13] Forster, R.E. 2d; Dodgson, S.J.; Storey, B.T.; Lin, L. Measurement of carbonic anhydrase activity inside cells and subcellular particles. Ann. N. Y. Acad. Sci. 429 (1984) 415-29.

[14] Wistrand, P.J. Human renal cytoplasmic carbonic anhydrase. Tissue levels and kinetic properties under near physiological conditions. Acta Physiol. Scand. 109 (1980) 239-48.

[15] Verpoorte, J.A.; Mehta, S.; Edsall, J.T. Esterase activities of human carbonic anhydrases B and C. J. Biol. Chem. 242 (1967) 4221-9.

[16] Dodgson, S.J.; Forster, R.E.; Sly, W.S.; Tashian, R.E. Carbonic anhydrase activity of intact carbonic anhydrase II-deficient human erythrocytes. J. Appl. Physiol. 65 (1988) 1472-1480.

[17] Masuda, Y.; Karasawa, T. Inhibitory effect of zonisamide on human carbonic anhydrase *in vitro*. Arzneimittelforschung 43 (1993) 416-418.

[18] Bayne, W.F.; Chu, L.C.; Theeuwes, F. Acetazolamide binding to two carbonic anhydrase isoenzymes in human erythrocytes. J. Pharm. Sci. 68 (1979) 912-913.

[19] Sly, W.S.; Hu, P.Y. Human carbonic anhydrases and carbonic anhydrase deficiencies. Ann. Rev. Biochem. 64 (1995) 375-401.

39. Synthesis of Labelled Advanced Glycation End Products Using N-Succinimidyl 4-[^{18}F]Fluorobenzoate

P. Mäding, Ch. Heichert, M. Scheunemann, R. Helling[1], T. Henle[1], J. Steinbach, B. Johannsen
[1]TU Dresden, Institut für Lebensmittelchemie

Introduction

The Maillard reaction between reducing carbohydrates and amino compounds, well studied in food systems over the last 80 years, turned to a new point of interest when various reaction products in human tissues were detected in the last few years.
Such "advanced glycation end products" (AGEs) were found to accumulate *in vivo* during aging as well as in diabetes or uremia. The physiological effects attributed to AGEs include cell activation, cytokine synthesis by monocytes, interaction with specific receptors (RAGE), an increase in oxidative stress and others [1, 2, 3, 4].
Whereas the endogenous formation of individual protein-bounded amino acids and their possible pathophysiological importance are intensively discussed, consequences resulting from dietary AGEs are still unknown. N^{ε}-Carboxymethyllysine (CML) and N^{ε}-carboxyethyllysine (CEL) proved to be AGE candidates from the nutritional and physiological point of view, because both amino acids are formed at proteins during food processing as well as under physiological conditions *in vivo* according to Scheme 1.

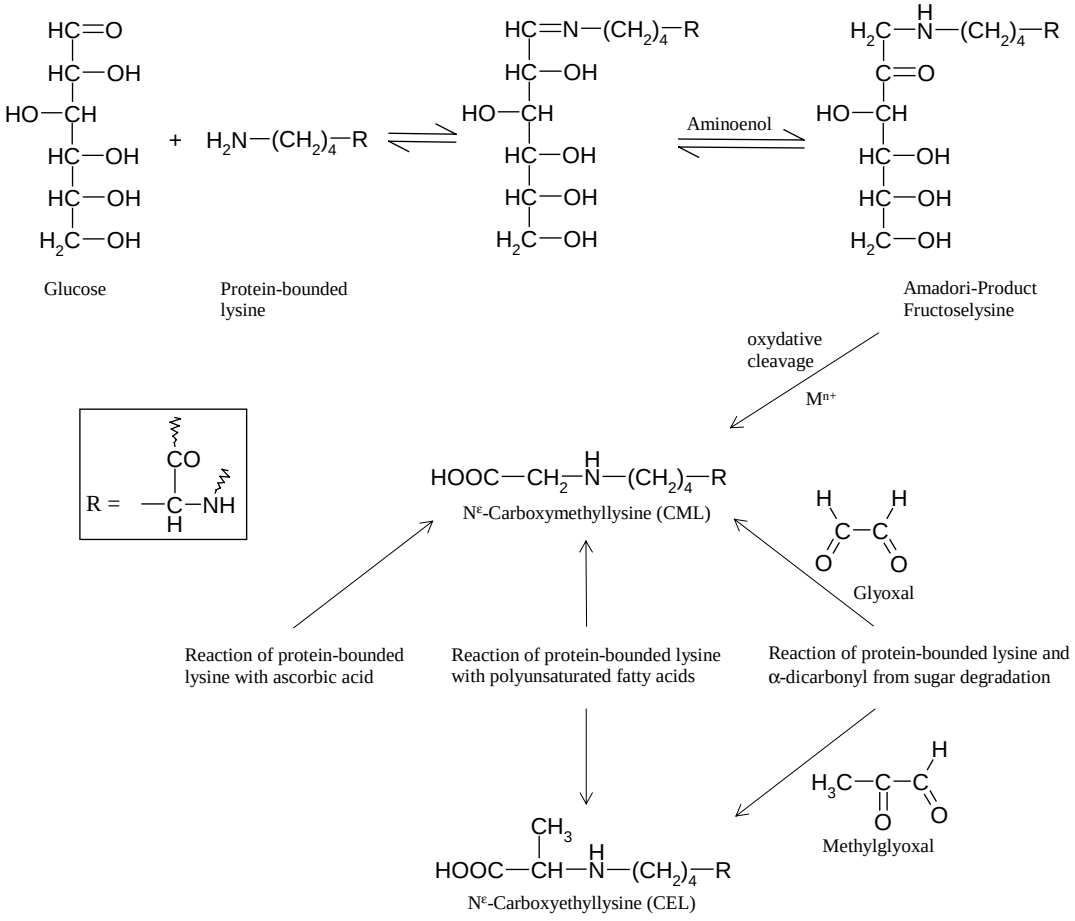

Scheme 1. Formation pathways of protein-bounded CML and CEL

Based on studies of the proteolytic release and resorption of peptide-bounded CML and CEL (especially as dipeptides or tripeptides), the *in vivo* distribution, metabolism and elimination kinetics of ^{18}F-labelled derivatives were to be investigated in comparison with ^{18}F-labelled lysine. For this purpose CML (**1a**) and CEL (**1b**) were modified at their free α-amino group, using N-succinimidyl

4-[^{18}F]fluorobenzoate ([^{18}F]SFB), to obtain the 4-[^{18}F]fluorobenzoylated derivatives **2a** or **2b** according to Scheme 2.

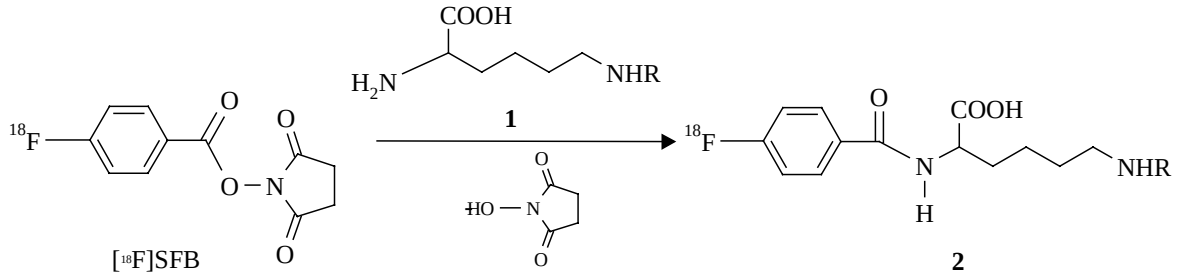

1a: R = CH_2COOH (CML)
1b: R = $CH(CH_3)COOH$ (CEL)
1c: R = Boc (N^{ε}-Boc-lysine)

2a: [^{18}F]FB-CML
2b: [^{18}F]FB-CEL
2c: [^{18}F]FB-N^{ε}-Boc-lysine

Scheme 2

The compounds **2a** and **2b** could be a useful model for dipeptides containing CML / CEL, possibly resulting from the digestion of glycated food proteins. In this case the fluorobenzoyl moiety acts as a surrogate for the second amino acid of the dipeptides.
The 4-[^{18}F]fluorobenzoylated derivative of lysine was used as a reference substance.

Experimental

Synthesis of the nonradioactive substances
CML and CEL were synthesized by means of reductive amination, starting from the sodium salt of N^{α}-acetyllysine and glyoxylic acid or pyruvic acid according to [2]. Reductive amination was carried out with Pd/C in a hydrogen atmosphere under pressure, followed by acidic deacetylation and purification, using ion exchange chromatography.
The nonradioactive fluorobenzoylated reference compounds were synthesized as follows. SFB (0.4 mmol) in dioxane (3 ml) and the amino acid (0.4 mmol) in water (8 ml) were well mixed, the pH was adjusted to 9 with 1 M NaOH. After stirring for 3 h at 50 °C, the reaction mixture was acidified with 1 M HCl to pH 3 and purified by preparative column chromatography on an RP-18 phase. Reaction products were identified by elemental analysis, NMR and ESI-MS studies.

Carrier-added radiosyntheses
[^{18}F]SFB was synthesized according to [5] with some modifications. The dried residue of [^{18}F]SFB was redissolved in 50 µl MeCN. A solution of SFB (1.34 µmol) in EtOH (100 µl) and a solution of CML, CEL or N^{ε}-Boc-lysine (1.53 µmol) in carbonate buffer (pH 8.9, 680 µl) were added. The reaction mixture was heated at 65 °C for 30 min. When CML or CEL were added, the reaction mixture was diluted with H_2O (1 ml) after heating and acidified by addition of HCl (1 M, 100 µl). The mixture was passed through an activated polystyrene cartridge (Merck, LiChrolut EN). The cartridge was washed with H_2O (3 ml), 5 % EtOH in H_2O (2 ml) and 16 % EtOH in H_2O (2 × 4 ml). About 35 % of the radioactive substances were eluted with the last two fractions as [^{18}F]FB-CML or [^{18}F]FB-CEL. After purity control by HPLC the 16 % ethanolic fractions were used for the biodistribution experiments.
The synthesis of [^{18}F]FB-lysine required a hydrolysis step for removing the Boc group at the end of the labelling reaction. For that reason HCl (6 M, 180 µl) was added and the reaction mixture was heated at 65 °C for another 20 min, diluted with H_2O (1 ml), and purified as described above.

Analysis
To determine the extent of conversion and the radiochemical purity and to identify the labelled products, an HPLC system (JASCO) was used, consisting of a pump, a Rheodyne injector with a 20 µl loop, a LiChrospher WP300 RP-18 column (5 µm, 250 mm x 3 mm, Merck) and a UV detector (230 nm) coupled in series with a radioactivity detector FLO-ONE\Beta 150TR (Canberra Packard). The HPLC analyses were carried out at a flow rate of 0.5 ml/min with mixtures of MeCN and water containing 0.2 % TFA. The gradient of the eluents was: 0 min - 10 % MeCN/ 90 % water; 14 min - 50 % MeCN/ 50 % water; 17 min - 100 % MeCN/ 0 % water; 20 min - 100 % MeCN/ 0 % water.

Results and Discussion

The synthesis of [^{18}F]SFB was carried out according to the three-step procedure described in [5]. The suitability of [^{18}F]SFB for [^{18}F]fluorobenzoylation of several peptides at their N-terminal α-amino group was investigated in [6, 7, 8] at the same time by another working group [9].
The conversion of [^{18}F]SFB with CML (**1a**), CEL (**1b**) or the N$^{\varepsilon}$-Boc-protected lysine (**1c**) was carried out in carbonate buffer (pH 8.9) at increased temperatures (65 °C). The labelling experiments were carrier-added syntheses, i.e. nonradioactive SFB was added to the reaction mixture of the amino acids **1** and [^{18}F]SFB. Under these conditions we obtained the 4-[^{18}F]fluorobenzoylated derivatives as predominant products together with smaller amounts of various unknown by-products, indicating that the α-amino group of the amino acids reacts preferably with [^{18}F]SFB.
The purification of the labelled derivatives was performed by means of solid phase extraction, using an adsorber resin cartridge. The 4-[^{18}F]fluorobenzoylated products were eluted with aqueous ethanol in radiochemical yields up to 35 % (decay-corrected) starting from [^{18}F]SFB. This is a fast and easy way of isolating the main products [^{18}F]FB-CML and [^{18}F]FB-CEL in radiochemical purities (90 to 96 %), which is sufficient for biochemical investigations.

References

[1] Raj, D.; Choudhury, D.; Welbourne, T.C.; Levi, M. Advanced glycation end products: A nephrologist`s perspective. Am. J. Kidney Dis. 35 (2000) 365-380.

[2] Liardon, R.; Weck-Gaudard, D. de; Phillippossian, G.; Finot, P.-A. Identification of N-ε-carboxymethyllysine : A new Maillard reaction product in rat urine. J. Agric. Food Chem. 35 (1987) 427-431.

[3] Schleicher, E. D.; Wagner, E.; Nerlich, A.G. Increased accumulation of the glycoxidation product CML. J. Clin. Invest. 99 (1997) 457-468.

[4] Ledl, F.; Schleicher, E. Die Maillard-Reaktion in Lebensmitteln und im menschlichen Körper - neue Ergebnisse zu Chemie, Biochemie und Medizin. Angew. Chem. 6 (1990) 597-734.

[5] Wester, H.J.; Hamacher, K.; Stöcklin, G. A comparative study of n.c.a. fluorine-18 labeling of proteins via acylation and photochemical conjugation. Nucl. Med. Biol. 23 (1996) 365-372.

[6] Mäding, P.; Scheunemann, M.; Steinbach, J.; Bergmann, R.; Iterbeke, K.; Tourwé, D.; Johannsen, B. Development of potential tumour imaging agents by 4-[^{18}F]fluorobenzoylation of neurotensin analogues. J. Labelled Compd. Radiopharm. 42 (1999) 1012-1013.

[7] Scheunemann, M.; Mäding, P.; Steinbach, J.; Bergmann, R.; Iterbeke, K.; Tourwé, D.; Johannsen, B. Fluorine-18 labelling of neurotensin analogues for the development of tumour imaging agents. J. Labelled Compd. Radiopharm. 42, Suppl. 1 (1999) 713-714.

[8] Scheunemann, M.; Mäding, P.; Bergmann, R.; Steinbach, J.; Johannsen, B. The utilization of [^{18}F]N-succinimidyl 4-fluorobenzoate ([^{18}F]SFB) for labelling bombesin derivatives. *Report July – December 1999*, Institute of Bioinorganic and Radiopharmaceutical Chemistry, FZR-283 pp. 61-62.

[9] Fredriksson, A.; Johnström, P.; Stone-Elander, S.; Jonasson, P.; Nygren, P.-A.; Ekberg, K.; Johansson, B.-L.; Wahren, J. Preparation of radiolabelled human C-peptide by conjugation with N-succinimidyl-4-[^{18}F]fluoro-benzoate. J. Labelled Compd. Radiopharm. 42, Suppl. 1 (1999) 546-548.

40. Aspects of the 6-[^{18}F]Fluoro-L-DOPA Preparation: Effective Chromatographic Purification of the Reaction Mixture and Determination of Radiochemical Purity

F. Füchtner, J. Steinbach, R. Lücke, E. Kraus

Introduction

The increasing number of PET centres using 6-[^{18}F]fluoro-L-DOPA ([^{18}F]FDOPA) as a radiotracer in PET studies [1] indicates the usefulness of this tracer for various medical indications. Accordingly, the number of papers dealing with [^{18}F]FDOPA applications in medicine is rather high. About 490 papers relating to [^{18}F]FDOPA are listed on the internet page of the U.S. Food and Drug Administration, the Center for Drug Evaluation and Research [2]. For 1999 and 2000 50 titles are listed.
Since the middle of the 1990s we have been dealing with studies related to the dopaminergic system using [^{18}F]FDOPA as a radiopharmaceutical. During this period more than 250 preparations according to the method described in [3] were performed.
In contrast to our results with the standard quality control method for the determination of the radiochemical purity we obtained indications of the presence of some [^{18}F]fluoride impurities in the final product. To improve the quality of the [^{18}F]FDOPA we were looking for more effective methods for purification of the reaction mixture by HPLC and for quality control.

Experimental

Purification
At first the [^{18}F]FDOPA crude product was synthesised by fluorination of the stannyl precursor by elemental [^{18}F]F_2 and hydrolysis of the protective groups. Afterwards the reaction mixture was directly transferred to a 10 ml injection loop passing through a 0.22 µm vented filter. After cooling down for 2 minutes the product was injected into the HPLC column. In Fig. 1 the chromatograms of semi-preparative HPLC using two different types of columns are shown.

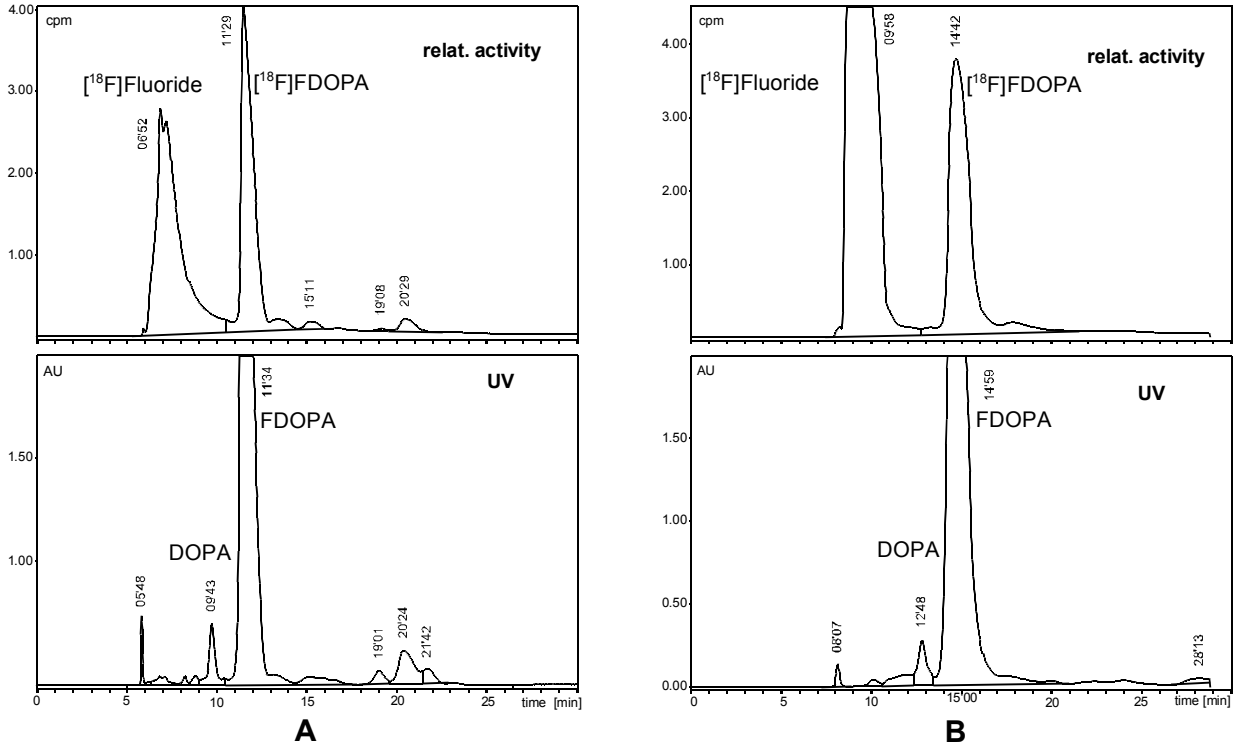

Fig. 1. Chromatograms of the semi-preparative separation of the reaction mixture
A - column: Nucleosil 120 C18, 7 µm, 250 x 10 and 50 x 10 mm, Macherey – Nagel,
B - column: PRP-1, 250 x 10 mm, 10 µm, two columns in line, Hamilton.

general

- sample volume: 4 ml,
- eluent: 105.6 mM of CH_3COONa and CH_3COOH, pH 4.7, isotonic, prepared with sterilised water (aqua ad iniectabilia),
- flow rate: 3 ml/min,
- detection: UV: 1 mm path length, 280 nm; radioactivity.

The eluent is fractionated by monitoring the radioactivity and the UV signal by switching a stream selection valve.

Radiochemical purity

For the determination of the radiochemical purity an analytical HPLC method is applied. Two different RP-chromatographic systems were tested for that purpose. Fig. 2 shows the chromatograms of the final product produced by semi-preparative HPLC purification as described in Fig. 1, using a silica-gel and a polymer-based RP column.

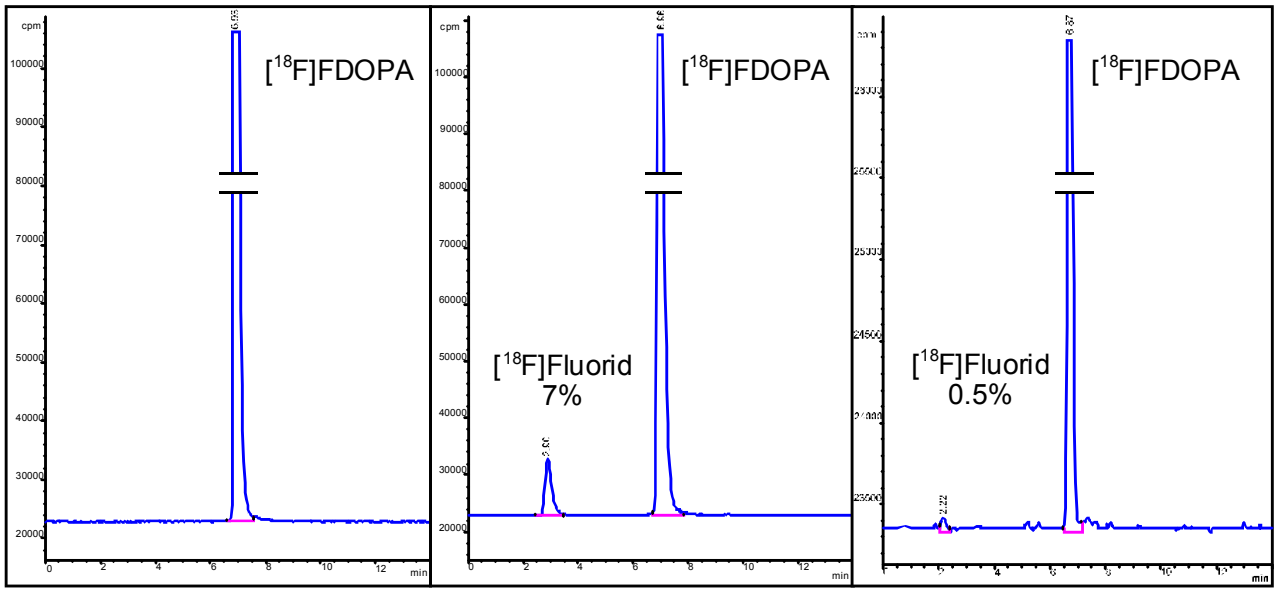

Fig. 2. HPLC chromatograms of the analytical separation of the final product

A - column: LiChrosorb RP-18, 7 µm, 250 x 4 mm, MERCK
- sample: product of semi-preparative HPLC purification, using silica-gel-based RP-18 material (see Fig. 1 A)

B - column: PRP-1, 150 x 4 mm, 5 µm, Hamilton,
- sample: product of semi-preparative HPLC purification, using silica-gel-based RP-18 material (see Fig. 1 A)

C - column: PRP-1, 150 x 4 mm, 5 µm, Hamilton,
- sample: product of semi-preparative HPLC purification, using polymer-based RP-18 material (see Fig. 1 B)

general

- sample volume: 10 µl,
- eluent: A: 70 mM KH_2PO_4, 1.5 mM octan-1-sulphonic acid sodium salt, 0.1 mM EDTA pH 3.40, adjustment with 1 M H_3PO_4
  B: acetonitrile : eluent A = 2 : 1
- gradient: linear, 0 – 100 % B (10 min)
- flow rate: 1 ml/min
- detection: radioactivity.

As the exact sample recovery is difficult to determine for column chromatography, we tried to use the TLC method for the quantification of the radiochemical purity. Fig. 3 shows the TLC chromatograms obtained from the final product, using a silica gel and a polymer-based RP column for semi-preparative purification. The TLC analysis was performed on RP-18 glass plates (5 x 10 cm, F_{254S}, MERCK). The chromatographic development was carried out in a chamber filled with 0.1 M acetic acid / ethanol (95 : 5). For visualisation the dried TLC plates were contacted with an imaging plate (IP-BAS-III, 20 x 25 cm, FUJI). The distribution of radioactivity on the TLC plate was recorded by an imaging analyser (BAS2000, FUJI).

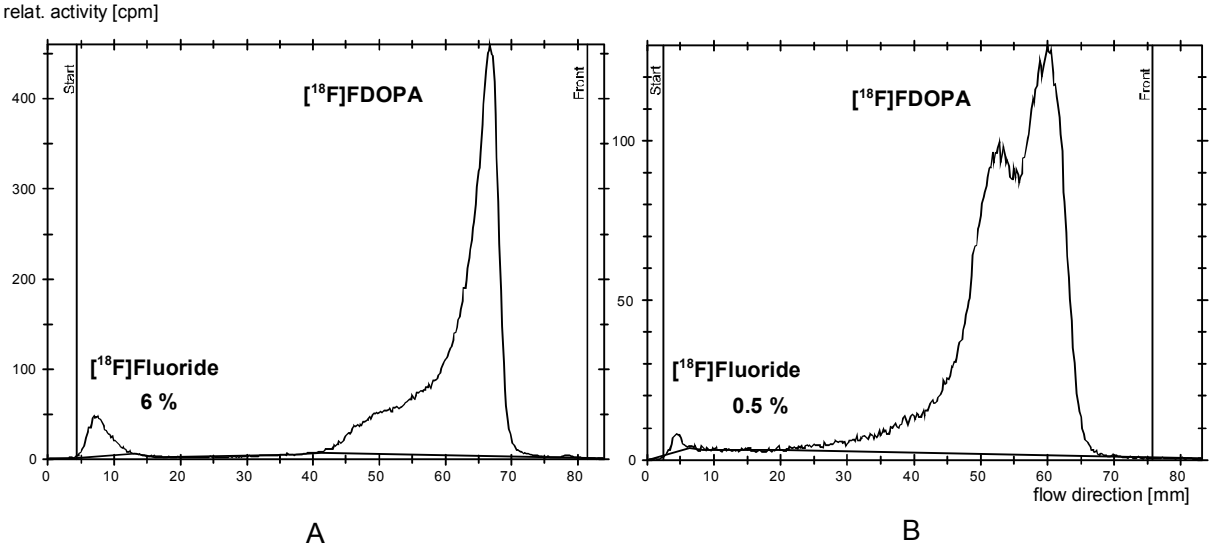

Fig 3. TLC chromatograms of the final product fraction as shown in Fig. 1. A: sample using silica-gel-based RP-18 material, B: sample using polymer-based RP-18 material.

Results and Discussion

During the purification of the crude product by semi-preparative HPLC the main radioactive peak ([^{18}F]FDOPA) is eluted after about A –11 minutes or B – 15 minutes. As shown in Fig. 1 A, the [^{18}F]FDOPA peak is eluted on the tailing of the [^{18}F]F-fluoride peak, using silica-based RP material. This is due to the anion exchange properties of the free OH groups of silica gel. Silica gel is the supporting material of the reversed phase stationary phase used.
Analysing a sample of this fraction by means of the frequently used reversed phase chromatography with C-18 as the stationary phase on the base of silica gel (see Fig. 2 A), we did not detect any radiochemical impurities. If a polymer-based RP column is used, approximately 7 % of [^{18}F]fluoride are detected in the same sample. The reason for this difference are again the anion exchange properties of the silica-gel supporting material. Accordingly, the small amount of fluoride is completely retained on the silica-based RP column, while on the inert polymer supporting material fluoride is not absorbed and therefore eluted with the death volume of the column (see Fig. 2 B).
This fact is supported by the results of a TLC analysis. Fig. 3 A also shows that about 6 % of [^{18}F]fluoride are included in sample 1 A. Unfortunately, we did not find a suitable method for the separation of catecholamines. As is well known, during the TLC runs catecholamines are very sensitive to oxidation. [^{18}F]FDOPA is therefore partially decomposed and shows a double peak. Nevertheless, TLC is an absolute analysing method without any problems in relation to the recovery of the sample. The separation into fluoride and FDOPA is sufficient for fluoride quantification.

The disadvantages of an incomplete fluoride isolation from the final product that are associated with the use of silica-based RP materials in the [^{18}F]FDOPA preparation can be overcome by using a polymer-based RP column (PRP-1 column) for this purpose. In this case the [^{18}F]FDOPA -containing peak is eluted after about 15 minutes in a high radiochemical purity. Analysing the obtained fraction by HPLC with the PRP-1 column less than 0.5 % [^{18}F]fluoride was found in the chromatogram (see Fig. 2 C). The same result was observed by TLC analysis. Fig. 3 B shows that only about 0.5 % [^{18}F]fluoride is present in the sample.

To sum up, it can be pointed out that by replacing the silica-gel-based HPLC column by a polymer-based one for semi-preparative separation of [^{18}F]FDOPA from the reaction mixture, the radiochemical purity of the final product can be increased up to > 99 %.
For the determination of the radiochemical purity by HPLC, polymer-based RP material gives more correct results. The radio TLC analysis as an absolute method for the determination of radiochemical purity would be the best analysing method.
However, we have to improve the stability of [^{18}F]FDOPA during the analysing run so that it shows only a single peak.

References

[1] Meyer, G.-J.; Waters, S.L.; Coenen, H.H. PET radiopharmaceuticals in Europe: current use and data relevant for the formulation of summaries of product characteristics (SPCs). Eur. J. Nucl. Med. 22 (1995) 1420-1432.

[2] http://www.fda.gov/cder/regulatory/pet/728f18dopa.htm, November 2000.

[3] Füchtner, F.; Günther, K.; Steinbach, J.; Lücke, R.; Scholz, R.; Hüller, R. High yield preparation of 6-[^{18}F]fluoro-DOPA , *Annual Report 1996*, Institute of Bioinorganic and Radiopharmaceutical Chemistry, FZR-165, pp.153-156.

41. Separation of Radioactively Labelled Compounds by on-line Combination of SEC and HPLC

H. Wittrisch, R. Bergmann, C. Heichert

Introduction

For biotransformation investigations of *in vivo* and *in vitro* studies, radioactively labelled compounds provide one of the most important tools to completely track the metabolites in complex biological matrices, such as blood, urine, faeces, bile and *in vitro* samples. Chromatographic techniques such as high performance liquid chromatography (HPLC) and capillary electrophoresis (CE) are used for separation of the metabolites. Due to the high affinity of various substances such as plasma proteins to the column packing, a preparation of the biological material is often needed to obtain reproducible results and extend the lifetime of the columns. Especially solid–phase extraction (SPE) [1, 2], columns with special “restricted access” material (RAM) [3, 4] and several liquid extraction mixtures are used to separate the compounds of interest from the biological matrix. However, the recovery from these techniques is often poor and they are moreover time consuming.
Size exclusion chromatography (SEC), often referred to as gel permeation chromatography (GPC), is an entropically controlled separation technique in which molecules are separated on the basis of their hydrodynamic molecular volume or size [5, 6]. With proper column calibration a separation of the analyte and the most parts of the matrix can be readily achieved. Sample preparation using SEC has been reported for residue analysis of pesticides and herbicides in agricultural products [7, 8], fat-containing foods and biota samples [9], veterinary drugs in foodstuffs [10], metabolites of polychlorinated biphenyls, dibenzo-p-dioxins and dibenzofurans in microsomal assay extracts [11].
In this study, the removal of matrix components using an on-line SEC clean-up column in tandem with an analytical RP-18 column is demonstrated. A new configuration of two six-port valves was used to transfer only the compounds within a certain range of molecular weight to the analytical LC column for final separation. The metabolically stabilized pseudopeptide [$Arg^{8}\Psi(CH_2NH)Arg^{9}$] NT (8-13) was used to optimize the separation conditions.

Material and Methods

The HPLC system (HP1100, Agilent Technologies, Waldbronn, Germany) consists of an autosampler, two HPLC pumps, two six-port valves, a variable-wavelength UV detector and a radio-chromatography detector Flo-one-ßeta (Canberra-Packard, Dreieich, Germany). The instrumental setup is shown in Figure 1. Pump 1 delivers the buffer for SEC (column ZORBAX GF-250, 4.6 mmID x 250 mmL), while pump 2 delivers the buffer for the analytical column (ZORBAX 300SB-C18, 4.6 mmID x 50 mmL). Both columns were protected by a short (4.6 mmD x 12 mmL) precolumn filled with the appropriate packing. Typically, 5 - 150 µl of neurotensin standard solution or rat urine were injected, without any sample pre-treatment,. In most cases a phosphate buffer adjusted to pH 7 was used for SEC (Fig. 1A). When the analytes were eluted from the SEC column both six-port valves were switched by the software (HP ChemStation for LC) (Fig. 1B). During this step the RP column was loaded with the sample (“transfer step”). Then the first valve switched back and the compounds were separated, using the analytical column under gradient conditions at 40 °C (Fig. 1C). Solvent A consisted of water with 0.05 % trifluoro acetic acid (TFA), and solvent B of acetonitrile with 0.04 % TFA. For UV detection the wavelength of 214 nm was used.

Results and Discussion

SEC conditions
The buffer substance, the buffer concentration, the flow rate and the temperature were varied to reach the fastest possible separation in view of the limited lifetime of the ^{18}F labelled analytes. A stock solution of the stabilized NT (8-13) was used to optimize the SEC conditions.
At first 100 mM acetate and phosphate buffers were tested at pH 7 (Fig. 2). With the phosphate buffer (Fig. 2A) a shorter elution time of stabilized NT (8-13) as well as a better signal-to-noise ratio were observed. Phosphate buffers were therefore used in all further separations.
Next the concentration of the phosphate buffer was varied (Fig. 3). Due to the increased ionic strength shorter elution times and better peak shapes were obtained at higher buffer concentrations. With concentrations above 300 mM no further significant reduction in elution time was observed.
Flow rates between 0.5 ml/min and 2 ml/min and temperatures between 20 °C and 40 °C were applied. By varying the temperature the best results were observed at 40 °C. Because of a significant increase in back pressure at higher flow rates, especially during the transfer step, a flow of 1 ml/min

was used. Furthermore, 5 % acetonitrile was added to the buffer to minimize unspecific adsorption effects of matrix compounds.

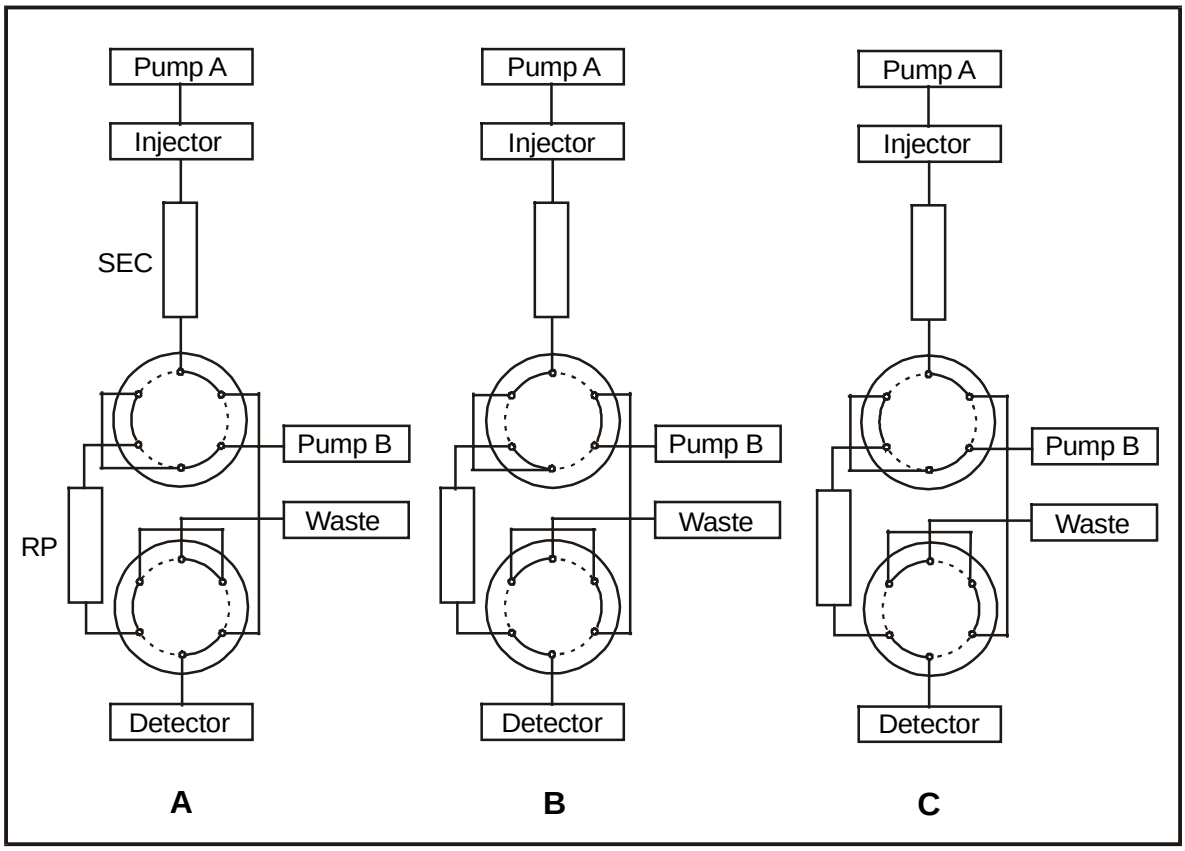

Fig. 1. Setup of the SEC-HPLC instrumentation

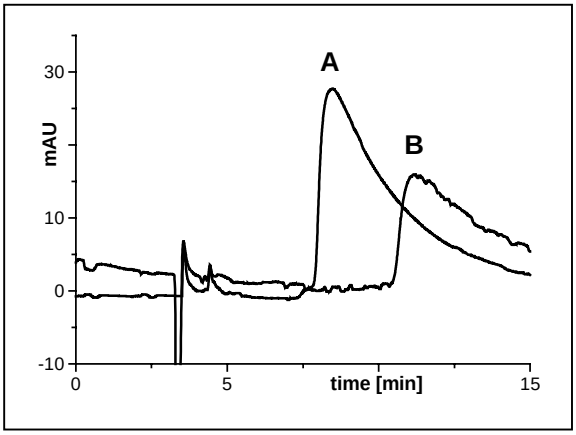

Fig. 2. SEC separation of NT(8-13) with a 100 mM phosphate buffer pH 7 (A) and a 100 mM acetate buffer pH 7 (B)

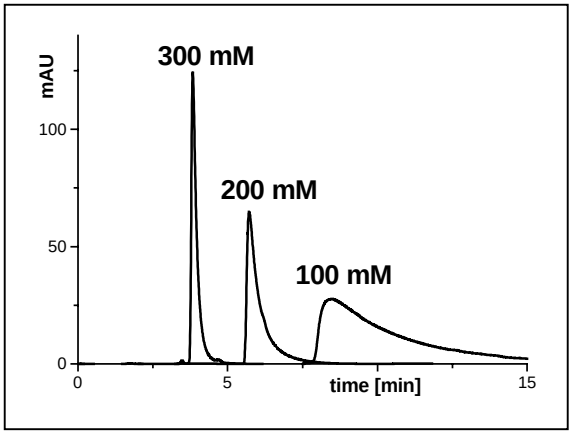

Fig. 3. SEC separation of NT(8-13) with different concentrated phosphate buffers

Transfer step
The time for switching the valves to transfer the analytes to the analytical column can be determined in various ways. One method is to use standard substances. The elution time observed in a separate run of the reference substance can be used for analysis of biological samples. However, wrong results could be obtained by this method, if the sample contains unknown metabolites with a big difference in molecular weight. In this case some metabolites are not transferred to the analytical column.

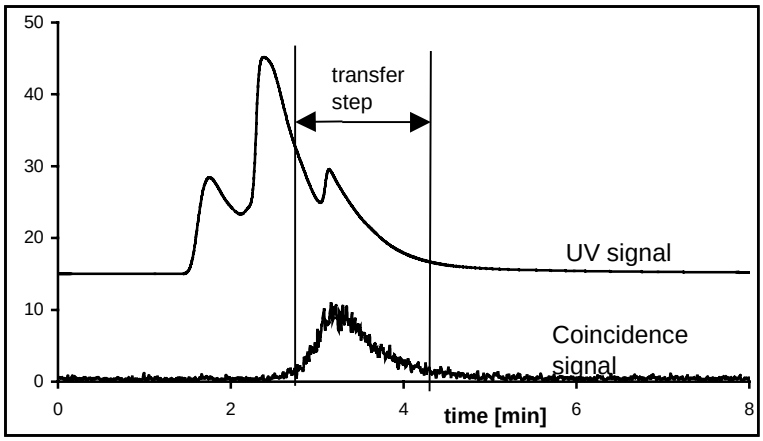

Fig. 4. SEC separation of [^{18}F]fluorbenzoyl labeled NT(8-13) and its metabolites in rat urine in 300 mM phosphate buffer with UV and coincidence detection

This problem is solved by using radioactively labelled substances. In this case the elution time of a compound and its metabolites is determined on-line with an X-ray detector. The SEC separation of rat urine containing [^{18}F]fluorobenzoyl-labelled NT (8-13) and its metabolites is shown in Fig. 4.

The UV signal shows that a large part of the biological matrix is flushed into the waste before the transfer step starts. With the coincidence signal it was observed, that the labelled NT(8-13) and its metabolites were eluted between 2.8 min and 4.3 min.

RP conditions
The analytical system was optimized for the separation of peptides. A special column packing (ZORBAX 300SB-C18) was therefore used. This material allows separation below pH 2. The separation of neurotensin derivatives was carried out with a varying acetonitrile / water gradient. Each of the solvents contained TFA in different concentrations. The gradient was varied, and so were the flow rate and the temperature. The best resolution was obtained with the conditions shown below:

eluent A:	water + 0.05 % TFA	
eluent B:	acetonitrile + 0.04 % TFA	
gradient:	0 – 8 min	5 % B
	8 – 12 min	from 5 % to 60 % B
	12 – 14 min	from 60 % to 80 % B
	14 – 15 min	80 % B
flow:	1 ml/min	
temperature:	40 °C	

Fig. 5 shows the separation of ^{18}FB[Arg$^{8}\Psi$(CH_2NH)Arg^{9}] NT (8-13) (compound A) and its metabolite ^{18}FB-Arg$^{8}\Psi$(CH_2NH)Arg^{9}Pro^{10} (compound B).

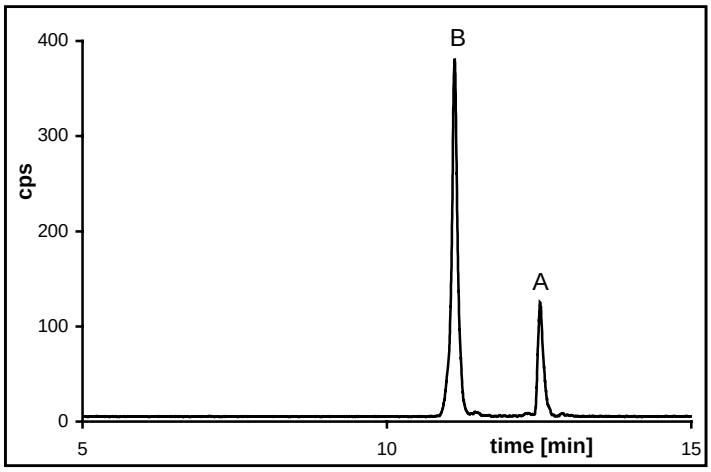

Fig. 5. Separation of the stabilized ^{18}FB-NT (8-13) (A) and its metabolite (B)

The results presented in this paper clearly demonstrate that the on-line combination of SEC and HPLC is a very useful tool for metabolism studies of radioactively labelled compounds. By using this method no further preparation of urine samples is necessary.

References

[1] Fleischer, C.T.; Boos, K.-S. Analyt-spezifische on-line Festphasenextraktion. GIT Spezial 20 (2000) 15-17.
[2] Papadoyannis, I.N. Determination of datura alkaloids by using chromatographic techniques: a review. Nat. Toxins 3 (1995) 310-316.
[3] Boos, K.-S.; Wilmers, B.; Schlimme, E.; Sauerbrey, R. On-line sample processing and analysis of diol compounds in biological fluids. J. Chromatogr. 456 (1998) 93-104.
[4] Boos, K.-S.; Wilmers, B.; Schlimme, E.; Sauerbrey, R. Development and performance of an automated analyzer for catecholamines. Chromatographia 24 (1987) 363-370.
[5] Barth, H.G.; Boyes, B.E.; Jackson, C. Size exclusion chromatography and related separation techniques. Anal. Chem. 70 (1998) 251R-278R.
[6] Barth, H.G.; Boyes, B.E.; Jackson, C. Size exclusion chromatography. Anal. Chem. 68 (1996) 445R-466R.
[7] Gelsomino, A.; Petrovicova, B.; Tiburtini, S.; Magnani, E.; Felici, M. Multiresidue analysis of pesticides in fruits and vegetables by gel permeation chromatography followed by gas chromatography with electron-capture and mass spectrometric detection. J. Chromoatogr. A 782 (1997) 105-122.
[8] Rimmer, D.A.; Johnson, P.D.; Brown, R.H. Determination of phenoxy acid herbicides in vegetation, utilising high-resolution gel permeation chromatographic clean-up and methylation with trimethylsilyldiazomethane prior to gas chromatographic analysis with mass-selective detection. J. Chromatogr. A 755 (1996) 245-250.
[9] Rimkus, G.G.; Rummler, M.; Nausch, I. Gel permeation chromatography-high performance liquid chromatography combination as an automated clean-up technique for the multiresidue analysis of fats. J. Chromatogr. A 737 (1996) 9-14.
[10] Biancotto, G.; Angeletti, R.; Piro, R.D.M. Detection of veterinary drugs in foodstuffs using gel permeation. Analyst (Cambridge, U. K.) 121 (1996) 229-232.
[11] Rozemeijer, M.J.C.; Green, N.; Jimenez, B.; Adrichem, M.A.; Olie, K.; de Voogt, P. Integrating gel permeation chromatography clean-up in the analysis of metabolites of polychlorinated biphenyls, dibenzo-p-dioxins and dibenzofurans extracted from a microsomal assay A comparison of different mobile phases. J. Chromatogr. A 755 (1996) 57-66.

42. Optimization of the Synthesis of [^{18}F]$FClO_3$

A. Jordanova, J. Steinbach

Introduction

The electrophilic introduction of no carrier added (n.c.a.) ^{18}F at electron rich sites of molecules as aromatic rings by electrophilic fluorinating agents is a challenging task. The development of appropriate techniques to fulfil this task is a prerequisite for labelling various compound of radiopharmaceutical interest.
Some carrier added (c.a.) electrophilic fluorinating agents [1, 2] were synthesised from readily accessible [^{18}F]F_2 precursor and used for labelling of biologically interesting compounds. Methods for synthesising n.c.a. electrophilic fluorinating agents from n.c.a. [^{18}F]fluoride have not been described so far in the literature.
Our method for 'Umpolung' of reactivity from the nucleophile [^{18}F]F^- to an electrophile ^{18}F-labelled fluorinating agent makes it possible to synthesise an n.c.a. ^{18}F-labelled electrophilic fluorinating agent. Previous studies [3] showed that [^{18}F]$FClO_3$ (perchloryl fluoride) could be synthesised starting from n.c.a. [^{18}F]fluoride. This is a one-pot procedure which combines two reactions. The reaction [4] results in the in-situ formation of [^{18}F]HSO_3F from n.c.a. [^{18}F]fluoride and oleum and [5] to the formation of [^{18}F]$FClO_3$ in the presence of $KClO_4$. The generation of perchloryl fluoride is confirmed by reactions with various compounds.
However, the radiochemical yield of obtained [^{18}F]$FClO_3$ is not at all satisfactory (0.5 % after 30 min) and not reproducible as the experimental conditions have not yet been optimised.
Based on the proposed formation of ClO_3^+ ions during the reaction of $KClO_4$ with an excess of HSO_3F [6] one can assume a reaction with HF forming $FClO_3$ as a mixed anhydride of HF and $HClO_4$. Hance the synthesis of [^{18}F]$FClO_3$ should be possible directly from n.c.a. [^{18}F]HF and anhydrous $HClO_4$.

Experimental

Reaction of n.c.a.[^{18}F]HF with anhydrous $HClO_4$ as one - pot procedure
Cold oleum (H_2SO_4, 65 % SO_3) was added to the cooled aquatic n.c.a. [^{18}F]HF. After $HClO_4$ (70 %) was distilled over P_4O_{10} and introduced into the vial with n.c.a. [^{18}F]HF and oleum. The reaction mixture was reacted within 30 min at RT. The formed [^{18}F]$FClO_3$ was not isolated and was led out by means of a nitrogen stream from the reaction mixture to the second reaction vessel containing the tracer substance and directly applied for the labelling reaction.

Reaction of [^{18}F]$FClO_3$ with the tracer substances
[^{18}F]$FClO_3$ was passed within 30 min through a cooled solution of phenyllithium in THF/diethylether or a solution of sodium malonic acid diethyl ester in THF. After stopping the reaction, an aliquot was taken from the reaction mixture and was analysed by radioluminiscence thin-layer chromatography (BAS2000, Fuji, Silicagel F_{254}, as a mobile phase - petroleum ether:diethyl ether = 9:1 for fluorobenzene and diethyl ether:petroleum ether = 2:1 for fluoromalonic acid diethyl ester). The presence of the ^{18}F-labelled products was proved by comparison with nonradioactive reference substances.

Results and Discussion

Using the described optimised synthetic procedure, [^{18}F]$FClO_3$ was prepared in yields corrected for decay ranging from approximately 3 to 6 %. [^{18}F]$FClO_3$ was not isolated. The radiochemical yield was estimated from the fluorinated radiotracer in the labelling reactions and based on the starting activity level of the n.c.a.[^{18}F]HF. Fig.1 shows radioluminescence thin–layer chromatograms of the products of the reaction of [^{18}F]$FClO_3$ with phenyllithium (a) and of the reaction of [^{18}F]$FClO_3$ with sodium malonic acid diethylester. In both cases the crude reaction mixture was analysed without any techniques for separation and purification of the final labelled product.
Phenyllithium was chosen in this reaction not only as a tracer substance for proving the synthesis of [^{18}F]$FClO_3$ by this method, but as a model compound of an unfunctionalized aryllithium for demonstrating the ability of [^{18}F]$FClO_3$ to label aromatic compounds. By this labelling procedure [^{18}F]fluorobenzene was prepared within 30 min in radiochemical yields of up to 6.4 % corrected for decay and based on the starting radioactivity of n.c.a. [^{18}F]HF. The share of [^{18}F]fluorobenzene (related to activity level at the beginning of synthesis) in the reaction mixture was 36 % as shown by the chromatogram (Fig. 1 (a)).

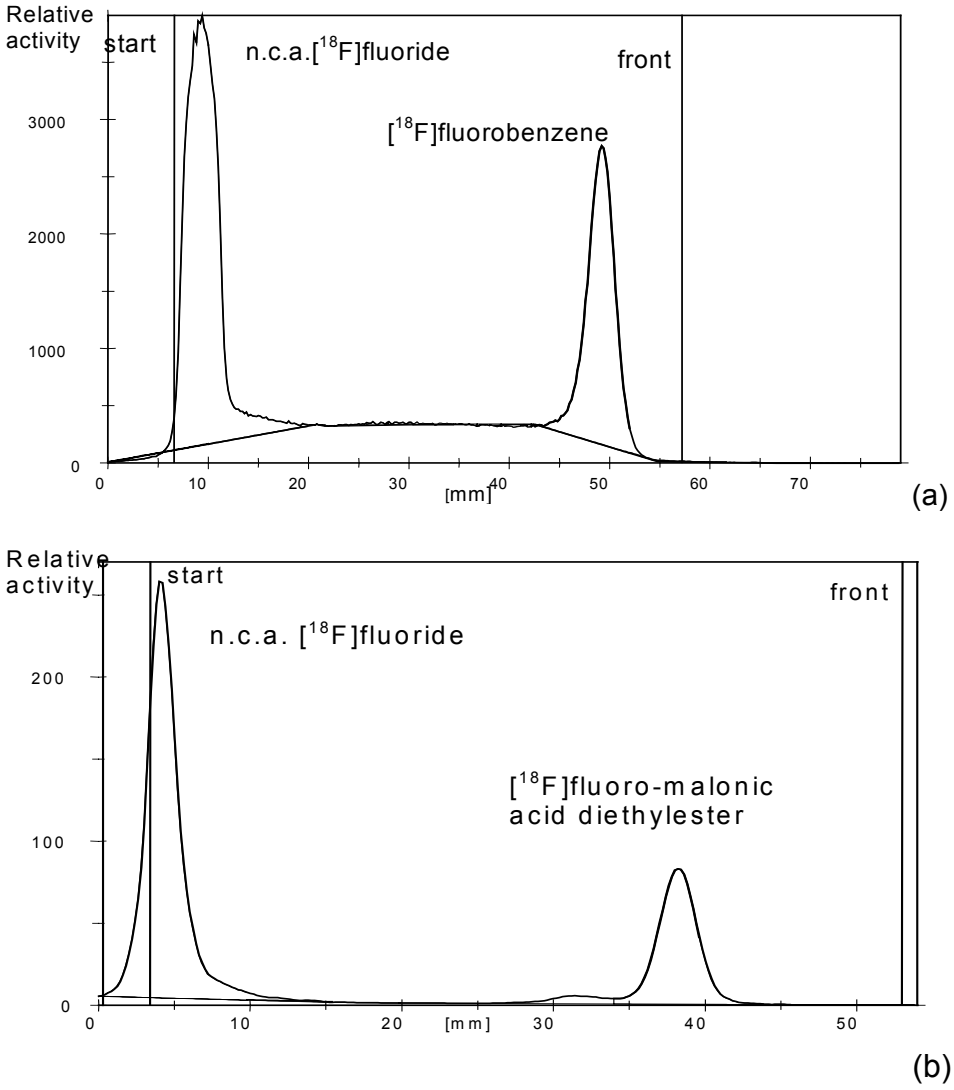

Fig. 1. Radioluminescence thin-layer chromatograms of the reaction mixture containing [^{18}F]fluorobenzene (a) and [^{18}F]fluoromalonic acid diethyl ester (b).

Nevertheless, a much better but still modest yield was achieved by this approach in the synthesis of [^{18}F]$FClO_3$ as well as of fluorinated products. The optimization took place on the basis of an alternative reaction pathway. The results obtained imply and provide a promising route for preparation of ^{18}F-labelled aromatics with potential biological function and interest.

References

[1] Lerman, Or.; Tor, Y.; Hebel, D.; Rozen, Shl. A novel electrophilic fluorination of activated aromatic rings using acetyl hypofluorite, suitable also for introducing ^{18}F into benzene nuclei. J. Org. Chem. 49 (1984) 806-813.

[2] Ehrenkaufer, R.; Robert, MacGr. Synthesis of [^{18}F]perchloryl fluoride and its reactions with functionalized aryl lithium. Int. J. Appl. Radiat. Isot. 34 (1983) 613-615.

[3] Fischer, Chr. Umpolung von nukleophilem n.c.a. [^{18}F]Fluorid zu elektrophilem n.c.a. [^{18}F]$FClO_3$ mit hoher spezifischer Aktivität. *Thesis*, TU Dresden (1998).

[4] Traube, W. Über Fluorsulfonsäure und ihre Salze. Chem. Ber. 46 (1913) 2525-2530.

[5] Barth-Wehrenalp, G. A new method for producing perchloryl fluoride ($FClO_3$). J. Inorg. Nucl. Chem. 2 (1956) 266.

[6] Woolf A.A. The intermediate in the preparation of perchloryl fluoride. J. Inorg. Nucl. Chem. 3 (1956) 250.

43. Quality Assurance in Manufacturing Radiopharmaceuticals for Positron Emission Tomography (PET)

K. Smolinka, R. Syhre, F. Füchtner, J. Steinbach

Introduction

The PharmPlantReg (Pharmaceutical Manufacturing Plant Regulations) [1] oblige all holders of a Manufacturing Authorization to follow the principles of Good Manufacturing Practice (GMP) expressed in the European Economic Community Guide to Good Manufacturing Practice for Medicinal Products (EEC GMP Guide) [2]. This guide calls for a functioning pharmaceutical quality assurance system (quality management system, QMS). The QMS should ensure that products are consistently produced and controlled to the quality standards appropriate to their intended use. It is a wide ranging concept which covers all matters which individually or collectively influence the quality of a product. It is therefore concerned with both production and quality control.

Activities in the Rossendorf PET Centre

The Rossendorf PET Centre has held a Manufacturing Authorization since 1997. Since then the facility has been continually developed. In particular the necessary staff are involved guaranteeing routine production. There are, for example, directors of production and quality control and the quality assurance manager. Many quality assurance activities have been carried out last year.
At the end of 1999 a quality assurance circle was established. The circle consists of members of the executive board of the Research Centre Rossendorf Inc. and of representatives of various areas (production, quality control, research). It meets once or twice a year to coordinate important future actions and to discuss fundamental questions. Evaluating this year´s inspection by the authority, the quality assurance circle decided to install a more effective changing zone (airlock) and to develop a quality manual. The latter should contain the complete standards of quality assurance in production, quality control, personnel, documentation and research based on the EEC GMP Guide and the ISO 9000 series.

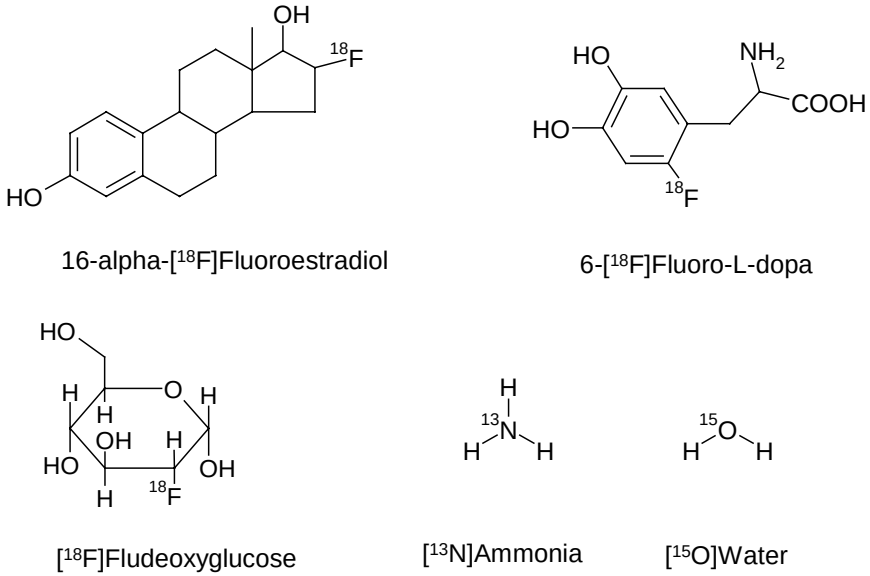

Fig. 1. Radiopharmaceuticals for Positron Emission Tomography (drug products) currently produced at the Rossendorf PET Centre

Five radioactive drug products are at present routinely produced at the Rossendorf PET Centre for medical research and routine diagnostic (see Fig. 1). This year, the 16α-[^{18}F]fluoroestradiol injection and the [^{13}N] ammonia injection were fully validated. This means that all analytical methods used in routine quality control were validated, at least three or more lots produced and the drug products subjected to extensive quality control.

The manufacturing of 16α-[^{18}F]fluoroestradiol injection was validated with three batches. We determined the radiochemical, radionuclidic and chemical purity, the bacterial endotoxin value before and after sterile filtration, the pH value, the sterility and the bioburden before sterile filtration, usually in double determinations. Additionally the content of heavy metals was quantified by ICP-MS and the radionuclidic impurities of the [^{18}O]water target were identified. The specifications were fully met. 16α-[^{18}F]fluoroestradiol injection is used in a clinical study for imaging breast cancer.
We produced seven batches for validation of the manufacturing of [^{13}N]ammonia injection. We determined the radiochemical purity by cation and anion exchange chromatography, the radionuclidic and chemical purity, the radionuclidic impurities before purification, the bacterial endotoxin value before and after sterile filtration, the pH value, the osmolality, the sterility and the bioburden before sterile filtration, usually in double determinations. One batch was produced for quantification of the aluminium specified in the monograph (draft) [3] of the European Pharmacopoeia and of heavy metals. The specifications were fully met. The [^{13}N]ammonia injection is used for imaging myocardial perfusion.
Future QMS activities will include validation of the manufacture of further drug products for PET, work on the quality manual and a thorough revision of the documentation.

References

[1] PharmPlantReg: Betriebsverordnung für Pharmazeutische Unternehmer (PharmBetrV), March 1985, last revision July 1998.
[2] European Economic Community Guide to Good Manufacturing Practice for Medicinal Products: EEC document III/2244/8, Rev. 3, January 1989.
[3] Draft Monograph: Ammonia (^{13}N) Injection, Pharmeuropa 10 (1998) 206–208.

44. Operation of the Rossendorf PET Cyclotron "CYCLONE 18/9" in 2000

St. Preusche, J. Steinbach

Routine operation

Our radionuclides produced in routine operation are $[^{18}F]F^-$, $[^{18}F]F_2$ and ^{11}C, which are used in the synthesis of different radiotracers, radiopharmaceuticals and for various experimental purposes. The routine production of ^{13}N was introduced in the fourth quarter of 2000. In the same period the radionuclide ^{15}O was made available as prerequisite for $[^{15}O]H_2O$.
The daily operating time of the CYCLONE 18/9 varies between two and four hours.
At the end of September we received an extended licence for routine operation from our authority. Now we are able to
increase the maximum target activity produced by the ^{18}F water target and the ^{11}C gas target
increase the maximum activity produced per year by the ^{13}N water target
We are subject to fewer limitations in terms of runs per days and weeks for all our radionuclides in the confirmed annual schedule as well.

Table 1 gives an overview of the 2000 radionuclide production.
The radionuclide ^{13}N was produced to optimize the irradiation and extraction conditions and to introduce $[^{13}N]$ammonia as a standard radiopharmaceutical while ^{18}F and ^{11}C are in routine use for the daily radiotracer and radiopharmaceutical production and for research purposes.

Table 1. Radionuclide production in 2000

RN	Radionuclide production	
	Number of Irradiations	$SumA_{EOB}$ GBq
$[^{18}F]F^-$	359	15350
$[^{18}F]F_2$	119*)	771
^{11}C	37	624
^{13}N	51	237
^{15}O	29	233

*) including pre-irradiations

Fig. 1 shows the number of irradiations of our radionuclides and Fig. 2 the total amount of activity produced from 1997 to 2000.

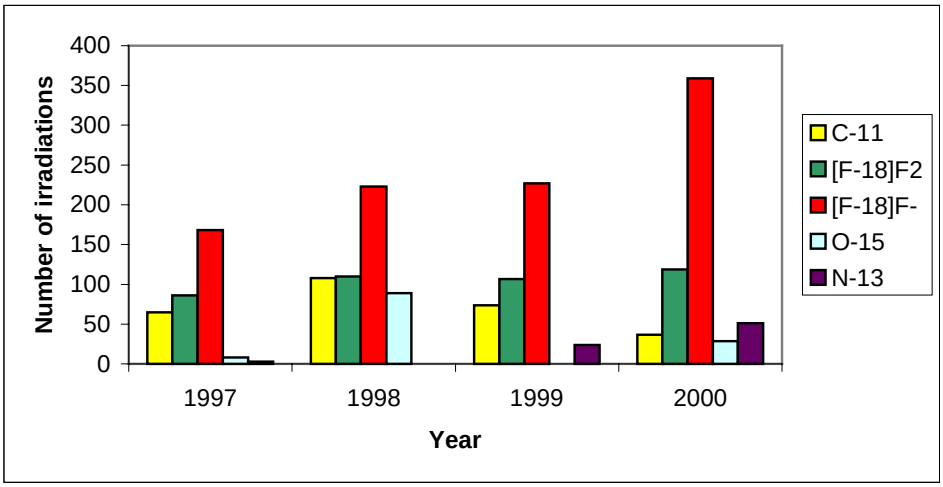

Fig. 1. Number of irradiations of radionuclides produced

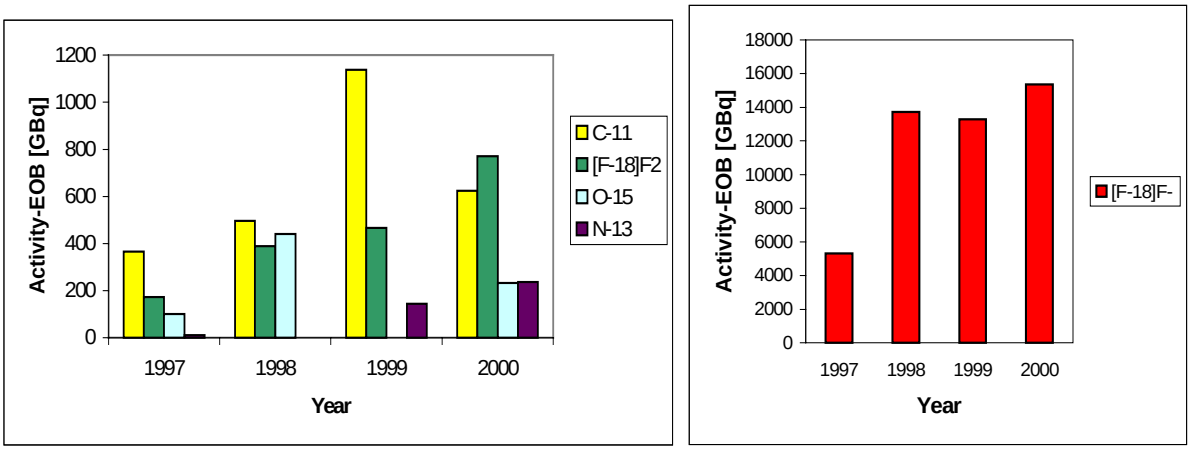

Fig. 2. Total amount of activity produced

Improvements at the cyclotron

- Modification of the ^{18}F water target loading procedure

The original IBA ^{18}F water target loading procedure with the syringe actuator system was designed for only one [^{18}O]H_2O grade. The request for ^{18}F to be utilized in the production of radiotracers and radiopharmaceuticals and for research purposes, varies strongly from day to day and from run to run. We therefore modified the ^{18}F water target loading procedure in the sense that it is now possible to fill the ^{18}F water target with [^{18}O]H_2O of two grades of enrichment. When there is only little demand for ^{18}F, recycled water of a low grade of enrichment can now be used. A modification of the IBA software was not necessary in our case [1].

- Modification of the PLC/PC hardware

The two seven-year-old PCs of our two control terminals were exchanged by IBA at the beginning of January for new ones with Windows NT as an operating system better adapted to the upgraded PLC system. The PCs received a new set-up and all communication tests between them and the PLC system were carried out successfully. Most of the cyclotron functions were tested with the new computers and found to be ready for routine operation.
In November the PLC central processor unit (CPU) as well as the communication processor (CP) were equipped by IBA with EPROMs instead of RAMs in order to solve finally the problem of data loss in case of failures in the CPU and CP boards [2].

Maintenance and service

Because of the great demand for radionuclides and the associated increases in operating time (Table 2) and also in wear of several cyclotron parts, the maintenance and service intervalls have become shorter. The cathodes of the ion sources and the puller electrodes have now to be replaced three times a year, the chimneys of the ion sources two to three times a year.

Table 2. Operation of the proton ion source for the production of ^{18}F

	1997	1998	1999	2000
Number of irradiations	168	223	227	359
Sum A_{EOB} / GBq	5307	13829	13300	15350
Ion beam on the target / h	108	197	204	283

According to Table 2 the operating time of the proton ion source increased in 2000 by about 40 per cent compared with 1999.

The main reasons for venting and opening the cyclotron were problems with the highly stressed proton ion source as well as maintenance and service work at both ion sources.
Unplanned turn-off periods:

Three days: - problems with the ventilation system (interlock signal) as a result of a destroyed heating system
- problems with the proton ion source.

The annual check of the CYCLONE 18/9 facility by the TÜV Sachsen organization (TÜV = Association for Technical Inspection) under § 76 of the German Radiation Protection Order took place in the middle of September. There were no objections to the further operation of the cyclotron.

Radiation protection

- Modification of the emission measurement system of radionuclides in the exhaust air

After the 41-year-old 120 cm cyclotron (U-120) was switched off at the end of 1999, the CYCLONE 18/9 is now the only emitter of radionuclides in the cyclotron building. The dose rate meter of the U-120 exhaust air tube was moved to the air tube of the hot cell 0 (cyclotron end terminal of the pneumatic transport system) of the CYCLONE 18/9 facility. If the emission of radionuclides exceeds the thresholds, the source of emission, i.e. the cyclotron or the loading process of the pneumatic rabbit, can now be identified as the responsible party.
Furthermore the monitoring system is now located in the control room of the CYCLONE 18/9.

- Emission of radionuclides with the exhaust air

The emission of radionuclides with the exhaust air is monitored. As shown in Table 3 it is far below the limit. The annual limit of emission of radionuclides from the cyclotron building was reduced by a factor of 30 after switching off the old 120 cm cyclotron.

Table 3: Emission of radionuclides with the exhaust air in 2000 as a result of operation of the CYCLONE 18/9

Radionuclide	Emission [Bq/a]
^{41}Ar	1.2E10
^{18}F	1.5E10
^{13}N	1.0E08
Sum	2.7E10
Percentage of the Annual limit	13.6

- Exposure to radiation of the cyclotron staff

The cyclotron staff belong to category A of occupational exposed persons. The average exposure to radiation was 1.8 mSv in 1997, 2.9 mSv in 1998, 3.5 mSv in 1999 and 4.4 mSv in 2000 (Jan. to Sep.). This is due to more frequent maintenance and shorter service intervals.

References

[1] Preusche, St.; Ross, H. Modification of the ^{18}F water target loading procedure. *This report*, pp.
[2] Preusche, St.; Ross, H.; Krug, H. Installation of surge protective devices for the CYCLONE 18/9 PLC system. *Report July - December 1999*, Institute of Bioinorganic and Radiopharmaceutical Chemistry, FZR-283, p. 70.

45. Modification of the ^{18}F Water Target Loading Procedure

St. Preusche, H. Ross

Introduction

The steep increase in the prices of enriched $[^{18}O]H_2O$ requires this target material to be used repeatedly as the basis of ^{18}F production. Unfortunately, after each cycle of irradiation and separation of ^{18}F the target water has to be refind, which results in decrease of enrichment. As the grade of enrichment linearly determines the ^{18}F yield, target water of various grades of enrichmnet has to be used as required. This requires separate equipment and procedures for handling of various $[^{18}O]H_2O$ grades.
The original IBA ^{18}F water target loading procedure with the syringe actuator system was designed for only one $[^{18}O]H_2O$ grade. The demand for ^{18}F to be used in the production of radiopharmaceuticals and for research purposes varies strongly from day to day and from run to run in our PET Center. We therefore modified the ^{18}F water target loading procedure in the sense that it is now possible to fill the ^{18}F water target with $[^{18}O]H_2O$ of two different grades of enrichment. For a low ^{18}F activity level, recycled enriched water is now available. A manually driven syringe system is used as a first step of modification and for getting experience. As we had no access to the programs of the control system, the modification was carried out without changing the IBA software.

Status before modification

The principle of the water target loading procedure is shown in Fig. 1. In the PLC controlled IBA water target loading procedure the target is filled by four strokes of a syringe actuator system within two minutes. One stroke consists of 15 seconds syringe loading and 15 seconds target loading. The $[^{18}O]H_2O$ is transferred into the target via a Rheodyne valve.

Solution
We installed:
A 24 V 3-way valve in the filling tube (see Fig. 1, dotted line), very close to the Rheodyne valve. The 3-way valve is normally open to the IBA syringe actuator system. It is operated by a push button to use our modification.
A switch in the + 24 V power line of the syringe actuator system (see Fig. 1, dotted line) for switching off the system.
A water supply vial with the recycled enriched water and a syringe with a manually driven 3-way valve.

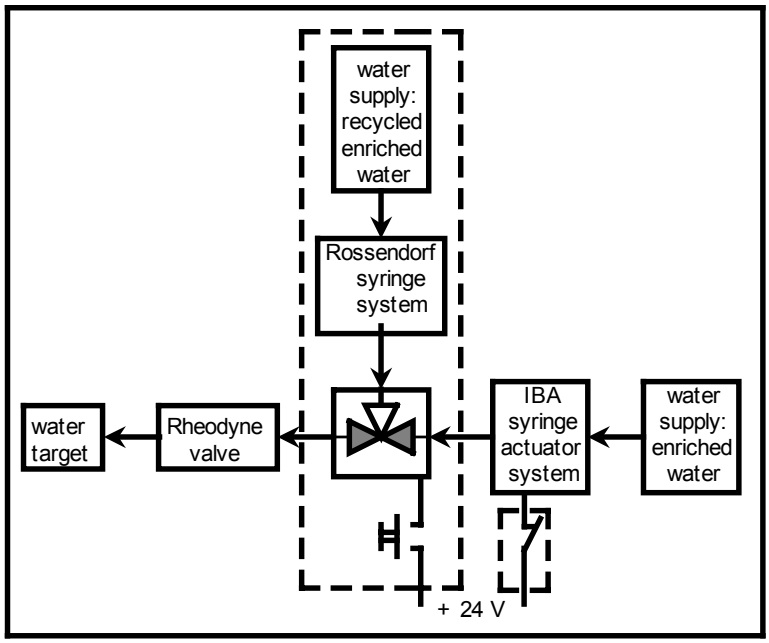

Fig. 1. Principle of the ^{18}F water target loading (dotted lines: our modification)

Course of a cycle
For using recycled enriched water, the 24 V power supply of the IBA syringe actuator system is first switched off. Our syringe is then manually loaded with 1.4 ml of recycled enriched water and the manually driven 3-way valve is turned towards the target filling tube. Now the IBA water target loading procedure can be started at the control terminal. In the two minutes when the Rheodyne valve is in the "target filling position" and the IBA syringe actuator system would normally work, the enriched water is filled into the target by switching the 3-way valve with the push button and acting our syringe. After two minutes the Rheodyne valve returned automatically to the "target irradiation position" and the water target loading procedure is finished. The 24 V power supply is again switched to the IBA syringe actuator system. The target is ready for irradiation.

Conclusion

The modified ^{18}F water target loading procedure has worked without any problems for half a year now. By this method it is possible to save the expensive enriched water (> 94 %) when there is only little demand for ^{18}F activity. Based on our experience with the manually driven syringe system we are planning to install a second IBA syringe actuator system.

46. Measurement of Recovery Coefficients for HR+ and their Application in a Correction Method

H. Linemann, E. Will, B. Beuthien-Baumann, H. Kutzner

Introduction

The concentration of the activity of small lesions is underestimated in PET measurements. Sphere phantom measurements show such underestimations for object sizes of up to four times the resolution of the PET camera (measured in FWHM) [1]. The resolution is determined by the camera characteristics and also by the reconstruction algorithm and by the filter conditions used. These deviations have to be corrected for quantitative evaluation. This is possible for simple shaped lesions, if their size and the spatial resolution in the reconstructed image are known and appropriate phantom measurements are available. From the PET image the lesion size can be approximately determined by the width of the profile.
The aim of the study was to determine the resolution as well as the hot spot recovery coefficients (HSRC) for small spheres by phantom measurements and to investigate whether it is possible to correct the underestimation, using the ratio of the two measured lesion values for reconstructions of clearly differing image resolution. The same conditions as for the patient measurements were used for the phantom reconstructions.

Materials and Methods

All measurements were carried out on an ECAT EXACT HR+ PET scanner with the software version V7.1 (Siemens, CTI) in the 2D mode. For measurement of the HSRC the IEC head phantom with the hollow spheres insert was used. These 6 spheres have inside diameters from 9.6 mm to 37.2 mm. Eight thin-walled glass spheres with inside diameters ranging from 5.0 mm to 8.6 mm were additionally examined. The phantom measurements were reconstructed by FBP (Ramp/0.5; Hann/0.5; Hann/0.4; Hann/0.3) and OSEM (iterations/subsets from 1/24 to 8/24).
The transverse resolution was measured with three line sources (inside diameters: 1.0 mm) in water. The average radial and tangential values were calculated.
The scatter correction was checked in accordance with the NEMA standard.
The HSRC were calculated from the activity in a ROI with a diameter equal to FWHM for each reconstruction. The measured activity of the largest sphere (37.2 mm) reconstructed by FBP (ramp/0.5) was used as the reference value. In each case the ROI was set into the slice (plane) with the highest value.
The patient measurements were analysed by calculating the image contrast (IC) of the lesion:

IC = (measured concentration of lesion - concentration of background) / concentration of background

Results

The transverse resolution is shown in Fig. 1 for an axial distance of up to 11.5 cm. The rise in FWHM with increasing axial distance is exclusively caused by the radial component.

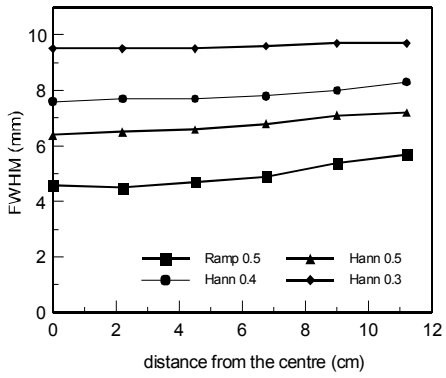

Fig. 1a. Resolution (FBP)

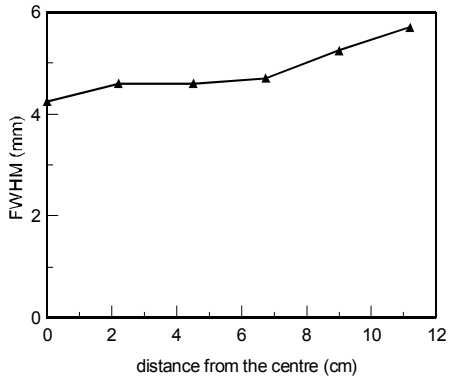

Fig. 1b. Resolution (OSEM 1/24)

Although scatter correction was applied, a scatter value of 5.3 % was observed in the case of FBP (without scatter correction 12.6 %). With OSEM a value of 6 % scatter is only achieved with a sufficiently large product of iteration and subset numbers (e.g. 8/24). In the case of OSEM (1/24) a "scatter" value of 16 % was obtained.
The HSRC measured for various reconstruction conditions (OSEM and FBP) are summarized in Fig. 2. By plotting the HSRC values against the diameter of the spheres (in FWHM of the reconstruction in question), all values are made to fit a common curve.

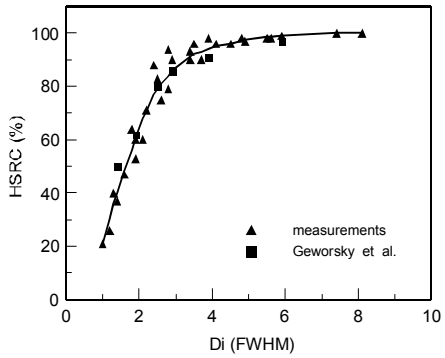

Fig. 2a. Hot spot recovery coefficients. Measurements with the 6 spheres of the EEC phantom (Di = 9.6...37.2 mm)

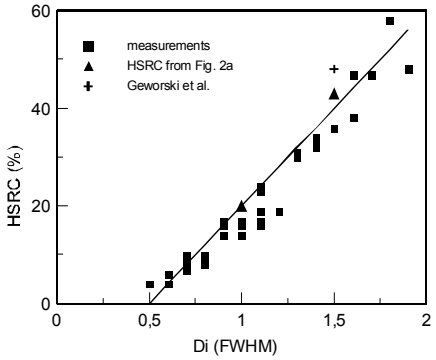

Fig. 2b. Hot spot recovery coefficients. Measurements with the 8 spheres of smaller diameter (Di = 5.0...8.6 mm)

The quotient of HSRC obtained from the reconstructions with OSEM 1/24 and FBP / Hann 0.4 over the sphere size is shown in Fig. 3. A significant change in the quotient is observed at sphere diameters smaller than approximately 15 mm.

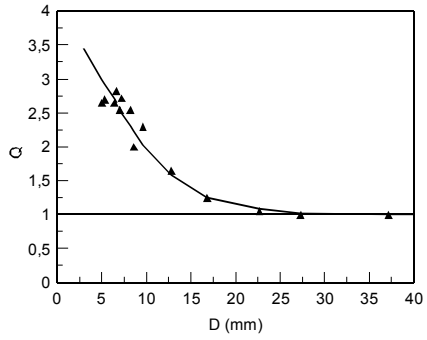

Fig. 3. Quotient Q calculated from HSRC(OSEM 1/24) divided by HSRC (FBP/Hann0.4) for all used spheres (distance from centre max. 7 cm)

Discussion

The HSRC dependence on the sphere size in units of resolution, as shown in Fig. 2, agrees with the values published by Geworski *et al.* [1].
The validity of the relationship CRC = HSRC
has to be presupposed to be able to use the dependence of the HSRC quotient, shown in Fig. 3 with various reconstruction conditions, for recovery correction in patient pictures. This condition is met if all influencing disturbances are completely corrected, except the recovery itself [1]. Under these conditions this method of recovery correction requires only the image contrast of the lesion to be determined. The filter conditions of the two reconstructions have to be so chosen that the resolutions of the images differ significantly. The combination of OSEM (1/24) and FBP (Hann/0.4) is only one example. Further investigations have to be carried out to show the limits of this method.
The recovery of a small structure for various reconstruction filters was used by Buchert *et al.* to distinguish between atrophy and reduced metabolism in brain studies [2].

Proposed procedure:

Prepare two images with different resolution of the same study.
Define ROIs with diameters corresponding to the FWHM into lesion [Rl] and surrounding background [Rb].
Image contrast = (Rl-Rb)/Rb for the same lesion in both images.
Q = image contrast(high resolution)/image contrast (low resolution) -> diameter of lesion (Fig. 3).
Convert the diameter of the lesion into FWHM (high resolution).
HSRC for lesion from calibration curve (Fig. 2).
Calculation of the object contrast OC = IC / HSRC, IC=IC (high resolution).

For application of the procedure to lesions on the periphery of the body, the dependence of the resolution on the axial distance has to be considered.

References

[1] Geworski, L.; Knoop, B.O.; Levi de Cabrejas, M.; *et al.*; Recovery correction for quantitation in emission tomography: a feasibility study. Eur. J. Nucl. Med. 27 (2000) 161-169.
[2] Buchert, R.; Väterlein, O.; Mester, J.; *et al.*, Differenzierung von Atrophie und reduzierter Traceraufnahme bei PET-Studien des Gehirns durch Ausnutzung des Recovery-Effects. Nuklearmedizin 38 (1999) A37.

TUMOUR AGENTS AND TUMOUR DIAGNOSIS

47. 3-*O*-Methyl-6-[^{18}F]Fluoro-L-DOPA – a Promising PET Tracer for Tumour Imaging. Autoradiographic Description of the Biodistribution in a Tumour-Bearing Nude Mouse and in the Rat Brain

M. Kretzschmar, P. Brust , F. Füchtner, J. Steinbach, B. Johannsen

Introduction

The synthesis of 3-*O*-methyl-6-[^{18}F]fluoro-L-3,4-dihydroxyphenylalanine (OMFD) was originally developed to correct human PET studies performed with 6-[^{18}F]fluoro-L-3,4-dihydroxyphenylalanine (FDOPA) for the transfer of this FDOPA metabolite into the brain. We recently found that there is a high accumulation of this amino acid in animal and human tumours [1 - 3]. Up to now the distribution of the compound in tumours and organs of animals was studied by dissection of rats and mice [3], a method which has a rather low spatial resolution. A whole-body autoradiography was therefore performed in this study in order to exactly match the image of the tracer distribution with the histological image of organs and tissues.
Previous [^{18}F]OMFD-PET studies of patients with glioblastoma multiforme showed an elevated tracer accumulation in the basal ganglia in addition to the tracer uptake in the brain tumour tissue [1, 4]. To be able to differentiate between the various substructures of the basal ganglia we studied the distribution of [^{18}F]OMFD in the rat brain by use of *ex-vivo* autoradiography.

Experimental

Whole-body autoradiography
A male nude mouse (weight: 39 g) bearing a FaDu human squamous cell carcinoma was intravenously injected with 1.75 MBq (20 GBq/µmol) [^{18}F]OMFD (dissolved in saline and 20 % ethanol). 60 min after injection the animal was sacrificed with ether, quickly frozen by immersion in an ethanol /dry-ice solution at – 70 ^{0} C and fixed in carboxymethyl cellulose gel on the microtome stage, using liquid nitrogen. The stage-mounted mouse was cut in a cryo-polycut microtome into 20 µm frontal sections which were attached to Tesa tape and dried by freeze drying (LGA 05, Janetzki, Leipzig) for 30 min. Thereafter the sections were apposed to standard imaging plates overnight. The plates were scanned in the bio-imaging analyser BAS 2000 (FUJI photo film Co,Tokyo) and the quantitative analysis of the in-vivo radioactivity distribution was performed with the AIDA software (Raytest, Straubenhardt).

Ex-vivo autoradiography
Two female Wistar rats (weight: 188 and 199 g) were intravenously injected with 18 – 19 MBq [^{18}F]OMFD (chemical dates see above). 2 hours later the animals were sacrificed as described above. The brains were quickly removed, immediately frozen by immersion in a 2-methylbutane / dry ice solution at –60 ^{0}C, weighed and measured in an automated γ counter (Capintec CRC-15-R) to determine their total radioactivity. Thereafter the stage–mounted brains were cut into 20 µm sagittal and horizontal sections, using a cryocut microtome. The sections were dried in a continous cold air stream for about 2 min. The autoradiographic technique was the same as described above.

Results and Discussion

Whole-body autoradiography
The in-vivo distribution of [^{18}F]OMFD was investigated in a male tumour-bearing nude mouse 60 min after i.v. injection to evaluate the tumour uptake of the tracer in relation to the other organs and tissues. The results of this whole-body autoradiographic study are shown in Fig. 1 and Table 1. Due to the rapid renal excretion of the tracer [3], we found the highest accumulation in the urinary bladder (50 % D/g). In addition to this, a high uptake was also found in the vital tumour (10 % D/g) and in the pancreas (10 % D/g). The skeletal muscles and the skin showed an intermediate uptake and the liver, digestive tract, lung and blood a very low uptake of [^{18}F]OMFD. The necrotic part within the tumour displayed only a small uptake (2.68 %D/g). The slightly greater accumulation of [^{18}F]OMFD in the muscles was also detected in rhesus monkeys [5] and rats [6]. In the nude mouse we obtained a high tumour uptake, good tumour to background ratios (tumour/liver and tumour/blood = 8, tumour/muscle = 4) and a low tracer retention in the body, which supports the use of [^{18}F]OMFD as a PET tracer for the visualization of various human tumour entities.

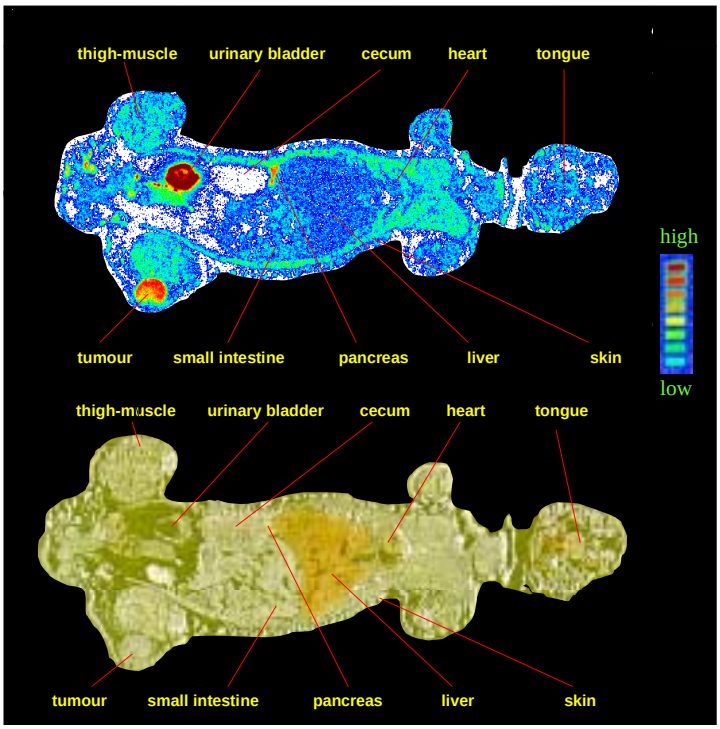

Fig. 1. Whole-body autoradiogram (above) in the frontal section level, radioactivity standard (right) and corresponding histological section (below) of a nude mouse bearing a human squamous cell carcinoma, 60 min after i.v. application of [^{18}F]OMFD.

Table 1. Uptake (%D/g) of [^{18}F]OMFD in a tumour-bearing nude mouse 60 min after i.v. application

Organ	[^{18}F]OMFD (%D/g)
Whole tumour	8.14 ± 1,29
Vital tumour	10.04 ± 1.36
Necrotic tumour	2.68 ± 0.88
Liver	1.24 ± 0.04
Skeletal muscle	2.64 ± 0.28
Skin	2.26 ± 0.50
Testicle	1.61 ± 0.08
Cecum	0.20 ± 0.05
Pancreas	10.55 ± 1.16
Small intestine	1.62 ± 0.17
Blood	1.20 ± 0.07
Lung	1.08 ± 0.15
Urinary bladder	50.69 ± 20.31
Bone	0.88 ± 0.09

Ex-vivo autoradiography

The [^{18}F]OMFD uptake in the brain was low (~0.15 % D/g) 2 hours after i.v. application. No selective accumulation was observed in most brain regions except in the nucleus accumbens (Fig. 2). The uptake in the nucleus accumbens was 0.25 % D/g tissue. A smaller uptake of between 0.17 and 0.19 %D/g tissue was found in the dorsal striatum, globus pallidus, subthalamic nucleus and substantia nigra. Similar values were also found in the cerebral cortex, thalamus and hippocampus. [^{18}F]OMFD is nearly stable metabolically in the brain of the rat. 92 % of the original compound was found in the brain 120 min after i.v. application [7]. We therefore expect that the higher ^{18}F uptake into the nucleus accumbens is caused by a regionally different tracer distribution rather than by differences in tracer metabolism. The volume of distribution of [^{18}F]OMFD was slightly higher also in the striatum of monkeys [5] and pigs [Füchtner *et al.*, in preparation] than in the other brain regions. However, the resolution of the PET images in these studies did not allow us to differentiate between the various nuclei.

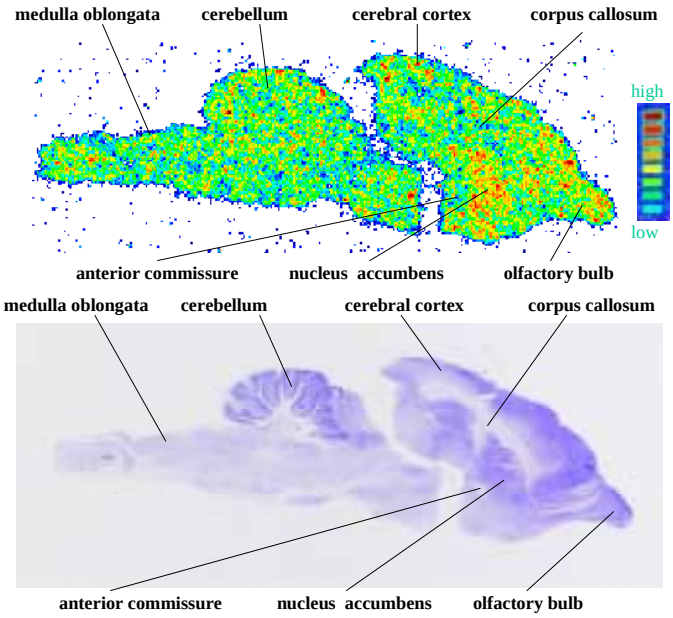

Fig. 2. In-vitro autoradiogram (above), radioactivity standard and corresponding histological image (below) of a sagittal brain section of the rat 2 hours after i.v. application of [^{18}F]OMFD.

To sum up, we found a low, rather homogeneous uptake of [^{18}F]OMFD in the rat brain. In keeping with studies performed on other species, a slightly higher uptake was found in the nuclei of the basal telencephalon [1, 4, 5]. In addition, we showed that this selective accumulation of [^{18}F]OMFD occurs only in the ventral extension of the striatum, the nucleus accumbens. This knowledge may contribute to the diagnostic accuracy of [^{18}F]OMFD PET studies in patients with intracerebral tumours.

References

[1] Alheit,H.; Bergmann,R.; Beuthien-Baumann,B.;Bredow, J.; Burchert, W.; Franke, W.G:; Füchtner, F.; Steinbach, J.; Syhre, R.; Zips,D. 3-*O*-methyl-6-[^{18}F]fluoro-L-DOPA ([^{18}F] OMFD) :development and first application of a new tracer for tumor detection with PET. J. Nucl. Med. 41 (2000) Supplement 43 P.

[2] Füchtner, F.; Steinbach, J.; Vorwieger, G.; Bergmann, R.; Syhre, R.; Brust, P.; Beuthien-Baumann, B.; Burchert, W.; Zips, D.; Baumann, M.; Johannsen, B. 3-O-methyl-6-[^{18}F]fluoro-L-DOPA – a promising substance for tumour imaging. J. Labelled Compd. Radiopharm. 42 (1999) Suppl.1, S267- S268.

[3] Syhre, R.; Brust, P.; Zips, D.; Füchtner, F.; Steinbach, J.; Johannsen, B. Distribution behaviour of 3-*O*-methyl-6-[^{18}F]fluoro-L-3,4-dihydroxyphenylalanine in Wistar rats, normal mice and tumour bearing nude mice. *Report July – December 1999*, Institute of Bioinorganic and Radiopharmaceutical Chemistry , FZR 283 pp. 1–11.

[4] Wahl, L.; Chirakal, R.; Firnau, G.; Garnett, E.S.; Nahmias, C. The distribution and kinetics of [^{18}F]6-fluoro-3-O-methyl-L-dopa in the human brain. J. Cereb. Blood Flow Metab. 14 (1994) 664–670.

[5] Doudet, D.J.; McLellan, C.A.; Carson, R.; Adams, H.R.; Miyake, H.; Aigner, T.G.; Finn, R.T.; Cohen; R.M. Distribution and kinetics of 3-O-methyl-6-[^{18}F]fluoro-L-dopa in the rhesus monkey brain. J. Cereb. Blood Flow Metab. 11 (1991) 726–734.

[6] Rose, S.; Jenner, P.; Marsden, C.D. The effect of carbidopa on plasma and muscle levels of L-DOPA, dopamine, and their metabolites following L-DOPA administration to rats. Movement Disord 3 (1988) 117–125.

[7] Vorwieger, G.; Bergmann, R.; Syhre, R.; Füchtner, F.; Steinbach, J.; Brust, P.; Johannsen, B. Metabolism of 6-[^{18}F]fluoro-3-*O*-methyl-L-3,4-dihydroxyphenylalanine in the rat. *Report January 1998 – June 1999*, Institute of Bioinorganic and Radiopharmaceutical Chemistry, FZR 270, pp. 13–16.

48. In-Vitro Evaluation of [^{18}F]FHPG and [$^{124/125}$I]FIAU for their Potential of Monitoring Gene Therapy

A. Friedrich, M. Scheunemann, R. Haubner[1], O.N. Koufaki[2], S. Noll, R. Bergmann, H. Stephan, B. Noll, N. Avril[1], P. Brust, B. Johannsen
[1]Department of Nuclear Medicine, Technische Universität München
[2]Department of Surgical Research, Technische Universität Dresden

Introduction

Gene therapy delivering genes into humans is a promising new approach to the treatment of cancer and other diseases [1] which has advanced from the experimental stage to the first successful clinical applications [2]. The transfer of the herpes simplex virus thymidine kinase (HSV-tk) gene was successfully employed in a variety of tumour models *in vitro* and *in vivo* [3 - 5]. It is based on the idea to use the selective expression of this gene in tumour cells for their destruction (suicide approach). Phase I/II clinical trials for brain, breast, colon and other tumours are currently being performed, but convincing positive results of the suicide gene therapy approach have not yet been reported.
Cancer gene therapy includes gene delivery to the tumour cells and the cellular expression of the specific transferred gene. But it is not yet known whether this gene is strongly enough expressed in the target tissue and how long the expression takes. To overcome this lack of information and to assess the distribution and duration of gene expression, strategies for monitoring the gene transfer by positron emission tomography (PET) have been developed [6, 7].
Two main categories of substrates for the HSV-TK, uracil nucleoside and acycloguanosine derivatives, have recently been investigated as reporter probes for imaging HSV-tk reporter gene expression [7]. The best compounds investigated for those two categories are [^{124}I]FIAU (5-iodo 2´-fluoro-2´-deoxy-1-ß-D-arabinofuranosyluracil) [8] and 9-[(3-[^{18}F]fluoro-1-hydroxy-2-propoxy)methyl]guanine (FHPG) [9, 10]. It is still an open question which lead structure is the most suitable for imaging HSV-tk reporter gene expression.
In this study we have compared two tracer for monitoring gene expression using the HSV-tk gene as a reporter gene. The uptake [^{18}F]FHPG and [^{125}I]FIAU was studied *in vitro* in four HSV-tk-transfected cell lines and compared with the uptake of tritiated acyclovir, a compound successfully used in the treatment of Herpes simplex virus infection [11].

Material and Methods

The animal experiments were performed in accordance with the German Law on the Protection of Animals. The study was approved by the Saxon State Government Committee for Animal Research (75-9185.81-4.6/95). Methods are described in detail elsewhere [12, 13].

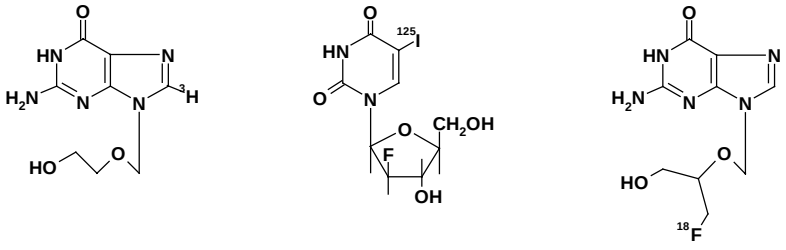

Fig. 1. Structures of the radioligands used in this study to monitor gene transfer. [^{3}H]Acyclovir: [8-^{3}H]-9-(2-hydroxyethoxy-methyl)guanine, [^{125}I]FIAU: 5-[^{125}I]iodo-2´-fluoro-2´-deoxy-1-ß-D-arabinofuranosyluracil, [^{18}F]FHPG: 9-[(3-[^{18}F]fluoro-1-hydroxy-2-propoxy)methyl]guanine.

Results

The transport and distribution of radioligands depends on their ability to cross the plasma membranes of cells. This process is influenced by the plasma membrane composition, the expression of transport systems and the lipophilicity of the radioligands. Partition experiments were therefore performed to estimate the partition coefficients of the various radioligands (Fig. 1) used in this study. The results are shown in Table 1. Data from the literature are included for comparison. We found that the 1-octanol/phosphate buffer partition coefficient of [^{125}I]FIAU is about 16 times that of acyclovir and 6

times that of [^{18}F]FHPG. For [^{18}F]FHPG no change of P_{oct} was observed between pH 5.2 and pH 8.0. P_{oct} of [^{125}I]FIAU only slightly decreased between pH 7.1 and pH 8.0 (data not shown).

Table 1. Partition coefficients of various nucleoside analogues used for monitoring gene therapy

Compound	Log P_{Oct}[1]
Ganciclovir	-2.10 ... –1.66[2]
[^{3}H]Ganciclovir	-1.94 ± 0.02
Acyclovir	-1.62 ... –1.22[3]
[^{18}F]FHPG	-0.96 ± 0.01
[^{125}I]FIAU	-0.20 ± 0.02

[1]Log P_{Oct} was determined from the tracer distribution in a 1:1 mixture of 1-octanol and phosphate buffer (pH 7.4); [2]Data from the literature: [14, 15]; [3]Data from the literature: [16 - 18].

The uptake of [^{3}H]acyclovir, [^{18}F]FHPG, and [^{125}I]FIAU was studied in four HSV-tk-expressing cell lines and their controls. Using [^{3}H]acyclovir, a low tracer uptake was measured in all cell lines with only small differences between HSV-tk-expressing (tk-positive) and non-expressing (tk-negative) cells (Fig. 2). The tk-positive/tk-negative cell uptake ratio after 240 min was between 1.45 (CMS-5) and 2.04 (T1115). The uptake after 240 min incubation increased for both series in the order: T1115 glioblastoma cells (514 ± 99 fmol/mg) followed by rat Morris hepatoma (MH3924A) cells (795 ± 145 fmol/mg), CMS-5 fibrosarcoma cells (990 ± 97 fmol/mg) and MCF7 mamma carcinoma cells (1048 ± 30 fmol/mg). The same order was found in the HSVtk-expressing cells (Fig. 2B), but the differences between the various cell lines were less pronounced.

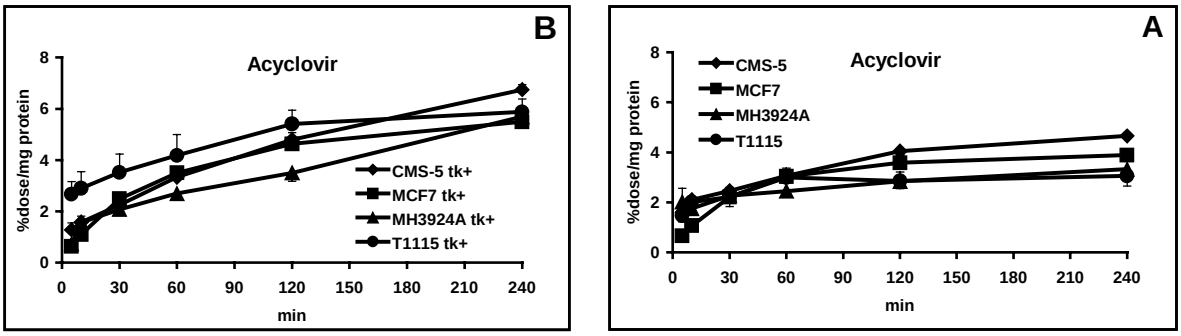

Fig. 2. Accumulation of [^{3}H]acyclovir in HSVtk-negative (left) and HSVtk-positive (right) cell lines as a function of the incubation time. Data are means ± S.E.M. (n = 6 - 12)

With [^{18}F]FHPG as a tracer, a relatively low uptake and a rather large variability between the cell lines was found (Fig. 3). In both groups, i.e. non-transfected HSVtk negative cells (Fig. 3A) and transfected tk^+ cells (Fig. 3B), the highest uptake was observed in the CMS-5 cell line. About 90% lower uptake values were measured in the T1115tk^- cells and T1115tk^+ cells. The tk^+/tk^- uptake ratios obtained with [^{18}F]FHPG as a tracer ranged from 2.1 (MCF7) to 6.6 (T1115) (Fig. 5).
With [^{125}I]FIAU as a tracer about 10 times higher uptake values than with [^{18}F]FHPG and 100 times higher uptake values than with [^{3}H]acyclovir were found (Fig. 4). The uptake ratios between transfected and non-transfected cells were also significantly higher. The lowest ratio was found for CMS-5 and the highest for MCF7 cells (Fig. 5). Therefore, *in vitro* the highest selectivity was observed for [^{125}I]FIAU. Furthermore, we found (cf. data from Table 1 and Figs. 2 - 4) that the tracer uptake in tk^+ cells correlated with the partition coefficient of the radioligand used. It is still unclear whether this observation reflects a causal relationship.

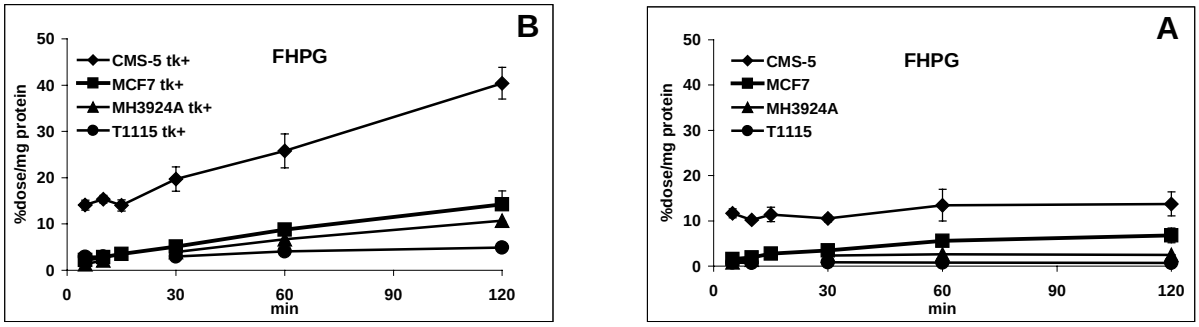

Fig. 3. Accumulation of [^{18}F]FHPG in HSVtk-negative (left) and HSVtk-positive (right) cell lines as a function of the incubation time. Data are means ± S.E.M. (n = 6 - 12)

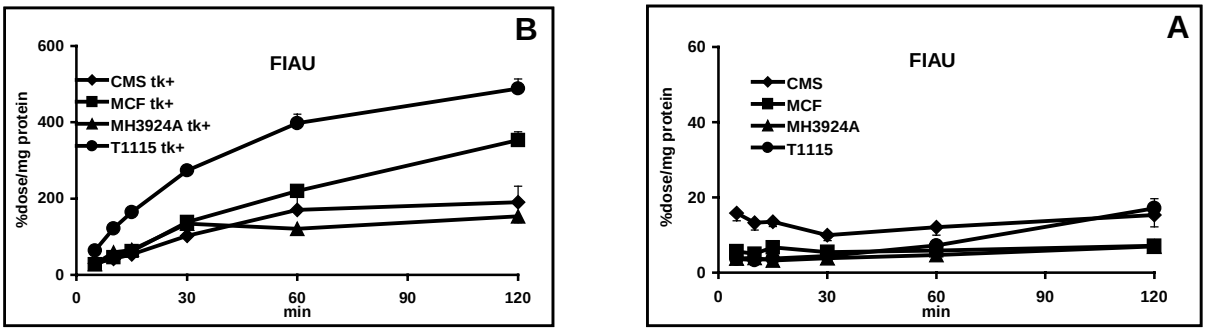

Fig. 4. Accumulation of [^{125}I]FIAU in HSVtk-negative (left) and HSVtk-positive (right) cell lines as a function of the incubation time. Data are means ± S.E.M. (n = 6 - 12).

Discussion

In this study we directly compared [^{18}F]FHPG and [^{125}I]FIAU *in vitro* using four HSV-tk transfected cell lines to evaluate the potential of the radiotracers to monitor gene therapy with PET.

Significant differences between the tumour cell lines were observed. While the uptake of acyclovir was similarly low in all tk-expressing cell lines the CMS-5 fibrosarcoma cells accumulated about 4 times more FHPG during 2 h incubation than the other cell types. And the uptake of FIAU into T1115 tk-expressing glioblastoma cells was more than two times that measured in the Morris hepatoma or CMS-5 cells. These differences are therefore assumed to be due to differences in the plasma membrane composition of the cells, including differences in the expression of specific transport systems. Cell-type-specific differences in the uptake rates of nucleosides were reviewed before [19] and may be related to both facilitated transport and non-mediated permeation.

The greatest variability between the various HSVtk expressing cell lines was seen using [^{18}F]FHPG. After 4 h incubation the highest uptake was found in CMS5-tk$^+$ cells (40.4 % dose/mg) and the lowest in T1115-tk$^+$ cells (5.0 % dose/mg). However, the greatest uptake ratio was found for the cell lines with the lowest uptake (MH, T1115). Our data are comparable to those previously published by others [20-22]. In cell lines of human origin the highest uptake ratio of [^{18}F]FHPG or [^{3}H]ganciclovir between HSVtk-expressing and non-expressing cells was 8.

The use of [^{18}F]FHBG, in which the ether oxygen in the side chain was substituted by carbon, increased this ratio by the factor 2 [23]. Cell lines derived from rat glioma generally showed a much higher ratio (between 35 and 100) [24, 25]. However, the C6 rat glioma model was criticised for its use in the investigation of gene therapy strategies [26]. De Vries *et al.* [24] compared this cell line with PA-317tk$^+$ cells derived from mouse fibroblasts and failed to demonstrate the selective uptake of [^{18}F]FHPG in PA-317-tk$^+$ cells while the toxicity of ganciclovir was comparable to C6-tk$^+$ cells. The uptake ratio between HSVtk-positive and HSVtk-negative C6 cells was drastically reduced by the introduction of ^{18}F in position 8 of ganciclovir ([^{18}F]ganciclovir). The same phenomenon was observed for penciclovir. Altogether these data support our observation that the [^{18}F]FHPG uptake depends very much on the specific tumour type. The reason for this could be the variability in transporter expression between the cells.

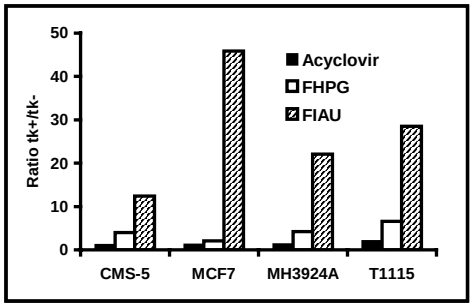

Fig. 5. Ratios of the tracer accumulation between HSVtk-positive and HSVtk-negative cell lines at 120 min incubation time.

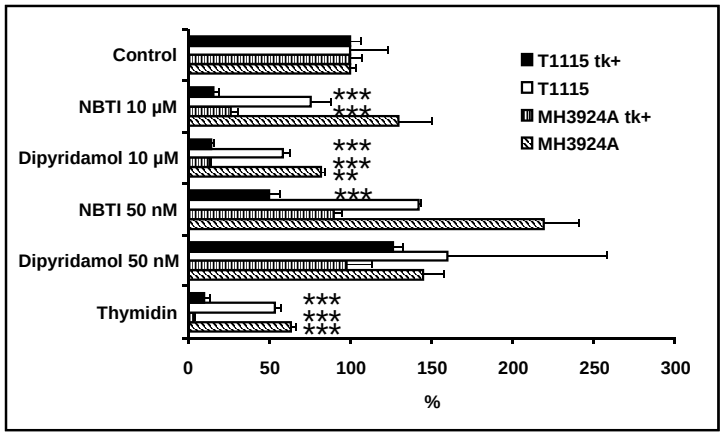

Fig. 6. Inhibition of [^{125}I]FIAU uptake in HSVtk-positive and HSVtk-negative MH3924A and T1115 cells. Data are means ± S.E.M. (n = 3 - 6)

The uptake of FIAU by tk-expressing cells is about ten times that of FHPG and 100 times that of acyclovir. Among the three radiotracers used in this study, FIAU is the only ligand which is only transported by nucleoside transport systems. Its uptake into MH3924A and T1115 cells was not inhibited by adenosine, uracil or hypoxanthine (unpublished data). It was strongly inhibited by thymidine and by high concentrations of nitrobenzylthioinosine (NBTI) or dipyridamol (Fig. 6). These data suggest that at least two different nucleoside transporters are involved in the transport of FIAU, i.e. the equilibrative-insensitive (ei) transporter and the concentrative (cit) transporter which accepts thymidine as permeant [for review see 27]. In T1115 cells but not in MH3924A cells part of the transport was sensitive to low concentrations of NBTI, which suggests a partial contribution of the equilibrative-sensitive (es) system.

Similar results were found for another uracil nucleoside derivative. The tritiated 5-fluoro-1-(2-deoxy-2-fluoro-ß-d-ribofuranosyl)uracil (FFUdR), a ribofuranosyl analogue of FIAU in which iodine was substituted by fluorine [28], was transported into MH3924A-tk$^+$ cells mainly via the equilibrative and concentrative nucleoside transporters but not by nucleobase transport systems [29]. About 7 – 8 % of the total radioactivity was found in the cells after 2 h incubation with the tracer, 35 - 40 times more than in the corresponding control cells [29]. We found a [^{125}I]FIAU uptake of between 15 % and 49 % of the total dose, which corresponds to between 12 times (CMS-5) and 50 times (MCF7) the uptake in HSVtk-negative cells.

This study compares two potential reporter probes for monitoring the HSV-TK activity after gene transfer. The study clearly demonstrates that in our direct comparison *in vitro* FIAU is a substantially better reporter probe than acyclovir or FHPG. But further studies are needed to decide whether the development of a suitable PET tracer should be primarily based on uracil nucleoside derivatives as the lead structures.

References

[1] Verma, I.M.; Somia, N. Gene therapy -- promises, problems and prospects. Nature 389 (1997) 239-242.

[2] Anonymus. Gene therapy: cautious optimism. Nat. Med. 6 (2000) 717.

[3] Moolten, F.L. Tumor chemosensitivity conferred by inserted herpes thymidine kinase genes: paradigm for a prospective cancer control strategy. Cancer Res. 46 (1986) 5276-5281.

[4] Culver, K.W.; Ram, Z.; Wallbridge, S.; Ishii, H.; Oldfield, E.H.; Blaese, R.M. *In vivo* gene transfer with retroviral vector-producer cells for treatment of experimental brain tumors. Science 256 (1992) 1550-1552.

[5] Caruso, M.; Panis, Y.; Gagandeep, S.; Houssin, D.; Salzmann, J.L.; Klatzmann, D. Regression of established macroscopic liver metastases after in situ transduction of a suicide gene. Proc. Natl. Acad. Sci. U S A 90 (1993) 7024-7028.

[6] Tjuvajev, J.; Stockhammer, G.; Desai, R.; Uehara, H.; Watanabe, K.; Gansbacher, B.; Blasberg, R. Imaging the expression of transfected genes *in vivo*. Cancer Res. 55 (1995) 6126-6132.

[7] Gambhir, S.S.; Barrio, J.R.; Herschman, H.R.; Phelps, M.E. Assays for noninvasive imaging of reporter gene expression. Nucl. Med. Biol. 26 (1999) 481-490.
[8] Tjuvajev, J.G.; Avril, N.; Oku, T.; Sasajima, T.; Miyagawa, T.; Joshi, R.; Safer, M.; Beattie, B.; DiResta, G.; Daghighian, F.; Augensen, F.; Koutcher, J.; Zweit, J.; Humm, J.; Larson, S.M.; Finn, R.; Blasberg, R. Imaging herpes virus thymidine kinase gene transfer and expression by positron emission tomography. Cancer Res. 58 (1998) 4333-4341.
[9] Monclus, M.; Luxen, A.; Van Naemen, J.; Damhaut, P.; Velu, T.; Cool, V.; Goldman, S. Development of PET radiopharmaceuticals for gene therapy: Synthesis of 9{(1-[^{18}F]fluoro-3-hydroxy-2-propoxy)methyl} guanine. J. Labelled Compd.Radiopharm. 37 (1995) 193-195.
[10] Alauddin, M.M.; Conti, P.S.; Mazza, S.M.; Hamzeh, F.M., Lever, J.R. 9-[(3-[^{18}F]-fluoro-1-hydroxy-2-propoxy)methyl]guanine ([^{18}F]-FHPG): a potential imaging agent of viral infection and gene therapy using PET. Nucl. Med. Biol. 23 (1996) 787-792.
[11] Elion, G.B. Acyclovir: discovery, mechanism of action, and selectivity. J, Med, Virol. Suppl 1 (1993) 2-6.
[12] Haubner, R.; Avril, N.; Hantzopoulos, P.A.; Gansbacher, B.; Schwaiger, M. *In vivo* imaging of herpes simplex virus type 1 thymidine kinase gene expression: early kinetics of radiolabelled FIAU. Eur. J. Nucl. Med. 27 (2000) 283-291.
[13] Brust, P.; Haubner, R.; Friedrich, A.; Scheunemann, M.; Gansbacher, B.; Koufaki, O.N.; Hauses, M.; Noll, S.; Noll, B.; Haberkorn, U.; Schackert, H.K.; Schackert, G.; Avril, N.; Johannsen, B. Comparison of [^{18}F]FHPG and [$^{124/125}$I]FIAU for their potential of monitoring gene therapy. Eur. J. Nucl. Med. 2001 (submitted).
[14] Benjamin, E.J.; Firestone, B.A.; Bergstrom, R.; Fass, M.; Massey, I.; Tsina, I.; Lin, Y.Y.T. Selection of a derivative of the antiviral agent 9-[(1,3-dihydroxy-2-propoxy)-methyl]guanine (DHPG) with improved oral absorption. Pharm. Res. 4 (1987) 120-125.
[15] Jensen, E.; Bundgaard, H. Synthesis, enzymatic hydrolysis and physico-chemical properties of N-sub-stituted 4-(aminomethyl)benzoate diester prodrugs of ganciclovir. Acta Pharm. Nord 3 (1991) 243-247.
[16] Kristl, A.; Vesnaver, G.; Mrhar, A.; Kozjek, F. Evaluation of partitioning and solubility data from some guanine derivatives in terms of mutual miscibility of octanol and water phase. Pharmazie 48 (1993) 608-610.
[17] Okamoto, H.; Hashida, M.; Sezaki, H. Effect of 1-alkyl- or 1-alkenylazacycloalkanone derivatives on the penetration of drugs with different lipophilicities through guinea pig skin. J. Pharm. Sci. 80 (1991) 39-45.
[18] Shao, Z.; Park, G.B.; Krishnamoorthy, R.; Mitra, A.K. The physicochemical properties, plasma enzymatic hydrolysis, and nasal absorption of acyclovir and its 2'-ester prodrugs. Pharm. Res. 11 (1994) 237-242.
[19] Plagemann, P.G.; Wohlhueter, R.M.; Woffendin, C. Nucleoside and nucleobase transport in animal cells. Biochim. Biophys. Acta. 947 (1988) 405-443.
[20] Haberkorn, U.; Altmann, A.; Morr, I.; Germann, C.; Oberdorfer, F.; van Kaick, G. Multitracer studies during gene therapy of hepatoma cells with herpes simplex virus thymidine kinase and ganciclovir. J. Nucl. Med. 38 (1997) 1048-1054.
[21] Haberkorn, U.; Khazaie, K.; Morr, I.; Altmann, A.; Müller, M., van Kaick, G. Ganciclovir uptake in human mammary carcinoma cells expressing herpes simplex virus thymidine kinase. Nucl. Med. Biol. 25 (1998) 367-373.
[22] Alauddin, M.M.; Shahinian, E.M.; Conti, P.S. Evaluation of F-18 9-(4-fluoro-3-hydroxymethylbutyl)guanine ([F-18]FHBG) as PET imaging agent for gene expression in tumor bearing nude mice. J. Nucl. Med. 40 (1999) 26P.
[23] Alauddin, M.M.; Conti, P.S. Synthesis and preliminary evaluation of 9-[(4-[^{18}F]-fluoro-3-hydroxy-methylbutyl]guanine ([^{18}F]-FHBG): a new potential imaging agent for viral infection and gene therapy using PET. Nucl. Med. Biol. 25 (1998) 175-180.
[24] De Vries, E.F.J.; van Waarde, A.; Harmsen, M.C.; Mulder, N.H.; Vaalburg, W.; Hospers, G.A.P. [^{11}C]FMAU and [^{18}F]FHPG as PET tracers for Herpes simplex virus thymidine kinase enzyme activity and human cytomegalovirus infections. Nucl. Med. Biol. 27 (2000) 113-119.
[25] Gambhir, S.S.; Barrio, J.R.; Wu, L.; Iyer, M.; Namavari, M.; Satyamurthy, N.; Bauer, E.; Parrish, C.; MacLaren, D.C.; Borghei, A.R.; Green, L.A.; Sharfstein, S.; Berk, A.J.; Cherry, S.R.; Phelps, M.E.; Herschman, H.R. Imaging of adenoviral-directed herpes simplex virus type 1 thymidine kinase reporter gene expression in mice with radiolabeled ganciclovir. J. Nucl. Med. 39 (1998) 2003-2011.

[26] Beutler, A.S.; Banck, M.S.; Wedekind, D.; Hedrich, H.J. Tumor gene therapy made easy: allogeneic major histocompatibility complex in the C6 rat glioma model. Hum. Gene Ther. 1 (1999) 95-101.
[27] Baldwin, S.A.; Mackey, J.R.; Cass, C.E.; Young, J.D. Nucleoside transporters: molecular biology and implications for therapeutic development. Mol. Med. Today 5 (1999) 216-224.
[28] Shields, A.F.; Grierson, J.R.; Kozawa, S.M.; Zheng, M. Development of labeled thymidine analogs for imaging tumor proliferation. Nucl. Med. Biol. 23 (1996) 17-22.
[29] Germann, C.; Shields, A.F.; Grierson, J.R.; Morr, I.; Haberkorn, U. 5-Fluoro-1-(2'-deoxy-2'-fluoro-beta-D-ribofuranosyl) uracil trapping in Morris hepatoma cells expressing the herpes simplex virus thymidine kinase gene. J.. Nucl. Med. 39 (1998) 1418-1423.

49. Separation of ^{18}F-Labelled Neurotensin Derivatives and its Metabolites

H. Wittrisch, R. Bergmann, K. Fischer, C. Heichert, P. Mäding, M. Scheunemann, P. Brust

Introduction

Neurotensin (NT) (pGlu-Leu-Tyr-Glu-Asn-Lys-Pro-Arg-Arg-Pro-Tyr-Ile-Leu) is a naturally occurring peptide hormone consisting of 13 amino acids. It is heterogeneously distributed throughout the central nervous system and also found in the gastrointestinal tract of various mammals [1]. This peptide displays a wide spectrum of biological activities. It is involved in hypotension, hyperglycemia, hypothermia, increased vascular permeability etc. Its various functions are evoked by interaction with specific neurotensin receptors.
Neurotensin receptors were also found in several tumours, such as Ewing's sarcoma, meningioma, astrocytoma and small cell lung cancer [2]. Previous studies showed that the hexapeptide NT (8-13) is the shortest sequence of the native peptide to maintain receptor binding [3]. NT (8-13)-based radiolabelled analogues were synthesized for diagnosis of cancer [4].
However, the labelled peptides are subject to rapid metabolism. Especially endopeptidase 24.15 and the angiotensin-converting enzyme are known to cleave the Arg^8-Arg^9 bond [5], while endopeptidases 24.11 and 24.16 cleave the Pro^{10}-Tyr^{11} bond [6]. Moreover, the angiotensin-converting enzyme can cleave the neurotensin between $Tyr^{11}$and Ile^{12} [7]. The separation of the resulting metabolites was usually performed by high performance liquid chromatography (HPLC) [8,9], ion exchange chromatography [10] or capillary electrophoresis [11]. Radioimmuno-assays were used for identification of the separated compounds [12].
The synthesis of [^{18}F]fluorobenzoyl-labelled NT (8-13) (^{18}FB-NT (8-13)) was recently described [13]. The separation of ^{18}FB-NT (8-13), the metabolically stabilized pseudopeptides [$Arg^8\Psi(CH_2NH)Arg^9$-Pro^{10}-Tyr^{11}-Ile^{12}-Leu^{13}] and [$Arg^8\Psi(CH_2NH)Arg^9$-Pro^{10}-Tyr^{11}-Tle^{12}-Leu^{13}] and their metabolites from *in-vivo* and *in-vitro* samples is shown in this study. The separation was performed by HPLC and the identification by mass spectrometry.

Material and Methods

For *in-vitro* studies rat blood was centrifuged at 14,000 rpm for 5 min. Blood or the plasma obtained was mixed with the pseudopeptide in question (0.5 MBq) and incubated at 37 °C for 1 to 480 min. For *in-vivo* experiments Wistar rats (male, 250 – 350 g) were used. About 25 MBq of the neurotensin derivatives (5 – 15 GBq / µmol) were injected into each rat. Plasma samples were taken after various periods (1 to 120 min). The plasma samples were directly used for HPLC analysis.
The HPLC system (HP1100, Agilent Technologies, Waldbronn, Germany) consists of an autosampler, two HPLC pumps, two six-port valves, a variable-wavelength UV detector and a radiochromatographic detector Flo-one-βeta® (Canberra Packard, Dreieich, Germany). Pump 1 delivers the buffer for the size exclusion chromatography (SEC) (column ZORBAX GF-250, 4.6 mmID x 250 mmL), while pump 2 delivers the buffer for the analytical column (ZORBAX 300SB-C18, 4.6 mmID x 50 mmL).
Typically, 10-150 µl plasma or urine samples were injected. A 300 mM phosphate buffer pH 7 containing 5 % acetonitrile (MeCN) was used for SEC. When the analytes were eluted from the SEC column, both six-port valves were switched by the software (HP ChemStation for LC). During this step the RP column was loaded with the sample. Than the first valve switched back and the compounds were separated, using the analytical column under gradient conditions at 40 °C and a flow rate of 1 ml/min. Solvent A consisted of water with 0.05 % trifluoro acetic acid (TFA), and solvent B of MeCN with 0.04 % TFA. The gradient contained the following steps: 0 – 8 min 5 % B, 8 – 12 min 5 % up to 60 % B, 12 – 14 min 60 % up to 80 % B, 14 – 15 min 80 % B. A wavelength of 214 nm was used for UV detection. The radioactivity concentration was continuously recorded during separation. After passing through the radiochromatographic detector, the HPLC fractions were collected with a Redi-Frac collector (Pharmacia Biotech, Sweden) and lyophilized. For identification of the metabolites a micromass Quattro LC system (micromass Limited, UK) was used. The instrument was operated in positive electrospray mode and a cone voltage of between 25 and 75 kV. The scan range was 50-1000 DA per minute. The ion source temperature was set to 250 °C.

Results and Discussion

[^{18}F]fluorobenzoyl-labelled NT (8-13)

The *in-vitro* stability of FB-NT (8-13) was investigated in the blood of Wistar rats. After only 5 min of incubation at 37 °C two metabolites were found (Fig. 1). One was identified as FB-Arg-Arg and the other as FB-Arg by mass spectrometry (Fig. 2). When the incubation was performed with plasma instead of blood, only FB-Arg was detected. This shows that the enzyme cleaving the Arg^{9}-Pro^{10} bond is located at blood cells such as leucocytes [14] or erythrocytes [15]. No FB-NT (8-13) was detected in the rat blood *in vivo*. Only 2 min after the injection of FB-NT (8-13) 49 % of the compound was metabolized into FB-Arg-Arg and 51 % into FB-Arg. A fast degradation of FB-Arg-Arg into FB-Arg occurred later.

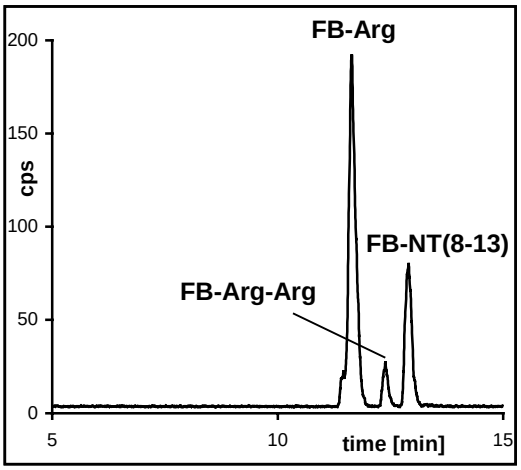

Fig. 1. Separation of rat blood containing FB-NT (8-13) and its metabolites FB-Arg-Arg and FB-Arg

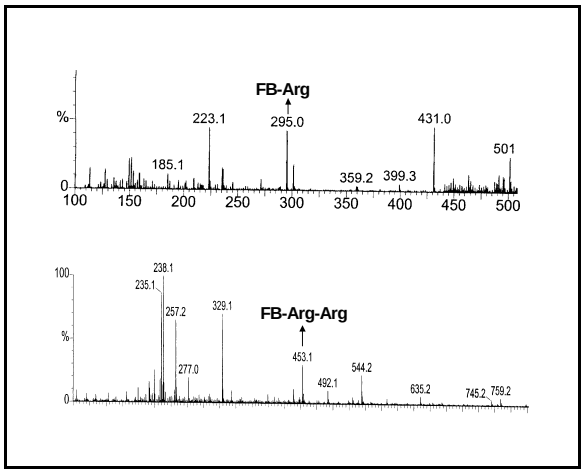

Fig. 2. Mass spectra of the peaks containing FB-Arg and FB-Arg-Arg

In the rat urine obtained 120 min after injection only the metabolites of FB-NT (8-13) were found (data not shown). Approximately 96 % FB-Arg and 4 % FB-Arg-Arg was detected.

[^{18}F]fluorobenzoyl-labelled [Arg^{8} Ψ(CH$_2$NH)Arg^{9}-Pro^{10}-Tyr^{11}-Ile^{12}-Leu^{13}]

For a higher stability of the neurotensin molecule the Arg^{8}-Arg^{9} bond was protected. After 5 min incubation of the stabilized NT derivative at 37 °C with rat blood or rat plasma, two metabolites were observed (Fig. 3).

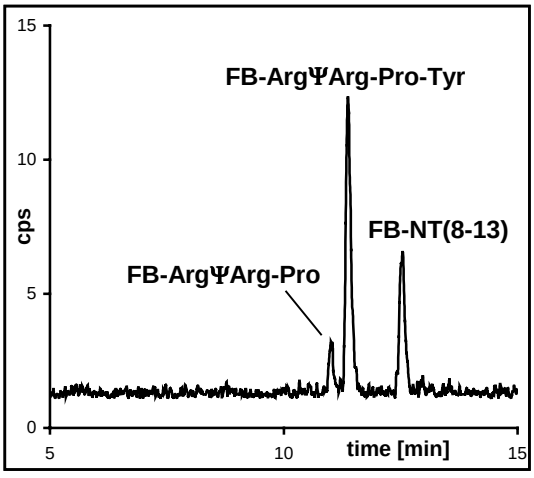

Fig. 3. Separation of rat blood plasma containing FB-[Arg^{8}Ψ(CH$_2$NH)Arg^{9}] NT (10-13) and its metabolites FB-ArgΨArg-Pro-Tyr and FB-ArgΨArg-Pro

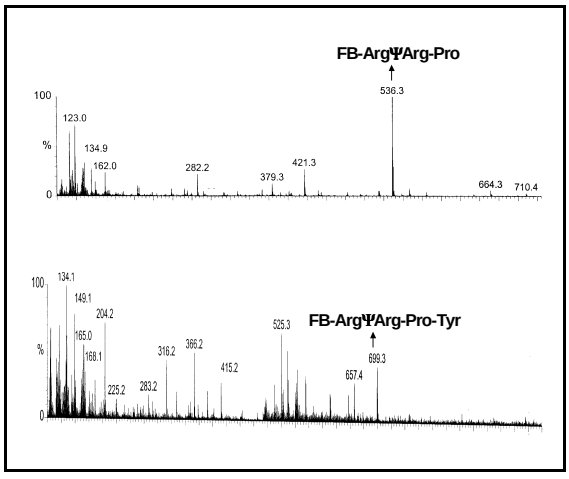

Fig. 4. Mass spectra of the peaks containing FB-ArgΨArg-Pro and FB-ArgΨArg-Tyr

FB-[Arg^{8}Ψ(CH$_2$NH)Arg^{9}-Pro^{10}-Tyr^{11}-Ile^{12}-Leu^{13}] was identified by chromatographic comparison with a reference substance. Mass spectrometry (Fig. 4) identified the first metabolite as FB-ArgΨArg-Pro-Tyr and the second as FB-ArgΨArg-Pro.
In accordance with the theoretical prediction an increased stability of the pseudopeptide was obtained. The unchanged compound was observed in rat blood up to 4 min after injection. During this time approximately 45 % of the pseudopeptide was metabolized into FB-ArgΨArg-Pro-Tyr and 53 % into FB-ArgΨArg-Pro. Due to the high activity of the peptidases (e.g. endopeptidase 24.11 and endopeptidase 24.16) the amount of FB-ArgΨArg-Pro-Tyr decreased very fast to a level of about 5 %.
Rat urine was obtained 120 min after injection. It coniained only 1 % unchanged FB-[Arg^{8}Ψ(CH$_2$NH)Arg^{9}-Pro^{10}-Tyr^{11}-Ile^{12}-Leu^{13}]. Approximately 97 % of the pseudopeptide was degraded into FB-ArgΨArg-Pro and 2 % into FB-ArgΨArg-Pro-Tyr.

[^{18}F]fluorobenzoyl-labelled [Arg^{8} Ψ(CH$_2$NH)Arg^{9}-Pro^{10}-Tyr^{11}-Tle^{12}-Leu^{13}]
Further metabolic stabilization of the peptide was achieved by replacing isoleucine by tertiary leucine. No degradation products were detected after incubation of the pseudopeptide in rat plasma for 8 hours at 37 °C. However, a cleavage of the Pro^{10}-Tyr^{11} bond was observed *in vivo*. Five min after injection approximately 20% of FB-ArgΨArg-Pro was detectable in rat plasma (Figs. 5, 6).

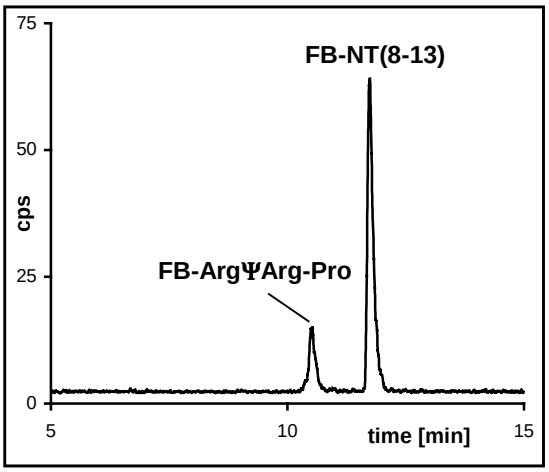

Fig. 5. Separation of rat blood plasma containing the double stabilized FB-NT (8-13) and its metabolite FB-ArgΨArg-Pro

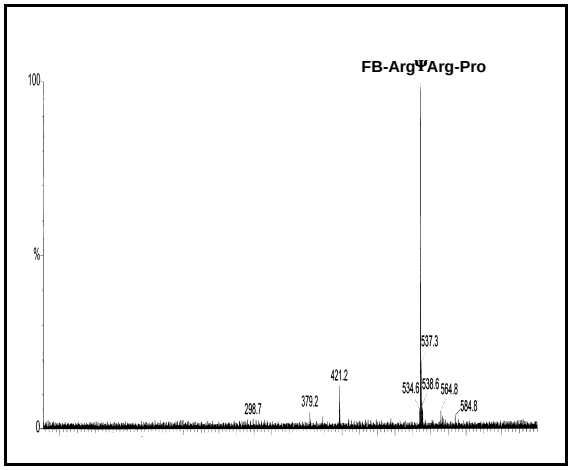

Fig. 6. Mass spectrum of the peak containing FB-ArgΨArg-Pro

Twenty-five min p. i. about 50 % of the double stabilized FB-NT (8-13) still remained in the plasma. Approximately 6 % unchanged pseudopeptide and 94 % FB-ArgΨArg-Pro were found in the urine 120 min after injection.

Our results clearly show that neurotensin derivatives and their metabolites can be separated under given HPLC conditions. The detected metabolites were identified by mass spectrometry. An increased stability of the [^{18}F]fluorobenzoyl-labelled neurotensin derivatives was observed.

This work was supported by the European Union (BMH4-CT98-3198).

References

[1] Tyler-McMahon B.M.; Boules M.; Richelson E. Neurotensin: peptide for the next millennium. Regul. Pept. 93 (2000) 125-136.
[2] Reubi, J.C.; Waser, B.; Schaer, J.C.; Laissue, J.A. Neurotensin receptors in human neoplasms: high incidence in Ewing's sarcomas. Int. J. Cancer 82 (1999) 213-218.
[3] Granier, C.; Van Rietschoten, J.; Kitabgi, P.; Poustis; C., Freychet, P. Synthesis and characterization of neurotensin analogues for structure/activity relationship studies. Eur. J. Biochem. 124 (1982) 117-125.
[4] Heppler, A.; Froidevaux, S.; Eberle, A.N.; Maecke H.R. Receptor targeting for localisation and therapy with radiopeptides. Curr. Med. Chem. 7 (2000) 971-994.

[5] Davis, T.P.; Gillespie T.J.; Konings P.N. Specificity of neurotensin metabolism by regional rat brain slices. J. Neurochem. 58 (1992) 608-817.
[6] Barelli, H.; Vincent, J.P.; Checler, F. Rat kidney endopeptidase 24.16. Purification, physico-chemical characteristics and differential specificity towards opiates, tachykinins and neurotensin-related peptides. Eur. J. Biochem. 211 (1993) 79-90.
[7] Checler F.; Vincent J.P.; Kitabgi P. Degradation of neurotensin by rat brain synaptic membranes: involvement of a thermolysin-like metalloendopeptidase (enkephalinase), angiotensin-converting enzyme, and other unidentified peptidases. J. Neurochem. 41 (1983) 375-384.
[8] Bennett, G.W.; Moss, S.H.; Forster C.D.; Marsden, C.A. Developmental changes in neurotensin and its metabolites in the neonatal rat. Brain Res. Dev. Brain Res. 111 (1998) 189-196.
[9] Kilts, C.D.; Knight, D.L.; Nemeroff, C.B. The simultaneous determination of neurotensin and its major fragments by on-line trace enrichment HPLC with electrochemical detection. Live Sci. 59 (1996) 911-920.
[10] Dizdaroglu, M.; Simic, M.G.; Rioux, F.; St-Pierre, S. Separation of diastereomers and analogues of neurotensin by anion-exchange high-performance liquid chromatography. J. Chromatogr. 245 (1982) 158-162.
[11] Koezuka, K.; Ozaki, H.; Matsubara, N.; Terabe, S. Separation and detection of closely related peptides by micellar electrokinetic chromatography coupled with electrospray ionization mass spectrometry using the partial filling technique. J. Chrommatogr. B. Biomed Sci. Appl. 689 (1997) 3-11.
[12] De Ceballos, M.L.; Taylor, M.D.; Jenner, P. Isocratic reverse-phase HPLC separation and RIA used in the analysis of neuropeptides in brain tissue. Neuropeptides 20 (1991) 201-209.
[13] Scheunemann, M.; Mäding, P.; Steinbach, J.; Bergmann, R.; Iterbeke, K.; Johannsen, B.; Tourwe, D. Fluorine-18 labelling of neurotensin analogues for the development of tumour imaging agents. J. Labelled Compd. Radiopharm. 42(Suppl.1) (1999) S713-S714.
[14] Rusu, I.; Yaron, A. Aminopeptidase P from human leukocytes. Eur. J. Biochem. 210 (1992) 93-100.
[15] Sidorowicz, W.; Canizaro, P.C.; Behal, F.J. Kinin cleavage by human erythrocytes. Am. J. Hematol. 17 (1984) 383-391.

50. Distribution of 16α-[^{18}F]Fluoro-Estradiol-3,17β-Disulphamate (FESDS) in Rats and Tumour-Bearing Nude Mice

P. Brust, H. Rodig, R. Bergmann, J. Römer, M. Baumann[2], H. Kasch[1], F. Füchtner, J. Steinbach
[1]idPharma, Jena, [2]Universitätsklinikum "Carl Gustav Carus" Dresden

Introduction

Estrogen sulphates are quantitatively the most important form of circulating estrogens during the menstrual cycle and in the post-menopausal period. Huge quantities of estrone sulphate and estradiol sulphate are found in the breast tissues of patients with mammary carcinoma. Many tumours in endocrine-sensitive tissues, such as the breast and endometrium, are hormone-dependent and hydrolysis of estrone sulphate to estrone by estrone sulphatase (ES) is a major source of estrogen in such tumours. It was demonstrated that various estrogen-3-sulphates (estrone-3-sulphate, estradiol-3-sulphate, estriol-3-sulphate) can provoke important biological responses in mammary cancer cell lines. [^{3}H]Estrone sulphate is converted into estradiol in a very high percentage in various hormone-dependent mammary cancer cell lines (MCF-7, R-27, T-47D), but very little or no conversion occurs in the hormone-independent mammary cancer cell lines (MDA-MB-231, MDA-MB-436) [1]. It is expected that control of the sulphatase will open new possibilities in the treatment of hormone-dependent mammary cancer. Administration of danazol was found to cause a fall in plasma estrone levels and to diminish the conversion ratio of estrone sulphate to estrone in breast cancer patients [2]. It also inhibited tissue sulphatase activity. Although this drug is only a weak sulphatase inhibitor, these observations indicate the potential value of developing more efficient sulphatase inhibitors.
Estrone-3-O-sulphamate (EMATE) was shown to be a potent ES inhibitor *in vitro* and *in vivo*. The administration of EMATE almost completely inhibited ES in the liver [3]. However, this compound still possesses a potent estrogenic activity [4]. A novel class of ES inhibitors was recently described. Estradiol-disulphamate and some of its derivatives exhibit a 2 to3 times higher potency of sulphatase inhibition [5]. Based on these findings 16α-[^{18}F]fluoroestradiol-3,17β-disulphamate ([^{18}F]FESDS) was developed as a potential PET tracer for imaging steroid-dependent breast tumours [6]. The suitability of [^{18}F]FESDS for imaging studies was investigated in this paper.

Material and Methods

Synthesis of [^{18}F]-FESDS
The synthesis of [^{18}F]FESDS was previously described [6].
Cell culture
MCF-7 cells (human breast adenocarcinoma; DSMZ No. ACC 115) were purchased from DSMZ Heidelberg. These cells were cultivated at 37 °C and 5 % CO_2 in RPMI 1640 medium with Glutamax I (Life Technologies GmbH, Karlsruhe) to which 10 % stripped fetal bovine serum (Greiner, Frickenhausen), 1 mM sodium pyruvate, 1 % MEM non-essential amino acids (Biochrom KG, Berlin), 20 mM Hepes buffer (Biochrom KG), 1 % penicillin/streptomycin (10 000 U/10 000 µg/ml; Biochrom KG), 10 µg/ml insulin and 5 nM ß-estradiol (Sigma, Deisenhofen) were added.
Tumour implantation
MCF-7 tumours were produced in nude mice by injection of 100 µl cell suspension (10^7 cells) into the axilla. To obtain good tumour growth 0.5 mg/kg/week ß-estradiolbenzoate (Sigma, Deisenhofen) was subcutaneously injected [7]. The dose was divided into three single injections per week. The hormone was dissolved in DMSO (0.1 mg/µl) and diluted with peanut oil in the ratio 1:200, of which 100 µl was injected.
FaDu is an established human hypopharyngeal squamous cell carcinoma. In nude mice FaDu grows as an undifferentiated carcinoma. For the experiments source tumours were excised, cleaned of necrotic tissue, cut into small pieces and subcutaneously transplanted into the right hindleg. No estradiol was given to the FaDu-tumour-bearing mice. When the tumours had reached a diameter of approx. 1 cm, the animals were sacrificed and the tumours frozen at –50 ^{o}C. After thawing, pieces of frozen FaDu tumours were cut up and subcutaneously injected into the thigh of the nude mice. Animals with a tumour diameter of between 0.7 and 1.0 cm were used for the biodistribution studies.
Biodistribution studies
Biodistribution studies were carried out in rats and in tumour-bearing nude mice according to the national regulations for animal research.
The animals were intravenously injected with approximately 125 kBq [^{18}F]FESDS per rat and about 85 kBq [^{18}F]FESDS per mouse. The animals were sacrificed and dissected between 5 and 60 min after the tracer injection. Tumours, blood, six brain regions, ovaries, uterus, pancreas, spleen, adrenals,

kidneys, fatty tissue, muscle, heart, lung, thymus (except nude mice), liver, femur and intestine were sampled and weighed, and the radioactivity in each tissue was measured. The results were expressed as the percentage of the injected dose per gram of tissue (mean ± S.E.M.). Inhibition studies were performed by i.v. injection of the inhibitor (10% DMSO in saline or 50% ethanol in saline) ten minutes before the tracer injection. The following drugs were used as inhibitors: acetazolamide 5mg/kg, ethoxyzolamide 5 mg/kg, quercetin 5 mg/kg, naringin 5 mg/kg, FESDS 0.05 mg/kg.

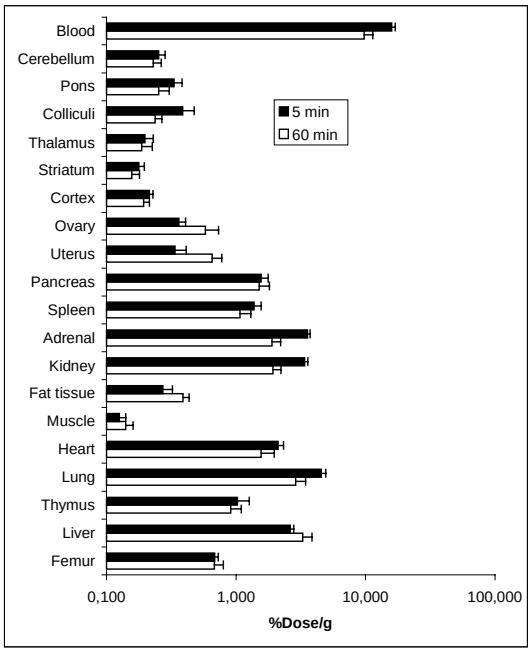

Fig. 1. Biodistribution of [^{18}F]FESDS in Wistar rats as a percentage of the injected dose per gram (mean ± S.E.M.)

Results

Table 1. Inhibition of the [^{18}F]FESDS uptake (% dose/g 60 min p.i.) into various organs of Wistar rats by a number of sulphatase inhibitors (mean ± S.E.M.)

	Control (n = 23)	Quercetin 5 mg/kg (n = 6)	Naringin 5 mg/kg (n = 5)	FESDS 0.05 mg/kg (n = 5)
Blood	10.951 ± 0.372	10.643 ± 2.015	12.789 ± 2.361	7.702 ± 0.987[b]
Cerebellum	0.265 ± 0.012	0.272 ± 0.056	0.324 ± 0.047	0.201 ± 0.011[a]
Pons	0.303 ± 0.017	0.262 ± 0.059	0.285 ± 0.031	0.230 ± 0.022
Colliculi	0.255 ± 0.028	0.287 ± 0.063	0.308 ± 0.090	0.236 ± 0.011
Thalamus	0.215 ± 0.013	0.209 ± 0.035	0.216 ± 0.028	0.163 ± 0.027
Striatum	0.190 ± 0.015	0.162 ± 0.027	0.211 ± 0.025	0.132 ± 0.012
Cortex	0.201 ± 0.010	0.200 ± 0.036	0.246 ± 0.021	0.146 ± 0.010[a]
Ovary	0.561 ± 0.072	0.815 ± 0.185	0.994 ± 0.175	0.536 ± 0.063
Uterus	0.577 ± 0.052	0.759 ± 0.174	1.066 ± 0.213	0.839 ± 0.137
Pancreas	1.434 ± 0.108	1.738 ± 0.268	1.785 ± 0.197	1.575 ± 0.067
Spleen	2.161 ± 0.159	1.384 ± 0.183[b]	1.438 ± 0.246[a]	1.598 ± 0.238
Adrenal	1.540 ± 0.222	1.647 ± 0.259	2.033 ± 0.459	0.996 ± 0.016
Kidney	1.863 ± 0.100	1.828 ± 0.301	2.049 ± 0.344	1.505 ± 0.200
Fat tissue	0.446 ± 0.042	0.764 ± 0.191	1.129 ± 0.250	0.490 ± 0.042
Muscle	0.284 ± 0.103	0.198 ± 0.045	0.281 ± 0.050	0.336 ± 0.167
Heart	1.775 ± 0.143	2.484 ± 0.524	2.630 ± 0.506	1.337 ± 0.153
Lung	2.866 ± 0.235	3.934 ± 0.880	4.186 ± 0.735	2.405 ± 0.277
Thymus	0.862 ± 0.067	1.323 ± 0.314	2.024 ± 0.425	0.674 ± 0.060
Liver	4.364 ± 0.272	2.434 ± 0.229[c]	2.589 ± 0.277[c]	3.981 ± 0.178
Femur	0.739 ± 0.032	1.056 ± 0.229	1.230 ± 0.192	0.766 ± 0.066

[a]$p < 0.05$, [b]$p < 0.01$, [c]$p < 0.001$

Fig. 1 shows the biodistribution of [^{18}F]FESDS in Wistar rats 5 min and 60 min p.i.. Surprisingly, most of the tracer remains in the blood. Clearance from the blood and all other organs is rather slow. Elimination is mainly by the enterohepatic route (~ 18 % dose in intestine vs. 0.5 % dose in urine 60 min. p.i.). Administration of 0.05 mg/kg FESDS 10 min before the tracer injection significantly diminished the uptake in the blood and in the brain (cerebellum and cortex) (Table 1). Estrone sulphatase inhibitors such as quercetin and naringin inhibited the uptake in the spleen by 36 % and 33 %. The uptake in the liver was reduced by 44 % and 41 %. The intestine showed a reduction in tracer uptake of more than 50 %.

Because of the structural relationship of FESDS with certain inhibitors of carbonic anhydrase (CA) (see Rodig *et al.*, this volume) the inhibition of the [^{18}F]FESDS uptake by acetazolamide and ethoxyzolamide was studied. Organs rich in carbonic anhydrase, such as blood, spleen, lung, heart and femur (bone marrow), showed a remarkable reduction. In equal doses (5 mg/kg), ethoxyzolamide was a stronger inhibitor than acetazolamide. The uptake into the intestine was about 3 times increased, indicating a much faster elimination of FESDS.

Table 2. Inhibition of the [^{18}F]FESDS uptake (% dose/g 60 min p.i.) into various organs of Wistar rats by a number of carbonic anhydrase inhibitors (mean ± S.E.M.)

	Control (n = 23)			Acetazolamide (5 mg/kg) (n = 5)			Ethoxyzolamide (5 mg/kg)(n = 5)		
Blood	10.213	±	0.340	0.585	±	0.071^{c}	0.390	±	0.031^{c}
Cerebellum	0.249	±	0.010	0.161	±	0.019^{c}	0.147	±	0.011^{c}
Pons	0.277	±	0.014	0.177	±	0.023^{b}	0.147	±	0.015^{b}
Colliculi	0.245	±	0.020	0.183	±	0.022	0.138	±	0.011^{a}
Thalamus	0.202	±	0.010	0.174	±	0.022	0.145	±	0.010^{a}
Striatum	0.177	±	0.011	0.175	±	0.017	0.138	±	0.011
Cortex	0.186	±	0.008	0.150	±	0.017	0.141	±	0.011
Ovary	0.498	±	0.051	0.663	±	0.076	0.467	±	0.061
Uterus	0.519	±	0.041	0.800	±	0.174	0.361	±	0.046
Pancreas	1.385	±	0.087	3.077	±	0.446	2.234	±	0.239
Spleen	2.051	±	0.112	0.354	±	0.046^{c}	0.259	±	0.018^{c}
Adrenal	1.305	±	0.161	0.962	±	0.150	0.614	±	0.033
Kidney	1.720	±	0.083	0.520	±	0.054^{c}	0.456	±	0.028^{c}
Fat tissue	0.429	±	0.031	0.614	±	0.074	0.331	±	0.075
Muscle	0.238	±	0.068	0.217	±	0.024	0.172	±	0.010
Heart	1.627	±	0.117	0.401	±	0.052^{c}	0.266	±	0.033^{c}
Lung	2.524	±	0.191	0.458	±	0.058^{c}	0.346	±	0.052^{c}
Thymus	0.747	±	0.061	0.249	±	0.030^{c}	0.212	±	0.020^{c}
Liver	4.310	±	0.180	4.055	±	0.143	4.841	±	0.234
Femur	0.722	±	0.027	0.359	±	0.031^{c}	0.148	±	0.023^{c}

$^{a}p < 0.05$, $^{b}p < 0.01$, $^{c}p < 0.001$

The uptake of [^{18}F]FESDS was also studied in tumour-bearing nude mice (Table 3). The highest uptake was found in organs rich in CA. As in rats, this uptake was drastically reduced by pre-injection of acetazolamide. Coinjection of FESDS did not further diminish but rather increased the uptake.

Two tumours were studied in the nude mice: human FaDu squamous cell carcinoma and human MCF-7 mamma carcinoma. [^{18}F]FESDS uptake into the estrogen dependent MCF-7 tumour was only 36 % higher than uptake into the non-estrogen dependent FaDu tumour. The tumour/muscle ratio was 1.39 and 1.89. The tumour uptake was only slightly inhibited by acetazolamide but not by FESDS.

Discussion

The aim of the study was to investigate the suitability of [^{18}F]FESDS as a PET tracer for tumour imaging. We found that [^{18}F]FESDS does not accumulate in FaDu squamous cell carcinoma and MCF-7 human breast carcinoma, the two types of tumours studied. In contrast to the FaDu tumours, MCF-7 tumours are expected to express large amounts of estrone sulphatase [8]. However, the comparison between these two tumours indicates that the binding of [^{18}F]FESDS to the enzyme represents less than 30 % of the total tracer accumulation in the tumour. To obtain a reasonable tumour-to-background ratio a specific tumour accumulation of the tracer of more than 90 % is needed.

The [^{18}F]FESDS accumulation in the tumour, uterus and ovaries was not reduced by the steroid sulphatase inhibitors quercetin and naringin, while a significant inhibition of about 40 to 50 % was observed in other organs (liver and spleen) with a high estrone sulphatase activity [9, 10]. 0.05 mg/kg FESDS only inhibited the accumulation of [^{18}F]FESDS in the blood and in the brain. Higher concentrations of this ligand (0.5 mg/kg and 5 mg/kg) showed an inhibitory effect only on the brain (data not shown).

Table 3. Inhibition of the [^{18}F]FESDS uptake (% dose/g 60 min p.i.) into various organs of tumour-bearing nude mice by pre-injection of acetazolamide and FESDS (mean ± S.E.M.)

	Control (n = 10)			Acetazolamide 5 mg/kg (n = 5)			Acetazolamide+FESDS 5 mg/kg (n = 4)		
Blood	32.557	±	4.251	3.198	±	0.811[c]	6.790	±	0.780
Cerebellum	0.999	±	0.067	0.387	±	0.044[c]	0.568	±	0.066
Colliculi	0.973	±	0.065	0.443	±	0.061[c]	0.522	±	0.013
Cortex	0.764	±	0.035	0.361	±	0.031[c]	0.491	±	0.027
Ovary	1.309	±	0.182	3.022	±	0.821	5.307	±	0.982
Uterus	1.392	±	0.172	6.794	±	2.893	7.431	±	1.287
Pancreas	3.230	±	0.235	8.086	±	1.519	9.545	±	1.530
Spleen	11.067	±	0.716	2.832	±	0.487[c]	7.488	±	0.340
Kidney	13.512	±	1.787	3.111	±	0.386[c]	10.356	±	0.565
Fat tissue	1.920	±	0.369	4.148	±	0.594	9.800	±	3.132
Muscle	0.553	±	0.047	0.668	±	0.106	2.479	±	0.262
Heart	6.138	±	1.628	1.181	±	0.280[a]	5.672	±	0.496
Lung	16.767	±	2.354	2.435	±	0.439[c]	9.338	±	0.476
Liver	9.550	±	0.712	11.684	±	1.486	26.634	±	1.176
Femur	1.670	±	0.095	1.283	±	0.251[a]	2.334	±	0.171
Tumour (FaDu)	0.768	±	0.125						
Tumour (MCF-7)	1.043	±	0.063	0.855	±	0.064[a]	3.315	±	0.479

[a] $p < 0.05$, [b] $p < 0.01$, [c] $p < 0.001$

The highest tracer accumulation of all organs was found in the blood, where it is mainly bound (>90 %) to the erythrocytes. A considerable part of the [^{18}F]FESDS accumulation measured in the organs is therefore due to the blood component, which is another disadvantage for a potential PET tracer. The strong binding of [^{18}F]FESDS to the erythrocytes is caused by the presence of large amounts of carbonic anhydrase in these cells. Sulphonamides have long been described as inhibitors of carbonic anhydrase [11].The two sulphonamide groups of FESDS are therefore expected to interact with CA. We have evidence to support this hypothesis because pre-injection of the well-known CA inhibitors acetazolamide and ethoxyzolamide reduced the [^{18}F]FESDS accumulation in the erythrocytes by about 95 %. A significant inhibition was also observed in other organs rich in CA, such as the lungs, kidneys and spleen. A decrease of about 20 % was also observed in tumours. However, the CA does not seem to be a useful target for tumour imaging [12].
To sum up, the in-vivo data obtained with [^{18}F]FESDS in this study indicate that this tracer is not suitable for tumour imaging, irrespective of whether the tumours express estrone sulphatase or not. The binding to estrone sulphatase seems to be negligible compared with the binding to carbonic anhydrase. Further studies are needed to test whether this enzyme could serve as a possible target of [^{18}F]FESDS.

References

[1] Pasqualini, J.R.; Chetrite, G.; Nestour, E.L. Control and expression of oestrone sulphatase activities in human breast cancer. J. Endocrinol. 150 (Suppl) (1996) 99-105.

[2] James, V.H.; Reed, M.J.; Purohit, A. Inhibition of oestrogen synthesis in postmenopausal women with breast cancer. J. Steroid Biochem. Mol. Biol. 43 (1992) 149-153.

[3] Purohit, A.; Williams, G.J.; Roberts, C.J.; Potter, B.V.; Reed, M.J. *In vivo* inhibition of oestrone sulphatase and dehydroepiandrosterone sulphatase by oestrone-3-O-sulphamate. Int. J. Cancer. 63 (1995) 106-111.

[4] Elger, W.; Schwarz, S.; Hedden, A.; Reddersen, G.; Schneider, B. Sulphamates of various estrogens are prodrugs with increased systemic and reduced hepatic estrogenicity at oral application. J. Steroid Biochem. Mol. Biol. 55 (1995) 395-403.
[5] Kasch, H.; Schumann, W.; Römer, J.; Steinbach, J. Steroid sulphamates, methods for preparation and use thereof. Patent PCT/DE 98/00813 (1998).
[6] Römer, J.; Füchtner, F.; Steinbach, J.; Kasch, H. Automated synthesis of 16α-[^{18}F]fluoroestradiol-3,17β-disulphamate. Appl. Radiat. Isot. 51, in press.
[7] Kubota, T.; Kubouchi, K.; Koh, J.; Enomoto, K.; Ishibiki, K.; Abe, O. Human breast carcinoma (MCF-7) serially transplanted into nude mice. Jpn. J. Surg. 13 (1983) 381-384.
[8] Pasqualini, J.R.; Schatz, B.; Varin, C.; Nguyen, B.L. Recent data on estrogen sulphatases and sulphotransferases activities in human breast cancer. J. Steroid Biochem. Mol. Biol. 41 (1992) 323-329.
[9] Nelson, K.; Keinanen, B.M.; Daniel, W.L. Murine arylsulphatase C: evidence for two isozymes. Experientia. 39 (1983) 740-742.
[10] Purohit, A.; Froome, V.A.; Wang, D.Y.; Potter, B.V.; Reed, M.J. Measurement of oestrone sulphatase activity in white blood cells to monitor *in vivo* inhibition of steroid sulphatase activity by oestrone-3-O-sulphamate. J. Steroid Biochem. Mol. Biol. 62 (1997) 45-51.
[11] Pesando, J.M.; Grollman, A.P. Proton magnetic resonance studies of carbonic anhydrase. III. Binding of sulphonamides. Biochemistry 14 (1975) 689-693.
[12] Nogradi, A. The role of carbonic anhydrases in tumors. Am. J. Pathol. 153 (1998) 1-4.

51. Identification of Cancer Tissue by a Combination of FTIR Spectroscopy and PET

T. Richter[1], G. Steiner[1], R. Bergmann, H. Rodig, B. Johannsen, R. Salzer[1]
[1]TU Dresden, Institut für Analytische Chemie

Introduction

Many diseases are caused or at least accompanied by chemical changes in constituents of the cells. Such chemical changes often occur before a disease can be diagnosed, although even the newest bioanalytical methods are often not capable of detecting these changes as early as necessary for successful therapy. One chance to improve the diagnostic capabilities is the combination of bioanalytical methods [1]. One of the promising combinations is based on *in vivo* Positron Emission Tomography (PET) and *ex vivo* FTIR spectroscopy. The great potential of both methods for diagnosing cancer was demonstrated before [2, 3].
Important compounds for *in vivo* cancer diagnostics by PET are 2-[^{18}F]fluoro-2-deoxy-D-glucose ([^{18}F]FDG) and 3-O-methyl-6-[^{18}F]fluoro-dihydroxyphenylalanine ([^{18}F]OMD). The accumulation of both compounds in cancer tissue is based on their enhanced glucose or amino acid metabolism. But non-cancer-specific accumulation of these radiotracers in the surrounding tissue or other organs is also detected. Another restriction on PET in cancer imaging and localization is the lateral resolution of PET, which is restricted to a few millimetres.
But the combination of infrared imaging and *ex-vivo* autoradiography should result in a powerful tool for obtaining images of greater diagnostic value for tissue properties. FTIR imaging was successfully used to study cancer with a spatial resolution down to 20 µm in histological sections [4, 5]. Furthermore by using mid-infrared fibres [6] *in vivo* spectroscopic measurements should be feasible during surgery in tissue localized by PET examination.
For the tissue section studies in this project the common PET modality was favourably substituted by imaging with BAS 2000 high resolution autoradiography (100 µm lateral resolution), which was combined with FTIR mapping of the sections. Tissue sections of mouse muscles were investigated. Some first results of the in-vivo detection of enhanced metabolic activity and the subsequent discrimination between healthy and cancer tissue by FTIR mapping will be demonstrated.

Materials and Methods

All experiments were carried out on mice according to the relevant national regulations. 5 MBq of the lipophilic ^{99m}Tc cation hexakis(2-methoxy-isobutyl-isonitrile)technetium(I), [^{99m}Tc]sestamibi (Cardiolite, Du Pont Pharma GmbH, Bad Homburg, Germany) and 2 MBq of 2-[^{18}F]fluoro-2-deoxy-D-glucose ([^{18}F]FDG) were simultaneously injected into the tail veins of 25 g athymic nude mice bearing a solid tumour from human squamous (FaDu) cells or from human colon adenocarcinoma HT-29 cells. All tumours were smaller than 10 mm in diameter. 30 min after the injection the mice were sacrificed by heart puncture under ether anaesthesia. Selected organs were isolated for weighing and counting. The samples were assayed for gamma radioactivity in a multichannel well-type sodium iodine gamma counter (COBRA II, Packard Instrument Company, Meriden, CT, USA) using two energy windows (^{99m}Tc: 110 - 180 keV and ^{18}F: 450 - 1500 keV). For autoradiography and infrared spectroscopy a 10 µm tissue section was cut from the tissue block. The section was transferred onto a 10 x 10 x 1mm CaF_2 window and air dried.
A Nicolet 5PC FTIR spectrometer (Nicolet, Offenbach, Germany) equipped with an IR microscope (IR-Plan, SpectraTec Ltd, Brichwood, UK) and MCT detector were used to record the infrared spectra. 64 spectra were co-added at 4 cm^{-1} resolution. Infrared maps were generated by an automatic XY stage controlled by the spectrometer. The stage was moved by increments of 90 µm in X and Y directions. At first a background spectrum was recorded from a sample-free area of the CaF_2 window. After every 10 sample spectra a new background was recorded at the same position as the first. Principal component analysis was performed, using the Unscrambler software (Camo, Trondheim, Norway) and the Matlab 5 package (MathWorks Inc. Natric, MA, USA).
For histological characterization one section of the sample was stained with Papanicolaous solutions [7] 1a, 2a and 3a (Merck, Darmstadt, Germany) and dehydrated in an ethanolic Rotihistol solution (Roth, Karlsruhe, Germany). Finally the samples were covered with Rothi-Histokitt (Roth, Karlsruhe, Germany) and overlaid by a thin glass slide. After staining the cell nucleus shows a blue colouring, the cytoplasm of acidophilic cells a pink or red colouring, and the cytoplasm of basophilic cells a bluish-green one. Parallel to the histological characterization the autoradiogram of the non-stained sample was obtained, using a standard imaging plate (BAS MP 2040, Raytest, Straubenhardt, Germany). The sample was scanned at constant time intervals in order to obtain the ^{18}F and ^{99m}Tc radioactivity contri-

butions. A bio-imaging analyzer BAS 2000 (FUJI Photo Film Co, Tokyo, Japan) was used. After an hour the radioactivity levelled off. All data were gathered as a percentage of the injected dose per g tissue (% ID/g tissue).

Results and Discussion

Fig. 1 shows a black-and-white reproduction of an optical micrograph of a section across the tumour and the surrounding tissue. Connective tissue is indicated as a small band between the growing tumour tissue and the muscle cells. The connective tissue region is characterized by an exceedingly high concentration of normal cells due to the growth of the adjacent cancer tissue.

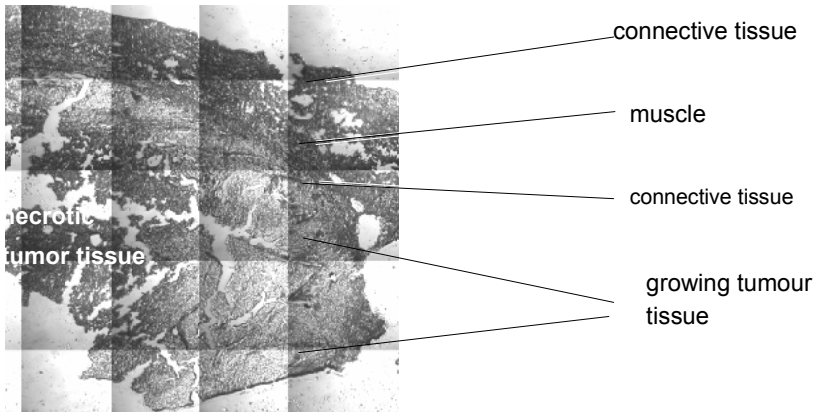

Fig. 1. Black-and-white reproduction of an optical micrograph of a non-stained tissue section.

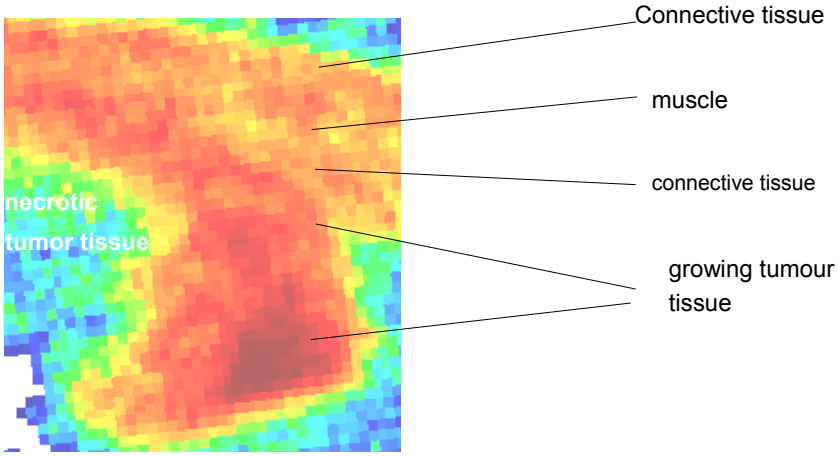

Fig. 2. Autoradiogram of the tissue section adjacent to the sample shown in Fig. 1. Dark colour indicates regions of high radioactivity. The cancer region is highlighted by a surrounding line.

Fig. 2 shows a typical autoradiogram of the FDG distribution in the tissue section. Despite the restricted lateral resolution the autoradiogram clearly renders the morphology of the sample. Areas depicted in dark colour indicate an enhanced metabolism. The growing zone of the tumour is clearly discernible due to its high metabolism. It has to be noted, though, that differences in sample thickness are also reflected in the autoradiogram. Such thickness variations have to be expected for air-dried samples. A greater sample thickness may more or less contribute to the enhanced activity detected in the dark area at the lower centre of Fig. 2. In contrast to the optical micrograph shown in Fig. 1, the PET autoradiogram shown in Fig. 2 does not permit sharp discrimination of the boundary between

cancer tissue and healthy tissue. Two reasons may be responsible for this situation. On the one hand, the cancer grows towards healthy cells, i.e. the healthy is compressed. A higher density of healthy cells per volume unit results, and the autoradiogram indicates enhanced activity for this volume unit. On the other hand, the narrow boundary between tumour tissue and healthy tissue is averaged out due to the limited lateral resolution achieved by the PET method. Whichever of the reasons is the predominant one, the discussion clearly indicates the need for a complementary analytical method, such as FTIR spectroscopy.

After PET autoradiography the samples were mapped by FTIR spectroscopy. Fig. 3a shows an optical micrograph of a non-stained section together with FTIR spectra taken under the microscope. Scanned areas are marked by an overlaid grid. Single spectra were recorded in order to map the complete sample area. Full squares denote regions in which the spectra shown in Fig. 3b originate. These spectra are typical of muscle tissue, connective tissue, and cancer.

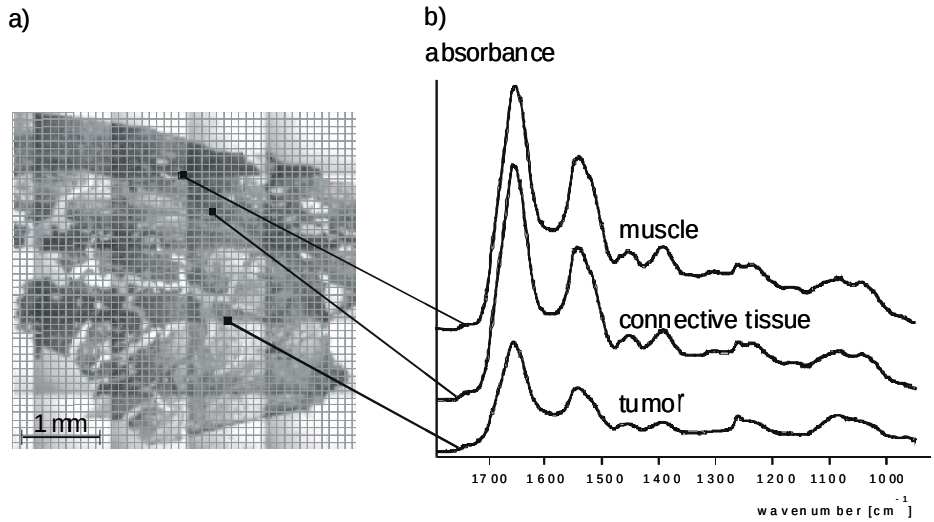

Fig 3. a) Black-and-white reproduction of an optical micrograph of the non-stained tissue section of Fig. 2 together with a measuring grid; b) typical infrared spectra of cancer, connective tissue and muscle (from bottom to top).

The spectra in Fig. 3b are dominated by amide bands (1,650 and 1,540 cm^{-1}). Weaker ν C-H and ν PO_2 bands can be observed between 1,000 and 1,400cm^{-1}. Simple IR maps of the functional group do not yield unambiguous results. In order to improve the utilization of the wealth of information contained in the IR spectra, a principal component analysis (PCA) was carried out. Only the wave number range with the highest information content (fingerprint range) between 1,800 and 950 cm^{-1} was considered so as to ensure an effective data analysis. The first derivatives were calculated from the genuine experimental spectra, then the derivatives were normalized. The best PCA results were obtained by assessing a weight factor of three to the phosphate band region between 1,080 and 1,380 cm^{-1}. The PCA scores were imported into the Matlab software package and finally evaluated as colour code images.

IR Maps of the Tissue Section based on PCA

1st component

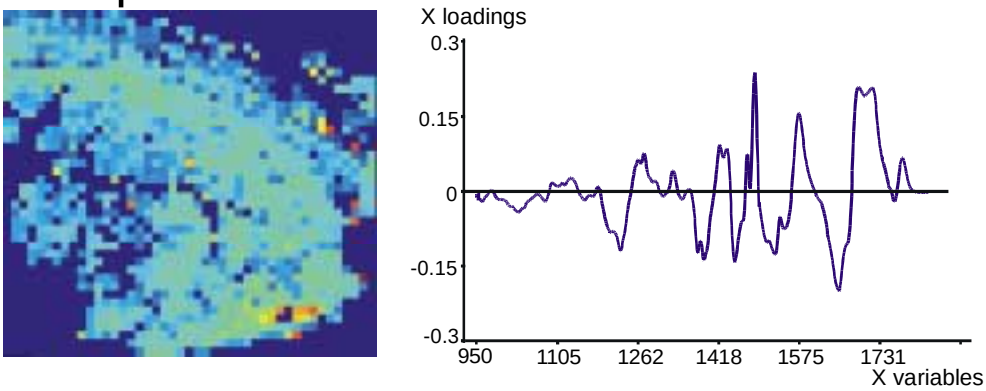

2nd component

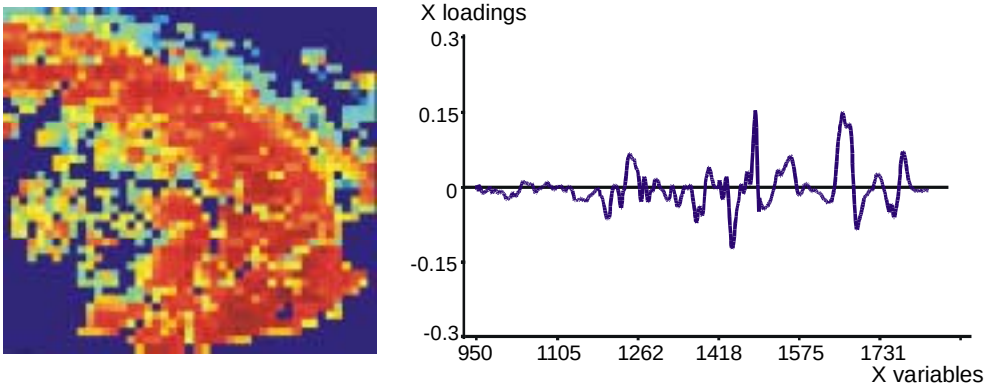

3rd component

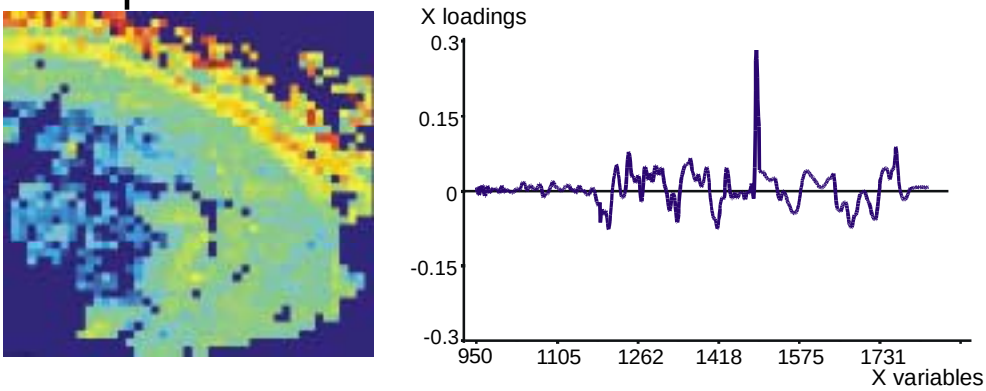

Fig. 4. IR maps of the tissue section in fig. 3and graphs of the PC loadings: a) first, b) second, c) third PC.

Of the 10 computed principal components (PCs) the first three permit a clear discrimination between morphologically different tissue areas. An example is given in Fig. 4. The full information content develops only for images displayed in colour. Grey scale images merely indicate the sample topology and the boundaries between tissue areas.
The first three PCs are given in Fig. 4. Maps are displayed on the left, the corresponding graphs of the PC loading on the right. The first PC mainly depicts the topology of the sample. The second and third PCs reveal very good consistency with the histological results (Fig. 1). Both PCs permit unambiguous discrimination between cancer and healthy tissue. The cancer growing area is particularly well displayed in the second PC, while connective tissue is emphasized by the third PC. The PC evaluation of the biochemical information contained in the FTIR microspectra clearly indicates the different distribution of tumour and healthy tissue across the section. In combination with PET a better demarcation of the tumour should be possible.
This study illustrates how FTIR spectroscopic mapping can support modern bioanalytical methods such as PET in the differentiation of tissue. Spectra in the range of 1,800 – 950 cm^{-1} were measured over a complete tissue section. Using the principal component analysis, chemical maps were evaluated and compared with the autoradiogram of the same tissue section. Fundamental changes from normal to malignant tissue were found in the 2^{nd} and 3^{rd} principal component. In contrast to the autoradiogram a sharp demarcation of tumour tissue was demonstrated. The combination of the two methods promises to improve identification of cancer and to open a new approach to *in vivo* diagnostics.

Acknowledgments

This work was supported by the Sächsischen Staatsministerium für Wissenschaft und Kunst 4-7531.50-03-0370-98/3.

References

[1] Steinberg, F.; Rohrborn, H.J.; Scheufler, K.M.; Asgari, S.; Trost, H.A. ; Seifert, V.; Stolke, D. NIR reflection spectroscopy based oxygen measurements and therapy monitoring in brain tissue and intracranial neoplsms: correlation to MIR and angiography. Exp. Med. Biol. 428 (1997) 553-560.
[2] Rigo, P. Oncological application of positron emission tomography with fluorine-18 fluorodeoxyglucose. Eur. J. Nucl. Med. 23 (1996) 1641-1674.
[3] Jackson, M.; Keith, K.; John, T.; Mansfield, J.R.; Dolenko, B.; Somorjai, R.L.; Orr, W.F.; Watson, P.H.; Mantsch, H.H. Cancer diagnosis by infrared spectroscopy: methodical aspects. Proc. SPIE-Int. Soc. Opt. Eng. 3257 (Infrared Spectroscopy: New Tool in Medicine*)* (1998), pp. 24-34.
[4] Mendelson, R.; Hasankhani, A.; DiCarlo, E.; Boskey, A.L. FT-IR microscopy of endochondral ossification at 20 µm spatial resolution. Calcif. Tissue internat. 44 (1989) 20-29.
[5] Paschalis, E.P.; Jacenko, O.; Olsen, B.R.; Mendelsohn, R.; Boskey, A.L. FT-IR microspectroscopic analysis identifies alternations in mineral properties in bones from mice transgenic for type x collagen. Bone 19 (1996) 151-156.
[6] Afanasyeva, N.; Bruch, R.; Katzir, A. Infrared fiberoptic evanescent wave spectroscopy: applications in biology and medicine. Proc. SPIE-Int. Soc. Opt. Eng. 3596 (Speciality Fiber Optics for Medical Applications) (1999), pp. 152-163.
[7] Burck, H.-C. Histologische Technik (1988) Thieme, Stuttgart.

52. Evaluation of FDG-PET in the Diagnostic Work-up of Patients with Squamous Cell Carcinomas of the Oral Cavitiy

M. Hlawitschka[1], J. Bredow[2], B. Beuthien-Baumann[2], E. Neise[1], U. Eckelt[1], W.-G. Franke[2]
TU Dresden, [1]Klinik und Poliklinik für Mund-Kiefer- und Gesichtschirurgie, [2]Klinik und Poliklinik für Nuklearmedizin, PET-Zentrum Rossendorf

Introduction

For individual treatment planning and prognostic evaluation knowledge of the dimension of the tumour and the lymph node status is mandatory for this tumour entity [1 - 3]. In addition to clinical investigation, tumour staging and the evaluation of cervical lymph nodes in terms of possible metastatic spread is based on magnetic resonance imaging (MRI) and computed tomography (CT) and Ultrasound (US). With CT morphologic tumour representation is often degraded by scatter due to metallic inlays or prothetic restauration, especially in the dental area. In MRI motion artefacts can limit the diagnostic validity concerning tumour localization and extension. The aim of this prospective study was to investigate whether the primary tumour can be better delineated by its metabolic characteristics by FDG-PET than by MRI or CT, and whether lymph node metastases are detected more frequently and with higher accuracy by FDG-PET than by US, CT or MRI.

Patients and Methods

Patients
38 patients (28 males, mean age 59 $\pm$ 11 years and 10 females, mean age 66 $\pm$ 14 years) with biopsy-confirmed squamous cell carcinomas of the oral cavity were evaluated prior to surgical treatment. The preoperative tumour staging included FDG-PET (n = 38), MRI (n = 35), CT (n = 31) and US of the head and neck region (n = 38). All patients were treated by radical tumour resection and cervical lymph node dissection. In 30 patients a cervical lymph node dissection was performed on both sides of the neck, in 8 it was only performed on the side of the primary tumour.
Diagnostic imaging
Sixty min after intravenous injection of 300 MBq ^{18}F-FDG a PET scan in 2D-mode (ECAT EXACT HR+, Siemens/CTI) was performed. The acquisition comprised the area from the inguinal region up to the orbits. Measured attenuation was performed at least in the head and neck region, after implementation of the software, measured attenuation correction of all bed positions and iterative reconstruction of the data was performed. The scans were qualitatively and quantitatively evaluated via standard uptake values (SUVs) of areas suspected to be malignant [4]. A SUV exceeding 2.0 was considered highly suspicious of being malignant.
CT of the head and neck region (Somatom DRH, Siemens) was performed in axial direction in a slice thickness of 5 mm before and after application of intravenous contrast media (Ultravist®).
The MRI scan (Magnetom 1.5 tesla, Siemens) of the head and neck region was performed applying 0.5 mm/0.5 slice thickness in T1 and T2 mode in axial and coronal view. Gadolinium DTPA (Magnevist®) was used as the intravenous contrast medium. The classification of malignant and benign lymph nodes visible in CT or MRI was performed according to the radiological criteria defined by Van den Brekel *et al.* 1990 (axial diameter, grouping, evidence of necrosis, uptake of contrast media). Ultrasound of the head and neck region was performed with a 7.5 MHz transducer and an annular probe (Tosbee). The horizontal and vertical diameters of the lymph node were documented. All lymph nodes detected by ultrasound were classified as being malignant.
Statistics: Sensitivity, specificity, positive and negative predictive value (PPV, NPV) and accuracy were determined for each diagnostic modality, using the two by two frequency table [5]. Statistical evaluation was performed with the software package SPSS for Windows, applying the PearsonChi^2-test for independent examples. A value of $p \leq 0.05$ was defined as being significant.

Results and Discussion

Primary tumour
By CT the visualization of the primary tumour was positive only in 22 of 31 cases. CT was negative for seven T1 and two T2 tumours, resulting in the lowest sensitivity (80 %) of all imaging modalities for the oral cavity (Table 1). The missed tumours were located in the dental area of the alveolar process, the lateral base of the oral cavity or the margin of the tongue.
In contrast to CT, by MRI all primary tumours, except one carcinoma in situ, were visualized, resulting in the highest sensitivity (97 %).

With FDG-PET 35 of 38 primary tumors were correctly identified. Two intermediate differentiated (G2) T1 tumours 6 and 8 mm in diameter in the anterior-lateral base of the oral cavity and the margin of the tongue, as well as one carcinoma located in the retromolar area and derived from a papillary leucoplakia did not show the typical increased FDG uptake. The sensitivity of FDG-PET therefore reached 92%.

Table 1. Detection rate of the primary tumour with FDG-PET, MRI and CT. TP/ FN: true/ false positive/ negative

Imaging modality	TP	FN	Sensitivity (%)
PET	35 / 38	3 / 38	92
MRT	34 / 35	1 / 35	97
CT	22 / 31	9 / 31	80

Cervical lymph node metastases

In 12 of the 38 patients (15 of 68 neck sides) the histopathological work-up of all neck sides revealed 1 to 7 lymph node metastases. Altogether 38 lymph node metastases were histologically detected. The prevalence of lymph node metastases in our group of patients was 22 %.

The results of the morphologic and functional investigations are summarized in Table 2. Four of the 14 neck sides with lymph node metastases were identified by CT, which is a sensitivity of 29 %. With MRI it was possible to detect lymph node metastases in 7 of 13 cases, resulting in a sensitivity of 54 %. Ultrasound, with a sensitivity of 80 % showed a high detection rate. Only 3 neck sides harbouring regional lymph node metastases were missed. FDG-PET identified 14 of 15 neck sides with histologically proven lymph node metastases. Only in 1 patient an ipsilateral lymph node metastasis of a diameter of 4 mm was not detected. The smallest lymph node metastasis, identified by FDG-PET, had a diameter of 6mm. FDG-PET showed the highest sensitivity in the detection of cervical lymph node metastases (93 %).

Table 2. Detection of lymph node metastases with FDG-PET, MRI, CT und US on the basis of histologically investigated neck sides (NS). PPV/NPV: positive/negative predictive value for a prevalence of 22 %.

Imaging modality	NS	Sensitivity %	Specificity %	PPV %	NPV %	Accuracy %
PET	68	93	83	61	98	85
US	68	80	62	38	92	66
MRT	63	54	84	49	87	78
CT	57	29	93	54	82	77

The predictive value of a positive PET result (positive predictive value, PPV) was 61 %. The predictive value of a negative PET result (negative predictive value, NPV) of 98 % was confirmed by histology. With FDG-PET 58 of 68 neck sides were preoperatively correctly classified as being N+ or N-, resulting in an accuracy of 85 %.

In three patients FDG-PET showed additional foci of increased uptake, in 2 patients in the lungs, and in one patient in the area of the epipharynx. One focus in the lung was identified as tuberculosis After biopsy and resection the other two areas were identified as secondary squamous cell carcinomas.

It was shown in this study that FDG-PET can identify tumour-related increases in the glucose metabolism of tumours of the oral cavity with high sensitivity. Concerning the primary tumour, when compared with other imaging modalities, no additional diagnostic gain was established if MRI or CT were of high quality. PET seems to be indicated if the quality of CT and MRI are limited by artefacts. An increase in sensitivity by image fusion of the functional modality PET and the anatomical information by CT/MRI can be expected.

In accordance with most of the results published in the literature [6 - 10](LIT), FDG-PET revealed better results for the detection of cervical lymph node metastases than MRI, CT and US. Due to the high

sensitivity and high negative predictive value of FDG-PET concerning the exclusion of cervical lymph node metastases, a more restrictive attitude towards lymph node surgery might be feasible.
PET, applied in the whole body mode, seems to be the most effective diagnostic tool for the detection of secondary tumours and distant metastases.

References

[1] Snow, G.B.; Annyas, A.A., van Slooten, E.A.; Bartelink, H.; Hart, A. A. Prognostic factors of neck node metastasis. Clin. Otolaryngol. 7 (1982) 185-192.

[2] Grandi, C.; Alloisio, M., Moglia, D., Podrecca, S., Sala, L., Salvatori, P., Molinari, R. Prognostic significance of lymphatic spread in head and neck carcinomas: therapeutic implications. Head Neck Surg. 8 (1985) 67-73.

[3] Sham, J.S.; Choy, D. Prognostic factors of nasopharyngeal carcinoma: a review of 759 patients. Br. J. Radiol. 63 (1990) 51-58.

[4] Reske, S.N.; Bares, R.; Bull, U., Guhlmann, A., Moser, E.; Wannenmacher, M.F. [Clinical value of positron emission tomography (PET) in oncologic questions: results of an interdisciplinary consensus conference. Schirmherrschaft der Deutschen Gesellschaft for Nuklearmedizin]. Nuklearmedizin 35 (1996) 42-52.

[5] Dawson-Saunders, B.; Trapp, R. Basic and clinical biostatistics. East Norwalk: Appleton & Lange, 1990.

[6] McGuirt, W.F., Greven, K., Williams, D. 3rd; Keyes, J.W., Jr.; Watson, N.; Cappellari, J.O., Geisinger, K.R. PET scanning in head and neck oncology: a review. Head Neck. 20 (1998) 208-215.

[7] Paulus, P.; Sambon, A.; Vivegnis, D.; Hustinx, R., Moreau, P.; Collignon, J.; Deneufbourg, J.M.; Rigo, P. ^{18}FDG-PET for the assessment of primary head and neck tumors: clinical, computed tomography, and histopathological correlation in 38 patients. Laryngoscope 108 (1998) 1578-1583.

[8] Laubenbacher, C.; Saumweber, D.; Wagner-Manslau, C.; Kau, R.J., Herz, M.; Avril, N.; Ziegler, S.; Kruschke, C.; Arnold, W.; Schwaiger, M. Comparison of fluorine-18-fluorodeoxyglucose PET, MRI and endoscopy for staging head and neck squamous-cell carcinomas. J. Nucl. Med. 36 (1995) 1747-1757.

[9] Braams, J.W.; Pruim, J.; Freling, N.J.; Nikkels, P.G.; Roodenburg, J.L.; Boering, G.; Vaalburg, W.; Vermey, A. Detection of lymph node metastases of squamous-cell cancer of the head and neck with FDG-PET and MRI. J. Nucl. Med. 36 (1995) 211-216.

[10] Adams, S.; Baum, R.P.; Stuckensen, T.; Bitter, K.; Hor, G. Prospective comparison of ^{18}F-FDG PET with conventional imaging modalities (CT, MRI, US) in lymph node staging of head and neck cancer. Eur. J. Nucl. Med. 25 (1998) 1255-1260.

53. Assessment of 16α-[^{18}F]Fluoro-17β-Estradiol (FES) and 2-[^{18}F]Fluoro-2-Deoxy-D-Glucose (FDG) PET in the Pre-Operative Diagnosis of Breast Cancer

J. Bredow[1], B. Richter[2], B. Beuthien-Baumann[1], J. Römer, F. Füchtner, W. Distler[2], W.-G. Franke[1], B. Johannsen
[1]Klinik und Poliklinik für Nuklearmedizin, [2]Klinik und Poliklinik für Frauenheilkunde und Geburtshilfe, Universitätsklinikum "Carl Gustav Carus" Dresden

Introduction

To estimate the diagnostic value of 2-[^{18}F]fluoro-2-deoxy-D-glucose (FDG) in breast cancer, many studies have been performed until today [1 - 5]. For detection of estrogen-receptor positive tumours with PET, the radiolabelled 16α-[^{18}F]fluoro-17β-estradiol (FES) was developed by KATZENELLEN-BOGEN *et al.* in 1980 [6]. Some first results of the clinical application of this radiotracer were published by MINTUN *et al.* and DEHDASHTI *et al.* [7, 8], who reported a good correlation between the post-operative estrogen-receptor status and the PET findings. Knowledge of the extent of the tumour, its multicentricity, evidence of axillary lymph-node metastases, and estrogen-receptor status is decisive for the planning of the surgical procedure. The purpose of this prospective study is to compare the results of PET with FES and FDG in patients with known breast cancer to validate the agreement between tumour estrogen-receptor status (ER) as determined by FES and to assess the relationship between tumour metabolic activity determined by FDG and tumour ER status.

Materials and Methods

20 patients with suspected breast cancer of the clinical stage cT2 or higher were included in the study. They were randomized and investigated either with FES or FDG. For the PET studies a dedicated PET system (ECAT EXACT HR+, Siemens/CTI, Knoxville, TN) was used. The scanner contained a full-ring system (32 rings, BGO crystals) with a ring diameter of 827 mm. The spatial resolution at 1 cm was 4.0 mm (axial) and 4.2 mm (transaxial). The axial field of view was 15,5 cm. The images consisted of 63 planes of a thickness of 2.46 mm.
In the FES studies the patients were injected with about 222 MBq, and the acquisition of a static study of the axillary and breast region in prone position, using a special cushion, started 90 min p.i. Afterwards a second scan of the wole body was carried out in supine position in 2D mode. A transmission scan for attenuation correction using ^{68}Ga/^{68}Ge rod sources was performed in all studies. Coronal, sagittal and transaxial tomograms were reconstructed, using an iterative algorithm. The image data were visually and semiquantitatively evaluated (ROI technique). In the FDG studies 290 to 370 MBq were administered, and the waiting period p.i. was 60 min; otherwise the acquisition parameters were the same as for FES.
Five patients were investigated in this study with FES and 4 patients with FDG.

Results and Discussion

Table 1. Results of the PET studies in comparison with histological findings (tumour stage, lymph node metastases, estrogen-receptor status)

No.	Diagnosis postoperative	Tracer	PET: T/Ln_{all}	ER [%]	Comparison PET - histological findings				
					T	MC	Ln_{ax}	ER	SUV
1	pT4NxM1G3L1 (MC)	FDG	+/-	0	RP	RP	(FN)*		2.0
2	pT4bN1M1G2	FES	-/-	0	RN	RN	RN	RN	0.2
3	pT2N0M0G2L0V0	FDG	+/-	0	RP	RN	RN		6.8
4	pT2N1M0G3L1 (MC)	FES	+/+	>80	RP	RP	RP	RP	4.3
5	pT2N0M0G2L0V0	FES	+/-	>80	RP	RN	RN	RP	1.5
6	pT4N1M1G3L1	FDG	+/+	20	RP	RP	RP		4.5
7	pT2N0M0 Dcis (MC)	FDG	+/-	0	RP	FN	RN		1.8
8	pT2N1M0L1V1 (MC)	FES	+/-	0	RP	RP	FN	FP	1.6
9	pT4NxM1 (MC)	FES	+/+	>90	RP	RP	(RP)**	RP	7.3

PET: T = tumour detected, Ln_{all} = lymph node metastases in general, MC = multicentricity, Ln_{ax} = axillary lymph node metastases, SUV = standardized uptake value, RN: right negative, RP: right positive FP: false positive, FN: false negative, *not histologically proven; but clinical findings and MRI indicate lymph node metastases, **only tumour biopsy, lymph node metastases not histologically proven.

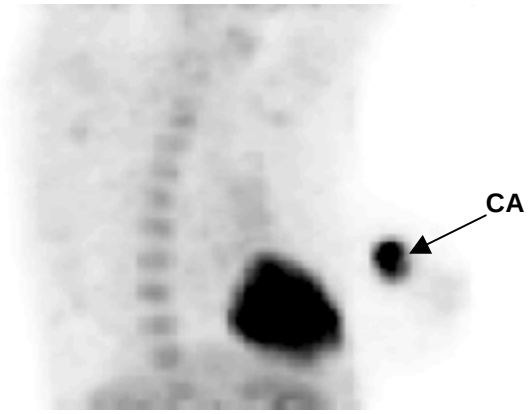

Fig. 1. [^{18}F]FDG PET scan (projection) of a 37 year old woman with clinically suspected breast carcinoma (CA) without lymph node metastases (histologically proven)

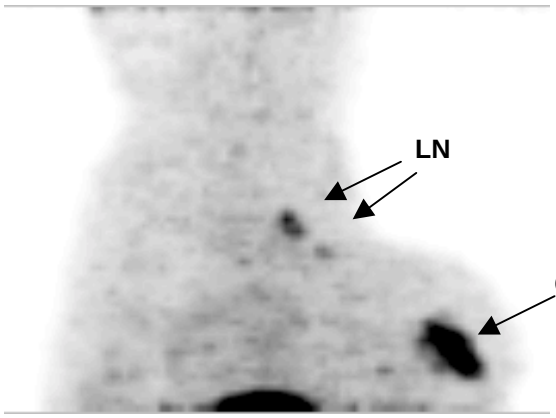

Fig. 2. [^{18}F]FES PET scan (projection) of a 60 year old woman. Multicentric carcinoma (CA) of the right breast with evidence of axillary lymph node metastases (LN) (histologically proven)

The results (Table 1) obtained with both radiotracers were found to correspond as regards the primary tumour and multicentricity. But some false positive and false negative results had to be registered in terms of the detection of axillary lymph node metastases and the estrogen-receptor status, using FES. Our first results indicate the usefulness of FES in the pre-operative diagnosis of breast cancer with PET. To improve the validity, the studies will be continued.

References

[1] Wahl, R.L.; Dody, R.L.; Hutchins, G.D. *et al.* Primary and metastatic breast carcinoma: Initial clinical evaluation with PET with the radiolabeled glucose analogue 2-[F-18]-Fluoro-2-deoxy-D-glucose. Radiology 179 (1991) 765-770.

[2] Nieweg, O.E.; Kim, E.E.; Wong, W.H. *et al.* Positron emission tomography with Fluorine-18-Deoxyglucose in the detection and staging of breast cancer. Cancer 71 (1993) 3920-5.

[3] Dehdashti, F.; Mortimer, J.E.; Sieger, B.A. *et al.* Positron tomographic assessment of estrogen receptors in breast cancer: Comparison with FDG-PET and *in vitro* receptor assays. J. Nucl. Med. 36 (1995) 1766-1774.

[4] Rigo, P.; Paulus, P.; Kaschten, B.J. *et al.* Oncological applications of positron emission tomography with fluorine-18 fluorodeoxyglucose. Eur. J. Nucl. Med. 23 (1996) 1641-1674.

[5] Harris, J.; Morrow, M.; Norton, L. Malignant tumors of the breast. In: DeVita, V.T. Jr.; Hellman, S.; Rosenberg, S.A. (eds.). Cancer. Principles and practice of oncology. Lippincott-Raven. Philadelphia. 1997, pp. 1557-1616.

[6] Katzenellenbogen, J.A.; Carlson, K.E.; Heiman, D.F. *et al.* Receptor-binding radiopharmaceuticals for imaging breast tumors: Estrogen-receptor interactions and selectivity of tissue uptake of halogenated estrogen analogs. J. Nucl. Med. 21 (1980) 550-558.

[7] Mintun, M.A.; Welch, M.J.; Siegel, B.A. *et al.* Breast cancer: PET imaging of estrogen receptors. Radiology 169 (1988) 45-48.

[8] Dehdashti, F.; Mortimer, J.E.; Sieger, B.A. *et al.* Positron tomographic assessment of estrogen receptors in breast cancer: Comparison with FDG-PET and *in vitro* receptor assays. J. Nucl. Med. 36 (1995) 1766-1774.

54. Parametric Imaging of Oncological Brain PET Studies Using [^{18}F]OMFD

R. Hinz, J. Bredow[1]
[1]Department of Nuclear Medicine, Dresden University of Technology

Introduction

As reported before [1], a number of patients suffering from recurrent glioblastoma multiforme after neurosurgical and radiotherapeutic treatment were investigated by the amino acid derivative 3-*O*-methyl-6-[^{18}F]fluoro-L-DOPA ([^{18}F]OMFD). Within an acceptable time after administration, this PET tracer shows a high uptake in the tumour in contrast to normal brain tissue. The aim of this work was to compute parametric images of the volume of distribution of [^{18}F]OMFD in the brain tissue as a possible means of quantitative assessment of the grade of malignancy of the tumour.

Material and Methods

Fig. 1 depicts the general two compartment model for reversible tracers. The assumptions are that the influx of tracer from the blood to the tissue is determined by the rate constant K_1 and that the efflux from the tissue to venous blood can be described by the rate constant k_2. Within the tissue compartment the tracer is neither irreversibly trapped nor metabolised.

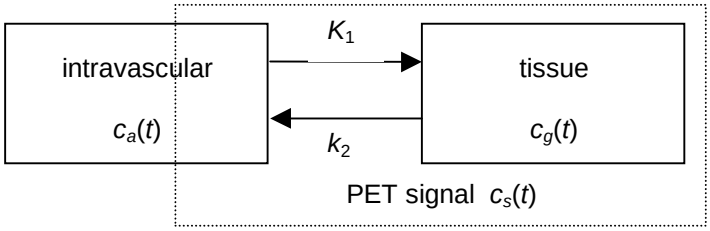

Fig. 1. The compartmental model used to describe the kinetic behaviour of reversible PET radiotracers.

The ordinary differential equation for the description of this single-tissue compartment model is

$$\frac{\mathrm{d}\, c_g(t)}{\mathrm{d}\, t} = K_1 \cdot c_a(t) - k_2 \cdot c_g(t)$$

where

$c_g(t)$ (in Bq·ml^{-1}) denotes the concentration of the activity in the tissue as a function of time t (in s),
$c_a(t)$ (in Bq·ml^{-1}) is the concentration of the activity in the arterial blood,
K_1 (in ml·ml^{-1}·min^{-1}) is the blood to tissue rate constant,
k_2 (in min^{-1}) is the rate constant of the elimination from tissue.

Because of the limited spatial resolution of PET, the measured total PET signal $c_s(t)$ comprises both label in the extravascular tissue, which is a function of $c_a(t)$ as given above, and also label in the vasculature:

$$c_s(t) = (1 - tbv) \cdot c_g(t) + tbv \cdot c_a(t)$$

denoting the vascular volume fraction *tbv* (total blood volume). The above equations are written in terms of decay-corrected variables $c(t)$.

The dynamic PET scans were performed on a high resolution scanner ECAT EXACT HR+ after intravenous injection of 330 MBq [^{18}F]OMFD. 34 frames were acquired within an overall scan time of about 90 minutes. The images were iteratively reconstructed using the Brain Mode of the ECAT 7.2 software (CTI PET Systems, Knoxville, TN, USA). 6 iterations, 16 subsets and a Hanning filter with 4 mm full width at half maximum were chosen.

The arterial input function was obtained from a region of interest (ROI) at the base of the skull from the A. carotis interna. Since the amount of labelled metabolites of [^{18}F]OMFD in the blood is less than 2 per cent, no metabolite correction was applied [2].

Prior to parameter estimation on a pixel-by-pixel basis, the images were smoothed by a three-dimensional Savitzky-Golay filter [3] to reduce noise and to improve the statistical significance of the estimated parameters. The three free parameters K_1, k_2 and *tbv* were estimated for every pixel from a linearised formulation of the model equation, taking the correction for the blood volume in a two-step procedure into account [4].

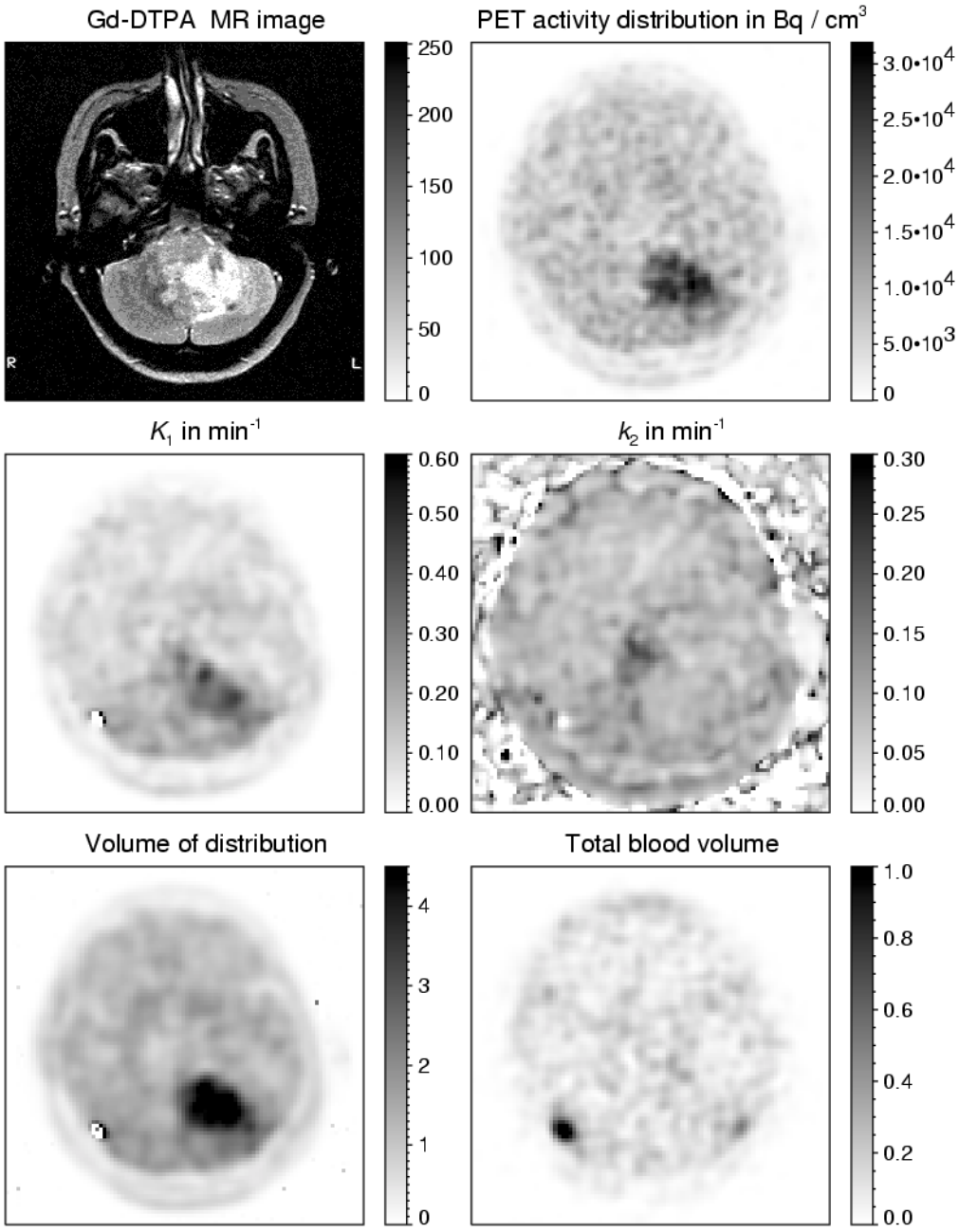

Fig. 2. Transaxial slices of a patient image.

The nuclear magnetic resonance (MR) image after administration of the contrast agent gadolinium diethylenetriaminepentaacetic acid (Gd-DTPA) as a T2-weighted image sequence is to be seen in the top row on the left side. The tumour can be recognised by the enrichment of the contrast agent in the bright region of the cortex. The measured PET activity distribution from a frame 60 minutes after tracer administration is depicted by the top row right image. On account of its high tracer accumulation, the tumour can clearly be detected.

In the central row are the maps of the computed rate constants K_1 and k_2. The values of K_1 are increased in the sector of the occipital cortex. The parametric image of k_2 is relatively noisy and of low contrast. The sinus sigmoideus (venous blood vessel) in the lower left part of the image is represented by a white spot of k_2 values very close to zero.

The same vessel is visible as a dark area in the total blood volume map (bottom right) because it is filled with blood. The volume of distribution image (bottom left) shows a high uptake of tracer in the area of the glioblastoma and a violation of the modelling assumptions at the vessel.

Results and Discussion

In Fig. 2 a representative slice of a computed parametric volume data set is shown. Based on the estimated parameters K_1 and k_2, the volume of distribution V_d is computed by the equation:

$$V_d = K_1 / k_2.$$

This is the ratio of the total tissue volume to the volume occupied by the tracer at equilibrium. It is a virtual volume (the volume the tracer would need to distribute within if it would adopt the same concentration in the tissue as in the blood).
The value of V_d is an indicator of the amino acid transporter activity in the cells. The expression of transporters for neutral amino acids are supposed to be a characteristic feature of tumour cells but not of normal brain tissue. After iterative image reconstruction and generation of parametric images of V_d, the image quality was superior to that of the original dynamic images of the activity distribution. Since the images are visually assessed by the nuclear medicine physician, the parametric images may help to improve the accuracy of diagnosis.

References

[1] Burchert, W.; Beuthien-Baumann, B.; Alheit, H.; Bredow, J.; Steinbach, J.; Johannsen, B.; Franke, W.-G. First results of 3-O-methyl-6-[^{18}F]fluoro-DOPA ([^{18}F]3-OMFD) in patients with glioblastoma multiforme. *Report January 1998 – June 1999*, Institute of Bioinorganic and Radiopharmaceutical Chemistry, FZR-270, pp. 24-25.

[2] Vorwieger, G.; Brust, P.; Bergmann, R.; Bauer, R.; Walter, B.; Füchtner, F.; Steinbach, J.: Metabolism of 6-[^{18}F]fluoro-3-*O*-methyl-L-3,4-dihydroxyphenylalanine in newborn piglets. *Report January 1998 – June 1999*, Institute of Bioinorganic and Radiopharmaceutical Chemistry, FZR-270, pp. 21-23.

[3] Press, W.H.; Teukolsky, S.A.; Vetterling, W.T.; Flannery, B.P. Numerical Recipes in C: The Art of Scientific Computing 2nd ed. Cambridge University Press, 1994, pp. 650-655.

[4] van den Hoff, J. Regionale Quantifizierung myokardialer Funktionsparameter in der Positronen-Emissions-Tomographie. Habilitationsschrift Med. Hochschule Hannover, 1998, pp. 83-86.

BRAIN BIOCHEMISTRY

55. Characterization of [^{11}C]McN5652 in Various Animal Species: Implications for Tracer Development

P. Brust, M. Kretzschmar, J. Zessin, R. Bergmann, A. Friedrich, F. Füchtner, R. Hinz, J. Steinbach

Introduction

Transport systems for neurotransmitters such as the serotonin transporter (SERT) play a key role in synaptic transmission in the brain. Located in presynaptic terminals, they serve to reduce high synaptic cleft concentrations of released neurotransmitters by facilitating re-uptake. Disturbances in this system are thought to contribute to various brain diseases. Reductions in the transporter in various brain regions were observed in the postmortem tissue of patients with Alzheimer´s [1, 2] and Parkinson´s disease [3, 4]. Dysfunction of the SERT has also been implicated in depression [5 - 7], suicidal behaviour [8 - 10] and obsessive compulsive disorders [11, 12].

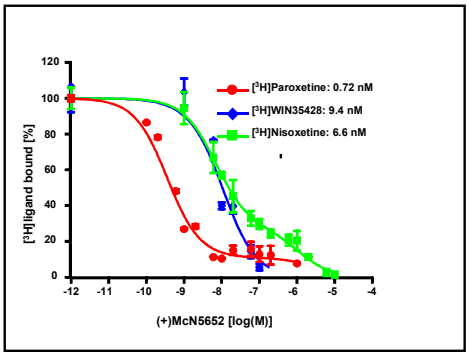

Fig. 1. Binding affinity of (+)McN5652 to SERT, DAT and NET

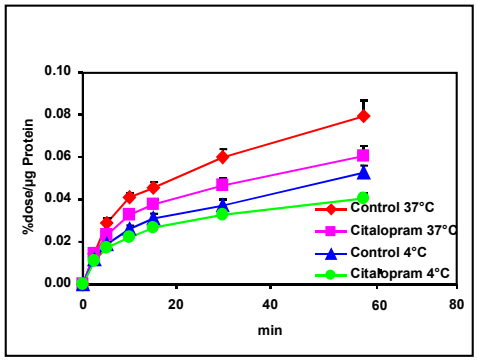

Fig. 2. Uptake of [^{11}C]McN5652 by a human SERT expressing cell line (JAR cells)

The development of suitable radioligands for neroimaging of the SERT in the human brain is therefore important. Most compounds investigated to date had a low specific binding to serotonin uptake sites in the living brain, and the approach to equilibrium binding was often too slow for PET experiments using short-lived isotopes [13 - 15]. [^{11}C](+)McN5652 is the only PET radioligand available for clinical use [16, 17]. But this compound is not optimal because of its rather slow kinetics and high non-specific binding in the human brain [14]. For evaluation of further radioligands in animal experiments a comparison with [^{11}C](+)McN5652 is recommended. We therefore studied the binding and distribution of [^{11}C](+)McN5652 in various animal species.

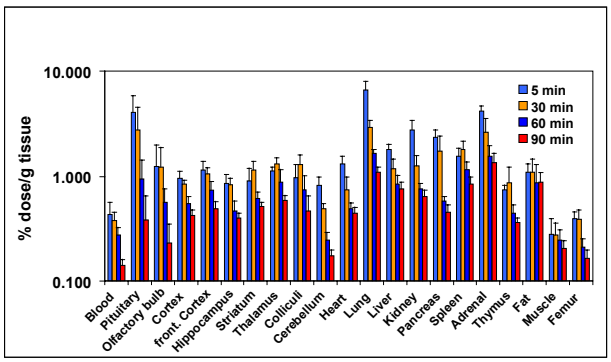

Fig. 3. Distribution of [^{11}C]McN5652 in rats

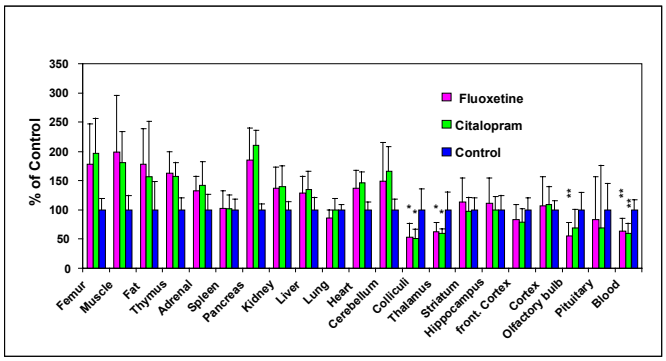

Fig. 4. Inhibition of [^{11}C]McN5652 binding *in vivo* (60 min. p.i.)

Material and Methods

The *in-vitro* binding of [^{11}C](+)McN5652 was studied on tissue homogenates and slices of rat and porcine brain and on the SERT-expressing human placental cell line JAR. The *in-vivo* binding of [^{11}C](+)McN5652 was investigated in rats, mice and pigs. 35 Wistar rats (age: 8 weeks) were injected with 20 MBq [^{11}C](+)McN5652 and sacrificed 5, 30, 60, or 90 min p.i. Eleven rats were additionally treated with 5 mg/kg i.v. fluoxetine or citalopram 5 min before the tracer injection. Six mice were injected with 80 - 200 MBq [^{11}C](+)McN5652 and sacrificed 60 min p.i. The brains were quickly removed and frozen for autoradiography. Three six-week-old farm-bred female pigs were studied with PET (31 frames, 120 min) under general anesthesia (0.5 - 0.75 % isoflurane in N_2O/O_2. Forty-six to forty-eight arterial blood samples were obtained at defined time points. Additional arterial samples were withdrawn for detection of metabolites, using thin-layer chromatography. A three-compartment model was used to analyse the transport and binding of [^{11}C](+)McN5652 in the brain. The distribution of radioactivity occurs between the intravascular space (compartment 1), the extravascular pool of the free ligand (compartment 2) and extravascular pool of the bound ligand (compartment 3). The transfer constants K_1 and k_2 describe the blood-brain and brain-blood transfer of [^{11}C](+)McN5652. The rate constants k_3 and k_4 describe the reversible binding of [^{11}C](+)McN5652 to the serotonin transporter.

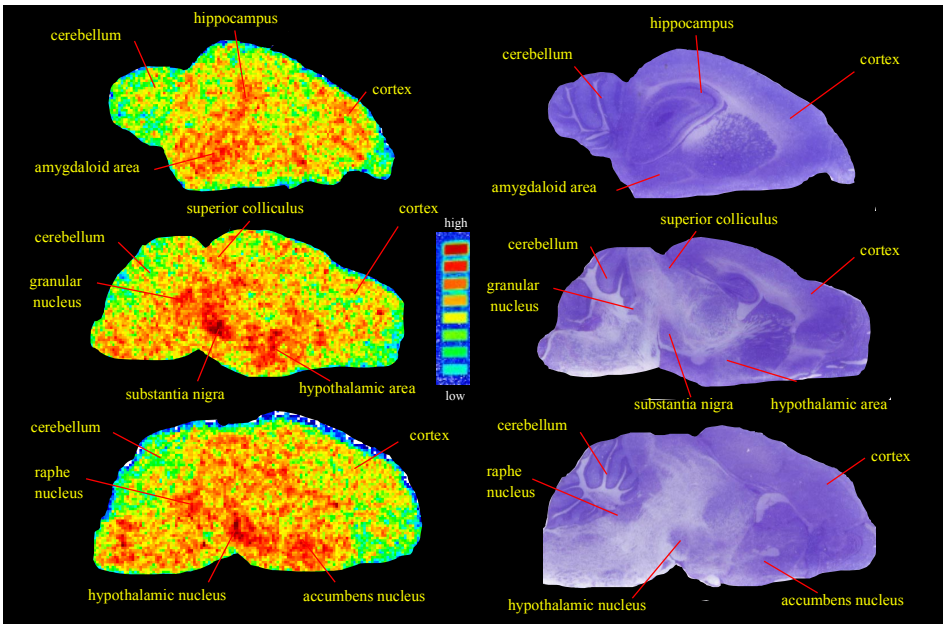

Fig. 5. Binding of [^{11}C]McN5652 in mouse brain 60 min after i. v. application . Left radioluminogram, centre radioactivity standard, right histological image of the corresponding section.

Results

Evidence of a significant binding of [^{11}C](+)McN5652 not only to SERT (IC_{50} = 0.72 nM) but also to the norepinephrine (NET) and dopamine transporters (DAT) was found *in vitro*. IC_{50} values of 6.6 and 9.4 nM for NET and DAT were measured (Fig. 1). SERT-expressing JAR cells were used to study the mechanism of the cellular uptake of [^{11}C](+)McN5652 (Fig. 2).

The nonspecific uptake (defined by 10 µM citalopram) was 76 %, which is close to the values measured at 4 ^{o}C (66 %). The same reduction in [^{11}C](+)McN5652 "uptake" was found at 37 ^{o}C (24 %) and 4 ^{o}C (23 %), indicating that this fraction represents binding to SERT rather than uptake by the SERT.

In rats a high brain uptake was found, with the highest values measured in the thalamus, colliculi and olfactory bulb (~1.3 % g^{-1}). Only in these regions and in the striatum the uptake increased between 5 and 30 min p.i. (Fig. 3). A significant inhibition (38 – 48 %) by fluoxetine and citalopram was found in the thalamus, colliculi and olfactory bulb but not in the striatum (Fig. 4). It is therefore assumed that the high striatal uptake is a result of the binding to the DAT. Similar results were obtained by autoradiography in mice (Fig. 5). The highest binding was observed in the substantia nigra and the thalamus.

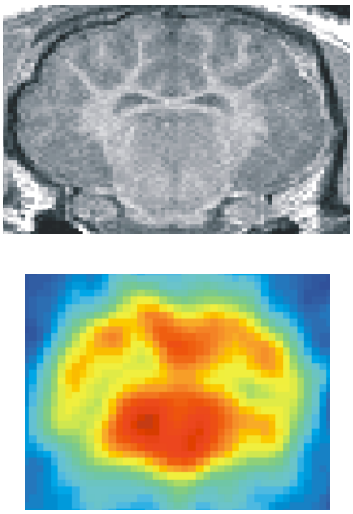

Fig. 6. MRI and corresponding PET image of porcine brain after injection of [^{11}C]McN5652

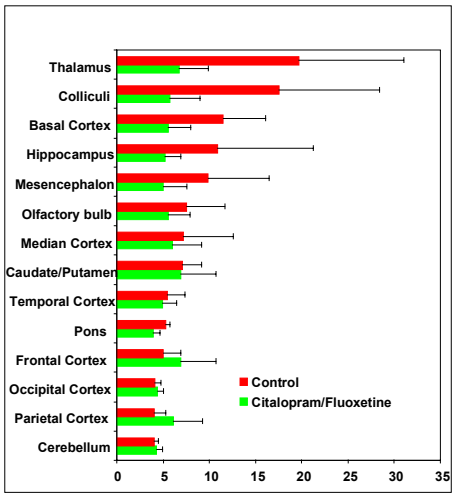

Fig. 7. Binding potential of [^{11}C]McN5652 in porcine brain

After 60 min the ratio thalamus:cerebellum was 3.2 in mice as compared to 3.6 in rats. The PET data obtained from pigs revealed a high blood-brain transfer of [^{11}C](+)McN5652 (K_1: 0.22-0.43 ml g^{-1} min^{-1}) (Table 1). The initial brain uptake is thus assumed to depend on the blood flow. A significant binding of [^{11}C](+)McN5652 was observed in all brain regions studied (k_3: 0.018 - 0.044 min^{-1}). The highest binding potential was found in thalamus and colliculi (Fig. 7). Pre-injection of citalopram or fluoxetine reduced k_3 by 30 to 70 % (Fig. 8). A rapid metabolism of the tracer was also observed. More than 50 % metabolites were found 12 min p.i. (Fig. 9).

Table 1. Transfer coefficients of [^{11}C]McN5652 in various regions of the porcine brain

Region	K_1 (ml g^{-1} min^{-1})	k_2 (min^{-1})	k_3 (min^{-1})	k_4 (min^{-1})
Thalamus	0.3813	0.0326	0.0343	0.0025
Colliculi	0.3264	0.0311	0.0289	0.0025
Basal Cortex	0.3367	0.0352	0.0374	0.0038
Hippocampus	0.3090	0.0349	0.0269	0.0033
Mesencephalon	0.3146	0.0313	0.0435	0.0039
Olfactory Bulb	0.3731	0.0421	0.0300	0.0036
Caudate/Putamen	0.3819	0.0385	0.0287	0.0043
Pons	0.2219	0.0256	0.0314	0.0040
Frontal Cortex	0.4274	0.0425	0.0204	0.0032
Occipital Cortex	0.2821	0.0370	0.0195	0.0038
Cerebellum	0.2870	0.0378	0.0317	0.0062

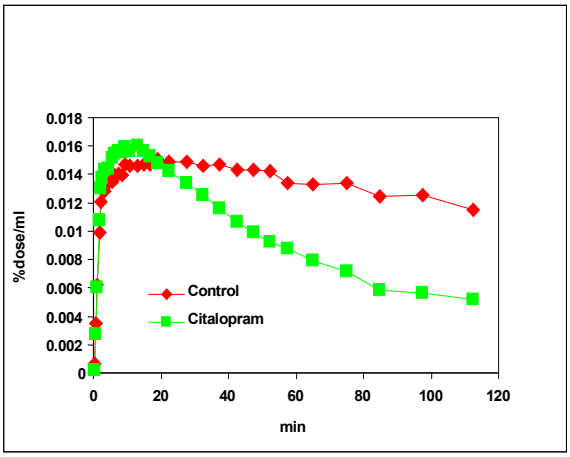

Fig. 8. Kinetics of [^{11}C]McN5652 in the porcine thalamus

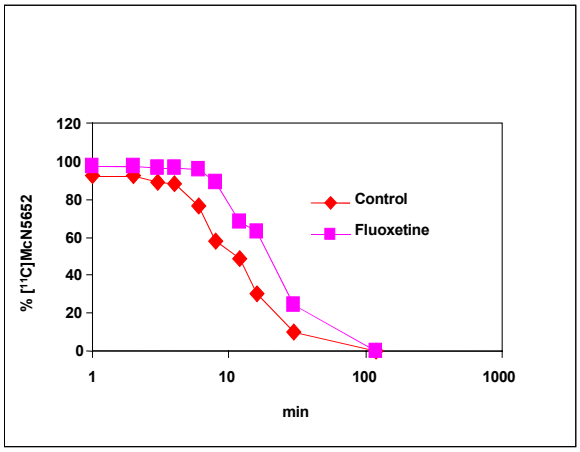

Fig. 9. Metabolism of [^{11}C]McN5652 in the porcine plasma

Discussion

[^{11}C]McN5652 was introduced as a new radioligand for PET to selectively label the SERT *in vivo* [18 - 20]. It has a high binding potency for the SERT. Its (+) optical/trans geometrical isomer has a sub-nanomolar inhibitory constant for the synaptosomal 5-HT uptake (K_i = 0.40 nM) [101, 102]. The potency of (+)McN5652 is similar to that of paroxetine and sertraline, two high affinity ligands for the SERT. It is the only PET radioligand that is so far available for clinical use [16, 17]. But the complicated chemistry of the compound restricts its use among PET facilities. The kinetics of the uptake into the human brain is rather slow and a correction for non-specific binding using [^{11}C](-)McN5652 is necessary for good quantification. There is therefore still a need for the development of other radioligands for SERT imaging, for which [^{11}C](-)McN5652 may be used as a reference. In this study the binding and distribution of [^{11}C](-)McN5652 was investigated in various animal species: mice, rats and pigs. The *in vitro* and *in vivo* studies in these species proved to be highly consistent. The data revealed a displaceable binding in target regions with the highest SERT density but also a significant binding potential in other regions, such as the caudate/putamen, which is not reduced by SERT inhibitors. This may be due to binding to other targets, such as the NET and DAT. The location of serotonin uptake sites in the porcine brain appears to be similar to that found in rats and mice [this presentation, 19], which makes pigs a suitable animal model for the development of radioligands for studying serotonergic functions with PET as was recently suggested [21].

References

[1] D'Amato, R.J.; Zweig, R.M.; Whitehouse, P.J.; Wenk, G.L.; Singer, H.S.; Mayeux, R.; Price, D.L.; Snyder, S.H. Aminergic systems in Alzheimer's disease and Parkinson's disease. Ann. Neurol. 22 (1982) 229-236.

[2] Chessell, I.P.; Francis, P.T.; Webster, M.T.; Procter, A.W.; Heath, P.R.; Pearson, R.C.; Bowen, D.M. An aspect of Alzheimer neuropathology after suicide transport damage. J. Neural. Transm. Suppl. 44 (1994) 231-243.

[3] Cash, R.; Raisman, R.; Ploska, A.; Agid, Y. High and low affinity [^{3}H]imipramine binding sites in control and parkinsonian brains. Eur. J. Pharmacol. 117 (1985) 71-80.

[4] Raisman, R.; Cash, R.; Agid, Y. Parkinson's disease: decreased density of ^{3}H-imipramine and ^{3}H-paroxetine binding sites in putamen. Neurology 36 (1986) 556-560.

[5] Fritze, J.; Deckert, J.; Lanczik, M.; Strik, W.; Struck, M.; Wodarz, N. Status of amine hypotheses in depressive disorders. Nervenarzt 63 (1992) 3-13.

[6] Bourin, M.; Baker, G.B. The future of antidepressants. Biomed. Pharmacother. 50 (1996) 7-12.

[7] Lesch K.P.; Gross J.; Franzek E.; Wolozin B.L.; Riederer P.; Murphy D.L. Primary structure of the serotonin transporter in unipolar depression and bipolar disorder. Biol. Psychiatry 37 (1995) 215-223.

[8] Collier, D.A.; Stober, G.; Li, T.; Heils, A.; Catalano, M.; Di Bella, D.; Arranz, M.J.; Murray, R.M.; Vallada, H.P.; Bengel, D.; Muller, C.R.; Roberts, G.W.; Smeraldi, E.; Kirov, G.; Sham, P.; Lesch,

K.P. A novel functional polymorphism within the promoter of the serotonin transporter gene: possible role in susceptibility to affective disorders. Mol. Psychiatry 1 (1996) 453-460.
[9[Kasper, S.; Schindler, S.; Neumeister, A. Risk of suicide in depression and its implication for psychopharmacological treatment. Int. Clin. Psychopharmacol. 11 (1996) 71-79.
[10] Mann, J.J.; Henteleff, R.A.; Lagattuta, T.F.; Perper, J.A.; Li, S., Arango, V. Lower ^{3}H-paroxetine binding in cerebral cortex of suicide victims is partly due to fewer high affinity, non-transporter sites. J. Neural. Transm. 103 (1996) 1337-1350.
[11] Klein, D.F. Pharmacotherapy of obsessive-compulsive disorder. Encephale 16 (1990) 331-334.
[12] Insel, T.R.; Zohar, J.; Benkelfat, C.; Murphy, D.L. Serotonin in obsessions, compulsions, and the control of aggressive impulses. Ann. N. Y. Acad. Sci. 600 (1990) 574-585
[13] Cumming, P.; Gjedde, A. Kinetics of the uptake of [^{3}H]paroxetine in the rat. Synapse 15 (1993) 134-39.
[14] Brust, P.; Scheffel, U.; Szabo, Z. Radioligands for the study of the 5-HT transporter *in vivo*. IDrugs 2 (1999) 129-145.
[15] Pike, V.W. Positron-emitting radioligands for studies *in vivo* – probes for human psychopharmacology. J. Psychopharmacol. 7 (1993) 139-158.
[16] Szabo, Z.; Kao, P.F.; Mathews, W.B.; Ravert, H.T.; Musachio, J.L.; Scheffel, U.; Dannals, R.F. Positron emission tomography of 5-HT reuptake sites in the human brain with C-11 McN5652 extraction of characteristic images by artificial neural network analysis. Behav. Brain Res. 73 (1996) 221-224.
[17] Szabo, Z.; Scheffel, U.; Mathews, W.B.; Ravert, H.T.; Szabo, K.; Kraut, M.; Palmon, S.; Ricaurte, G.A.; Dannals, R.F. Kinetic analysis of [^{11}C]McN5652: a serotonin transporter radioligand. J. Cereb. Blood Flow Metab. 19 (1999) 967-981.
[18] Suehiro, M.; Scheffel, U.; Dannals, R.F.; Ravert, H.T.; Ricaurte, G.A.; Wagner, H.N. Jr. A PET radiotracer for studying serotonin uptake sites: carbon-11-McN-5652Z. J. Nucl. Med. 34 (1993) 120-127.
[19] Suehiro, M.; Scheffel, U.; Ravert, H.T.; Dannals, R.F.; Wagner, H.N. Jr. [^{11}C](+)McN5652 as a radiotracer for imaging serotonin uptake sites with PET. Life Sci. 53 (1993) 883-892.
[20] Suehiro, M.; Ravert, H.T.; Dannals, R.F.; Scheffel, U.; Wagner, H.N. Jr. Synthesis of a radiotracer for studying serotonin uptake sites with positron emission tomography: ^{11}C-McN-5652. J. Lab. Compds. Radiopharm. 31(1992) 841-848.
[21] Smith, D.F.; Jensen, P.N.; Gee, A.D.; Hansen, S.B.; Danielsen, E.; Andersen, F.; Saiz, P.A.; Gjedde, A. PET neuroimaging with [^{11}C]venlafaxine: serotonin uptake inhibition, biodistribution and binding in living pig brain. Eur. Neuropsychopharmacology 7 (1997) 195-200.
[22] Cumming, P.; Kretzschmar, M.; Brust, P.; Smith, D.F. Quantitative radioluminography of serotonin uptake sites in the porcine brain. Synapse (in press).

56. Ex-Vivo Autoradiographic Studies to Investigate the Pharmacological Specificity and Selectivity of [^{99m}Tc]TRODAT Binding in the Rat Brain

M. Kretzschmar, I. Heimbold, S. Seifert, P. Brust

Introduction

The ^{99m}Tc-labelled tropane derivative [^{99m}Tc] TRODAT was successfully introduced by Kung *et al.* [1] for imaging cerebral dopamine transporters (DAT) [2 – 6] . The goal of our studies was to map and verify the specific and selective regional brain distribution of the compound in the rat by ex-vivo autoradiography.

Experimental

Five male rats (weight 150 – 170 g) were intravenously injected with 0.5 ml of a saline solution containing 27 – 47 MBq [^{99m}Tc]TRODAT-1. The radiotracer was prepared by reduction of 2.0 ml (500 MBq) of pertechnetate eluate with 20 µl $SnCl_2$ (1.5 mg $SnCl_2$ dissolved in 5 ml 0.1 N HCl) in a solution of 1.0 ml of propylene glycol, 0.2 ml of 0.1 N NaOH and 1.0 mg TRODAT dissolved in 0.2 ml of ethanol [7]. Sixty minutes after the injection the animals were sacrificed by CO_2 inhalation. The brains were rapidly removed and immediately frozen by immersion in a 2-methylbutane / dry ice solution at -70 ^{0}C. Before cutting , the frozen brains were weighed and the radioactivity concentration was determined , using an automated γ counter (Capintec-15-R). Then the stage-mounted brains were cut in a cryocut microtome into 40 µm horizontal and sagittal sections, thaw–mounted on microscope slides , and dried under a continuous air stream for about 2 min.
The blocking studies were carried out by pretreating the rat with GBR 12909 (5 mg/kg i.v.) or citalopram (5 mg/kg i.v.) 5 min prior to the tracer injection .
For radioluminography the slides containing the brain sections were apposed to imaging plates in an autoradiographic cassette for approximately 24 h and scanned in the bio-imaging analyser BAS 2000 (FUJI photo film Co,Tokyo). The quantitative analysis of the in-vivo distribution was carried out with the AIDA program (Raytest, Straubenhardt).

Results and Discussion

Figs. 1 – 3 illustrate the distribution of [^{99m}Tc] TRODAT-1 in the rat brain. The highest tracer accumulation was found in the striatum and in the ventricles (0.12 % D/g) followed by the pyramidal cell layer of the hippocampus (0.06 % D/g tissue). Pretreatment of the rats with GBR 12909, a dopamine transporter ligand, diminished the uptake only in the striatum but not in the pyramidal cell layer and ventricles, i.e. in regions which do not express DAT.

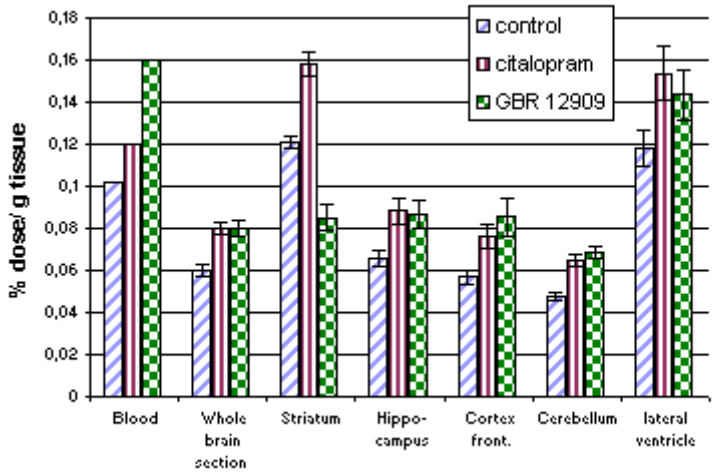

Fig. 1. Effect of pretreatment with citalopram and GBR 12909 on the distribution and regional brain uptake of [^{99m}Tc]TRODAT-1 in rats 60 min after the injection (% D/g tissue).

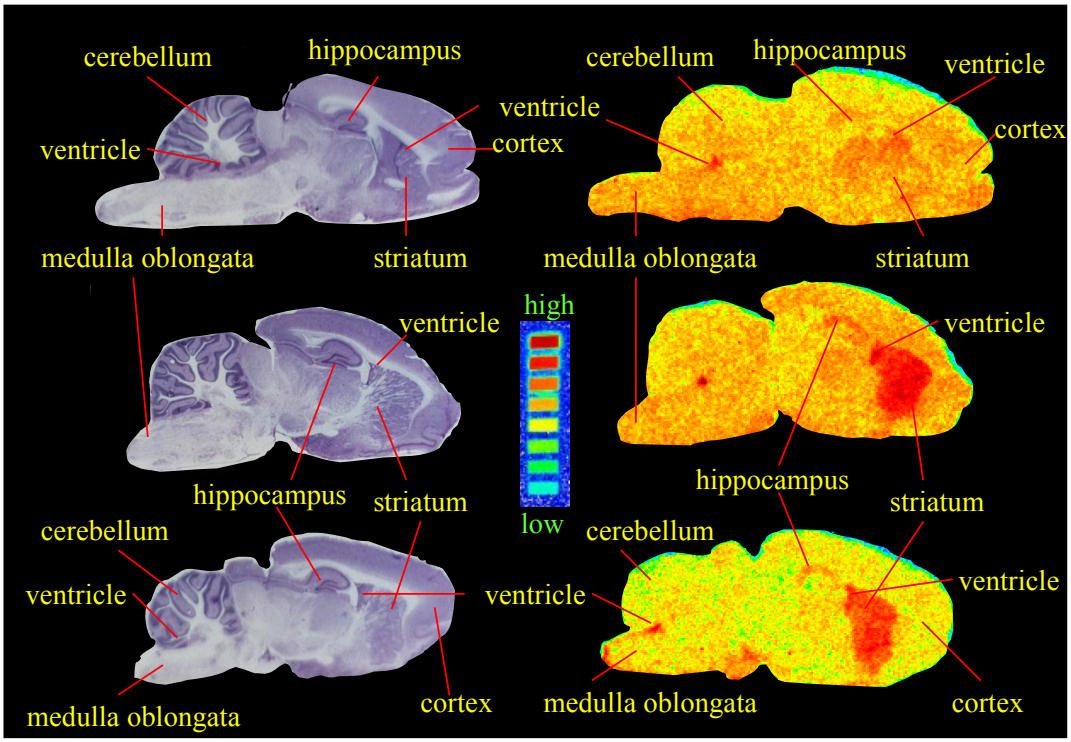

Fig. 2. Ex-vivo autoradiogram (right) radioactivity standard and corresponding histological image (left) of sagittal brain sections of rats 60 min after i.v. application of [^{99m}Tc]TRODAT-1, after pretreatment with isotonic saline (below) and with citalopram (middle) and GBR 12909 (above)

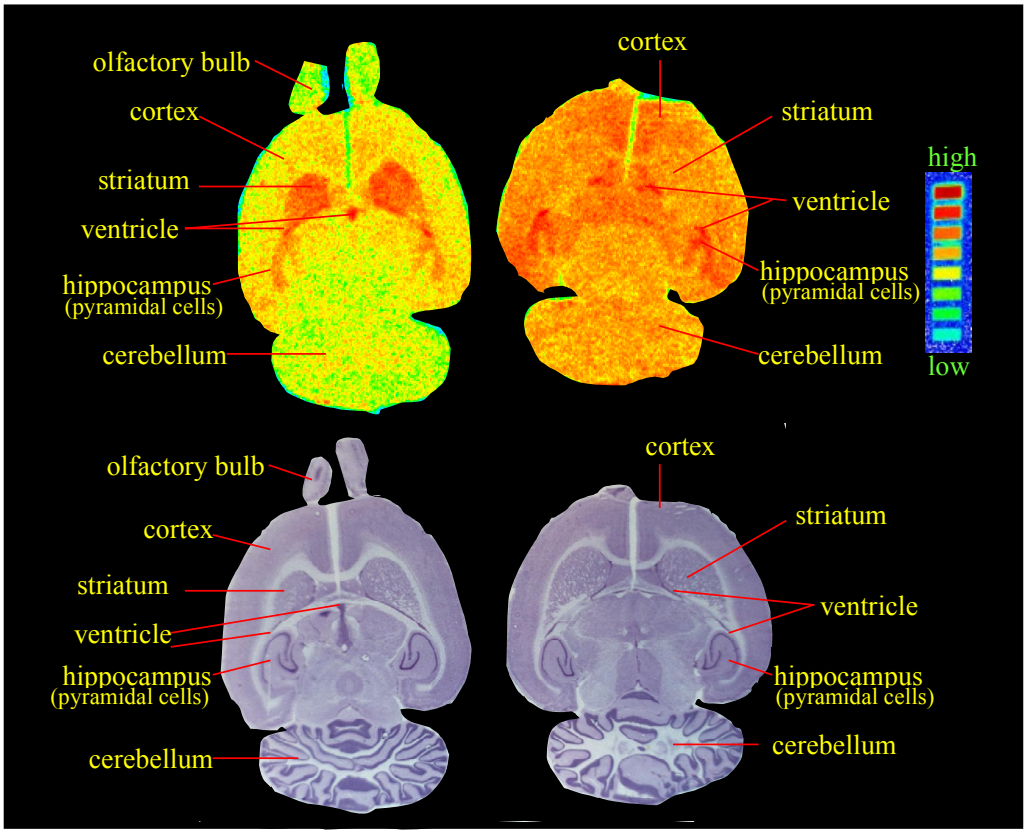

Fig. 3. Ex-vivo autoradiogram (above) radioactivity standard and corresponding histological image (below) of horizontal brain sections of rats 60 min after i.v. application of [^{99m}Tc]TRODAT-1, after pretreatment with isotonic saline (left) and with GBR 12909 (right)

An increased uptake was observed in all other structures of the brain after administration of GBR 12909. The administration of citalopram, a potent serotonin transporter ligand , did not compete with the [^{99m}Tc]TRODAT-1 uptake in several brain regions. An increased uptake of the compound was observed in the whole brain.
To sum up, we can say that our findings are consistent with those previously reported by Kung and coworkers [1]. [^{99m}Tc]TRODAT-1 accumulates selectively and specifically in the striatum, a region which expresses the dopamine transporter. The striatum to cerebellum ratio was 2.5. However, a significant affinity of [^{99m}Tc]TRODAT-1 to the 5-HT transporter was not demonstrable in our experiments, while Dresel *et al.* clearly showed the capacity of the tracer for imaging also the 5-HT transporter in their baboon studies [8]. The pretreatment with ligands of DAT and 5-HT transporters resulted in an increased uptake of [^{99m}Tc]TRODAT-1 in all nontarget regions of the brain, probably in consequence of a blockade of metabolizing enzymes.
In this study we used the method of radioluminography instead of the traditional photofilm autoradiography. It provides the same quality of images with only 10 % of the injected dose.

References

[1] Kung, M.P.; Stevenson, D.A.; Plössl, K.; Meegalla, S.K.; Beckwith, A.; Essman, W.D.; Mu, M.; Lucki, I.; Kung, H.F. [^{99m}Tc]TRODAT-1: a novel technetium-99m complex as a dopamine transporter imaging agent. Eur. J. Nucl. Med. 24 (1997) 372 – 380.

[2] Dresel, S.; Kung, M.-P.; Huang, X.-F.; Plössl, K.; Hou, C.; Meegalla, S.K.; Patselas, G.; Mu, M.; Saffer, J.R.; Kung, H.F. Simultaneous SPECT studies of pre- and postsynaptic dopamine binding sites in baboons. J. Nucl. Med. 40 (1999) 600 – 666.

[3] Kung, H.F.; Kim, H.J.; Kung, M.-P.; Meegalla, S.K.; Plössl, K.; Lee, H.-K. Imaging of dopamine transporters in humans with technetium 99m TRODAT-1. Eur. J. Nucl. Med. 23 (1996) 1527–1530.

[4] Meegalla, S.K.; Plössl, K.; Kung, M.-P.; Chumpradit, S.; Stevenson, D.A.; Kushner, S.A.; McElgin, W.T.; Mozley, P.D.; Kung, H.F. Synthesis and characterization of technetium-99m labeled tropanes as dopamine transporter-imaging agents. J. Med. Chem. 40 (1997) 9-17.

[5] Mozley, D.P.; Schneider, J.S.; Acton, P.D.; Plössl, K.; Stern, M.B.; Siderowf, A.; Leopold, N.A.; Li, P.Y.; Alavi, A.; Kung, H.F. Binding of [^{99m}Tc] TRODAT-1 to dopamine transporters in patients with Parkinson`s disease and in healthy volunteers. J. Nucl. Med. 41 (2000) 584 – 589.

[6] Mozley, P.D.; Stubbs, J.B.; Plössl, K.; Dresel, S.H.; Barraclough, E.D.; Alavi, A.; Araujo, L.I.; Kung, H.F. The biodistribution and dosimetry of a [Tc- 99m] tropane for imaging dopamine transporters. J. Nucl. Med. 39 (1998) 2069 – 2076.

[7] Heimbold, I.; Hoepping, A.; Seifert, S. Investigations for an improved synthesis of TRODAT. *Report January 1998 – June 1999*, Institute of Bioinorganic and Radiopharmaceutical Chemistry, FZR- 270, pp. 104 – 106.

[8] Dresel, S.; Kung, M.-P.; Huang, X.F.; Plössl, K.; Hou, C.; Shiue, C.; Karp, J.; Kung, H.F. SPECT imaging using [Tc-99m]Trodat-1: in vivo binding to the serotonin transporter. Joint Congress of European Association of Nuclear Medicine and the World Federation of Nuclear Medicine and Biology, Berlin, 30.08.-04.09.1998.

57. Intrauterine Growth Restriction Induces Upregulation of Cerebral Aromatic Amino Acid Decarboxylase Activity in Newborn Piglets

P. Brust, R. Bauer[1], B. Walter[1], R. Bergmann, G. Vorwieger, E. El-Hallag[1], A. Fritz[1], R. Hinz, F. Füchtner, J. Steinbach, U. Zwiener[1]
[1]Institute of Pathophysiology, Friedrich Schiller University Jena

Introduction

The importance of the intrauterine environment for the fetal brain development was revealed by studies showing persistent behavioral abnormalities in prenatally stressed animals [1]. Inadequate nutritional supply, mainly due to uteroplacental insufficiency or restricted maternal protein intake in the late gestation period, is mostly responsible for asymmetrical intrauterine growth restriction (IUGR) [2]. The immature dopaminergic system appears to be sensitive to inadequate prenatal nutritional supply followed by IUGR in offspring, because the dopamine content of the brainstem of fetal IUGR guinea-pigs is increased despite an unchanged oxygen delivery [3], and an altered dopamine release persists in IUGR born rats after maternal protein malnutrition [4]. This is suggested to contribute to etiological factors of the attention deficit hyperactivity disorder, a highly prevalent neurodevelopmental disorder with a prefrontal [5 - 7] and nigrostriatal [8, 9] dysfunction. However, the effects of IUGR on regional in-vivo brain dopamine metabolism have not yet been determined. We therefore determined the AADC activity, the ultimate enzyme in the dopamine synthesis as well as the regional cerebral blood flow (CBF), the brain tissue PO_2 and the cerebral metabolic rate of oxygen ($CMRO_2$) in newborn normal weight (NW) and IUGR piglets. We used a morphometrically well-characterized state of asymmetrical intrauterine growth restriction in newborn piglets [10] and included animals with optimal vital conditions early after birth [11]. We postulated that IUGR may activate the brain dopamine turnover.

Table 1. Organ weights of newborn piglets following normal growth and intrauterine growth restriction.

	NW piglets n = 10	IUGR piglets n = 10
Body weight (g)	2142 ± 373	908 ± 109 &
Brain weight (g)	36 ± 2	30 ± 1 &
Liver weight (g)	63 ± 15	22 ± 5 &
Brain/liver ratio	0.61 ± 0.16	1.42 ± 0.24 &

Values are presented as mean ± SD; & P < 0.01, comparison between normal weight (NW) newborn piglets andd intrauterine growth restricted (IUGR) ones.

Material and Methods

The animal experiments were performed according to the German Law on the Protection of Animals. The study was approved by the Saxon State Government Committee for Animal Research (75-9185.81-4.6/95). Methods are described in detail elsewhere [12, 13].

Results

In IUGR piglets the body weight was significantly reduced (42 % of NW group; Table 1). The naturally occurring growth restriction in pigs is asymmetrical with an increase in the mean ratio of the brain weight to the liver weight from 0.61 ± 0.16 to 1.42 ± 0.24 (P < 0.01). The reduction in brain weight was quite small (83 % of NW group). By contrast, the decrease in liver weight (35 % of NW group) was similar to that in body weight (42 % of NW group). All differences in organ weights were significant (P < 0.01).
The physiological values measured for newborn NW and IUGR piglets were consistent with other data obtained from mildly anaesthetized and artificially ventilated newborn piglets [14, 15]. The arterial blood pressure, the heart rate, and the arterial glucose content were slightly but significantly lower in IUGR piglets (P < 0.05). Other physiological values obtained, such as the $CMRO_2$, the brain tissue PO_2, and the regional CBF, were similar in NW and IUGR piglets (data not shown). But the regional CBF distribution showed marked differences. The mesencephalic and cerebellar blood flow in NW and IUGR piglets was increased compared with the forebrain structures (Fig. 1, P < 0.05).

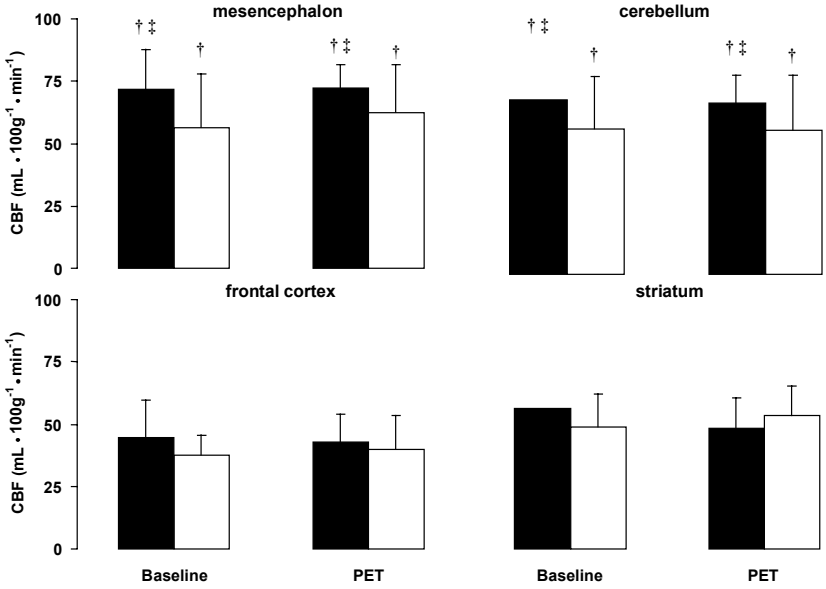

Fig. 1. Regional cerebral blood flow (CBF) in normal-weight (NW; n=10; filled columns) and intrauterine growth-restricted (IUGR; n=10; open columns) newborn piglets. Regional CBF was similar in NW and IUGR piglets and remained unchanged throughout the experiment. How-ever there were marked regional differences in the lowest CBF values in the frontal cortex. (Values are mean + SD, † ‡ $P < 0.05$, † indicates a significant difference to the frontal CBF values, ‡ indicates significant difference to the striatal CBF values).

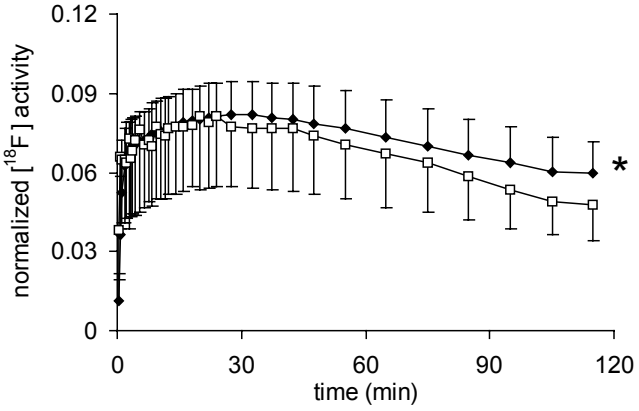

Fig. 2. The measured ^{18}F activity (mean ± SD) in the striatum of normal-weight (NW, n = 10, open squares) and intrauterine growth restricted piglets (IUGR, n = 10, filled circles). The coincidence counts detected by PET were divided by the injected activity and corrected for the differences in the body weight. Note the larger amount of ^{18}F activity accumulated in striatum of IUGR piglets (* $P < 0.05$, significant difference in ^{18}F activity in the striatum between NW and IUGR at the end of acquisition).

Fig. 2 shows the time course of the ^{18}F activity accumulated in the striatum, measured by PET. The data are normalized to the injected activity and corrected for differences in body weight. A distinctly larger amount of ^{18}F activity accumulated in the striatum of IUGR piglets ($P < 0.05$). The regional transport of FDOPA to the brain indicated by K_1^{FDOPA} and PS^{FDOPA}, and the clearance rate of labelled metabolites from brain tissue ($k_{cl}^{FDA+acids}$) were similar (Table 2) in both groups. However, the regional rate constants for the backflux from the brain (k_2^{FDOPA}) were markedly increased in IUGR piglets in the striatum (72 %) and the frontal cortex (83 %) ($P < 0.05$).

Table 2. Transfer coefficients and *PS* product of FDOPA of various brain regions calculated from the tracer activities in arterial blood and brain of normal weight (NW) and intrauterine growth restricted (IUGR) piglets

	K_1^{FDOPA} (mL • g^{-1} • min^{-1})		k_2^{FDOPA} (min^{-1})	
	NW	IUGR	NW	IUGR
Mesencephalon	0.070 ± 0.020	0.068 ± 0.029	0.087 ± 0.045	0.100 ± 0.068
Cerebellum	0.086 ± 0.028	0.076 ± 0.029 [1,3]	0.096 ± 0.025	0.104 ± 0.075
Frontal Cortex	0.062 ± 0.018 [1,2]	0.056 ± 0.018	0.057 ± 0.026 [2]	0.104 ± 0.058 *
Striatum	0.072 ± 0.016	0.064 ± 0.022	0.072 ± 0.020	0.124 ± 0.076 *
	$k_{cl}^{FDA+acid}$ (min^{-1})		PS^{FDOPA} (mL • g^{-1} • min^{-1})	
	NW	IUGR	NW	IUGR
Mesencephalon	0.009 ± 0.014	0.012 ± 0.007	0.074 ± 0.022	0.073 ± 0.033
Cerebellum	0.012 ± 0.006	0.014 ± 0.007	0.093 ± 0.031[1,3]	0.081 ± 0.033
Frontal Cortex	0.006 ± 0.014	0.013 ± 0.008	0.066 ± 0.020	0.060 ± 0.020 [1,2,4]
Striatum	0.011 ± 0.012	0.011 ± 0.007	0.079 ± 0.019	0.068 ± 0.025

Values are mean ± SD; *, [1,2,3,4] $P < 0.05$, * indicates significant differences between NW and IUGR piglets; [1,2,3,4] indicates significant differences within NW and IUGR piglets to [1] mesencephalon, [2] cerebellum. [3] frontal cortex, [4] striatum.

In all brain regions of IUGR piglets studied the rate constant of FDA production (k_3^{FDOPA}) was markedly increased by between 48 % (cerebellum) and mesencephalon (91 %) (Figure 3; $P < 0.05$), indicating a distinct upregulation of AADC activity. Cerebellar k_3^{FDOPA} was significantly lower than the mesencephalic and striatal k_3^{FDOPA} in the IUGR piglets.

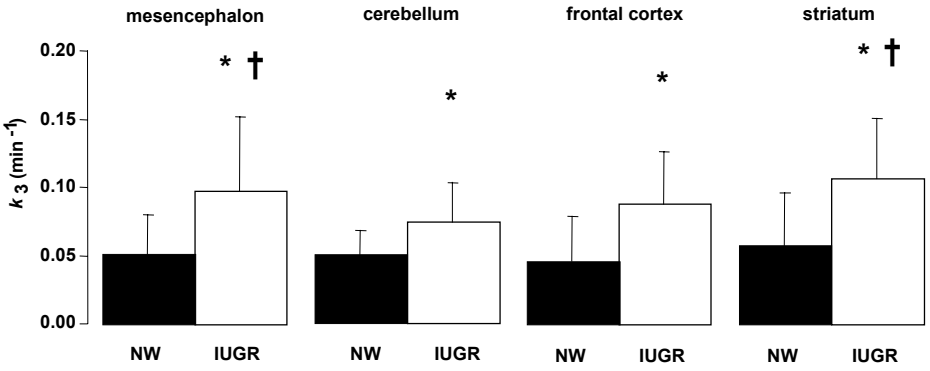

Fig. 3. Marked increase in the rate constants of FDA production (k_3^{FDOPA})in various brain regions of intrauterine growth-restricted piglets (IUGR, n = 10) compared with those of normal weight (NW, n = 10). (Values are mean ± SD, * $P < 0.05$, indicates significant difference between NW and IUGR piglets.)

Discussion

The main new finding in this study is that IUGR induces a markedly increased dopamine production within the mesencephalon (91 %) and in two major projection areas of the mesotelencephalic dopaminergic system, indicated by an increased AADC activity of 85% in the striatum and 93 % in the frontal cortex ($p < 0.05$). The changes in AADC activity are obviously not linked to brain oxygen delivery or brain tissue PO_2. This is noteworthy, because the immature cerebral dopaminergic system is sensitive to altered brain oxidative metabolism. There is obviously no "oxygen reserve" to protect the dopamine release and metabolism from a decrease in oxygen pressure, since the reduction in brain tissue PO_2 in the brain of the newborn piglet causes a significant increase in the striatal extracellular dopamine content in a dose-response relationship [16]. We recently found that the synthesis rate of fluorodopa-

mine from FDOPA also increases under those circumstances [13]. The upregulation of AADC activity found in this study may indicate an accelerated maturity of the dopaminergic system. The AADC is mainly localized in the presynaptic dopaminergic neurons and an increased expression of both D1 and D2 dopamine receptors occurs during postnatal development (for review see ref. [17,18]. No conclusions concerning the cause for the AADC upregulation in the dopaminergic system due to IUGR can be drawn from this study. There is, however, evidence that an altered glucocorticoid metabolism in IUGR fetuses due to disturbed placental clearance function for maternal glucocorticoids may influence brain dopaminergic activity in IUGR offspring. As the concentration of the circulating corticosteroid is two to ten times higher in the mother than in the fetus [19], fetal protection against maternal corticosteroid intoxication is normally effected by an appropriate placental 11β-hydroxysteroid dehydrogenase activity which rapidly converts physiological glucocorticoids into inactive products [20]. This is obviously changed during IUGR pregnancies. It was shown that the placental 11β-hydroxysteroid dehydrogenase activity was markedly reduced in the late gestational period of maternal protein-malnutrition causing IUGR offspring [21]. In addition, IUGR rats exhibited elevated liver and brain activities of specific glucocorticoid-inducible marker enzymes [22], suggesting an increased glucocorticoid action in brain and liver. Diaz *et al.* also showed that prenatal glucocorticoid administration induces a disturbed dopamine metabolism in juvenile rats with concomitant short-term and long-term neurobehavioral alterations [23,24]. The upregulation of AADC activity due to IUGR occurred mainly in the mesencephalon and in two major projection areas of the mesotelencephalic dopaminergic system, i.e. striatum and frontal cortex, which is fully developed at birth. A functional role of dopamine already in the early postnatal period is therefore suggested [25]. However, the cerebellar AADC activity was also moderately increased in IUGR. An “unspecific” AADC activity seems thus to be similarly sensitive to IUGR.

In summary, this study shows that the intrauterine growth restriction is associated with a marked increase in AADC activity in the mesostriatal and mesotelencephalic dopaminergic system of the brain of the immature piglet. However, the brain oxidative metabolism remains unchanged.

References

[1] Weinstock, M.; Fride, E.; Hertzberg, R. Prenatal stress effects on functional development of the offspring. Prog. Brain Res. 73 (1988) 319-331.

[2] Neerhof, M.G. Causes of intrauterine growth restriction. Clin. Perinatol. 22 (1995) 375-385.
Jensen, A.; Klonne, H.J.; Detmer, A.; Carter, A.M. Catecholamine and serotonin concentrations in fetal guinea-pig brain: relation to regional cerebral blood flow and oxygen delivery in the growth-restricted fetus. Reprod. Fertil. Dev. 8 (1996) 355-364.

[3] Chen, J.C.; Turiak, G.; Galler, J.; Volicer, L. Effect of prenatal malnutrition on release of monoamines from hippocampal slices. Life Sci. 57 (1995) 1467-1475.

[4] Mattes, J.A. The role of frontal lobe dysfunction in childhood hyperkinesis. Compr. Psychiatry 21 (1980) 358-369.

[5] Benton, A. Prefrontal injury and behavior in children. Dev. Neuropsychol. 7 (1991) 275-281.

[6] Heilman, K.M.; Voeller, K.K.; Nadeau, S.E. A possible pathophysiologic substrate of attention deficit hyperactivity disorder. J. Child. Neurol. 6 Suppl. (1991) S76-81.

[7] Lou, H.C.; Henriksen, L.; Bruhn, P.; Borner, H.; Nielsen, J.B. Striatal dysfunction in attention deficit and hyperkinetic disorder. Arch. Neurol. 46 (1989) 48-52.

[8] Ernst, M.; Zametkin, A.J.; Matochik, J.A.; Jons, P.H.; Cohen, R.M. DOPA decarboxylase activity in attention deficit hyperactivity disorder adults. A [fluorine-18]fluorodopa positron emission tomographic study. J. Neurosci.18 (1998) 5901-5907.

[9] Bauer, R.; Walter, B.; Hoppe, A.; Gaser, E.; Lampe. V.; Kauf, E.; Zwiener, U. Body weight distribution and organ size in newborn swine (sus scrofa domestica) -- a study describing an animal model for asymmetrical intrauterine growth retardation. Exp. Toxic. Pathol. 50 (1998) 59-65.

[10] De Roth, L.; Downie, H.G. Evaluation of viability of neonatal swine. Can. Vet. J. 17 (1976) 275-279.

[11] Brust, P.; Bauer, R.; Walter, B.; Bergmann, R.; Füchtner, F.; Vorwieger, G.; Steinbach, J.; Johannsen, B.; Zwiener, U. Simultaneous measurement of [F-18]FDOPA metabolism and cerebral blood flow in newborn piglets. Int. J. Dev. Neurosci. 16 (1998) 353-364.

[12] Brust, P.; Bauer, R.; Vorwieger, G.; Walter, B.; Bergmann, R.; Füchtner, F.; Steinbach, J.; Zwiener, U.; Johannsen, B. Upregulation of the aromatic amino acid decarboxylase under neonatal asphyxia. Neurobiol. Dis. 6 (1999) 131-139.

[13] Lerman, J.; Oyston, J.P.; Gallagher, T.M.; Miyasaka, K. A. G.; Volgyesi, G.A.; Burrows, F.A. The minimum alveolar concentration (MAC) and hemodynamic effects of Halothane, Isoflurane, and Sevoflurane in newborn swine. Anesthesiology 73 (1990) 717-721.
[14] Eisenhauer, C.L.; Matsuda L.S.; Uyehara C.F. Normal physiologic values of neonatal pigs and the effects of isoflurane and pentobarbital anesthesia. Lab. Anim. Sci. 44 (1994) 245-252.
[15] Huang, C.C.; Lajevardi, N.S.; Tammela, O.; Pastuszko, A.; Delivoria Papadopoulos, M.; Wilson, D.F. Relationship of extracellular dopamine in striatum of newborn piglets to cortical oxygen pressure. Neurochem. Res. 19 (1994) 649-655.
[17] Schambra, U.B.; Duncan, G.E.; Breese, G.R.; Fornaretto, M.G.; Caron, M.G.; Fremeau, R.T., Jr. Ontogeny of D1A and D2 dopamine receptor subtypes in rat brain using in situ hybridization and receptor binding. Neuroscience 62 (1994) 65-85.
[18] Guennoun, R.; Bloch, B. Ontogeny of D1 and DARPP-32 gene expression in the rat striatum: an in situ hybridization study. Mol. Brain Res. 12 (1992) 131-139.
[19] Beitins, I.Z.; Bayard, F.; Ances, I.G.; Kowarski, A.; Migeon, C.J. The metabolic clearance rate, blood production, interconversion and transplacental passage of cortisol and cortisone in pregnancy near term. Pediatr. Res. 7 (1973) 509-519.
[20] Seckl, J.R.; Brown, R.W. 11-beta-hydroxysteroid dehydrogenase: on several roads to hypertension. J. Hypertens. 12 (1994)105-112.
[21] Langley Evans, S.C.; Phillips, G.J.; Benediktsson, R.; Gardner, D.S.; Edwards, C.R.; Jackson, A.A.; Seckl, J.R. Protein intake in pregnancy, placental glucocorticoid metabolism and the programming of hypertension in the rat. Placenta 17 (1996) 169-172.
[22] Langley Evans, S.C.; Gardner, D.S.; Jackson, A.A. Maternal protein restriction influences the programming of the rat hypothalamic-pituitary-adrenal axis. J. Nutr. 126 (1996)1578-1585.
[23] Diaz, R.; Ogren, S.O.; Blum, M.; Fuxe, K. Prenatal corticosterone increases spontaneous and d-amphetamine induced locomotor activity and brain dopamine metabolism in prepubertal male and female rats. Neuroscience 66 (1995) 467-473.
[24] Diaz, R.; Fuxe, K.; Ogren, S.O. Prenatal corticosterone treatment induces long-term changes in spontaneous and apomorphine-mediated motor activity in male and female rats. Neuroscience 81 (1997) 129-140.
[25] Schmidt, R.H.; Bjorklund, A.; Lindvall, O.; Loren, I. Prefrontal cortex: dense dopaminergic input in the newborn rat. Brain Res. 281 (1982) 222-228.

58. Transport of Carnitine at the Brain Endothelium *in vitro*

A. Friedrich, V. Ganapathy[1], P. Brust
[1]Department of Biochemistry and Molecular Biology, Medical College of Georgia, Augusta, USA

Introduction

Treatment of brain diseases is often limited by poor brain drug uptake due to the restrictive nature of the blood-brain barrier (BBB), particularly for hydophilic, water soluble substances [1]. There are numerous methods to improve the brain drug delivery, such as increasing the drug lipid solubility. An alternative approach is to study the expression of saturable nutrition transporter systems at the BBB to use this knowledge for the design of drugs which are transported by these transporters.
Carnitine, which is important for the intracellular transport of fatty acids, was found to inhibit choline transport [2]. It was therefore possible that the accessibility of choline and acetyl moieties, transported by a carnitine carrier, was a limiting factor for the synthesis of the neurotransmitter acetycholine [3]. There was a carnitine transport reported at the immortalized rat brain endothelial cell line (RBE4) [4] which was sodium independent. This transporter was only described by functional and not by molecular studies. On the other hand, another specific transporter for carnitine was cloned and functionally identified (OCTN2). This transporter is sodium dependent [5] and has not been described at the BBB up to now. In this study we characterized the transport of carnitine at an in-vitro model of the BBB by functional and molecular methods. We obtained evidence that the OCTN2 transporter is also expressed at the BBB.

Methods

The RBE4 cell line was used as an in-vitro model of the BBB. The cells were cultured as described [6] and it was shown that these cells express typical BBB markers such as γ-glutamyltransferase and alkaline phosphatase [6].
Tracer uptake studies were performed in 24 multi-well plates using buffers containing 25 mM Hepes/Tris (pH 7.5), supplemented with 0.5% albumin, 5 mM glucose, 5.4 mM KCl, 1.8 mM $CaCl_2$, 0.8 mM $MgSO_4$ and 140 mM NaCl. Whenever Na^+-free buffers were used, NMDG chloride replaced NaCl isoosmotically. Cells were washed with the uptake buffer before starting the uptake studies and then incubated at 37°C with [^{3}H]L-carnitine (20 nM, Moravek Biochemical, St. Louis, CA) added to the incubation buffer. K_m values and V_{max} values were calculated from the uptake data using computer programs for nonlinear regression (Fig. P and Sigma Plot). Specific inhibitors (L-carnitine, MPP, TEA, 2 mM) of the transporter were added to the incubation buffer to study the specificity of the process.
RT-PCR with mRNA derived from RBE4 cells and rat kidney was performed using specific primers. The primers were designed on the basis of of the cDNA sequence of the rat OCTN2 transporter [7]. The upper primer was 5‘ CCT TCA TTT CGG GAC AGC 3‘ (position 570-587) and the lower primers was 5‘ GAC AGG ACT TCT CGG TGG 3‘ (position 1894-1911). An RBE4 cell cDNA library was constructed, using the Superscript plasmid system. This plasmid cDNA library, grown on NitroPure transfer membranes, was screened by the colony screening method as described by Vogeli and Kaytes [8]. The cDNA probe used for screening was 2.1 kb pair long and consisted of most of the coding region of rOCTN2 cDNA. The probe was labelled with [α-^{32}P]dCTP using the ready-to-go oligolabelling kit, and used to screen the RBE4 cDNA library under low stringency conditions. The cDNA was functionally expressed in HeLa cells by the vaccinia virus expression system [9]. Transport measurements were made at room temperature using the same uptake buffer as described above without albumin.

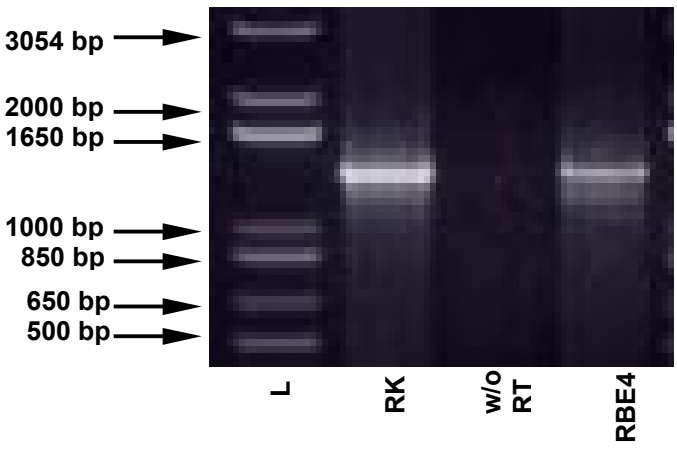

Fig. 1. RT-PCR with specific primers of the rat OCTN2 and mRNA derived from RBE4 cells (RBE4) and rat kidney (RK) as a positive control. As a negative control mRNA from RBE4 cells without reverse transcriptase (w/o RT) was used.

Results and Discussion

The RT-PCR with specific primers of the rat OCTN2 transporter shows clearly that OCTN2 is expressed in RBE4 cells (Fig. 1). The uptake studies with [^{3}H]L-carnitine at the RBE4 cells exhibit a linear time course over 4 hours. The estimated K_t value for the carnitine uptake at 37 °C in RBE4 cells is 45 µM and the V_{max} value is 161 pmol/mg/h (Fig. 2). It is reported that carnitine is accumulated by neuronal cells in a sodium dependent way [10]. The K_t value of this uptake is 123 µM, which is about 3 times the value found in RBE4 cells. On the other hand, the OCTN2 transporter derived from rat placenta [7] was cloned into HRPE cells and mediates a sodium dependent carnitine transport with a K_t of 14.8 µM which is about 3.5 times lower than at RBE4 cells.

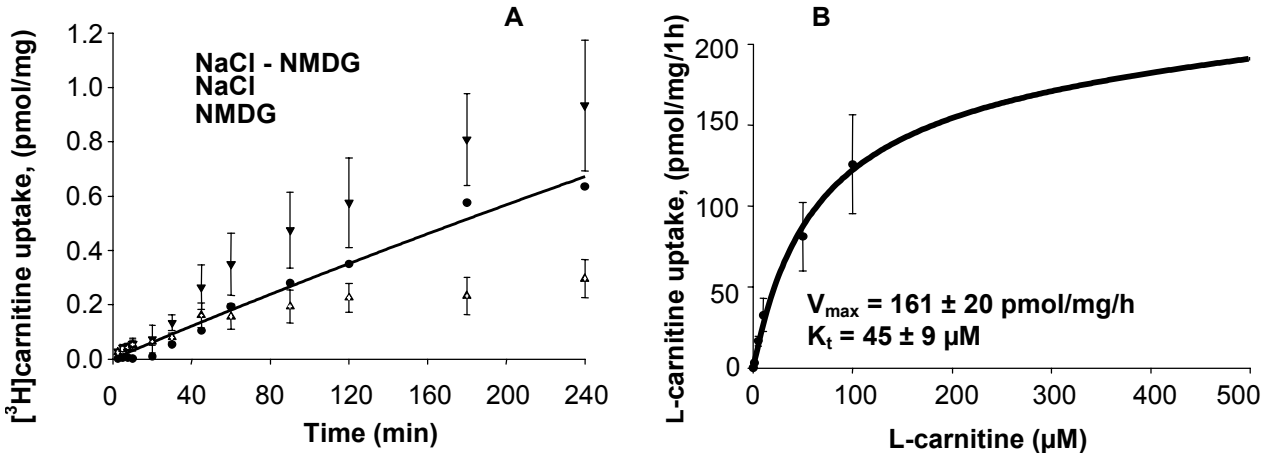

Fig. 2. Time course (A) and kinetics (B) of L-carnitine uptake in RBE4 cells at 37 °C in buffer with sodium (NaCl) and isoosmotic replacement of sodium by NMDG (NMDG). (NaCl - NMDG) resembles the specific sodium dependent L-carnitine uptake in the RBE4 cells.

In primary cultures of porcine brain capillary endothelial cells Mroczkowska *et al.* described a sodium-independent carnitine uptake with a K_t of 28 µm [11]. The same authors also found a sodium independent carnitine uptake in RBE4 cells [4]. However, we found that the RBE4 cells also take up fatty acid esters of carnitine such as propion-L-carnitine and acetyl-L-carnitine (data not shown), which is known for the OCTN2 [7] and was not observed by Mroczkowska *et al.*.

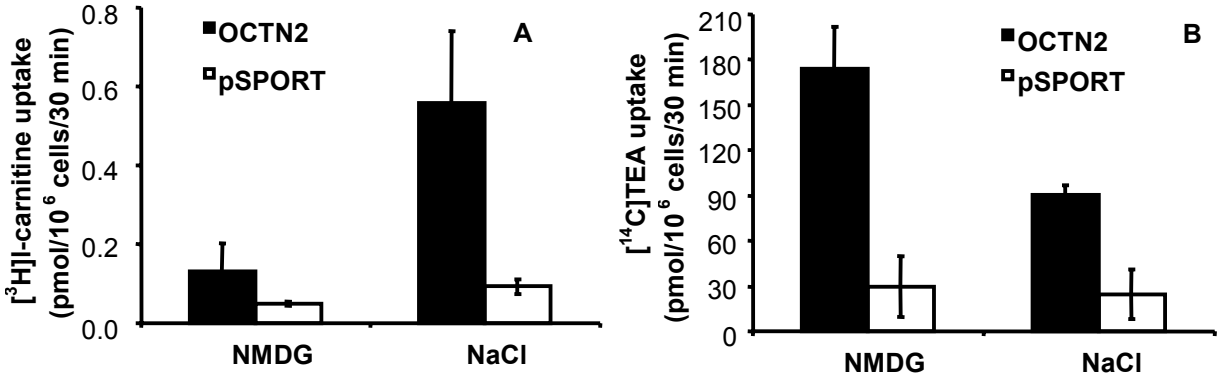

Fig. 3. Na-dependence of [^{3}H]L-carnitine (A) and [^{14}C]TEA (B) uptake at room temperature in HeLa cells transfected with the OCTN2 clone from RBE4 cells or the empty pSPORT vector as a control.

To further characterize the OCTN2 transporter of the RBE4 cells we isolated a full-length OCTN2 clone from the RBE4 cDNA library. HeLa cells transfected with this clone also show a Na^+-dependent carnitine uptake but a Na^+-independent uptake of tetraethylammonium (TEA) (Fig. 3) as described for OCTN2 [7]. Several organic cations (MPP^+ and TEA) known to be inhibitors of the OCTN2 transporter

[7] inhibit the carnitine uptake expressed in HeLa cells by the OCTN2 cDNA clone from RBE4 cells (Fig. 4).

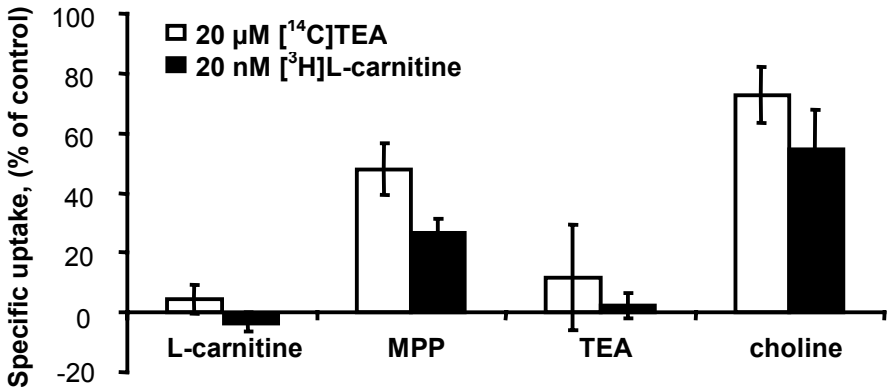

Fig. 4. Influence of specific inhibitors (2 mM) of organic cation transporters on the uptake of [^{3}H]l-carnitine and [^{14}C]TEA at room temperature in HeLa cells transfected with the OCTN2-clone from RBE4 cells.

In summary the sodium dependent carnitine transport at the RBE4 cells seems to be mediated by the OCTN2 transporter. The expression of OCTN2 at the BBB may help to understand the way the brain is supplied with acetyl groups for the synthesis of acetylcholine and lipids. It was suggested that the accessibility of choline and acetyl moieties could be a limiting factor for the acetylcholine synthesis [3]. Furthermore, knowledge of the expression of these transporters may be useful for the development of new drugs and radiotracers for brain diagnostics and treatment of brain diseases.

References

[1] Begley, D.J. The blood-brain barrier: Principles for targeting peptides and drugs to the central nervous system. J. Pharm. Pharmacol. 48 (1996) 136-146.

[2] Conford, E.M.; Braun, L.D.; Oldendorf, W.H. Carrier mediated blood-brain barrier transport of choline and certain choline analogs. J. Neurochem. 30 (1978) 299-308.

[3] Wawrzenzyk, A.; Nalecz, K.A.; Nalecz, M.J. Synergistic effect of choline and carnitine on acetylcholine synthesis in neuroblastoma NB-2a cells. Biochem. Biophys. Res. Commun. 202 (1994) 354-359.

[4] Mroczkowska, J.E.; Roux, F. S.; Galla, H.-J.; Nalecz, M.J.; Nalecz, K.A. Transport of carnitine in RBE4 cells – an *in vitro* model of blood-brain barrier Neurosci. Res. Commun. 19 (1996) 153-160.

[5] Tamai, I.; Ohashi, R.; Nezu, J.; Yabuuchi, H.; Oku, A.; Shimane, M.; Sai, Y.; Tsuji, A. Molecular and functional identification of sodium ion-dependent, high affinity human carnitine transporter OCTN2. J. Biol. Chem. 273 (1998) 20378-20382.

[6] Roux, F.; Durieu-Trautmann, O.; Chaverot, N.; Claire, M.; Mailly, P.; Bourre, J.-M.; Strosberg, A. D.; Couraud, P.-O. Regulation of gamma-glutamyl transpeptidase and alkaline phosphatase activities in immortalized rat brain microvessel endothelial cells. J. Cell. Physiol. 159 (1994) 101–113.

[7] Wu, X.; Huang, W.; Prasad, P.D.; Seth, P.; Rajan, D.P.; Leibach, F.H.; Chen, J.; Conway, S.J.; Ganapathy, V. Functional characteristics and tissue distribution pattern of organic cation transporter 2 (OCTN2), an organic cation/carnitine transporter. J. Pharmacol. Exp. Ther. 290 (1999) 1482-1492.

[8] Vogeli, G.; Kaytes, P.S. Amplification, storage and replication of libraries. Methods Enzymol. 152 (1987) 407-415.

[9] Ramamoorthy, S.; Leibach, F.H.; Mahesh, V.B.; Han, H.; Yang-Feng, T.L.; Blakely, R.D.; Ganapathy, V. Functional characterization and chromosomal localization of a cloned taurine transporter from human placenta. Biochem. J. 300 (1994) 893-900.

[10] Nalecz, K.A.; Korzon, D.; Wawrzenczyk, A.; Nalecz, M.J. Transport of carnitine in neurobalstoma NB-2a cells. Arch. Biochem. Biophys. 322 (1995) 214-220.

[11] Mroczkowska, J.E.; Galla, H.-J.; Nalecz, M.J.; Nalecz, K.A. Evidence for an asymmetrical uptake of l-carnitine in the blood-brain barrier *in vitro*. Biochem. Biophys. Res. Commun. 241 (1997) 127-131.

59. Transport of L-Tryptophan at the Brain Endothelium *in vitro*

A. Friedrich, V. Ganapathy[1], P. Brust
[1]Department of Biochemistry and Molecular Biology, Medical College of Georgia, Augusta, USA

Introduction

Immortalized brain endothelial cell lines are used as an in-vitro model to characterize the transport of drugs across the blood-brain barrier (BBB). We recently showed that the RBE4 cell line [1] expresses the drug efflux pump P-glycoprotein which determines the uptake of certain ^{99m}Tc-labelled radiopharmaceuticals [2]. Various centrally acting drugs and radiopharmaceuticals are neutral amino acids which are transported across the BBB by a special transporter expected to be system L [3] later designated LAT [4]. Among them are 3,4-dihydroxyphenylalanine (L-Dopa) which is used for the treatment of Parkinson´s disease [5, 6], the tyrosine hydroxylase inhibitor α-methyltyrosine [7] and the antihypertensive drug α-methyldopa [8]. The radiopharmaceutical L-3,4-dihydroxy-6-[^{18}F]fluorophenyl-alanine (FDOPA) is used for the imaging of dopaminergic diseases [9], and 3-*O*-methyl-[^{18}F]FDOPA is a promising tracer for brain tumour imaging [10].
In this study we showed that the transport of amino acids into immortalized rat brain endothelial cells (RBE4) is characterized by similar features as the transport at the brain endothelium *in vivo*. The RBE4 cell line can therefore be used as an in-vitro model to study the BBB transport of new drugs and radiotracers which are analogues of amino acids.

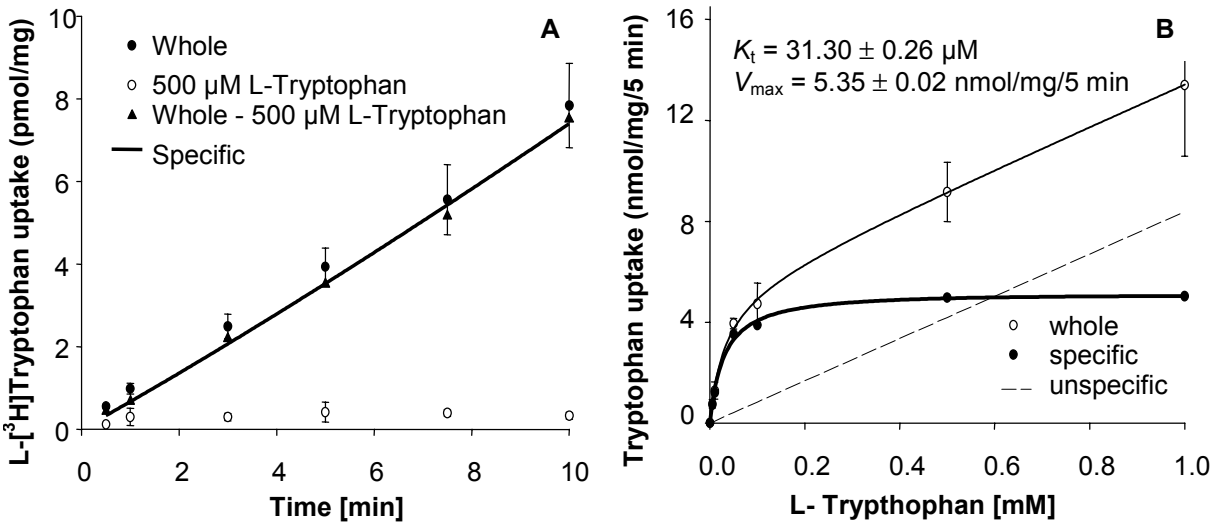

Fig. 1 Time course (A) and kinetics (B) of the L-[^{3}H]tryptophan uptake in RBE4 cells at room temperature. Unspecific uptake was determined with 500 µM L-tryptophan in the uptake buffer.

Methods

RBE4 cells were cultured as described in a preceding report in this volume [11].
Tracer uptake studies with RBE4 cells were performed in 24 multi-well plates using buffer containing 25 mM Hepes/Tris (pH 7.5), supplemented with 0.5% albumin, 5 mM glucose, 5.4 mM KCl, 1.8 mM $CaCl_2$, 0.8 mM $MgSO_4$ and 140 mM NaCl. Whenever Na^+-free buffers were used, NMDG chloride replaced NaCl isoosmotically. Cells were washed with the uptake buffer before starting the uptake and then incubated at room temperature with L-[^{3}H]tryptophan (50 nM) added to the incubation buffer. K_t values and V_{max} values were calculated from the uptake data using computer programs for nonlinear regression (Fig. P, Sigma Plot). Specific inhibitors (BCH, 1 mM; tryptophan, 500 µM) of the transporter and several amino acids (1 mM) were added to the incubation buffer to study the specificity of the uptake process.
RT-PCR with mRNA derived from RBE4 cells and rat brain was performed using specific primers. The primers were designed based on the cDNA sequence of the rat LAT1 subunit [12]. The upper primer was 5' GGG CTG TGT GCG GCG TCT 3' (position 332-349) and the lower primer was 5' CCA GAA GGA CAC GGC GAT GAG 3' (position 1414-1434). PCR products were run on a 1 % agarose gel,

cDNA bands were cut from the gel and purified using the Qiaex II gel extraction kit (Qiagen). The purified PCR products were then enzymatically digested with the restriction endonuclease BamH1 and digestion products were run on a 1 % agarose gel.

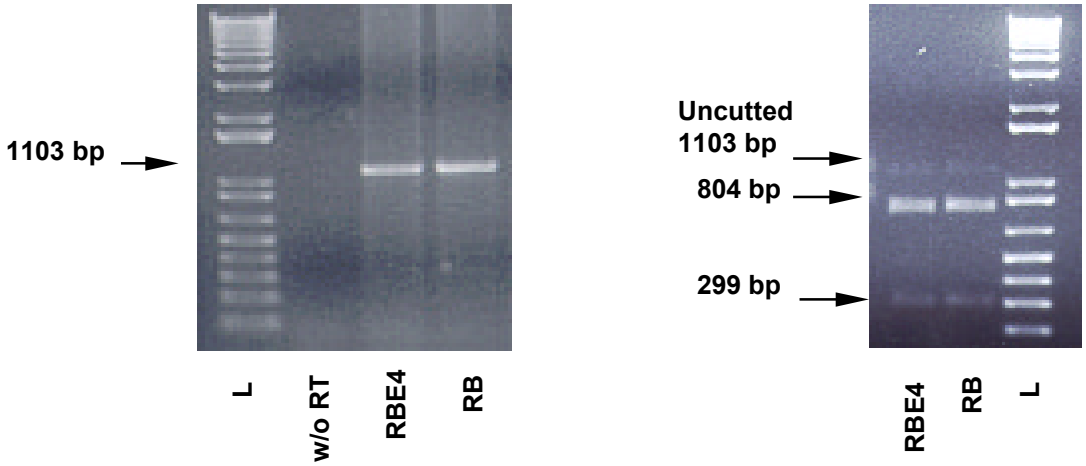

Fig. 2A. RT-PCR with specific primers for rat LAT1, mRNA derived from RBE4 cells (RBE4) and rat brain (RB) as a positive control and RBE4 cell mRNA without reverse transcriptase (w/o RT) as a negative control. B: Digestion of the RT-PCR products with restriction endonuclease BamH1.

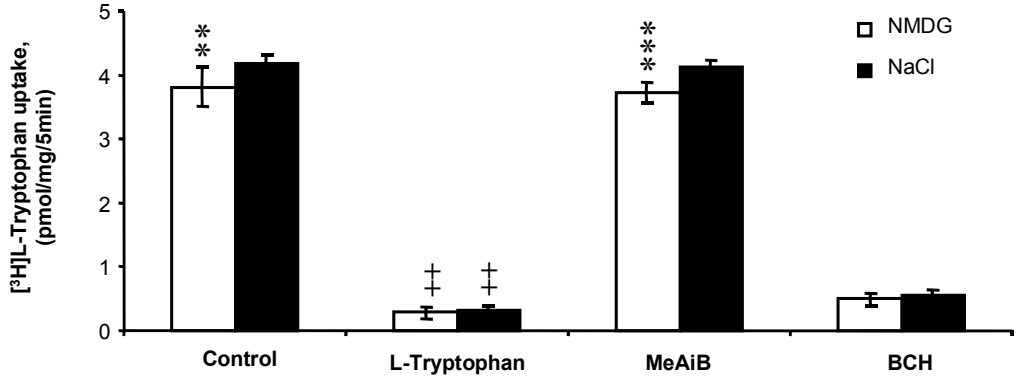

Fig. 3. Influence of specific inhibitors (1 mM) for system L (BCH) and system A (MeAiB) on the uptake of L-[^{3}H]tryptophan into RBE4 cells at room temperature. The uptake buffer contained either NaCl (open columns) or it was isoosmotically replaced by NMDG chloride (filled columns).
NMDG vs. NaCl (one-tailed t-Test): **- p<0.01, ***- p<0.001
L-tryptophan vs. BCH (two-tailed t-Test): ++- p<0.01

Results and Discussion

The uptake of L-[^{3}H]tryptophan into RBE4 cells is linear over a period of up to 10 minutes (Fig. 1A). The uptake measurement in further studies were therefore performed for 5 minutes. Fig. 1B shows that the transport of L-[^{3}H] tryptophan has a saturable and a non-saturable component. For the saturable component the half-saturation constant K_t of 31.3 µM and the transport capacity V_{max} of 5.35 nmol/mg/5min were determined. The transporter affinity is in the same range as published for the rat BBB *in vivo* (K_t = 52 µM) [13], the cloned bLAT1 obtained from bovine brain endothelium (K_t = 31.5 µm) [14] and the cloned hLAT1 obtained from human placenta (15 µM) [15]. This carrier of the BBB is sodium independent, bidirectional, and therefore an equilibrative transport system [16]. Kanai *et al.* [12] cloned a protein from rat C6 glioma cells which mediates the Na+-independent transport of neutral amino acids when coexpressed in Xenopus laevis oocytes with the heavy chain of the 4F2 antigen (CD98). This protein, designated rLAT1, is not capable of transporting amino acid on its own, but as a heterodimer with the heavy chain of the 4F2 antigen (4F2hc), rLAT1 possesses amino acid transport

activity with the characteristics of system L. In this study, using the RT-PCR, we demonstrated the presence of the rLAT1 subunit at the RBE4 cells. Fig. 2A shows the expression of the L-system subunit LAT1 in the RBE4 cells in comparison to the rat brain. The PCR products of 1103 bp were specifically digested by BamH1 to confirm them as parts of the LAT1 cDNA from rat. The expected fragments after digestion with BamH1 were 804 bp and 299 bp and are shown in Fig 2B.

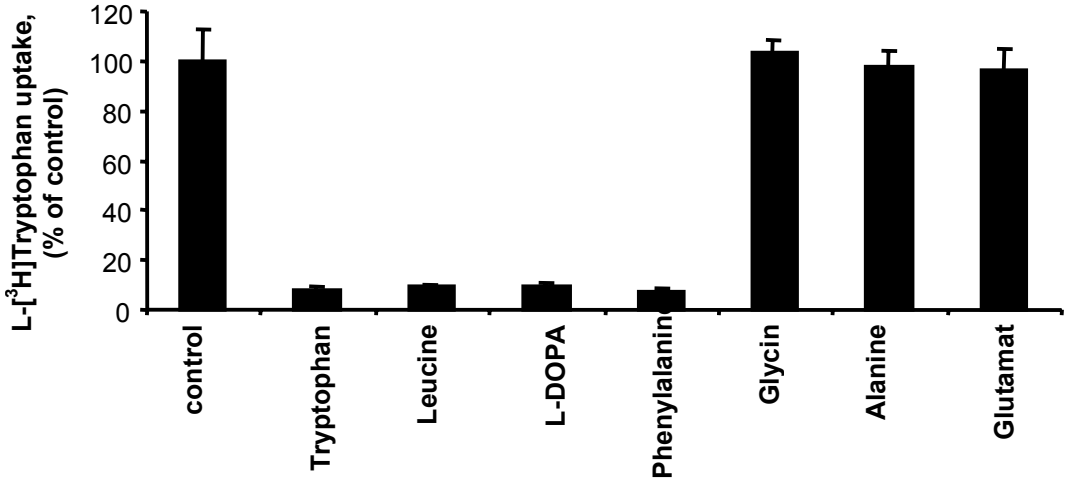

Fig. 4. Influence of various L-amino acids (1 mM) on the uptake of L-[^{3}H]tryptophan in RBE4 cells at room temperature.

Furthermore, we showed that the uptake of L-[^{3}H]tryptophan is sodium independent (Fig. 3) and that the specific LAT inhibitor BCH clearly reduces the tracer uptake into the RBE4 cells by about 87% while MeAiB, an inhibitor of system A, has no effect. Several large neutral amino acids such as tryptophan, leucine and phenylalanine inhibit the [^{3}H]L-tryptophan uptake into RBE4 cells while small neutral amino acids such as glycine and alanine or acidic amino acids (glutamate) do not (Fig. 4). These features characterize the transport of L-[^{3}H]tryptophan as primarily LAT1 mediated. However, a small part of about 8.5 % seems to be sodium-dependent because replacement of NaCl by NMDG significantly reduced the uptake of L-[^{3}H] tryptophan. L-tryptophan also showed a much greater inhibition than BCH at similar affinities of those two amino acids [16]. Measuring the uptake of L-[^{3}H]phenylalanine into vesicles prepared from bovine brain endothelium, Sanchez del Pino *et al.* [16] found a small sodium-dependent component which was sensitive to BCH. If tryptophan has a higher affinity to this transporter than BCH, this could explain our finding. It is unlikely that the sodium-dependent uptake of L-[^{3}H]tryptophan is caused by y^+LAT1, a transporter which mediates the efflux of basic amino acids in exchange for the Na^+-dependent uptake of neutral amino acids [17.] This transporter cannot be inhibited by BCH but it does not seem to take up L-tryptophan above background levels [10]. On the other hand, it should be taken into consideration that an affinity of L-tryptophan to other sodium-dependent transporters which at present are not known to exist at the BBB was described [17].
In conclusion we showed that the RBE4 cells may be used as a model to study the BBB transport of neutral amino acids via the Na^+-independent system L. The cells highly express LAT1. The affinity of this transporter to L-tryptophan and its selectivity for various amino acids is comparable to *in-vivo* studies and to investigations using isolated brain microvessels or primary brain endothelial cells.

References

[1] Roux, F.; Durieu-Trautmann, O.; Chaverot, N.; Claire, M.; Mailly, P.; Bourre, J.M.; Strosberg, A.D.; Couraud, P.O. Regulation of gamma-glutamyl transpeptidase and alkaline phosphatase activities in immortalized rat brain microvessel endothelial cells. J. Cell Physiol. 159 (1994) 101-113.

[2] Bergmann, R.; Brust, P.; Scheunemann, M.; Pietzsch, H.-J.; Seifert, S.; Roux, F., Johannsen B. Assessment of the *in vitro* and *in vivo* properties of a 99mTc-labeled inhibitor of the MDR gene product P-glycoprotein. Nucl. Med. Biol. 27 (2000) 135-141.

[3] Pardridge, W.M. Blood-brain barrier carrier-mediated transport and brain metabolism of amino acids. Neurochem. Res. 23 (1998) 635-644.

[4] Christensen, H.N.; Albritton, L.M.; Kakuda, D.K.; MacLeod, C.L. Gene-product designations for amino acid transporters. J. Exp. Biol. 196 (1994) 51-57.

[5] Carlsson, A. Development of new pharmacological approaches in Parkinson's disease. Adv. Neurol. 45 (1987) 513-518.
[6] Wade, L. A.; Katzman, R. Synthetic amino acids and the nature of L-Dopa transport at the blood-brain barrier. J. Neurochem. 25 (1975) 837-842
[7] Brogden, R.N.; Heel, R.C.; Speight, T.M.; Avery, G.S. alpha-Methyl-p-tyrosine: a review of its pharmacology and clinical use. Drugs 21 (1981) 81-89.
[8] Markovitz, D. C.; Fernstrom, J. D. Diet and uptake of aldomet by the brain: competition with large neutral amino acids. Science 197 (1977) 1014-1015.
[9] Barrio, J.R.; Huang, S.C.; Phelps, M.E. Biological imaging and the molecular basis of dopaminergic diseases. Biochem. Pharmacol. 54 (1997) 341-348.
[10] Füchtner, F.; Steinbach, J.; Vorwieger, G.; Bergmann, R.; Syhre, R.; Brust, P.; Beuthin-Baumann, B.; Burchert, W.; Zips, D.; Baumann, M.; Johannsen, B. 3-O-Methyl-6-[^{18}F]fluoro-L-DOPA - a promising substance for tumour imaging. J. Labelled Cpd. Radiopharm. 42 (1999) S267-S269.
[11] Friedrich, A.; Ganapathy, V.; Brust, P. Transport of carnitine at the blood-brain barrier *in vitro* (this volume)
[12] Kanai, Y.; Segawa, H.; Miyamoto, K. I.; Uchino, H.; Takeda, E.; Endou, H. Expression cloning and characterization of a transporter for large neutral amino acids activated by the heavy chain of 4F2 antigen (CD98). J. Biol. Chem. 273 (1998) 23622-23632.
[13] Pardridge,W. M.; Choi, T. B. Neutral amino acid transport at the blood-brain barrier. Fed. Proc. 45 (1986) 2073-2078.
[14] Boado, R. J.; Li, J. Y.; Nagaya, M.; Zhang,C.; Pardridge, W. M. Selective expression of the large neutral amino acid transporter at the blood-brain barrier. Proc. Natl. Acad. Sci. USA 96 (1999) 12079-12084.
[15] Prasad, P. D.; Wang, H.; Huang, W.; Kekuda, R.; Rajan, D. P.; Leibach, F. H.; Ganapathy, V. Human LAT1, a subunit of system L amino acid transporter: molecular cloning and transporter function. Biochem. Biophys. Res. Commun. 255 (1999) 283-288.
[16] Sanchez del Pino, M.M.; Peterson, D.R.; Hawkins, R.A. Neutral amino acid transport characterization of isolated luminal and abluminal membranes of the blood-brain barrier. J. Biol. Chem. 270 (1995) 14913-14918.
[17] Pfeiffer, R.; Rossier, G.; Spindler, B.; Meier, Ch.; Kühn, L.; Verrey, F. Amino acid transport of y+L-type by heterodimers of 4F2hc/CD98 and members of the glycoprotein-associated amino acid transporter family. EMBO J. 18 (1999) 49-57.
[18] Centanni, M; Canettieri, G; Viceconti, N; Sibilla, R; Bei, A; Andreoli, M. Effect of tryptophan on the early tri-iodothyronine uptake in mouse thymocytes. Eur. J. Endocrinol. 143 (2000) 119-123.

60. Changes in the Cerebral Glucose Metabolism of Patients with Wilson's Disease

W. Burchert, B. Kunath[1], B. Beuthien-Baumann[2], U. Reuner[1], W.-G. Franke[2]
TU Dresden, [1]Klinik und Poliklinik für Neurologie und [2]Klinik und Poliklinik für Nuklearmedizin /PET-Zentrum Rossendorf

Introduction

Wilson's disease is an inherited abnormality of the hepatic excretion of copper that results in toxic accumulation in the liver, the brain and other organs [1 - 3]. Subsequent changes in the cerebral glucose metabolism (MRGlc) were reported in the striatum, the thalamus, the cerebellar cortex and also in some other cortical areas [4 - 8]. The aim of the study was to evaluate whether the regional glucose metabolism can be used to characterize the cerebral disease activity.

Materials and Methods

Patients
22 consecutive patients (12 male, 10 female; 38.2 ± 11.8 (19 - 63) years) with Wilson's disease were included in this study. At the time of positron-emission tomography (PET) the duration of the disease was 18.6 ± 13.0 (0 - 42) years. The PET scan was performed on all patients under continued drug treatment (penicillamine, TTD). The patients were divided into two groups. The first group showed distinct neurological symptoms (wilson+; n = 13) while the second group of patients had no neurological signs and symptoms (wilson-; n = 9). These patients were compared with 7 controls (6 male, 1 female; 36.7 ± 12.8 (26 - 59) years).

Positron emission tomography
Prior to the PET scan patients fasted for at least 6 hours. The scan was performed in a dimmed room in supine position with eyes closed and ears unplugged. After an intravenous injection of 300 MBq [^{18}F]-fluorodeoxyglucose (FDG) a dynamic data acquisition (scan time period 60 minutes) was started. The data were recorded by a Siemens/CTI ECAT EXACT HR+ scanner with a 15.2 cm field of view and a reconstructed resolution of about 7 mm FWHM. During the reconstruction process (filtered backprojection) the data were corrected for attenuation (transmission scan, 10 minutes) and decay. The resulting images were calibrated in absolute activity concentration units. To provide an arterial input function arterialized venous blood samples from the patient`s heated hand were taken according to the midframe times during the scan period.

Data analysis
Quantitative images of regional metabolic rates of glucose were generated from the dynamic image data and the arterial input function on a pixel-by-pixel basis, using the GJEDDE/PATLAK Plot [9, 10]. The resulting quantitative 3D volumes were normalized into the TALAIRACH stereotactical space [11] (MEDx, Sensor Systems). Standardized validated ROI sets were used for regional analysis of the glucose metabolism. Student's t-test was used to evaluate the observed regional differences of metabolic values between patient groups. A p-value of < 0.05 was considered to be significant.

Results and Discussion

Patients with Wilson's disease showed no significant differences in their global cerebral metabolic rates of glucose as compared with the controls (Fig. 1; Table 1).

In patients with Wilson's disease exhibiting distinct neurological symptoms a reduced glucose metabolism was found in the putamen and the caudate nuclei on both sides. An increased metabolism was observed in the thalami. By contrast, patients with Wilson's disease but without neurological symptoms showed a normal metabolism of the basal ganglia. Almost in all patients the observed changes in the glucose metabolism were symmetrical (Fig. 2; Table 1).

A decreased glucose metabolism in the lateral temporal cortex was found in all patients with Wilson's disease as compared with the controls, regardless of the presence of neurological symptoms (Fig. 3; Table 1).

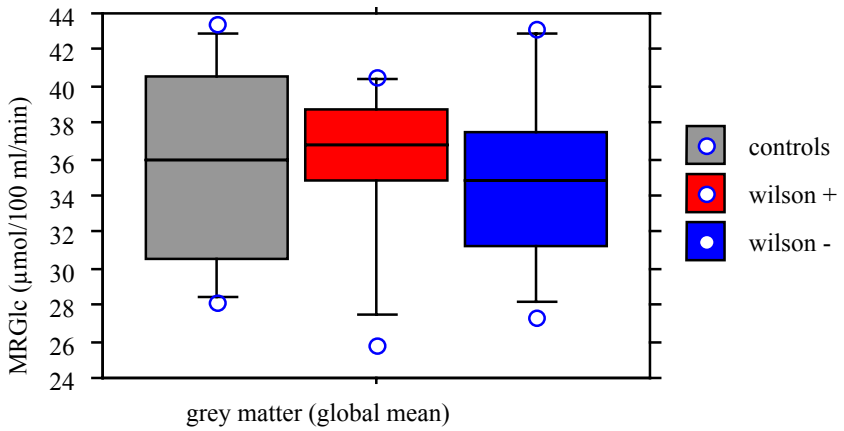

Fig. 1. Mean global glucose metabolism of the grey matter of controls and patients with Wilson's disease, with (wilson+) and without (wilson-) manifest neurological symptoms.

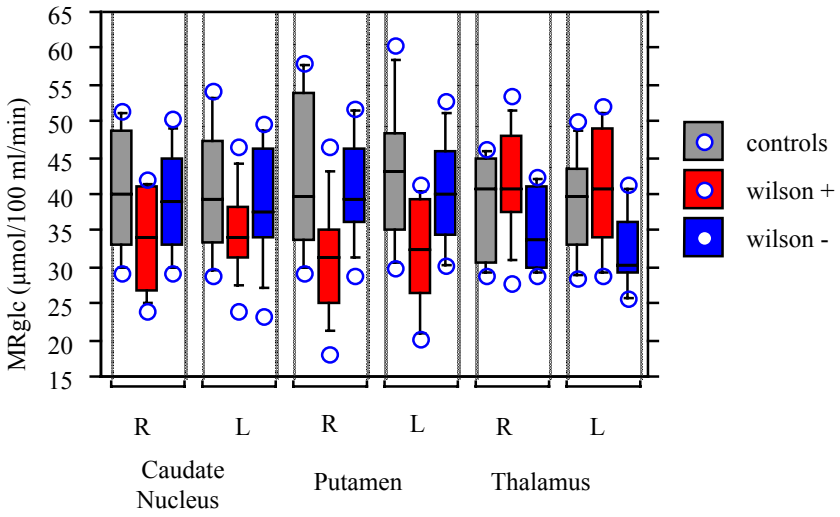

Fig. 2. In patients with distinct neurological symptoms (wilson +) a bilateral decrease in the glucose metabolism was found in the caudate nuclei and the putamen, while the thalami showed an increased metabolic activity. In patients without neurological symptoms normal values of the basal ganglia were found.

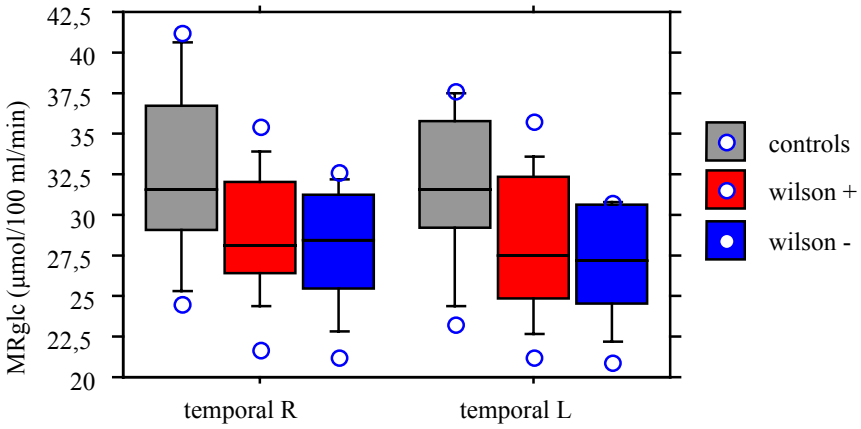

Fig. 3. A bilateral reduction in the glucose metabolism in the lateral temporal cortex was observed in patients with Wilson's disease, regardless of the manifestation of neurological symptoms (wilson +/-) as compared with the controls.

Table 1. rMRGlc in Wilson‘s disease and controls. Relation to neurological symptoms (+/-)

	Controls rMRGlc	Wilson - rMRGlc	Wilson + rMRGlc	(c/w-) p	(c/w+) p	(w-/w+) p
Gbl. gray matter	35.8 ± 5.9	35.4 ± 4.8	34.9 ± 5.3	n.s.	n.s.	n.s.
Caudate nucleus	40.5 ± 8.6	38.7 ± 7.4	34.2 ± 6.2	n.s.	0.07	n.s.
Putamen	43.0 ± 10.3	40.7 ± 7.3	31.4 ± 7.5	n.s.	0.008	0.008
Thalamus	38.6 ± 7.2	34.1 ± 5.4	40.8 ± 7.6	n.s.	n.s.	0.03
Front. cortex	39.3 ± 8.0	35.2 ± 5.4	36.2 ± 4.7	n.s.	n.s.	n.s.
Temp. cortex	32.1 ± 4.9	27.6 ± 3.5	28.6 ± 4.1	0.05	0.09	n.s.
Parietal cortex	37.9 ± 7.7	35.0 ± 5.1	35.5 ± 5.5	n.s.	n.s.	n.s.
Cerebellar cortex	33.6 ± 5.9	28.5 ± 5.6	30.7 ± 5.3	n.s.	n.s.	n.s.

MRGlc in µmol/100ml/min; significance of regional differences by student's t-test; Controls or c = control group; Wilson- or w- = Wilson patients without neurological symptoms; Wilson+ or w+ = Wilson patients with distinct neurological symptoms.

Examples of typical distributions of the regional cerebral glucose metabolism are shown in Figure 4. An unimpaired cerebral glucose metabolism was found in the basal ganglia and thalamus of a patient with Wilson's disease but without clinical symptoms. Patients with neurological symptoms exhibited a severe symmetrical impairment of the metabolism in the putamen and the caudate nuclei.

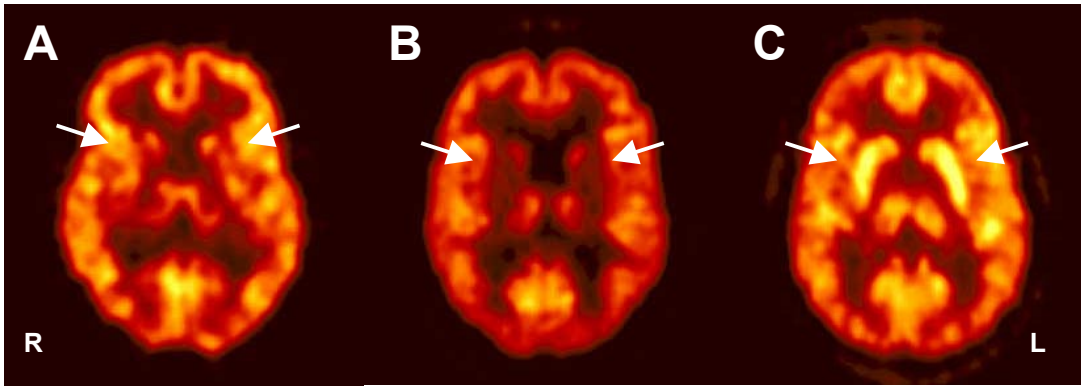

Fig. 4. FDG-PET of patients with Wilson's disease. Transaxial slices at the height of the basal ganglia. (A) 29-year-old female with symptoms for 11 years and a homozygote gene defect. PET was performed when Wilson`s disease was first diagnosed, without any previous treatment. Distinct neurological symptoms were observed. Decreased regional glucose metabolism in the area of the caudate nuclei and putamen. (B) 29-year-old male with a known Wilson‘s disease for 13 years. Treatment for six months with penicillamine. Distinct neurological symptoms. A severe reduction in the regional glucose metabolism in the caudate nuclei and the putamen was also found. (C) 30-year-old male with Wilson‘s disease known for 2 years. Tomography was performed under continued drug treatment with penicillamine. Clinically no neurological symptoms. Normal regional glucose metabolism.

FDG-PET may therefore be a useful parameter to support the clinical diagnosis of patients with Wilson‘s disease. Metabolic impairment was mostly bilateral. A moderate reduction in the glucose metabolism of the lateral temporal cortex was found in all patients with Wilson‘s disease. A decreased glucose metabolism in the basal ganglia was only observed in Wilson patients with clinically manifest neurological symptoms.

References

[1] Bacon, B.R.; Schilsky, M.L. New knowledge of genetic pathogenesis of hemochromatosis and Wilson's disease. Adv. Intern. Med. 44 (1999) 91-116.

[2] Brewer, G.J. Recognition, diagnosis, and management of Wilson's disease. Proc. Soc. Exp. Biol. Med. 223 (2000) 39-46.

[3] Wilson, S.A.K. Progressive lenticular degeneration. A familial nervous disease associated with cirrhosis of the liver. Brain 34 (1912) 295-307.

[4] Cordato, D.J.; Fulham, M.J.; Yiannikas, C. Pretreatment and posttreatment positron emission tomographic scan imaging in a 20-year-old patient with Wilson's disease. Mov. Disord. 13 (1998) 162-6.

[5] Hawkins, R.A.; Mazziotta, J.C.; Phelps, M.E. Wilson's disease studied with FDG and positron emission tomography. Neurology 37 (1987) 1707-11.

[6] De Volder, A.; Sindic, C.J.; Goffinet, A.M. Effect of D-penicillamine treatment on brain metabolism in Wilson's disease: a case study. J. Neurol. Neurosurg. Psychiatry 51 (1988) 947-9.

[7] Hefter, H.; Kuwert, T.; Herzog, H.; Arendt, G.; Stremmel, W.; Feinendegen, L.E. Relationship between striatal glucose consumption and copper excretion in patients with Wilson's disease treated with D-penicillamine. J. Neurol. 241 (1993) 49-53.

[8] Kuwert, T.; Hefter, H.; Scholz, D.; Milz, M.; Weiss, P.; Arendt, G.; Herzog, H.; Loken, M.; Hennerici, M.; Feinendegen, L.E. Regional cerebral glucose consumption measured by positron emission tomography in patients with Wilson's disease. Eur. J. Nucl. Med. 19 (1992) 96-101.

[9] Patlak, C.S.; Blasberg, R.G. Graphical evaluation of blood-to-brain transfer constants from multiple-time uptake data. Generalizations. J. Cereb. Blood Flow Metab. 5 (1985) 584-90.

[10] Patlak, C.S.; Blasberg, R.G.; Fenstermacher, J.D. Graphical evaluation of blood-to-brain transfer constants from multiple-time uptake data. J. Cereb. Blood Flow Metab. 3 (1983) 1-7.

[11] Talairach, J.; Tournoux, P. Co-planar stereotaxic atlas of the human brain. 2nd ed. Stuttgart: Thieme Verlag; 1988.

61. Integration of Functional Brain PET Images and Intraoperative Brain Mapping Data into the BrainLab VectorVision Neuronavigation System

R. Steinmeier[1], S. B. Sobottka[1], B. Beuthien-Baumann[2], J. Bredow[2], G. Reiss[1], R. von Kummer[3], W.-G. Franke[2], G. Schackert[1].
TU Dresden, [1]Klinik und Poliklinik für Neurochirurgie, [2]Klinik und Poliklinik für Nuklearmedizin /PET-Zentrum Rossendorf, [3]Abteilung für Neuroradiologie am Institut und Poliklinik für Radiologische Diagnostik

Introduction

In order to safely resect lesions close to eloquent brain areas, knowledge of their spatial distribution is essential. The classic technique is to perform surgery in the conscious patient under local anaesthesia, using brain-mapping techniques [1]. As an alternative, the location of eloquent areas can be visualized by preoperative functional brain imaging techniques, including positron emission tomography [2 - 7]. Both methods were combined by integration into a neuronavigation system (BrainLab) and were used to monitor speech-eloquent areas.

Patients and Methods

Speech-eloquent areas were preoperatively localized in five patients with left-sided lesions, using fluoro-18-desoxy-glucose PET. The patients were first scanned under conditions of silence and in a second study with speech activation, using a verb generation paradigm. The two scans were matched, the image maxima were adjusted, and the “zero” scan was subtracted from the activation study. The net activation was then superimposed on the “zero” scan (Fig. 1). This PET data set was transferred to a neuronavigation workstation and matched with a preoperative 3D-MRI, using a new image fusion algorithm. Intraoperative localization was performed, using brain-mapping techniques under local anaesthesia with bipolar stimulation. The stimulator position was mapped into the MRI-PET data set by neuronavigational tracking of the instrument.

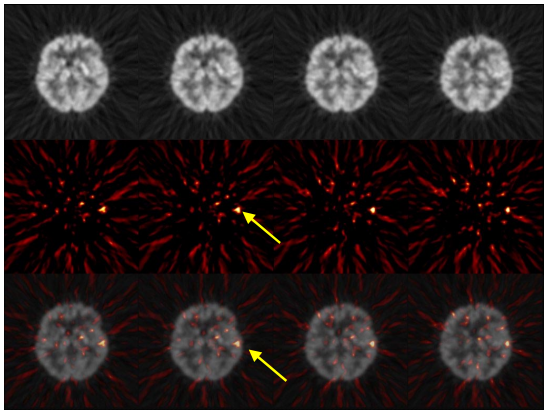

Fig. 1. Upper row: FDG-PET under conditions of silence (“zero” scan). Middle row: Net activation. Lower row: Net activation superimposed on the “zero” scan.

Results and Discussion

Using this novel technique, which is not yet commercially available, the preoperative activation PET and MRI can be exactly matched (Fig. 2). By integration of functional PET images and position tracking of the brain mapping electrode into neuronavigation, both methods can be compared and exactly transferred to the operative field. Five patients were operated according to this protocol, confirming the technical feasibility. Interestingly, the eloquent areas localized by speech-activation PET differed slightly from intraoperative areas of speech disturbance. These differences might be accounted for by slightly varying activation procedures during PET and the intraoperative setting. Further modifications of the activation paradigms might therefore be necessary. Apart from the speech activation itself, further experience with this new technique will have to be gathered to identify pos-

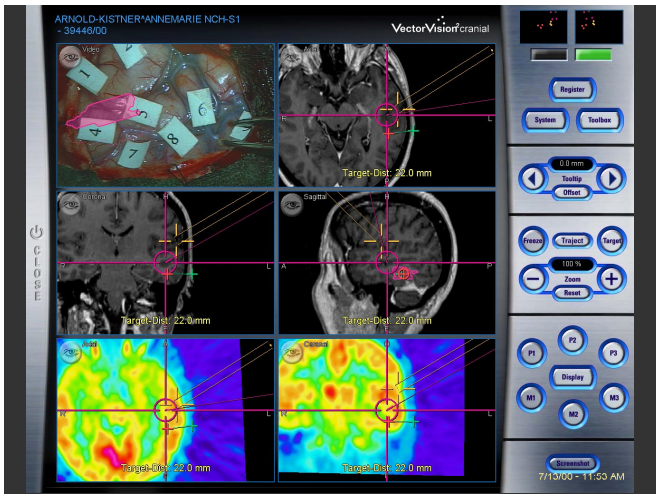

Fig. 2. Intraoperative display of the neuronavigation system. Intraoperative situs (upper left) MRI (upper right and middle row) and FDG-PET are visualized on one screen, superimposing the current position of the stimulator on each modality.

sible technical influences such as intraoperative brain shift, regional image distortion of MRI or the spatial resolution of the reference method (bipolar stimulation).
The new technique is suitable for monitoring eloquent speech areas during surgical resection of extended left-sided low-grade gliomas. By allowing a comparison with intraoperative electrophysiological brain mapping findings, the sensitivity and specificity of new functional imaging techniques can be evaluated by reconciling the data with the intraoperative situs.

References

[1] Ojemann, G.; Ojemann, J.; Lettich, E.; Berger, M. Cortical language localization in left, dominant hemisphere. An electrical stimulation mapping investigation in 117 patients. J. Neurosurg. 90 (1989) 591-598.

[2] McCarthy, G., Blamire, A.M.; Rothman, D.L.; Gruetter, R., Shulman, R.G. Echo-planar magnetic resonance imaging studies of the frontal cortex activation during word generation in humans. Proc. Natl. Acad. Sci. USA 90 (1993) 4952-4956.

[3] Fitzgerald. D.B.; Cosgrove, G.R.; Ronner, S.; Jiang, H.; Buchbinder, B.R.; Belliveau, J.W.; Rosen, B.R.; Benson, R.R. Location of language in the cortex: a comparison between functional MR imaging and electrocortical stimulation. Am. J. Neuroradiol. 18 (1997) 1529-1539.

[4] Simos, P.G.; Breier, J.I.; Maggio, W.W.; Gormley, W.B.; Zouridakis, G.; Willmore, L.J.; Wheless, J.W.; Constantinou, J.E.; Papnicolaou, A.C. Atypical temporal lobe language representation: MEG and intraoperative stimulation mapping correlation. Neuroreport 10 (1999) 139-142.

[5] Simos, P.G.; Papanicolaou, A.C.; Breier, J.I.; Wheless, J.W.; Constantinou, J.E.; Gormley, W.B.; Maggio, W.W. Localizatioin of language-specific cortex by using magnetic source imaging and electrical stimulation mapping. J. Neurosurg. 91 (1999) 787-796.

[6] Herholz, K.; Thiel, A.; Wienhard, K.; Pietrzyk, U.; von Stockhausen, H.M.; Karbe, H.; Kessler, J.; Bruckbauer, T.; Halber, M.; Heiss, W.D. Individual functional anatomy of verb generation. Neuroimage 3 (1996) 185-194.

[7] Duncan, J.D.; Moss, S.D.; Bandy, D.J.; Manwaring, K.; Kaplan, A.M.; Reiman, E.M.; Chen, K.; Lawson, M.A.; Wodrich, D.L. Use of positron emission tomography for presurgical localization of eloquent brain areas in children with seizures. Pediatr. Neurosurg. 26 (1997) 144-156.

62. Longitudinal PET Study of the Cerebral Glucose Metabolism in Major Depression: Acute State and Clinical Remission

V. A. Holthoff[1], B. Beuthien-Baumann[2], W. Burchert, A. Triemer[1], P. Winiecki[1], W.-G. Franke[2], O. Bach[1]
TU Dresden, [1]Klinik und Poliklinik für Psychiatrie und Psychotherapie und [2]Klinik und Poliklinik für Nuklearmedizin /PET-Zentrum Rossendorf

Introduction

Although regional changes in the cerebral glucose metabolism and blood flow have been well described in depressed subjects, enduring abnormalities in longitudinal studies are less reliably identified [1 - 4]. Medication effects are an important design limitation because the brain metabolism and blood flow have been shown to change under the influence of psychotropic drugs. The following prospective longitudinal PET study aims to determine brain areas associated with depressive illness in patients with first episode and recurrent unipolar depression (DSM-IV) carefully matched for medication status and to define correlates of acute and remitted illness.

Patients and Methods

Study design
We measured the pattern of change in the regional cerebral glucose metabolism (rCMRGlu) with PET (Siemens-CTI Exact HR Plus) in patients scanned during acute major depression (DSM-IV) and in those patients optimally matched for antidepressant drugs following clinical remission. Patients were considered to be in remission when their HAM-D scores remained lower than 7 for at least 12 weeks. An additional clinical assessment was carried out 6 months after the follow-up PET. Patients were initially investigated with MRI and subjected to neuropsychological tests in the acute and remitted state.

Patients
A total of 33 patients (8 male/25 female, mean age 44.5 years) were investigated by PET in acute depression. HAMD-21 at entry into study was 27.7 ± 3.8. Up to now 18 patients have been evaluated by PET in clinical remission. The mean HAMD-21 at this point in time was 1.7 ± 1.6. The cerebral glucose metabolism from both studies was compared with data from 7 normal controls (6 male/1 female, mean age 36.9 years).

PET
The PET scans were performed on a dedicated PET scanner (ECAT EXACT HR+). A transmission scan for measured attenuation correction was performed. A dynamic acquisition over 60 min was started with an intravenous injection of 300 MBq FDG. Pseudoarterial blood samples were taken for a quantitative analysis.
The dynamic emission data was transformed into a parametric data set (Gjedde-Patlak Plot), followed by spatial normalization into Talairach space (medx sensor system). On these spatially normalized data a standardized evaluation was performed with predefined regions of interest (ROI) according to the Brodmann (Br.) areas (Fig. 1). The values of the regional brain metabolism of each investigation were normalized to the mean of the whole brain grey matter.
For statistical analysis the paired t-test and the Mann-Whitney U-test were applied (Statview, SAS).

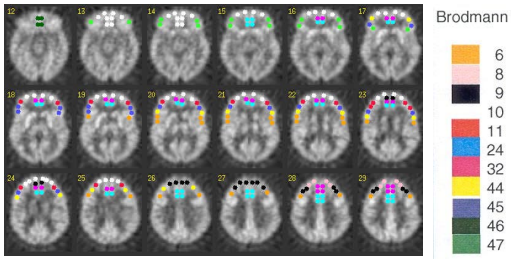

Fig. 1. ROI set of the frontal cortex according to the Brodmann areas.

Results and Discussion

Qualitative evaluation
Patients in acute depression showed areas of decreased tracer uptake in the prefrontal cortex (Fig. 2a). In clinical remission (Fig. 2b) these prefrontal areas showed incomplete increases in 8/18 patients, in 10/18 patients the pattern was unchanged.

Quantitative evaluation
Absolute metabolic values:
No significant differences were found between the mean of the whole brain grey matter values of the acute state (37.1± 8.4 µmol/100ml/min), clinical remission (37.7± 6.0) and the controls (36.9± 6.4).
Normalized data (Table 1):
Compared with the control group, significantly lower values were found in Br. 6, 8 and 46 in the right hemisphere in the acute state and in clinical remission. A significant asymmetry (left<right) in Br. 10, 32, 44,45 and 46 was observed in the acute state, persisting in remission only in Br. 46. No significant differences were seen in additional frontal areas, other cortical, subcortical or cerebellar regions.

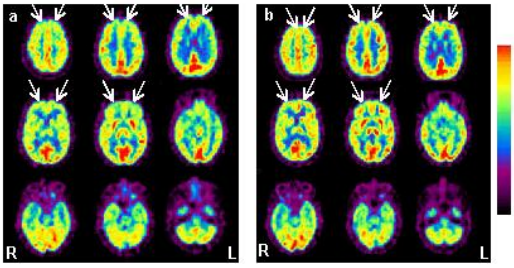

Fig. 2. A 59-year-old female depressive patient in the acute state (a) and in clinical remission (b). The glucose metabolism in the prefrontal and anterior cingulate cortex is markedly decreased during acute depression and increases upon recovery, although some metabolic impairment persists compared with the normal control.

Table 1. Normalized data of the frontal cortex. Acute state versus clinical remission

	Patients (n = 33) acute phase		Patients (n = 18) acute phase		remission	
ROI	right mean (SD)	left mean(SD)	right mean (SD)	left mean (SD)	right mean (SD)	left mean(SD)
Br. 6	1.02 ± 0,16**	1.03 ± 0.16	1.01 ± 0,17**	1.05 ± 0.14	0.99 ± 0.15**	1.06 ± 0.16
8	0.93 ± 0.15*	0.94 ± 0.20	0.93 ± 0.15*	0.96 ± 0.20	0.90 ± 0.15*	0.95 ± 0.16
10	1.00 ± 0.18	0.95 ± 0.18	1.01 ± 0.19	0.95 ± 0.18*	0.97 ± 0.17	0.93 ± 0.17
32	1.04 ± 0.13	0.99 ± 0.14	1.02 ± 0.13	0.98 ± 0.14*	1.00 ± 0.15	0.97 ± 0.15
44	1.07 ± 0.14	1.02 ± 0.15	1.07 ± 0.15	1.02 ± 0.15**	1.05 ± 0.14	1.01 ± 0.15
45	1.08 ± 0.15	0.99 ± 0.17	1.08 ± 0.16	1.00 ± 0.18***	1.04 ± 0.14	0.99 ± 0.15
46	1.11 ± 0.16*	0.98 ± 0.20	1.11 ± 0.17*	0.98 ± 0.21***	1.08 ± 0.14*	0.95 ± 0.19***

*p<0,01; **p< 0,005 patients versus controls
*p<0,01; **p<0,005; ***p<0,0001 left versus right hemisphere

An acute depressive state was associated with a significant asymmetry localized in specific prefrontal regions. In the recovered state the asymmetry was no longer present. It may therefore represent a state marker of depression. Altered rCMRGlu in Br. 6, 8 and 46 that persists upon recovery may be related to histopathological changes that have been revealed by a recent morphometric study [5].

References[1] Bench, C.J.; Frackowiak, R.S.; Dolan, R.J. Changes in regional cerebral blood flow on recovery from depression. Psychol. Med. 25 (1995) 247-61.
[2] Videbech, P. PET measurements of brain glucose metabolism and blood flow in major depressive disorder: a critical review. Acta Psychiatr. Scand. 10 (2000) 11-20.
[3] Drevets, W.C. Functional neuroimaging studies of depression: the anatomy of melancholia. Ann. Rev. Med. 49 (1998) 341-61.
[4] Soares, J.C.; Mann, J.J. The functional neuroanatomy of mood disorders. J. Psychiatr. Res. 31 (1997) 393-432.
[5] Rajkowska, G.; Miguel-Hidalgo, J.J.; Wie, J.; Delley, G.; Pittman, S.D.; Meltzer, H.Y.; Overholser, J.C.; Roth, B.L.; Stockmeier, C.A. Morphometric evidence for neuronal and glial prefrontal cell pathology in major depression. Biol. Psychiatry 45 (1999) 1085-1098.

II. PUBLICATIONS, LECTURES, PATENTS AND AWARDS

PUBLICATIONS

Bauer, R.; Brust, P.; Walter, B.; Vorwieger, G.; Bergmann, R.; Füchtner, F.; Steinbach, J.; El-Hallag, E.; Fritz, A.; Johannsen, B.; Zwiener U.
Relation between brain tissue pO_2 and dopamine synthesis of basal ganglia - A ^{18}FDOPA-PET study in newborn piglets.
J. Perinat. Med. 28 (2000) 54-60.

Bergmann, R.; Brust, P.; Scheunemann, M.; Pietzsch, H.-J.; Seifert, S.; Roux, F.; Johannsen, B.
Assessment of the in vitro and in vivo properties of a ^{99m}Tc-labeled inhibitor of the multidrug resistant gene product P-glycoprotein.
Nucl. Med. Biol. 27 (2000) 135-141.

Beuthien-Baumann, B.; Hamacher, K.; Oberdorfer, F.; Steinbach J.
Preparation of fluorine-18 labelled sugars and derivatives and their application as tracer for positron-emission-tomography.
Carbohydr. Res. 327 (2000) 107-118.

Brust, P.; Friedrich, A.; Krizbai, I. A.; Bergmann, R.; Roux, F.; Ganapathy, V.; Johannsen, B.
Functional expression of the serotonin transporter in immortalized rat brain microvessel endothelial cells.
J. Neurochem. 74 (2000) 1241-1248.

Friebe, M.; Spies, H.; Seichter, W.; Leibnitz, P.; Johannsen, B.
Neutral '3+1' mixed-ligand oxorhenium(V) complexes with tridentate [S,N,S] chelates and aminoalkanethiols: synthesis, characterization and structure determination.
J. Chem. Soc., Dalton Trans. (2000) 2471-2575.

Friebe, M.; Mahmood, A.; Spies, H.; Berger, R.; Johannsen, B.; Mohammed, A.; Eisenhut, M.; Bolzati, C.; Davison, A.; Jones, A. G.
'3+1' Mixed-ligand oxotechnetium(V) complexes with affinity for melanoma: Synthesis and evaluation in vitro and in vivo.
J. Med. Chem. 43 (2000) 2745-2752.

Friebe, M.; Suda, K.; Spies, H.; Syhre, R.; Berger, R.; Johannsen, B.; Chiotellis, E.; Kramer, S. D.; Wunderli-Allenspach, H.
Permeation studies in vitro and in vivo of potential radiopharmaceuticals with affinity to neuroreceptors.
Pharm. Res. 17 (2000) 754-760.

Linemann, H.; Will, E.; Beuthien-Baumann, B.
Untersuchung zur Strahlenbelastung des medizinischen Personals bei [^{18}F]FDG-PET-Studien.
Nuklearmedizin 39 (2000) 77-81.

Mäding, P.; Steinbach, J.
Synthesis of [1-^{11}C]phenol.
J. Labelled Compd. Radiopharm. 43 (2000) 557-563.

Mäding, P.; Steinbach, J.; Johannsen, B.
No-carrier-added ^{11}C-labelling of benzenoid compounds in ring positions by condensation of nitro-[^{11}C]methane with pyrylium salts.
J. Labelled Compd. Radiopharm. 43 (2000) 565-583.

Nock, B.; Pietzsch, H.-J.; Tisato, F.; Maina, T.; Leibnitz, P.; Spies, H.; Chiotellis, E.
Oxorhenium mixed-ligand complexes with the 2,6-dimercaptomethylpyridine ligand. Crystal structure of [2,6-dimercaptomethylpyridinato][p-methoxybenzenethiolato] oxorhenium(V).
Inorg. Chim. Acta 304 (2000) 26-32.

Nock, B.; Maina, T.; Tsortos, A.; Pelecanou, M.; Raptopoulou, C.P.; Papadopoulos, M.; Pietzsch, H.-J.; Stassinopoulou, C.; Terzis, A.; Spies, H.; Nounesis, G.; Chiotellis, E.
Glutathione interaction with SNS/S mixed ligand complexes of oxorhenium(V): Kinetic aspects and characterization of the products.
Inorg. Chem. 39 (2000) 4433-4441.

Pietzsch, H.-J.; Gupta, A.; Reisgys, M.; Drews, A.; Seifert, S.; Syhre, R.; Spies, H.; Alberto, R.; Abram, U.; Schubiger, P. A.; Johannsen, B.
Chemical and biological characterization of technetium(I) and rhenium(I) tricarbonyl complexes with dithioether ligands serving as linkers for coupling the $Tc(CO)_3$ and $Re(CO)_3$ moieties to biologically active molecules.
Bioconjugate Chem. 11 (2000) 414-424.

Römer, J.; Füchtner, F.; Steinbach, J.
Synthesis of 16α-[^{18}F]fluoroestradiol-3,17β-disulphamate.
J. Labelled Compd. Radiopharm. 43 (2000) 425-436.

Seifert, S.; Künstler, J.-U.; Gupta, A.; Funke, H.; Reich, T.; Hennig, C.; Rossberg, A.; Pietzsch, H.-J.; Alberto, R.; Johannsen, B.
EXAFS analyses of technetium(I) carbonyl complexes - stability studies in solutions.
Radiochim. Acta 88 (2000) 239-245.

Seifert, S.; Drews, A.; Gupta, A.; Pietzsch, H.-J.; Spies, H.; Johannsen, B.
Stability studies on ^{99m}technetium(III) complexes with tridentate/monodentate thiol ligands and phosphine ("3+1+1" complexes).
Appl. Radiat. Isot. 53 (2000) 431-438.

Stephan, H.; Spies, H.; Johannsen, B.; Kaufmann, C.; Vögtle, F.
pH-controlled inclusion and release of oxyanions by denrimers bearing methyl orange moieties.
Org. Lett. 2 (2000) 2343-2346.

Skaddan, M.B.; Wüst, F.R.; Jonson, S.; Syhre, R.; Welch, M.J.; Spies, H.; Katzenellenbogen, J.A.
Radiochemical synthesis and tissue distribution of Tc-99-labeled 7alpha-substituted estradiol complexes.
Nucl. Med. Biol. 27 (2000) 269-278.

PROCEEDINGS

Pietzsch, H.-J.; Scheunemann, M.; Kretzschmar, M.; Seifert, S.; Syhre, R.; Johannsen, B.
Design and biological evaluation of technetium(V) complexes for serotonin-5-HT_{2A} receptor binding.
IAEA Technical Document (IAEA TECDOC), December 2000.

Steiner, G.; Richter, T.; Salzer, R.; Bergmann, R.; Rodig, H.; Johannsen, B.
Identification of cancer cells by a combination of FTIR spectroscopy and PET.
Proceedings SPIE, Photonics West 2000, “Spectral Imaging: Instrumentation, Applications and Analysis" (3920), San Jose, CA, USA, 22.01.–28.01.2000.

Stephan, H.; Spies, H.; Johannsen, B.; Kauffmann, C.; Schwanke, F.; Vögtle, F.
Dendritic receptors for binding and transport of oxyanions.
ISSC IX 2000, XIth International Symposium on Supramolecular Chemistry, ACROS FUKUOKA, Fukuoka/Japan, 30.07.–04.08.2000, Abstractband PD27

ABSTRACTS

Abedin, Z.; Spies, H.
Synthesis characterization and stability studies of some potential brain-seeking agents - trialkyl (triaryl) siloxyalkyl-thiolato-3-thiapentane-1,5-dithialato oxorhenium(V) complexes
Nükleer TIP, Turk. J. Nucl. Med. 9 (2000) 92.

Ahlheit, H.; Bergmann, R.; Beuthien-Baumann, B.; Burchert, W.; Franke, W. G.; Füchtner, F.; Steinbach, J.; Syhre, R.; Zips, D.
3-O-Methyl-6-[^{18}F]Fluor-DOPA ([^{18}F]OMFD) zur Tumordiagnostik: Entwicklung eines neuen Tracers und erste Anwendung am Patienten.
Nuklearmedizin 39 (2000) A43.

Ahlheit, H.; Bergmann, R.; Beuthien-Baumann, B.; Bredow, J.; Burchert, W.; Franke, W. G.; Füchtner, F.; Steinbach, J.; Syhre, R.; Zips, D.
3-O-Methyl-6-[^{18}F]fluoro-L.DOPA ([^{18}F]OMFD): Development and first application of a new tracer for tumor detection with PET.
J. Nucl. Med. 41 (2000) (Suppl. 5) 43P.

Bergmann, R.; Scheunemann, M.; Brust, P.; Mäding, P.; Steinbach, J.; Tourwe, D.; Johannsen, B.
^{18}F-markierte Peptide zur Darstellung von Neurotensin- und Bombesin-Rezeptoren mit der Positronen-Emissions-Tomographie.
Nuklearmedizin 39 (2000) A12.

Bergmann, R.; Scheunemann, M.; Mäding, P.; Rodig, H.; Kretzschmar, M.; Chavatte, K.; Tourwé, D.; Zips, D.; Brust, P.; Johannsen, B.
New ^{18}F-labelled neurotensin(8-13) analogs for positron emission tomography (PET): Pharamcological and biochemical charakterisation.
Nucl. Med. Commun. 21 (2000) 565-566.

Brust, P.; Zessin, J.; Kretzschmar, M.; Bergmann, R.; Friedrich, A.; Füchtner, F.; Hinz, R.; Steinbach, J.; Johannsen, B.
Characterization of [^{11}C]McN5652 in various animal species: Implications for tracer development.
NeuroImage 11 (2000) S66.

Chavatte, K.; Bergmann, R.; Terriere, D.; Iterbeke, K., Tourwé, D.; Mertens, J.; Bossuyt, A.
3-^{125}I-4-HO-Phenylacetyl-[Lys-Psi(CH_2=NH)-Arg-Phe^{11}-t-Leu^{12}-]NT(10-13): Radiosynthesis and characterisation.
Nucl. Med. Commun. 21 (2000) 568.

Dinkelborg, L. M.; Tepe, G., Noll, B., Muschick, P.; Duda, S. H.
^{186}Re labeled stents for prophylaxis of restenosis: First animal results.
J. Nucl. Med. 41 (2000) 7P.

Franke, W.-G.; Ahlheit, H., Beuthien-Baumann, B., Bergmann, R., Bredow, J., Brust, P., Burchert, W.; Füchtner, F.; Johannsen, B.; Kretzschmar, M., Steinbach, J., Syhre, R.; Zips, D.
3-O-Methyl-6-[^{18}F]fluor-L.DOPA (OMFD) - First experiences in brain tumor imaging.
Nükleer TIP, Turk. J. Nucl. Med. 9 (2000) 64.

Friebe, M.; Mahmood, A.; Bolzati, C.; Spies, H.; Johannsen, B.; Mohammed, A.; Eisenhut, M., Davison, A.; Jones, A. G.
N,N-(Dialkylamino)-alkyl substituted ^{99m}Tc-amineamidedithiol (AADT) complexes as diagnostic probes for melanoma.
J. Nucl. Med. 41 (2000) 120P.

Hinz, R.; Enghardt, W.; Hasch, B. G., Lauckner, K., Pawelke, J., Pönisch, F., Sobiella, M.
PET zur in-situ Dosislokalisation bei der Schwerionen-Tumortherapie.
Nuklearmedizin 39 (2000) A45.

Iterbeke, K.; Chavatte, K.; Terriere, D.; Bergmann, R.; Johannsen, B.; Tourwe, D.; Mertens, J.
Optimization of a neurotensin(8-13) analogue for radioiodination.
Nucl. Med. Commun. 21 (2000) 588-589.

Kropp, J.; Naumann, R.; Schirmer, L.; Tipolt, C.; Beuthien-Baumann, B.; Franke, W.-G.; Ehninger, G.
Comparison of dedicated PET with hybrid PET in patients with malignant lymphomas.
J. Nucl. Med. 41 (2000) Supplement 71P.

Kutzner, H.; Linemann, H.; Will, E.; Beuthien-Baumann, B.
Auswirkungen unterschiedlicher Rekonstruktionsparameter auf die Bildqualität bei der Positronen-Emissions-Tomographie (PET).
Nuklearmedizin 39 (2000) A99.

Pinkert, J., Wunderlich, G.; Bergmann, R.; Hliscs, J.; Kropp, J.; Franke, W. G.
Re-188 markierte HSA-Mikrosphären für die intraarterielle Tumorembolisation.
Nuklearmedizin 39 (2000) A44.

Zessin, J.; Eskola, O.; Steinbach, J.; Bergman, J.; Marjamäki, P., Brust, P.; Solin, O.; Johannsen, B.
Synthese und erste biologische Evaluierung des [^{18}F]Fluormethyl-Analogons von (+)-McN5652, einem Tracer zur Darstellung des Serotonintransporters.
Nuklearmedizin 39 (2000) A36.

LECTURES AND POSTERS

Abedin, Z.; Spies, H.
Synthesis characterization and stability studies of some potential brain-seeking agents - trialkyl (triaryl) siloxyalkyl-thiolato-3-thiapentane-1,5-dithialato oxorhenium(V) complexes.
VII. Asia and Oceania Congress of Nuclear Medicine and Biology & IV. International Congress of Nuclear Oncology, Istanbul/Turkey, 01.-05.10.2000.

Ahlheit, H.; Bergmann, R.; Beuthien-Baumann, B.; Burchert, W., Franke, W. G.; Füchtner, F.; Steinbach, J.; Syhre, R.; Zips, D.
3-O-Methyl-6-[^{18}F]Fluor-DOPA ([^{18}F]OMFD) zur Tumordiagnostik: Entwicklung eines neuen Tracers und erste Anwendung am Patienten.
Nuklearmedizin 2000, 38. Intern. Jahrestagung DGN, München, 29.03.-01.04.2000.

Ahlheit, H.; Bergmann, R.; Beuthien-Baumann, B.; Bredow, J.; Burchert, W.; Franke, W. G.; Füchtner, F.; Steinbach, J.; Syhre, R.; Zips, D.
3-O-Methyl-6-[^{18}F]fluoro-L.DOPA ([^{18}F]OMFD): Development and first application of a new tracer for tumor detection with PET.
47th Annual Meeting of the Society of Nuclear Medicine, St. Louis/USA, 03.-07.06.2000.

Berger, R.; Spies, H.; Friebe, M.; Johannsen, B.
Lipophilicity and pK_a measurements of technetium and rhenium complexes as potential radiopharmaceuticals by using RP-HPLC.
LogP2000, The Second Lipophilicity Symposium: ”Lipophilicity in Drug Disposition: Practical and Computational Approaches to Molecular Properties Related to Drug Permeation, Disposition and Metabolism” Lausanne, March 05.–09.03.2000.

Bergmann, R.; Scheunemann, M.; Brust, P.; Mäding, P.; Steinbach, J.; Tourwe, D.; Johannsen, B.
^{18}F-markierte Peptide zur Darstellung von Neurotensin- und Bombesin-Rezeptoren mit der Positronen-Emissions-Tomographie.
Nuklearmedizin 2000, 38. Intern. Jahrestagung DGN, München, 29.03.-01.04.2000.

Bergmann, R.; Scheunemann, M.; Mäding, P.; Rodig, H.; Kretzschmar, M., Chavatte, K.; Tourwé, D.; Zips, D., Brust, P.; Johannsen, B.
New ^{18}F-labelled neurotensin(8-13) analogs for positron emission tomography (PET): Pharamcological and biochemical charakterisation.
International Congress on Peptide Radiopharmaceuticals in Diagnosis and Therapy, Rome, 25.-28.05.2000.

Brust, P.; Zessin, J.; Kretzschmar, M.; Bergmann, R.; Friedrich, A.; Füchtner, F.; Hinz, R.; Steinbach, J.; Johannsen, B.
Characterization of [^{11}C]McN5652 in various animal species: Implications for tracer development.
Third International Symosium on Functional Neuroreceptor Mapping, New York, 09.-11.06.2000.

Chavatte, K.; Bergmann, R.; Terriere, D.; Iterbeke, K.; Tourwé, D.; Mertens, J.; Bossuyt, A.
3-^{125}I-4-HO-Phenylacetyl-[Lys-Psi(CH_2=NH)-Arg-Phe^{11}-t-Leu^{12}-]NT(10-13): Radiosynthesis and characterisation.
International Congress on Peptide Radiopharmaceuticals in Diagnosis and Therapy, Rome, 25.-28.05.2000.

Dinkelborg, L.M.; Tepe, G.; Noll, B.; Muschick, P.; Duda, S.H.
^{186}Re labeled stents for prophylaxis of restenosis: First animal results.
47th Annual Meeting of the Society of Nuclear Medicine, St. Louis/USA, 03.-07.06.2000.

Friebe, M.; Mahmood, A.; Bolzati, C.; Spies, H.; Johannsen, B.; Mohammed, A.; Eisenhut, M.; Davison, A.; Jones, A.G.
N,N-(Dialkylamino)-alkyl substituted ^{99m}Tc-amineamidedithiol (AADT) complexes as diagnostic probes for melanoma.
47th Annual Meeting of the Society of Nuclear Medicine, St. Louis/USA, 03.-07.06.2000.

Friedrich, A.; Ganapathy, V.; Brust, P.
Transport of choline and carnitine at the blood-brain barrier in vitro.
Symposium Signal Transduction in the Blood-Brain Barrier, Potsdam, 22.-24.09.2000.

Füchtner, F.; Steinbach, J.; Johannsen, B.
PET radiopharmaceutical production - a unit of preparation and quality control.
Sixth TESLA Workshop: Positron Emission Tomography at the Cyclotron Center of the Slovak Republic, Castá-Papiernicka, Slovak Republic, 24.-25.10.2000.

Gloe, K.; Chartroux, C.; Rambusch, T.; Stephan, H.; Vögtle, F.
Binding of metal ions by dendrimers.
Workshop "Aspects of Dendrimers in Drug Targeting", FZ Rossendorf, 08.05.2000.

Hinz, R.; Enghardt, W.; Hasch, B.G.; Lauckner, K.; Pawelke, J.; Pönisch, F.; Sobiella, M.
PET zur in-situ Dosislokalisation bei der Schwerionen-Tumortherapie.
Nuklearmedizin 2000, 38. Jahrestagung DGN, München, 29.03.-01.04.2000.

Iterbeke, K., Chavatte, K.; Terriere, D., Bergmann, R., Johannsen, B.; Tourwe, D.; Mertens, J.
Optimization of a neurotensin(8-13) analogue for radioiodination.
International Congress on Peptide Radiopharmaceuticals in Diagnosis and Therapy, Rome, 25.-28.05.2000.

Jordanova, A.; Steinbach, J.
Synthese von Radiofluor-markiertem [^{18}F]Perchlorylfluorid im pikomolaren Konzentrationsbereich.
Deutsche Fluortage Schmitten/Taunus, 24.-27.09.2000.

Künstler, J.-U.; Seifert, S.; Reich, T., Funke, H.; Johannsen, B.
EXAFS analyses of technetium(I) and rhenium(I) tricarbonyl complexes - ligand exchange studies.
Second Euroconference and NEA Workshop on Speciation, Techniques, and Facilities for Radioactive Materials at Synchrotron Light Sources, Grenoble, France, 10.09 - 12.09. 2000.

Kutzner, H.; Linemann, H., Will, E.; Beuthien-Baumann, B.
Auswirkungen unterschiedlicher Rekonstruktionsparameter auf die Bildqualität bei der Positronen-Emissions-Tomographie (PET).
Nuklearmedizin 2000, 38. Intern. Jahrestagung DGN, München, 29.03.-01.04.2000.

Linemann, H.; Will, E.; Beuthien-Baumann, B.; Kutzner, H.
Measurements of recovery coefficients for the HR+ and their application in a correction method.
CTI-Tagung Barcelona, Spanien, 28.08.-01.09.2000.

Pietzsch, H.-J.; Johannsen, B.
Technetium and Rhenium in Nuclear Medicine
Congress of the South American Pharmaceutical Federation, Montevideo/Uruguay, 26.-28.04.2000
Identification of cancer cells by a combination of FTIR spectroscopy and PET.

Pietzsch, H.-J.
Development of ^{99m}Tc complexes for imaging the serotonin-5HT$_{2A}$ receptor in the central nervous system.
3rd Research Co-ordination Meeting on"Development of Agents for Imaging CNS Receptors Based on 99mTc", Montevideo, Uruguay, 24.-28.04.2000.

Pietzsch, H.-J.
Tc complexes as ligands for CNS receptors: state of the art (1993-1999).
3rd Research Co-ordination Meeting on"Development of Agents for Imaging CNS Receptors Based on 99mTc", Montevideo, Uruguay, 24.-28.04.2000.

Pietzsch, H.-J.; Scheunemann, M.; Kretzschmar, M.; Seifert, S.; Syhre, R.; Johannsen, B.
Design and biological evaluation of technetium(V) complexes for serotonin-5-HT$_{2A}$ receptor binding.
IAEA Research Coordination Meeting on CNS Receptors, Montevideo/Uruguay, 24.-28.04.2000.

Pietzsch, H.-J.; Spies, H.
A novel approach to robust Tc(III) mixed-ligand chelates as tools for conjugating biologically active molecules.
Meeting der COST B12 Action, WG 5, Rome, 29.05.2000.

Pietzsch, H.-J.; Seifert, S.; Drews, A.; Tisato, F.; Refosco, F.; Gupta, A.; Syhre, R.; Spies, H.
A novel approach to robust Tc(III) mixed-ligand chelates as tools for conjugating biologically active molecules.
34. International Conference on Coordination Chemistry, Edinburgh, 09.-14.07.2000.

Pinkert, J.; Wunderlich, G.; Bergmann, R.; Hliscs, J.; Kropp, J.; Franke, W. G.
Re-188 markierte HSA-Mikrosphären für die intraarterielle Tumorembolisation.
Nuklearmedizin 2000, 38. Jahrestagung DGN, München, 29.03.-01.04.2000.

Römer, J.; Füchtner, F.; Steinbach, J.; Kasch, H.
Rapid module-assisted synthesis of 16α[^{18}F]fluorestradiol-3,17β-disulphamate.
7th International Symposium on The Synthesis and Applications of Isotopes and Isotopically Labelled Compounds of the International Isotope Society, Dresden, 18.-22.06.2000.

Scheunemann, M.; Mäding, P.; Bergmann, R.; Steinbach, J.; Iterbeke, K.; Tourwé, D.; Johannsen, B.
F-18 peptide labelling: Neurotensin derivatives.
7th International Symposium on The Synthesis and Applications of Isotopes and Isotopically Labelled Compounds of the International Isotope Society, Dresden, 18.-22.06.2000.

Steinbach, J.*
Trägerarme Markierung aromatischer Verbindungen mit C-11 und F-18.
Institutsseminar, Institut für Nuklearchemie, Forschungszentrum Jülich, 28.05.2000.

Steinbach, J.*
Labelling of aromatic compounds with carbon-11.
7th International Symposium on The Synthesis and Applications of Isotopes and Isotopically Labelled Compounds of the International Isotope Society, Dresden, 18.-22.06.2000.

Steinbach, J.*
PET-Radiopharmaka: Stand und Perspektiven.
7. Jahrestagung, Berlin-Brandenburgische Gesellschaft für Nuklearmedizin e.V., Brielow, 11.11.2000.

Steiner, G.; Richter, T.; Salzer, R.; Bergmann, R.; Rodig, H.; Johannsen, B.
SPIE, Photonics West 2000, "Spectral Imaging: Instrumentation, Applications and Analysis" (3920) San Jose, CA, USA, 22.-28.01.2000.

Stephan, H.*
Functionalized dendrimers: Emerging opportunities for the application in medicine.
4-Center Meeting Amsterdam-Bologna-Bonn-Freiburg, Oegstgeest/Leiden (Netherlands) 24.-26.03.2000.

Stephan, H.; Johannsen, B.
Functionalized dendrimers in drug delivery systems.
Max Delbrück Center of Molecular Medicine, 07.04.2000.

Stephan, H.; Spies, H.; Syhre, R.
Dendrimers and their emerging medicinal applications.
Workshop "Aspects of Dendrimers in Drug Targeting", FZ Rossendorf, 08.05.2000.

Stephan, H.*
Development of complexing agents for binding Tc(VII) and An(III).
Kolloquium, Department of Materials Science, Japan Atomic Energy Research Institute, Tokai, Japan, 24.07.2000.

Stephan, H.*
Binding and transport of transition metals using tailor-made ligands.
Kolloquium, Department of Applied Chemistry, Saga University, Saga, Japan, 27.07.2000.

Stephan, H.; Spies, H.; Johannsen, B.; Kauffmann, C.; Schwanke, F.; Vögtle, F.
Dendritic receptors for binding and transport of oxyanions.
XIth Int. Symp. Supramolecular Chem., ACROS FUKUOKA, Fukuoka (Japan), 30.07.–04.08.2000.

Stephan, H.*
Dendrimere in der medizinischen Diagnostik und Therapie: Stand und Perspektiven.
Institutskolloquium, Universität Bonn, Institut für Organische Chemie und Biochemie, 06.10.2000.

Stephan, H.; Pietzsch, H.-J.; Spies, H.; Leibnitz, P.
Requirements for the development of complexing agents for technetium and actinides.
Institutskolloquium, Universität Heidelberg, Institut für Anorganische Chemie, 07.10.2000.

Zessin, J.; Eskola, O.; Steinbach, J.; Bergman, J.; Marjamäki, P.; Brust, P.; Solin, O.; Johannsen, B.
Synthese und erste biologische Evaluierung des [^{18}F]Fluormethyl-Analogons von (+)-McN5652, einem Tracer zur Darstellung des Serotonintransporters.
Nuklearmedizin 2000, 38. Intern. Jahrestagung DGN, München, 29.03.-01.04.2000.

Zessin, J.; Eskola, O.; Steinbach, J.; Mariamäki, P.; Bergman, J.; Brust, P.; Solin, O.; Johannsen, B.
Imaging of the serotonin transporter with the [^{18}F]fluoromethyl analogon of (+)-McN5652.
7th International Symposium on The Synthesis and Applications of Isotopes and Isotopically Labelled Compounds of the International Isotope Society, Dresden, 18.-22.06.2000.

PATENTS

Römer, J.; Füchtner, F.; Steinbach, J., Kasch, H.; Johannsen, B. ha 1173, AZ 10006155.9
Verfahren zur Herstellung von 16α-[^{18}F]Fluorestradiolsulfamaten.

AWARDS

Dr. Matthias Friebe
FZR-Doktorandenpreis 2000
Amingruppentragende Technetium(V)- und Rhenium(V)-Verbindungen: Synthese und Untersuchungen von Zusammenhängen molekularer Eigenschaften und dem Transport über die Blut-Hirn-Schranke.

PhD THESIS

Antje Gupta
In-vivo und in-vitro Stabilität und Metabolismus von Gemischtligandkomplexen.
Dresden University of Technology, 16.10.2000.

III. SCIENTIFIC COOPERATION

COOPERATIVE RELATIONS AND JOINT PROJECTS

In multidisciplinary research such as carried out by this Institute, collaboration, the sharing of advanced equipment and, above all, exchanges of ideas and information play an important role. Effective collaboration has been established with colleagues at universities, in research centres and hospitals.

Dresden University of Technology has been a major partner in our cooperative relations. Cooperation with various groups in the Department of Chemistry and the Faculty of Medicine was again significantly extended last year. Common objects of radiopharmacological and medical research link the Institute with the Dresden University Hospital, above all with its Department of Nuclear Medicine (Prof. Franke). A joint team of staff members from both the Institute and the Clinic of Nuclear Medicine are currently working at the Rossendorf PET Centre.
The Institute cooperates with the Department of Surgical Research (Prof. Schackert) on a project concerning gene therapy monitoring. The Institute of Analytical Chemistry (Prof. Salzer) plays an important part in tumour research.

Special thanks go to *Schering AG Berlin* (Dr. Dinckelborg).

Very effective cooperation exists with the *Federal Material Research Institute in Berlin* (Mr. Leibnitz, Dr. Reck), whose staff members carried out X-ray crystal structure analysis of new technetium and rhenium complexes.

Our Institute is linked with the Institute of Pathology (Prof. Zwiener, Dr. Bauer) of *Jena's Friedrich-Schiller University* by long-standing fruitful cooperation on the pathophysiological aspects of brain functions.

The fruitful collaboration with the *Paul Scherrer Institute* (Prof. Schubiger*)* of Villigen, Switzerland, which involves bioinorganic, radiochemical and biological topics, is much appreciated. PSI is also one of the main partners in the current BIOMED2 project on tumour-affine neuropeptides.

Cooperation in Tc chemistry exists with the *University of Ferrara* (Prof. Duatti, Dr. Bolzati), *CNR Padova* (Dr. Tisato, Dr. Refosco), and, more recently, with the *Instituto Tecnologico e Nuclear (ITN)*, Lisbon (Dr. Santos).

Our long-standing cooperation with the *"Demokritos" National Research Centre for Physical Sciences* in Athens (Dr. Chiotellis) has been continued. Various joint projects on technetium and rhenium chemistry were dealt with.

In the field of supramolecular chemistry, successful cooperation was established with the Institute of Organic Chemistry and Biochemistry (Prof. Schmidtchen) of *Technische Universität München* and with the Kekulé Institute of Organic Chemistry and Biochemistry (Prof. Vögtle) of the *University of Bonn.*

Cooperation in PET tracer chemistry and radiopharmacology has been established with the *Turku Medical PET Centre* (Dr. Solin).

In the field of PET tracers (steroid chemistry) the Institute works together with the *Hans-Knöll-Institute for Natural Products Research,* Jena (Prof. Hinnen, Dr. Kasch).

The further development of the regioselective labelling of compounds is the subject of a fruitful cooperation with *BASF*, Ludwigshafen (Dr. Schlecker).

The identification of common objects in PET radiopharmacy has led to collaborative research with the Department of Nuclear Medicine (Prof. Georgi) of the *University of Leipzig* as well as with the *Institut für Interdisziplinäre Isotopenforschung Leipzig* (Prof. Stöcklin).

Effective cooperation also exists with the *Riga Institute of Organic Chemistry* (Dr. Zablotskaya), Latvia.
The Institute works with the *Bar-Ilan University* in Ramat-Gan*,* Israel (Prof. Nudelman).

LABORATORY VISITS

A. Drews
Karolinska Institute Stockholm, Sveden
April 22 – 28, 2000

A. Gupta
Karolinska Institute Stockholm, Sveden
April 22 – 28, 2000

H. Spies
Latvian Institute of Organic Synthesis Riga, Latvia
July 14 – 17, 2000

A. Drews
Karolinska Institute Stockholm, Sveden
August 27 – September 3, 2000

A. Gupta
Karolinska Institute Stockholm, Sveden
August 27 – September 3, 2000

T. Knieß
Latvian Institute of Organic Synthesis Riga, Latvia
September 28 – October 1, 2000

J. Zessin
National PET-Centre Turku, Finland
October 30 – November 11, 2000

GUESTS

Dr. H. Li
Nuklearmedizinische Klinik und Poliklinik des Klinikums München-Großhadern
January 10 – 21, 2000

Dr. Patt
Institut für Interdisziplinäre Isotopenforschung Leipzig
January 10 – 11, 2000

Dr. Th. Stumpf
Forschungszentrum Karlsruhe
January 21 – 25, 2000

Dr. F. Tisato
CNR Padua, Italy
February 15 – 18, 2000

Dr. Ch. Bolzati
CNR Padua, Italy
February 15 – 18, 2000

A. Nicolopoulou
National Centre of Scientific Research Athens, Greece
March 5 - 26, 2000

Dr. A. Zablotskaya
Latvian Institute of Organic Synthesis Riga, Latvia
March 31 - April 27, 2000

Dr. T. Pajpanova
Institute of Molecular Biology Sofia, Bulgaria
April 6 - May 6, 2000

Dr. C.M. Fernandes
Instituto Tecnológico e Nuclear, Sacavém, Portugal
May 2 - June 2, 2000

Dr. A. Zablotskaya
Latvian Institute of Organic Synthesis Riga, Latvia
May 14 - July 3, 2000

Prof. E. Golovinsky
Institute of Molecular Biology Sofia, Bulgaria
July 4 - August 24, 2000

Dr. K. Chavatte
Vrije Universiteit Brussel, Belgium
July 5 - 14, 2000

G. Horváth
PET Center of the University School of Medicine, Debrecen, Hungary
September 1- November 30, 2000

Dr. A. Zablotskaya
Latvian Institute of Organic Synthesis Riga, Latvia
October 9 - December 19, 2000

Prof. K. Yoshizuka
Faculty of Science and Engineering, Saga University, Saga, Japan
November 11 -26, 2000

Dr. F. X. Sundram
Singapore General Hospital, Singapore
November 11 - 15, 2000

S. Somanesan
Singapore General Hospital
November 11 - 15, 2000, Singapore

Prof. Dr. S. Tachimori
Japan Atomic Energy Research Institute, Tokai, Japan
November 13, 2000

Dr. K. Chavatte
Vrije Universiteit Brussel, Belgium
November 17, 2000

Prof. J. Ostyk-Narbutt
Institute of Nuclear Chemistry and Technology, Warsaw, Poland
November 18 - December 2, 2000

MEETINGS ORGANIZED

Workshop
"Aspects of dendrimers in drug targeting"
May 8, 2000.

Two-days seminar on "Promisses and pitfalls in radiopharmaceutical research"
June 22 - 23, 2000

TEACHING ACTIVITIES

Winter term 1999/2000

B. Johannsen
One-term course on Radiopharmaceutical Chemistry

H. Spies
Laboratory course on Radiopharmaceutical Chemistry

Summer term 2000

B. Johannsen
One-term course on Metals in Biosystems

OTHER ACTIVITIES

B. Johannsen
Chairman of the DGN Working Group on Radiochemistry and Radiopharmacy.

B. Johannsen
Co-editor of the Journal “Nuclear Medicine and Biology“.

B. Johannsen
Co-organizer of the 7th International Symposium on “The Synthesis and Applications of Isotopes and Isotopically Labelled Compounds“ of the International Isotope Society.
Dresden, June 18 - 22, 2000.

IV. SEMINARS

TALKS OF VISITORS

Prof. Dr. P. Comba, Universität Heidelberg
Design, Synthese und Charakterisierung von biologisch relevanten Kupferverbindungen.
02.02.2000.

Dr. R. Reszka, Max-Delbrück-Zentrum Berlin
Liposomale in-vivo-Gentherapie mit dem HSV-tk-Gen/Ganciclovirsystem zur Behandlung von Glioblastomen.
18.02.2000.

Dr. M. Friebe, Havard Medical School Boston, USA
Technetium-99m probes with affinity for malignant melanoma: Synthesis and evaluation in vitro and in vivo.
28.04.2000.

Dr. G. Westera, Universitätsspital Zürich, Switzerland
Neuronale nAChR-Liganden auf der Basis von Epibatidin.
19.05.2000.

Dr. S. R.Waldvogel, Universität Münster
Supramolekulare Rezeptoren und Katalysatoren auf der Basis von funktionalisiertenTriphenylenketalen.
08.06.2000.

Dr. P. Kumar, University of Alberta, Canada
Nitroimidazoles in hypoxia management: Our activities.
16.06.2000.

Prof. Dr. H. F. Kung, University of Pennsylvania, Philadelphia, USA
Development of CNS receptor imaging agents for SPECT.
23.06.2000.

Prof. L. I. Wiebe, University of Alberta, Edmonton, Canada
Gene therapy imaging.
04.10.2000.

Dr. G. Horvath, PET-Center of the Univ. School of Medicine, Debrecen, Hungary
PET in Debrecen.
08.11.2000.

Prof. K. Yoshizuka, Saga University, Japan
Application of molecular modeling toward separation science of metallic ions.
17.11.2000.

Dr. S. Eichler, EU-Forschungskoordinatorin, Leipzig
Europäische Forschungsförderung auf dem Gebiet der Lebenswissenschaften (5.RP)
24.11.2000.

Prof. J. Ostyk-Narbutt , Institute of Nuclear Chemistry and Technology, Warsaw, Poland
Liquid-liquid partition and hydration of amphiphilic chelates of metal ions.
24.11.2000.

Dr. W. Mier, DKFZ Heidelberg
Rezeptorvermittelter Transport von Antisense-Oligodesoxynukleotid-Molekülen.
08.12.2000.

Prof. Inoue, Saga University, Japan
Development of lyophilic chitosan as novel solvent extraction reagents friendly environments.
18.12.2000.

INTERNAL SEMINARS

Scheunemann M.
Neue Ergebnisse zur ^{18}F-Markierung an NT- und BN-Derivaten.
05.01.2000.

Fischer K.
Möglichkeiten und Grenzen massenspektroskopischer Untersuchungen im Haus.
20.01.2000.

Zessin J.
Neue Radiotracer für 5HAT-Transporter.
26.01.2000.

Römer J.
Ergebnisse und Perspektiven der modulgestützten Synthese von fluorierten Estradiolsulfamaten.
09.02.2000.

Jordanova A.
Darstellung von n.c.a. [^{18}F]$FclO_3$-Optimierungsarbeiten.
23.02.2000.

Fischer K.
Massenspektroskopie (LC-MS)
01.03.2000.

Füchtner F.
3-O-Methyl-6-[^{18}F]fluor-DOPA - Ansatzpunkt für aussichtsreiche Tracer zur Tumordarstellung?
08.03.2000.

Rodig H.
Biologische Charakterisierung von [^{18}F]Fluorestradioldisulfamat.
22.03.2000.

Will E.
Rechnernetz und www.
12.04.2000.

Preusche S.
Betriebserfahrungen unter Nutzung der aktuellen Steuersoftware.
19.04.2000.

Steinbach J.
Elektrophile Fluorierung.
05.05.2000.

Künstler J.-U.
EXAFS-Untersuchungen von Re/Tc-Carbonylverbindungen.
24.05.2000.

Syhre R.
Die Ratte als Tiermodell zur Beurteilung des in vivo-Verhaltens von Radiotracern.
14.06.2000.

Drews A.
Rezeptoraffine Komplexe.
05.07.2000.

Rother A.
Stand zur Arbeit zu redox-aktiven Tc-Komplexen.
30.08.2000.

Noll St.
Synthese von Substraten der HSV-1-Thymidinkinase und der entsprechenden Präkursoren für die ^{18}F-Markierung.
20.09.2000.

Jordanova A.
Synthesis of [^{18}F]FCLO$_3$ and labelling of aromatics.
20.09.2000.

Mäding P.
Leuckart-Wallach-Reaktion mit 4-[^{18}F]Fluorbenzaldehyd.
29.09.2000.

Pawelke B.
Vorarbeiten zur Synthese kernmarkierter Benzoe- und o-Tolylsäurederivative.
04.10.2000.

Römer J.
Herstellung von [^{18}F]FES-Monosulfamaten.
11.10.2000.

Grote M.
Gentherapie.
11.10.2000.

Smolinka K.
AMG und AmRadV: Bedeutung und Konsequenzen für die Entwicklung radioaktiver Arzneimittel für PET.
25.10.2000.

Noll B.
^{186}Re/^{188}Re-markierte Stents zur Prävention von Restenosen.
08.11.2000.

Heichert C.
[^{18}F]FSB als Fluorbenzoylierungs-Reagens.
15.11.2000.

Füchtner F.
^{18}F-markierte Aminosäuren - Herstellung und Anwendung.
29.11.2000.

Pietzsch H.-J.
Rezeptorbindende Tc-Komplexe.
06.12.2000.

Zessin J.
Darstellung von Brom-[^{18}F]fluormethan.
06.12.2000.

Jung C.
Stand der Arbeit zu Tc-Komplexen mit modifizierten Fettsäureliganden.
20.12.2000.

V. ACKNOWLEDGEMENTS

ACKNOWLEDGEMENTS FOR FINANCIAL SUPPORT

The Institute is part of the Research Center Rossendorf Inc., which is financed by the Federal Republic of Germany and the Free State of Saxony on a fifty-fifty basis.

Two projects were supported by Commission of the European Communities:

Peptide radiopharmaceuticals in oncology
BIOMED II
in collaboration with Belgium, Greece and Switzerland
(PL 963198-SC), 04/1998 – 03/2001.

Radiotracers for *in vivo* assessment of biological function
COST B12
in collaboration with Sweden, Italy and Switzerland
02/1999 – 02/2004.

Three research projects concerning technetium tracer design, biochemistry and PET radiochemistry were supported by the Deutsche Forschungsgemeinschaft (DFG):

Tc labelled fatty acids for myocardium diagnosis
Sp 401/6-1 (H. Spies), 06/1999 – 05/2001.

Redox transport system for ^{99m}Tc radiopharmaceuticals
Sp 401/5-1 (H. Spies), 06/1999 – 06/2001.

The Sächsisches Staatsministerium für Wissenschaft und Kunst provided support for the follwing projects:

Technetium(VII) complexes with supramolecular receptors
SMWK-No. 4-7533-70-844-98/4, 07/1998 – 12/2000.

^{18}F labelled substrates of virus thymidine kinase for monitoring of gene therapy of cancer
SMWK-No. 4-7531.50-03-844-98/2, 07/1998 – 12/2000.

Molecular modelling of solid tumours by molecule spectroscopy in combination with PET
SMWK-No. 4-7531.50-03-0370-98/3, 07/1998 – 12/2000.

The International Atomic Energy Agency supported a co-ordinated research program: “Development of agents for imaging central neural system receptors based on Tc-99m“.
Agreement No. 8959 – 12/1995 – .

Three projects were supported by cooperations with the pharmaceutical industry:

Cooperation in nuclear diagnostic
Schering AG Berlin
07/1996 – 06/2002.

Cooperation in drug targeting
BASF Ludwigshafen
03/2000 - 02/2001

id-pharma Jena
01/2000 - 12/2000

Bilateral cooperation with Latvia:

Silyl group-functionalized Tc complexes
WTZ, LET-008-97, 07/1997 – 12/2001

Silyl group-functionalized Re complexes
NATO, 05/2000-04/2002

VI. PERSONNEL

per 31 December 2000

Director

Prof. Dr. B. Johannsen

Administrative Staff

L. Kowe
G. Neubert
M. Kersten

Scientific Staff

Dr. Bergmann, R.
Dr. Brust, P.
Dr. Füchtner, F.
Dr. Heichert, C.*
Dr. Heimbold, I.*
Dr. Hinz, R.*
Kretzschmar, M.
Mäding, P.
Dr. Noll, B.
Dr. Noll, St.
Dr. Pawelke, A.*
Dr. Pietzsch, H.-J.
Preusche, S.
Dr. Römer, J.*
Dr. Seifert, S.
Smolinka, K.*
Dr. Spies, H.
Dr. Steinbach, J.
Dr. Stephan, H.*
Dr. Syhre, R.
Dr. Will, E.

Technical Staff

Beyer, B.*
Dohn, N.
Fischer, K
Gläser, H.
Görner, H.
Große, B.
Hentges, A.*
Herrlich, R.
Herzog, W.*
Kasper, H.
Kolbe, U.
Krauß, E.
Kreisl, B.
Kunadt, E.
Landrock, K.
Lehnert, S.
Lenkeit, U.
Lipps, B.*
Lücke, R.
Roß, H.
Sterzing, R.
Suhr, A.*

Post Docs

Dr. Knieß, T.*
Dr. Wittrisch, H.*
Dr. Zessin, J.*

* term contract

PhD Students

Drews, A.
Friedrich, A.
Grote, M.
Jordanova, A.
Jung, Ch.
Künstler, J.-U.
Rodig, H.
Rother, A.

Former Personnel

(who left during the period covered by the report)

Scientific Staff: Dr. Scheunemann, M.

Technical Staff: Lösel, E.
Smuda, Ch.

PhD Students: Gupta, A.